Quantifying plasma membrane protein reduction during immune activation using mass spectrometry

Monika Stegmann

Sir William Dunn School of Pathology

Brasenose College

University of Oxford

A thesis submitted for the degree of Doctor of Philosophy

Trinity Term 2015

Abstract

The communication of immune cells through cell surface receptors is crucial for maintaining immune homeostasis, coordinating the immune response and pathogen clearance. The interaction of cell surface receptors with their cognate ligands is dependent on a key-lock principle and therefore only allows binding of partners in their correct conformational state. Reductive cleavage of labile disulfide bonds is a post-translational modification, capable of controlling protein function by mediating a conformational change. Activation of the immune system leads to the secretion of thiol isomerases that catalyse labile disulfide bond reduction and thereby are able to modulate protein function. A bioinformatics study and a mass spectrometry based screen have shown that many different plasma membrane proteins potentially contain labile disulfide bonds. To identify proteins with biologically relevant labile disulfide bonds it is necessary to quantify the reduction occurring as it is expected that only proteins that are reduced to a substantial amount affect cellular function.

In this study, a mass spectrometry based method to screen for proteins with labile disulfide bonds and quantify their reduction in primary cells was developed. It was then applied to study the plasma membrane redox proteome during immune activation and identified several proteins, mainly activating (CD132, gp130) and adhesion (integrins, ICAM1 and CD44) molecules, that are reduced to a major degree during immune activation. Furthermore, functional studies on the shared cytokine receptor gp130 showed that thioredoxin reduction inhibits IL-6 signalling.

These observations in conjunction with the literature suggest that labile disulfide bond reduction during immune activation is a mechanism to prevent over-activation of the immune system and excessive accumulation of leukocytes in sites of inflammation. Presenting a method to identify altered redox control of proteins in diseases such as autoimmunity provides the basis for the rational design of novel redox drugs.

Acknowledgements

First and foremost I would like to thank Prof. A. Neil Barclay who offered me the opportunity to do my DPhil in his lab. I am grateful for all the guidance and support throughout the project.

I thank everyone in the Barclay lab for providing a supportive environment. Special thanks go to Clive Metcalfe for the supervision in the lab. I have learned a lot from him and his ideas were instrumental for the success of this project. Thank you for reading my thesis and providing a critical feedback.

The Sir William Dunn School of Pathology and the Central Proteomics Facility have been an excellent environment to carry out research. A special thank goes to Svenja Hester for her support and advice in the acquisition of reproducible, high quality mass spectrometry data. Elisa Pappalardo helped me with the statistical analysis of the proteomics data and Phil Charles provided excellent advice throughout my project.

I would like to thank Alison for all the great OMPI-II sofa discussions, Patty for introducing me to yoga and sharing the joys and pain of the DPhil starting from day one, Johannes and Uli for great times in and around Oxford, the W1 and wNVL girls for great trainings, matches and socials, Andrea for her smile, Mariette for exploring Paris and London with me, Breanne and Carlos for our dinner-dates and Aline for her telepathic support.

Lastly, I would like to thank my family for their encouragements from close or from afar. I greatly enjoyed the hiking trips with my parents, exploring Cornwall with my brother, visiting English country gardens with my grandparents, catching up with my cousins Andreas, Martin and Sarah in Oxford, having a spontaneous dinner with Silvia and Giovanni at the Rickety Press and the London-Oxford adventure with Ruedi and Marianne.

Contents

Abstract ..... **i**

Acknowledgements ..... **ii**

Contents ..... **iii**

List of figures and tables ..... **iv**

Chapter I – Introduction **1**

1.1. Disulfide bonds and their function in proteins 4
1.2. Thiol isomerases cleave extracellular, labile disulfide bonds 9
1.3. Role of labile disulfide bonds in immune regulation and disease 12
1.3.1. Redox regulation of immune activation 12
1.3.2. Several viruses are dependent on labile disulfide bond reduction for host cell entry 14
1.4. Identification of labile disulfide bonds 17
1.5. Mass spectrometry based proteomics 20
1.6. Research objectives 28

Chapter II – Materials and Methods **30**

2.1. Culture of cells 32
2.2. Isolation of peripheral blood mononuclear cells 32
2.3. LPS-induced endotoxemia mouse model 32
2.4. Flow cytometric and ImageStream analysis of cell surface markers and cell surface thiol levels 33
2.5. Differential thiol labelling of cell surface proteins using SH-IQ (Thiol (-SH) identification and quantitation) 34
2.6. Differential thiol labelling of recombinant protein using the isotope pair NEM (N-ethylmaleimide) and d5NEM (deuterated (ethyl-D5) NEM) 36
2.7. Mass spectrometry analysis 36
2.8. Analysis of mass spectrometry data 37
2.9. IL-6 stimulation of INA-6 cells 38
2.10. Western blotting 39
2.11. Reduction of labile disulfide bonds followed by SDS-PAGE and in-gel analysis 40

Chapter III – Quantitation of labile disulfide bond cleavage **42**

3.1. Introduction 44
3.2. Results 45
3.2.1. Labile disulfide bonds are reduced in leukocyte cell surface proteins by TCEP 45
3.2.2. Quantitation of labile disulfide bond reduction using mass spectrometry 48
3.2.3. Tandem lectin-avidin purification maximises the detection of biotinylated cell surface proteins by mass spectrometry 54
3.2.4. SH-IQ quantifies the reduction of labile disulfide bonds in 32 plasma membrane proteins on leukocytes 61

3.3. Discussion 74

Chapter IV – Labile disulfide bonds are cleaved during immune activation 76

4.1. Introduction 78
4.2. Results 79
4.2.1. Reduction of labile disulfide bonds on PBMCs can be followed by flow cytometry 79
4.2.2. Cell surface thiol levels increase on PBMCs during immune activation 81
4.2.3. Cell surface thiol levels are highest on activated T cells 83
4.2.4. Thioredoxin inhibition prevents labile disulfide bond reduction during immune activation 85
4.2.5. SH-IQ identifies 29 proteins with labile disulfide bonds that are reduced on PBMCs during immune activation 87
4.2.6. Interesting observation: Thiol levels on splenocytes increase during inflammation 93
4.3. Discussion 100

Chapter V – Labile disulfide bonds in ADAM17 and gp130 104

5.1. Introduction 106
5.1.1. ADAM17 107
5.1.2. Gp130 and IL-6 signalling 109
5.2. Results 113
5.2.1. Free cysteines are formed upon ADAM17 reduction with TCEP and thioredoxin 113
5.2.2. Labile disulfide bond is located in the ADAM17 metalloproteinase domain 115
5.2.3. Structural analysis of gp130 reveals potential labile disulfide bonds 119
5.2.4. IL-6 induces tyrosine phosphorylation of STAT3 121
5.2.5. IL-6 signalling is inhibited by thioredoxin through the JAK-STAT3 but not the Ras-Raf-MEK-Erk pathway 123
5.2.6. Thioredoxin inhibits IL-6 induced STAT3 phosphorylation in a time-dependent manner 125
5.3. Discussion 127
5.3.1. ADAM17 127
5.3.2. Gp130 129

Chapter VI – Discussion 132

6.1. Quantitative analysis of labile disulfide bond reduction using mass spectrometry 134
6.2. Labile disulfide bonds are reduced in many different cell surface proteins 137
6.2.1. ICAM-1 137
6.2.2. Integrins 138
6.2.3. Tumor necrosis factor receptor superfamily member 8 (CD30) 140
6.2.4. CD44 141
6.3. Implications of labile disulfide bond reduction in disease 143

Bibliography 150

Abbreviations 174

Appendix **182**

1. Supplementary tables 184
2. Quantitation methods in proteomics 210
   - 2.1. SILAC 212
   - 2.2. ICAT 212
   - 2.3. iTRAQ and TMT 213
   - 2.4. NeuCode 214
   - 2.5. Label-free quantitation 216
3. Shared cytokine receptors 220
4. Papers 226
   - 4.1. Immunoregulation through membrane proteins modified by reducing conditions induced by immune reactions. 228
   - 4.2. CD44 binding to hylaruonic acid is redox regulated by a labile disulfide bond in the hylaruonic acid binding site. 230

List of figures and tables

Figure 1: **The human proteome is 50-times larger than the genome.** 5

Figure 2: **Disulfide bond conformations.** 6

Figure 3: **Thioredoxin reduces labile disulfide bonds via oxidoreductase cleavage.** 10

Figure 4: **DCs provide the reducing extracellular environment required for T cell activation.** 13

Figure 5: **Binding of HIV gp120 to leukocyte CD4.** 15

Figure 6: **Conceptual representation of tandem mass spectrometry.** 20

Figure 7: **Schematic of a QExactive mass spectrometer.** 22

Figure 8: **Fragmentation of peptides.** 23

Figure 9: **Fragmentation spectrum of the peptide DPPSEPSPLEAEFQR.** 24

Figure 10: **False discovery rate and posterior error probability.** 25

Figure 11: **Labile disulfide bonds are reduced on leukocytes by TCEP.** 46

Figure 12: **Labile disulfide bonds are reduced on the leukocyte cell surface by TCEP.** 47

Figure 13: **Differential labelling of cysteines for labile disulfide bond quantitation – three strategies.** 50

Figure 14: **Efficient enrichment of biotinylated cell surface proteins by tandem lectin-avidin purification.** 59

Figure 15: **Mass spectrometry workflow for the quantitation of labile disulfide bond reduction.** 60

Figure 16: **Normalisation of SH-IQ mass spectrometry data: Box and whisker plots.** 62

Figure 17: **SH-IQ: Diagnostic plots.** 63

Figure 18: **SH-IQ: Volcano plot.** 65

Figure 19: **Gene ontology and power analysis of SH-IQ data.** 67

Figure 20: **Verification of SH-IQ by Western blotting.** 71

Figure 21: **Internalisation of reduced CD44 is accelerated compared to native CD44.** 72

Figure 22: **Labile disulfide bonds are reduced on PBMCs by TCEP.** 80

Figure 23: **Thiol levels increase on the leukocyte cell surface during immune activation.** 82

Figure 24: **Cell surface thiol levels are highest on activated T cells.** 84

Figure 25: **Thioredoxin inhibition affects labile disulfide bond reduction and cell adhesion during immune activation.** 86

Figure 26: **Diagnostic plots of labile disulfide bond reduction on PBMCs after activation.** 88

Figure 27: **Schematic of the kinetics of labile disulfide bond reduction.** 89

Figure 28: **Kinetics of labile disulfide bond reduction during immune activation.** 92

Figure 29: **Labile disulfide bonds are reduced during inflammation.** 94

Figure 30: **Progenesis diagnostic plots for the quantitation of labile disulfide bond reduction during inflammation.** 95

Figure 31: **SINQ diagnostic plots for the quantitation of labile disulfide bond reduction during inflammation.** 96

Figure 32: **Splenocyte cell type composition is unchanged after immunisation with LPS.** 99

Figure 33: **ADAM17 activity is redox-controlled.** 108

Figure 34: **IL-6 signalling complex formation and functional implication of redox modulation.** 110

Figure 35: **Major IL-6 signalling cascades through JAK-STAT and Ras-Raf-MEK-Erk.** 112

Figure 36: **ADAM17 labile disulfide bond reduction followed by SDS-PAGE.** 114

Figure 37: **Labile disulfide bond is located in the ADAM17 metalloproteinase domain.** 116

Figure 38: **Structural analysis of ADAM17 metalloproteinase domain.** 118

Figure 39: **Structural analysis of gp130 disulfide bonds.** 120

Figure 40: **Dose-dependent phosphorylation of STAT3 by IL-6.** 122

Figure 41: **IL-6 signalling through JAK-STAT but not Ras-Raf-MEK-Erk is inhibited by thioredoxin.** 124

Figure 42: **Labile disulfide bonds are reduced on leukaemia cells by thioredoxin in a time-dependent manner.** 126

Figure 43: **Reduced ADAM17 cysteine-rich domain structure.** 128

Figure 44: **Immune cells secrete thiol isomerases upon activation.** 136

Figure 45: **Redox regulation of integrin $\alpha_{IIb}\beta_3$ activation on platelets.** 139

Figure 46: **Redox and cancer therapy.** 148

Table 1: **Classification of disulfide bonds based on the signs of the dihedral angles χ1, χ2, χ3, χ'2, χ'1.** 7

Table 2: **Effects of labile disulfide bond reduction on plasma membrane protein function**. ... 16

Table 3: **Comparison of quantitative proteomics strategies.** 27

Table 4: **Comparison of avidin and tandem lectin-avidin enrichment for selected proteins to assess the purification efficiency of biotinylated cell surface proteins.** 57

Table 5: **Quantitation of labile disulfide bond reduction in leukocyte cell surface proteins after TCEP reduction.** 69

Table 6: **Quantitation of labile disulfide bond reduction in splenocyte cell surface proteins during inflammation.** 98

Supplementary Table 1: **50 most abundant proteins identified from leukocyte whole cell lysate.** 185

Supplementary Table 2: **50 most abundant proteins identified after lectin purification.** 188

Supplementary Table 3: **SH-IQ: 50 most abundant proteins identified after avidin purification.** 191

Supplementary Table 4: **SH-IQ: 50 most abundant proteins identified after tandem lectin-avidin purification.** 194

Supplementary Table 5: **Quantitation of labile disulfide bond reduction in leukocyte cell surface proteins after TCEP reduction.** 197

Supplementary Table 6: **Analysis of splenocyte control experiments.** 203

Supplementary Table 7: **Kinetics of labile disulfide bond reduction during immune activation.** 204

Chapter I – Introduction

1.1. Disulfide bonds and their function in proteins

Proteins are large, complex molecules that are responsible for almost every task in the cell, including organisation, maintenance and communication. They are composed of a linear array of 20 different amino acids whose sequence defines the protein's characteristic three-dimensional structure and protein function. Cysteine is a particular member among the amino acids as it encompasses a sulphur-containing, highly reactive thiol (-SH) group which can easily oxidise to sulfenic acid (-SOH), sulfinic acid ($-SO_2H$) or cysteic acid ($-SO_3H$) and can form disulfide bonds between two cysteines. Disulfide bonds stabilise the intra-chain tertiary and inter-chain quaternary structure of proteins and can serve as centres of catalytic sites for thiol enzymes providing a strong reducing potential.

Generally, protein function is controlled by either the amount of protein present or by the modification state of the protein. The activity of a protein depends on the exact orientation of amino acids relative to each other which can be modulated by i) the covalent modification of amino acid side chains, ii) the cleavage or isomerisation of peptide bonds and iii) disulfide bond cleavage. Thus, slight changes in the conformation may result in altered function. Post-translational modification (PTM) of proteins is a rapid mechanism for the cell to adapt to environmental changes when needed which is independent of protein *de novo* synthesis. Moreover, PTM of proteins leads to a vast diversification of protein function. The human genome 'only' consists of around 25,000 genes (1) but the proteome contains over 1,000,000 proteins (2) (Figure 1). This is achieved by changes in transcription and PTM of proteins. Currently, there are over 200 covalent PTMs characterised, including phosphorylation and ubiquitination, which allows a single protein to carry out different functions or to localise to different cellular compartments.

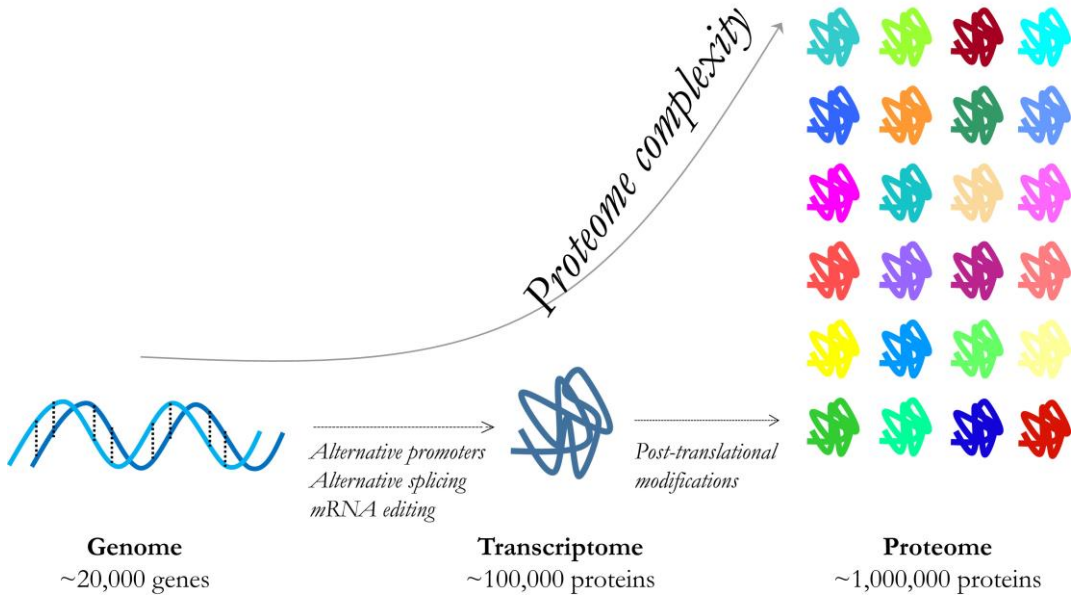

Figure 1: **The human proteome is 50-times larger than the genome.** Changes in transcription (alternative promoters, alternative splicing, mRNA editing) and post-translational modification of proteins increases the size of the human proteome (~1,000,000 proteins) vastly relative to the genome (~20,000 genes). This increases the functional diversity of the proteome and allows the cell to post-translationally control protein function.

Most disulfide bonds are of structural nature and assist protein stability. However, there is a subset of disulfide bonds termed labile disulfide bonds that can be post-translationally cleaved leading to functional effects. Reductive cleavage of labile disulfide bonds is capable of controlling protein function by mediating allosteric conformational changes. Therefore, these disulfide bonds are also called allosteric disulfide bonds (allos = 'other', steros = 'solid' or 'three-dimensional') (3).

Not all disulfide bonds are alike in their function, nor are they in their geometry. Based on their structure, disulfide bonds can be classified into 20 different classes (Table 1) which can be further divided into three different groups: i) spirals, ii) hooks, and iii) staples (Figure 2 B). The disulfide bond groups are defined by the torsion angle of the three $\chi 2$, $\chi 3$, and $\chi' 2$ bonds (Figure 2 A). A positive sign of the $\chi 3$ angle makes the bond right handed and negative sign left handed (Table 1). The most abundant class of disulfide bonds are the –LHSpirals (4). Catalytic disulfide bonds are mostly found in

the hook conformation (-LHHook and -/+RHHook) whereas labile disulfide bonds are mainly contained in the -RHStaple and to a lesser extent in the -LHHook and -/+RHHook groups (5). -RHStaple disulfide bonds have a high dihedral strain energy (DSE) (18.1 kJ mol^{-1} on average) compared to the average disulfide bond (14.8 kJ mol^{-1} on average) (5, 6). Interestingly, structural disulfide bonds have a relatively low DSE (10.1 kJ mol^{-1} on average) and catalytic disulfide bonds a high DSE (20.8 kJ mol^{-1} on average). This highlights that structural disulfide bonds are the least strained and thus the most stable disulfide bonds and labile disulfide bonds the most strained and thus the most reactive disulfide bonds. The high DSE of labile disulfide bonds was suggested to arise from a relatively short Cα-Cα' distance (4.32 Å on average) (Figure 1 A), compared to the mean Cα-Cα' distance (5.63 Å on average), forcing the disulfide bond to bend (5) (reviewed in (7)). All-atom molecular-dynamics simulation recently revealed that -RHStaple and -/+RHHook are indeed more stressed than other disulfide bond conformations displaying a higher tension force due to stretching of the disulfide bond rather than the previously suggested DSE (4). This high mechanical force facilitates cleavage of labile disulfide bonds (8) which is consistent with their functional role.

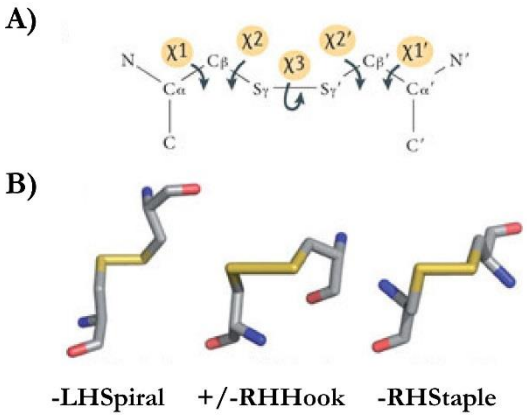

Figure 2: **Disulfide bond conformations.** A) Disulfide bonds can be classified based on their geometry which is defined by the χ torsion angles linking the two Cα of the two cysteine residues (Cα – Cα'). The χ angles can be either negative or positive, the sign of the χ3 angle defines whether a disulfide bond is right handed (positive sign) or left handed (negative sign). B) Disulfide bond configurations -LHSpiral, +/-RHHook and -RHStaple). Figure from (7).

Table 1: **Classification of disulfide bonds based on the signs of the dihedral angles χ1, χ2, χ3, χ'2, χ'1.** The χ1 and χ'1 angle define the sign of the disulfide bond, the χ3 angle defines whether a bond is left handed (LH, -) or right handed (RH, +) and the χ2 and χ'2 the group of the disulfide bond (spiral [-/-] or [+/+], hook [-/+] or [+/-] and staple [-/-] or [+/+]. Indicated in bold are labile disulfide bond configurations and in grey the most abundant disulfide bond configuration amongst all disulfide bonds.

Class	**χ1**	**χ2**	**χ3**	**χ'2**	**χ'1**	**Class**	**χ1**	**χ2**	**χ3**	**χ'2**	**χ'1**
+/-LHSpiral	+	-	-	-	-	**-RHStaple**	**-**	**-**	**+**	**-**	**-**
+/-RHSpiral	+	+	+	+	-	**-LHHook**	**-**	**-**	**-**	**+**	**-**
+RHSpiral	+	+	+	+	+	**-/+RHHook**	**-**	**+**	**+**	**-**	**+**
+RHHook	+	+	+	-	+	-RHSpiral	-	+	+	+	-
-/+LHHook	+	+	-	-	-	-RHHook	-	+	+	-	-
+/-LHStaple	+	+	-	+	-	-LHStaple	-	+	-	+	-
+LHStaple	+	+	-	+	+	+/-LHHook	+	-	-	+	-
+/-RHStaple	+	-	+	-	-	+/-RHHook	+	-	+	+	-
+RHStaple	+	-	+	-	+	+LHSpiral	+	-	-	-	+
-LHSpiral	-	-	-	-	-	+LHHook	+	-	-	+	+

Since cysteines and disulfide bonds have the unique ability to modulate protein function through cysteine oxidation, coordination of metals, redox catalysis and disulfide bond cleavage, it is not surprising that cysteine is the second most conserved amino acid after tryptophan (9, 10). Disulfide-bonded cysteines are even more conserved than unpaired cysteines and surpass tryptophan in terms of conservation (11). This can be explained due to the fact that the cysteine pair is required to form a disulfide bond which in turn is important for protein structure and function.

Interestingly, disulfide bonds are prevalent in plasma membrane and secreted proteins. About half of all disulfide bonds annotated in UniProt (16,538) are in fact found in membrane proteins (7264) (12). Disulfide bonds seem essential in maintaining the structural integrity of cell surface proteins in the harsh, oxidising extracellular environment. However, more recently it has been appreciated that disulfide bonds can also have a functional role through their redox-cleavage. This can lead to functional changes in cell surface proteins affecting the cell's ability to respond to environmental cues which is

anticipated to be of particular importance in the immune system as pathogen invasion and recognition, immune activation and the coordination of the immune response involve cell surface protein-mediated functions. Therefore, not only could labile disulfide bond reduction be crucial for the cell to modulate plasma membrane protein function but also for therapy as it potentially allows the redox-control of cell surface protein function.

1.2. Thiol isomerases cleave extracellular, labile disulfide bonds

Thiol isomerase enzymes such as protein disulfide isomerase (PDI) and thioredoxin (TRX) are a family of enzymes that are involved in catalysing labile disulfide bond formation, reduction and isomerization. They contain a double-cysteine motif (Cys-Gly-Pro-Cys) in their active site which catalyses the reversible reduction of disulfide bonds (13, 14). Thiol isomerase family members are found in the endoplasmic reticulum (ER) where they assist proper folding of proteins (15, 16). Despite their KDEL ER-retention sequence, they have been found in locations other than the ER such as the cell surface, the extracellular space, the cytosol, and the nucleus (13, 15). The human plasma proteome, for example, contains the thiol isomerases PDI, thioredoxin, glutaredoxin and flavoenzyme (17).

Labile disulfide bond reduction can occur through either thiol isomerase-mediated cleavage or thiol-disulfide exchange cleavage. Thiol isomerase-mediated cleavage occurs via a S_N2 (second-order nucleophilic substitution)-type reaction in which the two sulphur atoms contained in the substrate disulfide bond and the sulphur ion nucleophile (S^-) contained in the thiol isomerase are involved (Figure 3). They must arrange in a plane at a 180° angle for the reaction to be successful (18). The closer the orientation is to the 180° angle, the faster the reaction. Thiol isomerases can only reduce disulfide bonds with a bigger (less negative) redox potential, limiting their mode of action. When the sulfur ion nucleophile from the thiol isomerase attacks the disulfide bond in the substrate, a mixed disulfide intermediate is formed which spontaneously decomposes to the more stable reduced substrate and oxidised thiol isomerase. Once thiol isomerases are oxidised, they can be recycled back to their reduced dithiol form by thioredoxin reductase (Figure 3). The electrons required to catalyse this reaction are obtained from NADPH (nicotinamide adenine dinucleotide phosphate). Thiol-disulfide exchange cleavage is different in that it does not require any additional hydrogens and electrons in addition to the three sulphur atoms. The sulphur ion nucleophile is unreactive until it is brought in line with the disulfide bond which initiates cleavage.

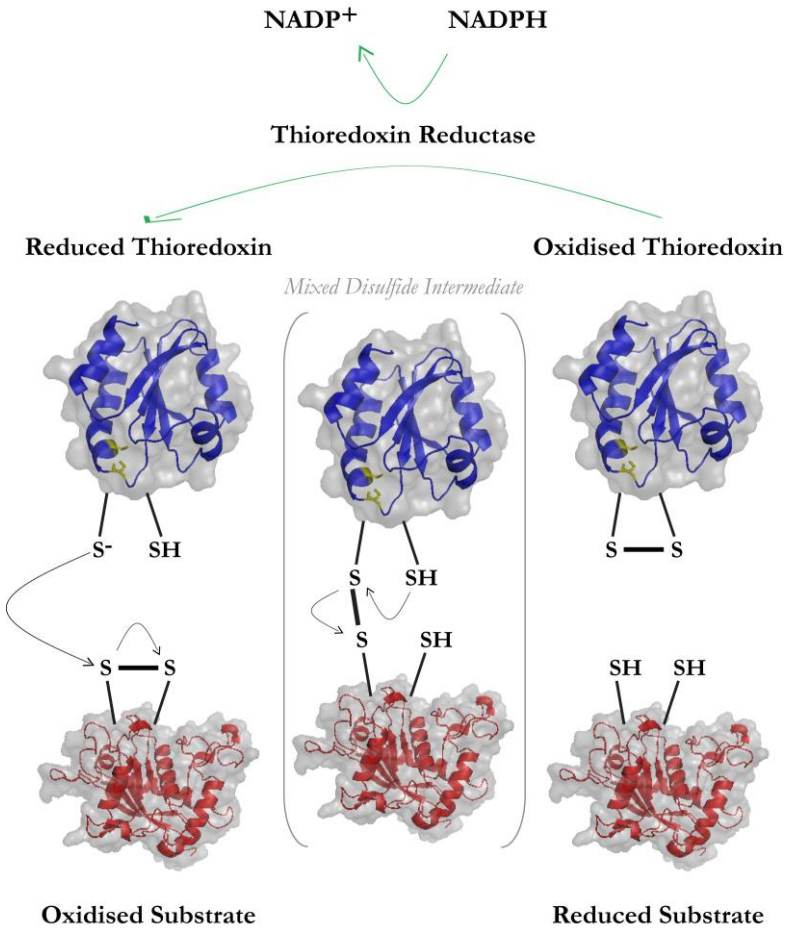

Figure 3: **Thioredoxin reduces labile disulfide bonds via oxidoreductase cleavage.** Reduced thioredoxin can cleave labile disulfide bonds in target proteins via a S_N2-type reaction in which the thioredoxin sulfur nucleophile (S^-) attacks the disulfide bond in the substrate. The intermediate mixed disulfide bonded complex can then spontaneously decompose via an intramolecular thiol-disulfide exchange, resulting in the more stable disulfide bond in thioredoxin and free thiols (-SH) in the substrate. Oxidised thioredoxin can be recycled back to its reduced state by thioredoxin reductase. The reducing potential required for this reaction is provided in the form of NADPH.

It is still unclear to what extent different thiol isomerases mediate the cleavage of different substrates whereas it is known that thiol isomerases are poly-specific. Thioredoxin, for example, cleaves labile disulfide bonds in CD132 (19) and CD44 (20). Although substrate specificity seems to be mostly overlapping between different thiol isomerases (i.e. gp120 is cleaved by thioredoxin, PDI and glutaredoxin (21–25)), there is evidence that different thiol isomerases can still reduce different substrates (26). In addition to substrate specificity, spatial distribution of target proteins and thiol isomerases is likely to provide an additional level of control to where and when labile disulfide bonds are cleaved.

1.3. Role of labile disulfide bonds in immune regulation and disease

Localization of thiol isomerases to the cell surface or the extracellular space can cause the reduction of labile disulfide bonds in plasma membrane proteins which is of particular relevance for the immune system. The interaction of leukocyte cell surface proteins with their cognate ligands forms the basis for detecting pathogens and enabling communication between immune cells, ensuring that immune homeostasis is maintained and pathogens cleared. It has been shown that labile disulfide bonds play a crucial role during immune activation (27), platelet activation (28), different diseases, such as rheumatoid arthritis, cancer, neurodegenerative- and cardiovascular diseases (29), and a broad range of viral infections. Understanding how labile disulfide bond reduction modulates protein function in immune regulation and disease is pivotal as it presents huge potential to translate this basic research into novel therapies.

1.3.1. Redox regulation of immune activation

A reducing extracellular environment has been shown to be important in T cell activation and proliferation which is provided by antigen presenting dendritic cells (DCs) (Figure 4) (30). Unlike other lymphocytes, naïve T cells do not express the cystine (Cys_2) transporter x_c- and therefore are dependent on extracellular cysteine (Cys) which tends to be present at low concentrations. DCs have been shown to provide the source of extracellular Cys for T cells by secreting reduced glutathione (GSH) which is then converted to Cys_2 and Cys by gamma-glutamyltranspeptidase and dipeptidase (31) (32). Regulatory T cells (T regs) can act on DCs and inhibit glutathione synthesis which subsequently decreases extracellular Cys levels available for T cells (33). Moreover, T regs and naïve T cells compete for Cys uptake. The importance of the Cys_2 transporter system x_c- in DCs in providing T cell with extracellular Cys required for activation is illustrated in the gut. Unlike peripheral blood monocytes, lamina propria macrophages do not express the x_c- transporter and are therefore unable to take up Cys_2 and provide Cys to the adjacent T cells (34). This might be crucial in maintaining the gut an immunotolerant environment since the T cells critically depend on an exogenous source of Cys. In ulcerative colitis and Crohn's disease, which are both chronic inflammatory conditions of the gastrointestinal tract, the x_c-

transporter is upregulated in contrast to the normal gut (34). As a result, inflammatory bowel disease gut DCs can provide the reducing environment T cells need for activation which may lead to the observed exaggerated immune response against luminal antigens of the commensal gut flora.

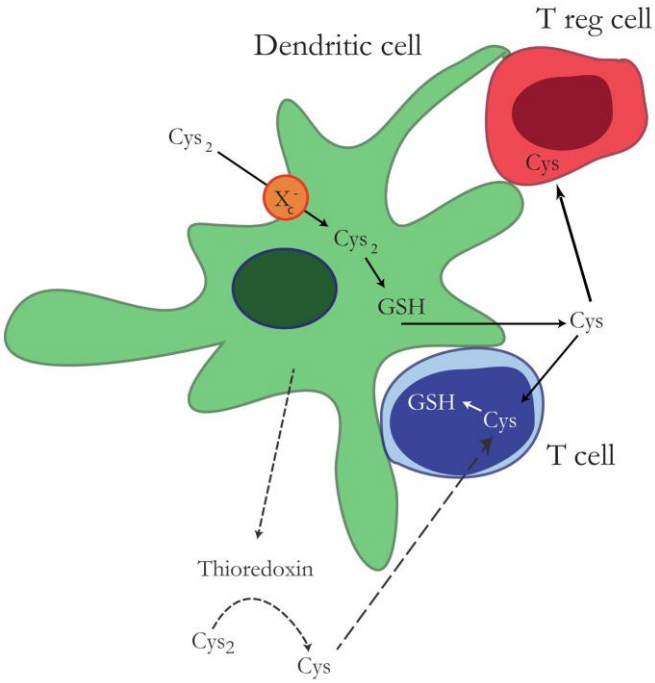

Figure 4: **DCs provide the reducing extracellular environment required for T cell activation.** Naïve T cells require an extracellular source of cysteine for activation as they lack the X_c^- transporter. This transporter, however, is expressed by DCs which allows them to generate glutathione (GSH) from imported cystine (Cys_2) which is then converted to cysteine (Cys) by gamma-glutamyltranspeptidase and secreted for the uptake by T cells. It initially has been thought that extracellular Cys_2 is converted to Cys by thioredoxin. Yet, this mode of action could never been proven. Regulatory T cells (T regs) are able to inhibit extracellular Cys by interaction with DCs and uptake of extracellular Cys.

Initially it was thought that DCs secrete thioredoxin to convert extracellular Cys_2 to Cys (Figure 4) (30). Indeed, thioredoxin could be detected in the supernatant of DCs when reacted with T cells, yet, neither cell type alone secrets thioredoxin, suggesting that either or both cell types secrete thioredoxin upon activation (32). Interestingly, when T cells are mitogen activated, thioredoxin expression and amount of protein are significantly increased (35) but not in lipopolysaccharide (LPS) activated DCs

(36). This indicates that the majority of thioredoxin secreted upon co-incubation of DCs with T cells originates from the T cells but there is no evidence that thioredoxin is involved to a significant extent in converting extracellular Cys_2 to Cys for the uptake by T cells. Although thioredoxin could not be shown to be involved in converting Cys_2 to Cys (32), it has a different role in T cell activation.

About 20 years ago, Lawerence *et al.* observed an increase in thiol levels when immune cells were activated (27). Henceforth, this direct relationship between increased thiol levels and immune activation could be confirmed by a number of different studies: These showed that thiol levels are increased i) in the spleen and lymph nodes after immunisation (35), ii) on PBMCs (peripheral blood mononuclear cells) of HIV (human immune deficiency virus) patients (27, 37) and iii) on splenocytes of mice with LCMV (lymphocytic choriomeningitis virus)-Armstrong-induced inflammation (38). Labile disulfide bond reduction, which leads to increased thiol levels, could be shown to be mediated by thiol isomerases as their inhibition with bacitracin blocks thiol formation during immune activation (27).

Furthermore, thioredoxin expression is induced in activated T cells (35) which could explain the phenomenon of increased thiol levels on leukocytes after immune activation. More specifically, cytotoxic T cells (T_C cells, CD8+) have been shown to contain more free thiols on the cell surface than helper T cells (T_H cells, CD4+) (27, 37, 38).

1.3.2. Several viruses are dependent on labile disulfide bond reduction for host cell entry

Enveloped viruses infect host cells by binding to target-cell receptors (overview of cell surface receptors targeted by viruses is reviewed in (39)). Whilst many viruses depend on low pH or proteolytic cleavage (40), others depend on reducing conditions for their entry into the host cell.

The best-known example is the human immune deficiency virus‘s (HIV) dependence on gp120 (glycoprotein 120) reduction for host cell entry. Gp120 possesses eighteen disulfide bonded cysteines of which several are cleaved by thioredoxin, PDI or glutaredoxin (21–25). It is proposed that disulfide bond cleavage in gp120 (Cys296-Cys331 (21)) leads to the exposure of hitherto hidden regions of the protein where co-receptors CXCR4 or CCR5 bind, initiating a conformational change in the non-

covalently bound gp41 allowing the fusion of the viral envelope with the host cell (Figure 5) (41). Moreover, CD4, the receptor for HIV, also contains a labile disulfide bond which is involved in multimer formation. HIV has been shown to preferentially bind to the reduced, monomeric CD4 (42). Gp120 binding to CD4 has been shown to facilitate the reduction of the disulfide bond on gp120. Compounds that are able to block the cleavage of the disulfide bond in gp120 or between CD4 multimers are therefore potential inhibitors for HIV entry and subsequent infection. The therapeutic potential of targeting labile disulfide bond reduction in HIV uptake has been extensively reviewed by Fennouillet *et al.* (39).

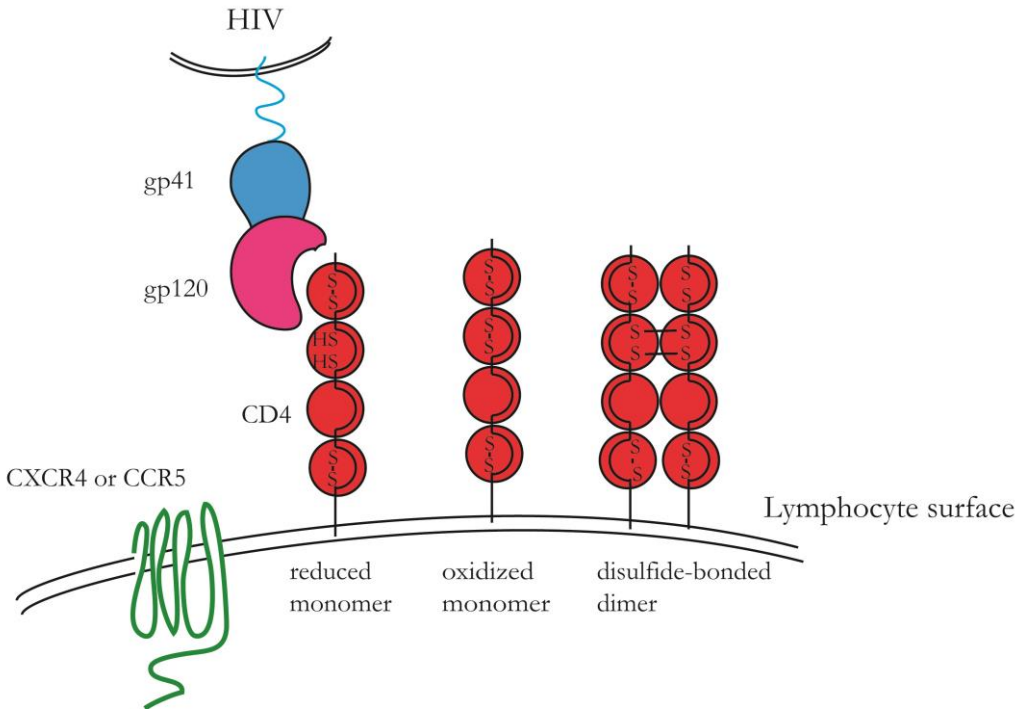

Figure 5: **Binding of HIV gp120 to leukocyte CD4.** HIV gp120 is reduced upon binding to its receptor CD4 which enables binding of the co-receptors CXCR4 or CCR5. This in turn initiates structural changes in the non-covalently linked gp41 which eventually leads to the fusion of the viral particle with the host cell. CD4 itself contains a labile disulfide bond and can therefore be present as a reduced monomer, an oxidised monomer or a disulfide-bonded dimer on lymphocytes.

Labile disulfide bond reduction is also important in the uptake of other viruses such as HCV (hepatitis C virus), Newcastle disease virus and others (43). HCV host cell entry has been shown to be dependent on nine disulfide bonds in the envelope proteins E1 and E2 as blocking disulfide bond reduction or rearrangement inhibited entry (44). Newcastle disease host cell fusion is mediated by hemagglutinin neuraminidase and fusion glycoprotein. Free thiols in the fusion glycoprotein are required for virus entry which can be suppressed by thiol isomerase inhibitors (45). Supporting this finding is the observation that overexpression of PDI resulted in increased virus-host cell fusion (46).

Table 2: **Effects of labile disulfide bond reduction on plasma membrane protein function**. Examples of cell surface proteins with labile disulfide bonds and the associated functional consequence of labile disulfide bond cleavage. *Red* (reduced), *Ox* (oxidised). Reviewed in (7, 47–52).

Protein name	Effect	Changes in
CD132	*Red* prevents IL-2 signalling through CD132	Ligand binding
IL-4	*Red* prevents Il-4 binding to its receptor IL-4Rα	
C-reactive protein	Different functions depending on whether multimer, *ox* monomer or *red* monomer	
β3 integrin	Activation is associated with *red* of several disulfide bonds	
CD44	*Red* prevents hyaluronic acid binding by CD44	
CD30	*Red* impairs CD30 ligand binding	
Angiotensinogen	*Ox* protein shows increased cleavage by renin leading to a raise in blood pressure, correlated with pre-eclampsia	Proteolysis
MICA	*Red* induces shedding	
Factor XI	*Red* leads to more efficient activation by thrombin	
CD4	Exists as disulfide-linked dimers and reduced or oxidised monomers	Oligomer formation
Vascular endothelial growth factors C and D	*Red* ablates activity of disulfide-linked homodimers	

1.4. Identification of labile disulfide bonds

Although it is well known that disulfide bonds stabilise protein structure, only more recently evidence has emerged that a subset of disulfide bonds, labile disulfide bonds, control protein function. The redox regulation of a number of plasma membrane proteins has been studied up to date (Table 2, reviewed in (7, 47–52)). To understand the role of labile disulfide bond reduction in immune activation and disease requires the identification of proteins with labile disulfide bonds that are reduced to an extent that is biologically relevant. This has remained a challenge due to the lack of suitable technology.

The Philip J. Hogg lab has developed a bioinformatics screen to identify labile disulfide bonds based on their geometry. In brief, they identified the -RHStaple, -LHHook and -/+RHHook disulfide bond conformations as signatures for labile disulfide bonds. They all display a relatively high tension force and/or a short Cα-Cα' distance. Unfortunately, this approach is hampered by the limited availability of plasma membrane protein crystal structures which is required for the analysis. Furthermore, proteins are dynamic structures of which only one form is represented in the crystal structure. Not being able to identify a labile disulfide bond configuration in a crystal structure therefore does not exclude that the disulfide bond can enter these configurations. Nevertheless, this bioinformatics approach is useful when the crystal structure is available and the candidate protein known but is not suitable for screening for novel candidates nor to quantify reduction in a biological system.

There has been an attempt to develop a cell-based screening method to systematically identify labile disulfide bond reduction in plasma membrane proteins by Laragione *et al.* combining 2-D gel electrophoresis with mass spectrometry by which they identified integrin α_4 to contain a labile disulfide bond (53). Although this method has been insightful, it has not provided a high throughput screen for labile disulfide bond containing proteins.

Mass spectrometry is a method that allows the simultaneous identification and quantitation of proteins and peptides from complex samples and therefore lends itself for the large-scale identification and quantitation of labile disulfide bond reduction.

Metcalfe *et al.* have developed a mass spectrometry based screen to identify plasma membrane proteins with labile disulfide bonds (26). This has yielded the identification of a vast number of proteins with putative labile disulfide bonds. To identify proteins with labile disulfide bonds whose function is likely to be affected by reducing conditions, it is crucial to quantify the reduction occurring. This will allow to rank proteins according to their degree of reduction. The more reduced a protein is, the more likely it is that this manifests in a biological effect. Furthermore, quantitation of labile disulfide bond reduction will allow to investigate the kinetics of labile disulfide bond reduction.

Quantifying labile disulfide bond reduction in plasma membrane proteins by mass spectrometry represents a challenge because of i) the low abundance of plasma membrane proteins relative to cytosolic proteins, ii) their hydrophobicity and iii) their heterogeneity introduced by glycosylation. Mass spectrometers have a limited dynamic range which affects the identification of peptides present in sub stoichiometric amounts. In order to be able to study labile disulfide bond reduction, the peptides of interest must be enriched to reduce sample complexity. Therefore, it is necessary to label cysteines of reduced labile disulfide bonds with an affinity tag to be able to enrich for cysteine-containing peptides prior to mass spectrometry analysis. The selective enrichment of modified peptides prior to mass spectrometry analysis is routinely carried out for phosphorylated peptides via immobilised metal affinity chromatography (IMAC) and/or titanium dioxide (TiO_2) beads (54) and for ubiquitinated (55, 56) or acetylated (57) peptides via antibody enrichment. Furthermore, the analysis of hydrophobic plasma membrane proteins is challenging because it requires their extraction from the membrane, solubilisation and the removal of glycosylation sites. Glycosylation can impair proteolytic cleavage efficiency through steric hindrance and identification of glycosylated peptides through sample heterogeneity. Extraction and solubilisation can be achieved by a variety of methods using detergents, organic solvents, organic acids and salt buffers. The use of detergents such as Triton X-100 (TX-100)

and sodium dodecyl sulfate (SDS) is most effective, however, not compatible with mass spectrometry analysis (58). Detergents can be removed from the sample using filter-aided sample preparation (FASP) (59) in which the filter is used as a detergent removal tool (60). Moreover, the use of FASP allows differential alkylation of cysteines in complex mixtures and recombinant proteins (19, 26). This exploits the principle that cysteines in labile disulfide bonds can be labelled with reagent X *in situ* or on the filter and all remaining cysteines with reagent Y on the filter. This freezes a given redox state of a cell or protein, a concept similar to pervanadate treatment of cells to freeze the phosphorylation state, which allows the analysis of the proteome by mass spectrometry and quantitation of labile disulfide bond reduction.

1.5. Mass spectrometry based proteomics

Proteomics is the systematic characterisation of proteins in a cellular compartment which uses tandem mass spectrometry (Figure 6). Proteins are digested to peptides, separated by liquid chromatography and ionised to enter the mass spectrometer. The peptide precursor-ion m/z (mass/charge) is analysed (MS1 or MS), precursor ions selected for fragmentation and the fragment spectrum analysed (MS2 or MS/MS). Protein composition of the sample is then deduced by peptide mass fingerprinting.

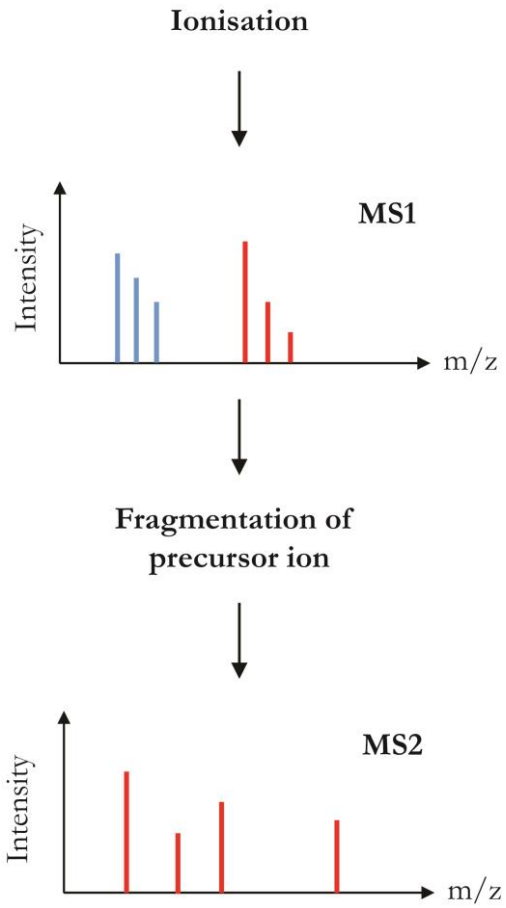

Figure 6: **Conceptual representation of tandem mass spectrometry.** In a first step peptides are ionised and their m/z is measured (MS1). Peptide A is represented in blue and peptide B in red. Specific precursor ions are then selected for fragmentation (peptide B in this example), giving rise to product ions which will be detected in the second mass analysis step (MS2) to produce the product ion spectrum.

The average human protein is composed of 375 amino acids (61) with a combined lysine and arginine frequency of ~11%. This leads to the generation of 37 tryptic peptides per protein. Analysing samples that contain multiple proteins therefore requires the separation of peptides prior to mass spectrometry analysis to reduce sample complexity in order to achieve the most complete analysis. To do so, a reversed phase liquid chromatography column is connected upstream of the mass spectrometer to separate peptides according to their hydrophobicity. To enter the mass spectrometer, peptides must be ionised and enter the gas phase which is achieved by passing the analyte through a conductive needle to which a voltage of approximately 2,000 V is applied. Peptides generated by trypsin contain two positive charges, one on the N-terminus and one on the C-terminus, donated by the acid in the loading buffer (62).

It is not sufficient to only measure the mass of the peptide ion (precursor ion) to unambiguously identify the peptide sequence. Many peptides of different sequence composition can have the same m/z value. Thus, to confidently identify the peptide sequence the precursor mass of peptides is measured in a survey scan, peptide ions selected (quadrupole) for fragmentation (HCD collision cell) and the fragment ion mass spectrum acquired (Orbitrap mass analyser) which allows peptide mass fingerprinting (Figure 7).

Quadrupole mass analysers consists of four parallel metal rods with adjacent rods having opposite voltage and opposite rods having the same voltage. This generates an alternating electric field that causes deflection or transmission of the peptide ions allowing the selection of specific precursor ions for fragmentation. In the Orbitrap mass analyser ions undergo a circular motion when placed in a magnetic field. The frequency of an ion is detected when the ions pass by conductive plates placed at opposite ends inducing a current. Fourier transformation is used to extract the individual frequencies present which can then be related to the m/z since the magnetic field is known. The longer the signal is measured, the better the spectrum, the more data points for final deduction. However, the longer the signal is measured, the less different spectra can be acquired. Orbitrap mass analysers have a high mass accuracy and a dynamic range of five orders of magnitude (10^5).

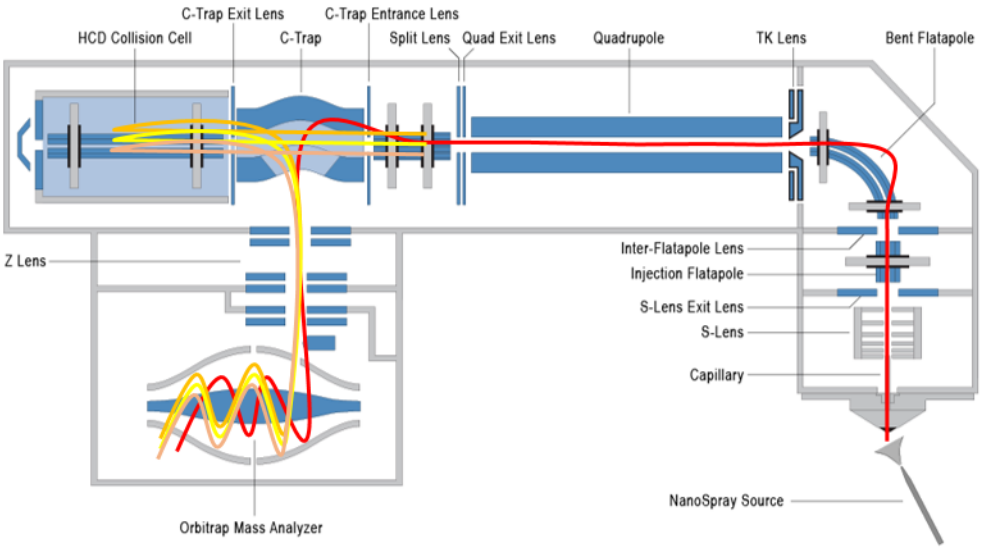

Figure 7: **Schematic of a QExactive mass spectrometer.** When running the instrument on a top20 method, the mass of all precursor ions is analysed in a survey scan (red) that is followed by the fragmentation of the 20 most abundant precursors in the HCD collision cell and subsequent MS/MS analysis (orange, yellow and beige lines represent three precursor ions selected for fragmentation).

Collision induced dissociation (CID) is a process in which peptide ions are accelerated and collided with an inert gas such as helium, leading to the release of the proton from the basic moiety. The conversion of kinetic energy to peptide bond vibration then causes the fragmentation of the peptide. When an amide bond is broken b- (keeping N-terminal portion of the peptide) and a y-ions (keeping the C-terminal portion of the peptide) are formed (Figure 8).

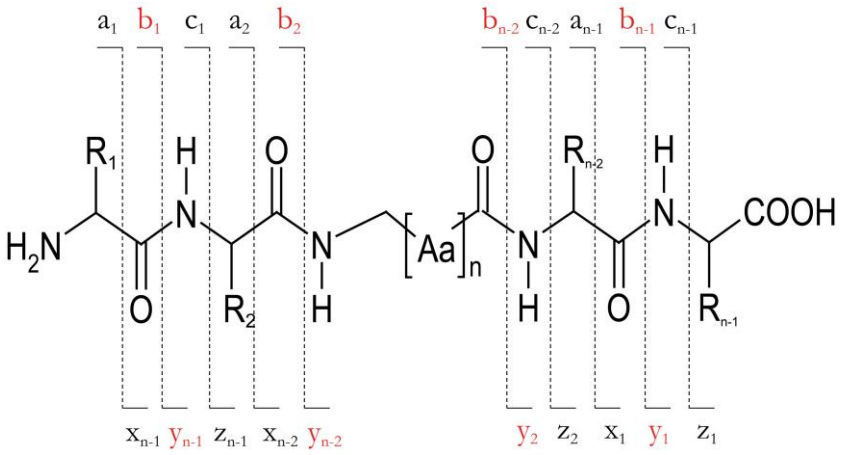

Figure 8: **Fragmentation of peptides.** Peptide fragments are labelled a_n, b_n c_n containing the N-terminal proportion of the peptide. The numbering of the fragments starts from the N-terminus. Fragments labelled x_n, y_n, z_n contain the C-terminal proportion and are numbered starting from the C-terminus. CID produces mainly b and y ions (indicated in red).

Once the mass spectra have been acquired, the challenge is to assign each mass spectrum to a peptide sequence. The peptide fragments in a series differ from each other by one amino acid and it is therefore possible to determine the amino acid sequence by considering the mass difference between two adjacent peptide fragments (Figure 9). Pattern matching search engines such as Mascot use databases (i.e. UniProt) to retrieve protein sequences and digest the proteome of interest *in silico* to generate a complete library of peptides and corresponding peptide fragments. Observed precursor masses and fragment spectra are then compared to the library to find the best match (peptide spectrum match – PSM). When matching observed peptide fragment patterns to theoretical peptide fragment patterns the degree of similarity between the two is determined and represented as a probability that the observed match is a random event (P-value). A protein can be considered as confidently identified if several statistically significant, unique peptides identify the protein.

A)

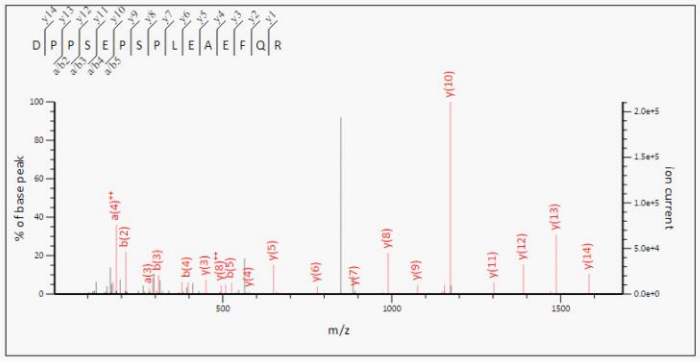

B)

#	Aa MW	a	b	Aa Seq.	y	#
1	88.0393	88.0393	116.0342	D		15
2	70.0651	**185.0921**	**213.0870**	P	*1583.7700*	14
3	70.0651	**282.1448**	**310.1397**	P	*1486.7172*	13
4	60.0444	369.1769	**397.1718**	S	*1389.6645*	12
5	102.0550	498.2195	**526.2144**	E	*1302.6325*	11
6	70.0651	595.2722	623.2671	P	*1173.5899*	10
7	60.0444	682.3042	710.2992	S	*1076.5371*	9
8	70.0651	**779.3570**	807.3519	P	*989.5051*	8
9	86.0964	**892.4411**	920.4360	L	*892.4523*	7
10	102.0550	1021.4837	1049.4786	E	*779.3682*	6
11	44.0495	1092.5208	1120.5157	A	*650.3257*	5
12	102.0550	1221.5634	1249.5583	E	*579.2885*	4
13	120.0808	1368.6318	1396.6267	F	*450.2459*	3
14	101.0709	1496.6904	1524.6853	Q	*303.1775*	2
15	129.1135			R	*175.1190*	1

Figure 9: **Fragmentation spectrum of the peptide DPPSEPSPLEAEFQR.** All y ions have been observed for this peptide and four b ions. A) The m/z of observed fragment ions is plotted versus the ion current. B) The table reports the observed m/z values of fragment ions in bold and the predicted molecular weight (MW) of each amino acid (aa).

Rapid advances in technology allow the identification of hundreds of proteins from one single mass spectrometry analysis. The challenge arising is to confidently identify the proteins present in the sample. When plotting the number of peptides observed versus the peptide identification scores, this shows a Gaussian-shaped distributions (63). The peak centered around the lower scores represents true negative identifications (random matches) whereas the one centering around higher scores represents true positive identifications (Figure 10). Mathematical modelling can now be used to determine the likelihood of a hit occurring by chance (probability P) for a given cut-off score. Increasing the search space (by searching against the whole mammalian database instead of database of the species or including variable modifications) leads to lower sensitivity (the scores stay the same but the false

matches increase) whereas decreasing the search space (limiting peptide mass accuracy to a few ppm) leads to a higher sensitivity. The advantage of mathematical, modelling which determines the cut-off score above which the likelihood of a hit occurring by chance is below 5%, is that is independent of the scoring system (reviewed in (64)). To normalise the scores from different search engines the posterior error probability (PEP) can be calculated (Figure 10). The PEP is the probability that the observed PSM is false – it is the local version of the false discovery rate (FDR). An alternative to this strategy is to calculate the FDR by generating a decoy set of peptides. The decoy database has to have the same size, a matching mass distribution and the same amino acid composition which is simply achieved by reversing the original sequence database. The peptides are then searched against both the true and the decoy database. In theory the observed fragments should only match the true database but not the decoy database. A disadvantage of this approach is that it can only estimate an overall FDR for a large group of fragment spectra. Moreover, it cannot be used on small datasets such as immunoprecipitations because the input is too small for a robust analysis.

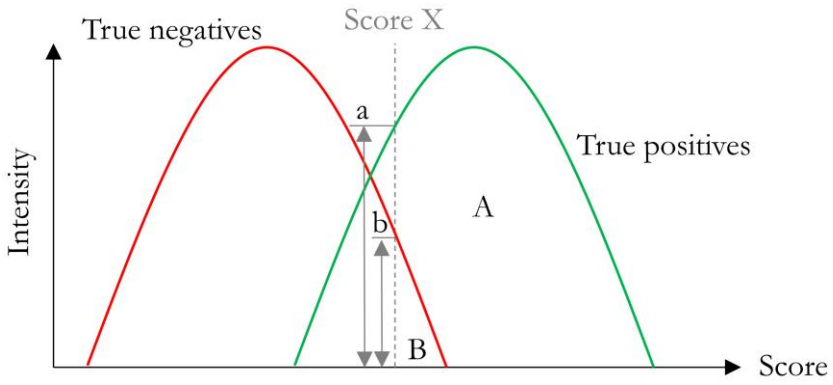

Figure 10: **False discovery rate and posterior error probability.** In a perfect experiment, all proteins identified correspond to peptides that are present in the sample. In practice, however, the data is represented in a Gaussian-shaped distributions when plotting the number of peptides observed versus the peptide identification scores. The peak associated with lower scores (indicated in red) represents true negatives and the peak with higher scores (indicated in green) true positives. Mathematical modelling allows to identify an ion score cut-off above which it is likely to observe true positives with a given likelihood. The PEP $\left(\mathrm{PEP} = \frac{b}{a}\right)$ describes the probability that the observed PSM is false (it is a local version of the FDR). An alternative way to calculate the FDR is to search the data against a true and a decoy dataset. To calculate the FDR, the number of matches to the decoy database is doubled and divided by the total number of matches ($\mathrm{FDR} = \frac{2 \times B}{A+B}$).

The field of proteomics has moved beyond simple protein identification and is now aiming to accurately quantify differences in protein abundances and post-translational modification states in health versus disease.

Quantitative proteomics comes in two flavours: i) stable isotope labelling and ii) label-free approaches. Common stable isotope labelling methods include metabolic labelling of proteins by incorporation of stable isotope labels with amino acids in cell culture (SILAC) (65), chemical labelling of proteins with isotope-coded affinity tags (ICAT) (66), chemical labelling of peptides with isobaric tags for relative and absolute quantitation (iTRAQ) (67), or tandem mass tags (TMT) (68, 69), labelling of primary amine groups using demethylation (DiMe) and neutron coded labelling (NeuCode) (70). The quantitation methods mentioned above are described in detail in the *Appendix - Quantitation methods in proteomics*.

When choosing a suitable quantitation strategy the aim is to identify and quantify as many proteins as possible with maximum accuracy (to observe the true fold change) and precision (error with which the fold change is observed) (Table 3). SILAC is the most accurate and precise method due to parallel sample processing, however, it cannot be applied to primary cells and can only compare a maximum of three conditions. Dimethyl labelling is as accurate as SILAC and can be applied to primary samples. However, this method is also restricted to three channels and due to the later incorporation of the label less precise than SILAC. To compare more than three samples TMT (up to 10) or label-free quantitation (∞) can be used. In order to be able to quantify labile disulfide bond reduction in primary cells and tissues and to be able investigate the kinetics of labile disulfide bond reduction, a label-free quantitation approach was chosen.

Table 3: **Comparison of quantitative proteomics strategies.** Greyed out are methods that are not widely used (71).

Labelling method	Benefits	Disadvantages	Number of channels
SILAC	• Excludes experimental variation by parallel sample processing • High accuracy • Identifies as many proteins as in unlabelled sample	• Expensive • Not applicable to primary cells and tissues • Limited to 3 channels	2, 3
ICAT	• Restricted to Cys containing peptides	• Expensive • Restricted to Cys containing peptides	2
Dimethyl labelling	• Cheap • High accuracy (as good as SILAC) • Applicable to primary cells and tissues	• Limited to 3 channels	3
iTRAQ		• iTRAQ identifies less proteins than TMT	4 or 8
TMT	• High accuracy • High precision	• Identifies less proteins than SILAC or dimethyl labelling (but quantifies more) • Dynamic range compression	2, 6, 10
NeuCode	• High accuracy • High precision • *NeuCode-SILAC* Wider dynamic range than TMT Identifies as many proteins as in unlabelled sample	• Instruments with high mass resolution are needed (480,000) • *NeuCode-Tag* Reduced number of peptides identified	4
Label-free	• No limit to number of samples to compare • Applicable to primary cells and tissues • Identifies the maximum number of proteins • Cheap	• Depends on consistent sample preparation	∞

1.6. Research objectives

The aim of this thesis was to establish the importance of labile disulfide bond reduction during immune activation. This required the completion of the following three main research objectives:

1. Develop a high through-put mass spectrometry based method to identify and quantify labile disulfide bond reduction (*Chapter III*).
2. Identify and quantify labile disulfide bond reduction during immune activation and inflammation to gain an insight of what proteins are affected and to what extent by labile disulfide bond reduction (*Chapter IV*).
3. Follow up novel labile disulfide bond-containing candidate proteins by characterising the functional consequences of labile disulfide bond reduction (*Chapter V*).

Chapter II – Materials and Methods

2.1. Culture of cells

2B4 Saito hybridoma T cells (72) were maintained at 37° C in a 10 % CO_2 atmosphere in DMEM medium (Sigma), supplemented with 10 % fetal calf serum (FCS, Sigma) and 100 U/ml penicillin (Gibco) and 100 µg/ml streptomycin (Gibco).

INA-6 cells (73) were maintained at 37° C in a 5 % CO_2 atmosphere in RPMI 1640 medium (Sigma), supplemented with 10 % FCS, 100 U/ml penicillin, 100 µg/ml streptomycin, 2 mM L-glutamine (Gibco), 1 mM sodium pyruvate (Sigma), 1 % MEM non-essential amino acids (Gibco) and 2.5 ng/ml human IL-6 (Peprotech).

Human peripheral blood mononuclear cells (PBMCs) were maintained at 37° C in a 5 % CO_2 atmosphere in RPMI 1640 medium, supplemented with 10 % FCS, 100 U/ml penicillin and 100 µg/ml streptomycin, 2 mM L-glutamine, 1 mM sodium pyruvate and 1 % MEM non-essential amino acids and 25 µM of the thiol isomerase inhibitor PX-12 (Sigma Aldrich) when indicated. In a mixed leukocyte reaction (MLR) PBMCs isolated from two donors were mixed at a 1:1 ratio to a final concentration of 1-2 x 10^6 cells/ml.

2.2. Isolation of peripheral blood mononuclear cells

Human PBMCs were isolated from leukocyte cones of healthy donors by standard gradient centrifugation using Ficoll Plaque PREMIUM (GE Healthcare Life Sciences). PBMCs were then harvested from the interface, washed with phosphate buffered saline (PBS, Lonza) at 400 g for 10 min and twice with PBS at 200 g for 20 min.

2.3. LPS-induced endotoxemia mouse model

Female C57BL/6 mice were obtained from the Charles River Laboratories and injected intraperitoneally with 100 µg lipopolysaccharide from *Escherichia coli* (LPS, serotype 055:B5, Sigma) to cause endotoxemia or PBS as a control and splenocytes were harvested 3 h after injection.

2.4. Flow cytometric and ImageStream analysis of cell surface markers and cell surface thiol levels

For flow cytometry, the following antibodies and reagents were used at the indicated concentrations: CD69-APC (Invitrogen, MHCD6905, d1/100), TCR α/β-PE (Biolegend, 306708, d1/100), TCR α/β-biotin (AbD Serotec, MCA1413B, d1/5), CD19-APC (Immuno Tools, 22220196, d1/40), IgG2a-APC (AbD Serotec, MCA1125APC, d1/10), F4/80-biotin (AbD Serotec, MCA497B, d1/5), CD11c-PerCP (BioLegend, 117325, d1/100), CD44-biotin IM7 (Affimetrix eBioscience, 13-0441, d1/500), streptavidin-FITC (AbD Serotec, STAR2B, d1/200), Alexa-488-Maleimide (Thermo Scientific, A-10254, 25 µM), live/dead marker (Thermo Scientific, L10120).

To analyse the expression of cell surface markers, 1 x 10^6 cells (2B4 T cells, PBMCs or mouse splenocytes) were stained with 100 µl of the indicated primary antibody in FACS buffer (0.25 % BSA and 0.1 % NaN_3 in PBS) for 30 min on ice, washed with 4 ml FACS buffer and incubated with 100 µl of the indicated secondary antibody for 30 min on ice. Cells were then washed with 4 ml FACS buffer and fixed in 2 % formaldehyde containing FACS buffer. The data was acquired on a FACSCalibur (BD Biosciences) and analysed with the FlowJo X software.

To analyse free cell surface thiols, 1 x 10^6 cells (2B4 T cells, PBMCs or mouse splenocytes) were incubated with 100 µl 25 µM Alexa-488-Maleimide for 20 min on ice, washed with 4 ml FACS buffer and incubated with 100 µl the live/dead marker for another 20 min. Cells were then washed, fixed in 2 % formaldehyde containing FACS buffer and analysed using a FACSCalibur and analysed with the FlowJo X software. Nonviable cells were gated out based on either the uptake of the live/dead label or size and granularity as is indicated for each experiment.

To follow internalisation rates of CD44 on control and reduced (2.5 mM TCEP in medium for 15 min) 2B4 T cells, cells were reduced, washed and resuspended in medium containing CD44 at d1/500 for 30 min. Cells were then processed as described before for the analysis of cell surface markers by flow cytometry.

The fluorescent cells were also analysied using an ImageStream (Amnis) which combines the advantages of flow cytometry and microscopy in a single cell assay. This allows the cell surface localisation of Alexa-488-Maleimide after TCEP reduction of 2B4 T cells.

2.5. Differential thiol labelling of cell surface proteins using SH-IQ (Thiol (-SH) identification and quantitation)

2B4 T cells (1 x 10^8 cells, counted using the NucleoCounter NC-3000 (chemometec) and Solution 13 (chemometec)) were washed with 50 ml PBS supplemented with 1 % BSA (bovine serum albumin, PBS/BSA) and incubated with 7.5 ml 2.5 mM Methyl-PEG_{12}-Maleimide (MPM, Thermo Scientific) for 20 min while rotating to block free cysteines on the cell surface. After washing the cells twice with 25 ml PBS/BSA to remove excess label, labile disulfide were reduced with 10 ml 2.5 mM TCEP (Sigma-Aldrich) in PBS/BSA for 15 min while rotating, washed twice with 25 ml PBS/BSA and labelled with 2.5 ml 2.5 mM Maleimide-PEG_2-Biotin (MPB, Thermo Scientific) for 20 min while rotating.

PBMCs (1 x 10^8 cells) were directly labelled with 2.5 ml 2.5 mM MPB for 25 min on ice.

The cells were then washed twice with 25 ml PBS/BSA, harvested by centrifugation for 5 min at 500 g and lysed in 2 ml PBS containing 1 % Triton X-100 (TX-100, Sigma-Aldrich) and 100 µl protease inhibitor cocktail (Sigma-Aldrich) for 20 min on ice. The lysate was cleared by centrifugation at 15,000 g for 15 min, the supernatant collected and equivalent amounts of protein (estimated with micro BCA protein assay kit following the user guidelines, Thermo Scientific) purified for membrane proteins with lentil lectin agarose beads (300 µl slurry was equilibrated with buffer A (PBS containing 0.1 % TX-100)). Lentil lectin binds proteins that contain α-D-mannose, α-D-glucose, and sterically related residues and is therefore suited to purify plasma membrane proteins as most of them are glycosylated. Membrane proteins were allowed to bind for 45 min while rotating. The resin was then washed three times with 5 ml buffer A and glycosylated proteins were eluted with 1.5 ml buffer B (buffer A containing 10 % α-methyl glucoside) for 45 min while rotating. The eluted membrane proteins were further purified for MPB-tagged proteins using monomeric avidin agarose beads (350 µl slurry, Thermo

Scientific). The beads were pre-washed with 5 ml buffer A twice, non-reversible biotin binding sites blocked with 2 ml buffer C (2.5 mM biotin in buffer A), washed twice with 5 ml 100 mM glycine (pH 2.5) and equilibrated with 10 ml buffer A. Biotinylated proteins were bound for 45 min while rotating, the beads washed four times with 5 ml buffer A and the biotinylated proteins eluted with 1 ml buffer C for 45 min while rotating.

The enriched biotinylated membrane protein sample fraction was transferred onto a 10 kDa cut-off filter (VIVAproducts) and the detergent washed off with four times 500 µl PBS. To test if all the detergent was removed, the tube containing the wash flow-through was shaken. A solution above the critical micelle concentration (critical micelle concentration of TX-100: 0.24 mM or 0.0155 %) forms bubbles whereas a solution below the critical micelle concentration does not. The proteins were then denatured with 400 µl 8 M urea for 45 min, the disulfide bonds reduced by adding TCEP to a final concentration of 10 mM for an additional 45 min and the cysteines alkylated with 500 µl 10 mM iodoacetamide (IAA, Sigma-Aldrich) for 45 min in the dark. Proteins were then deglycosylated with 500 units PNGaseF (NEB) in 200 µl over night at 37℃, the filter washed twice with 500 µl ammonium bicarbonate (AMBIC) and proteins digested over night with d1/20 µg trypsin in 200 µl 25 mM AMBIC. Peptides were eluted from the filter with 200 µl 0.1 % formic acid (FA) followed by 200 µl 0.1 % FA in 50 % acetonitrile (ACN) and 200 µl 0.1 % FA in 80 % ACN. The increase of ACN in the elution helps to elute hydrophobic peptides. Peptides containing 50% and more hydrophobic residues (A, F, I, L, M, P, V, W, Y) might be insoluble or only partly soluble in an aqueous solution such as 0.1 % FA. The sample was then dried in a vacuum centrifuge. The tryptic peptides were desalted on a C18 column (Thermo Scientific) and injected into an HPLC-coupled QExactive mass spectrometer (Thermo Scientific).

2.6. Differential thiol labelling of recombinant protein using the isotope pair NEM (N-ethylmaleimide) and d5NEM (deuterated (ethyl-D5) NEM)

1 µg of recombinant protein (human ADAM17, R&D Systems) was either incubated with PBS for 90 min, 2.5 mM TCEP for 15 min or 1 µM thioredoxin (human, Sigma-Aldrich) together with 0.1 pM thioredoxin reductase (from rat liver, Sigma-Aldrich) and 200 µM NADPH (Sigma-Aldrich) for 90 min. The protein was then transferred onto a 10 kDa cut-off spin filter, washed with PBS and reacted with 10 mM NEM (Sigma-Aldrich) for 30 min. The protein was denatured with 8 M urea, the disulfide bonds reduced with 10 mM TCEP and alkylated with 1 mM d5NEM (Cambridge Isotope Laboratories, Inc.). The protein was deglycosylated with 500 units PNGaseF and digested with 1 µg trypsin in 200 µl 25 mM AMBIC overnight. The tryptic peptides were desalted on a Pierece C18 spin column following the manufacturer's instructions (Thermo Scientific, 8 mg C18 resin, up to 30 µg of total peptide capacity) and injected into an HPLC-coupled QExactive mass spectrometer.

2.7. Mass spectrometry analysis

Peptides were reconstituted in 0.1 % FA / 2 % ACN and separated on an in-house packed 25 cm C18 column (75 µm inner diameter column, 3 µm diameter C18 Maisch phase) using an Ultimate 3000 nano HPLC (Dionex) in direct injection mode to a QExactive mass spectrometer (Thermo Fisher Scientific). Separation was conducted with a gradient of 5-30 % buffer B (0.1 % FA in ACN) for 90 min, followed by 30 % - 55 % buffer B for 20 min and 98 % buffer B for 5 min (buffer A: 0.1 % FA) at a flow rate of 300 nl/min. All data was acquired in a data-dependent mode, automatically switching from MS to collision induced dissociation MS/MS on the top 20 most abundant ions with a precursor ion scan range of 350 - 1650 m/z. Charge state 1^+ ions were rejected. Full scan MS spectra were acquired at a resolution of 70,000 and MS/MS scans at 17,000 at a target value 3×10^6 and 1×10^5 ions respectively. Dynamic exclusion was enabled with an exclusion duration of 40 s. This means that once a peptide was selected for MS/MS analysis it will not be selected again for 40 s.

2.8. Analysis of mass spectrometry data

SH-IQ data was analysed using the Progenesis QI for Proteomics software (Nonlinear Dynamics) to perform label-free quantitation of labile disulfide bond reduction in plasma membrane proteins. Progenesis firstly aligns the m/z and retention time features for every chromatographic run which is manually reviewed to ensure that like-for-like MS peaks are compared. Secondly, Progenesis uses feature detection to identify the isotope pattern of the MS peaks (peptides) to separate overlapping peptides and to quantify them by using a peak area method. Peptides and proteins are then identified using the external search engine Mascot (Matrix Science, Boston, MA). MS/MS spectra were searched against the UniProt_CP mouse or UniProt_SPHuman database. Precursor mass tolerance was set at 10 ppm and a fragment tolerance at 0.02 Da. The precursor ion charge state was 2^+, 3^+ and 4^+. Variable modifications were defined as deamidation on asparagine (N) and glutamine (Q), oxidation on methionine (M) and alkylation with MPB or IAA on cysteines (C). The enzyme specificity was set to trypsin with a maximum of two missed cleavages. The target-decoy-based false discovery rate (FDR) for proteins was set to 1 % and a minimum Mascot ion score of 20. Quantile normalisation (74) was applied to all repeats to reduce experimental variation and was analysed with the linear models for microarray data (Limma) statistical package (75) and an individual P-value computed. Benjamini-Hochberg correction (76) was applied to adjust for multiple testing. Only proteins identified and quantified in all three biological replicates were considered.

Where indicated, SH-IQ data was analysed using the in-house Central proteomics Facilities Pipeline (CPFP, http://cpfp-master.molbiol.ox.ac.uk:3001/auth/login (77)) platform which uses the search engines Mascot, X!Tandem (78) and OMSSA (79) using the parameters indicated previously. Quantitation was carried out using normalised spectral index quantification (SINQ) (80).

Data obtained from differentially NEM/d5NEM labelled recombinant protein (Δ m/z=2.5 for z=2) was analysed using MaxQuant (81) with the search parameters indicated previously. Only peptides identified and quantified in at least two measurements in the seven replicate experiments were considered.

To estimate the power of the mass of the SH-IQ method the analysis software program PS Power and Sample Size Calculations (82, 83) was used.

2.9. IL-6 stimulation of INA-6 cells

1 x 10^6 serum-starved (RPMI 1640 medium supplemented with 1 % FCS, 100 U/ml penicillin, 100 µg/ml streptomycin, 2 mM L-glutamine, 1 mM sodium pyruvate, and 1 % MEM non-essential amino acids for 4 h) INA-6 cells were washed twice with 25 ml PBS, resuspended in 500 µl RPMI 1640 and put on ice. Cells were then stimulated with the indicated IL-6 concentration at 37° C and lysed in ice-cold lysis buffer (1 % digitonin, 1 mM NaF (to in inhibit protein phosphoseryl and phosphothreonyl phosphatases), 1 mM Na_3VO_4 (to inhibit alkaline phosphatases and protein-phosphotyrosine phosphatases) and protease inhibitor cocktail) for 20 min on ice. The lysate was cleared by centrifugation at 15,000 g for 15 min and subjected to SDS-PAGE (84) and Western blotting (85) as described below.

2.10. Western blotting

The following primary and secondary antibodies and reagents were used: Stat3 124H6 (Cell Signaling Technology, d1/1,000), phopho-Stat3 Tyr705 D3A7 (Cell Signaling Technology, d1/2,000), Akt 40D4 (Cell Signaling Technology, d1/1,000), phospho-Akt Ser473 (Cell Signaling Technology, d1/1,000), p44/42 MAPK 3A7 (Cell Signaling Technology, d1/1,000), phopho-p44/42 MAPK Thyr202/Tyr204 197G2 (Cell Signaling Technology, d1/1,000), β-actin 8H10D10 (Cell Signaling Technology, d1/1,000), CD44-biotin IM7 (Affymetrix eBiosience, d1/3,000), goat anti-rabbit DyLight800 (Thermo Scientific, d1/5,000), goat anti-mouse DyLight680 (Thermo Scientific, d1/5,000), streptavidin DyLight680 (Thermo Scientific, d1/5,000) and streptavidin DyLight800 (Thermo Scientific, d1/5,000).

For western blot analysis (85), samples were separated by molecular weight using SDS-PAGE (84) gels and transferred to a nitrocellulose membrane (LiCor). The membrane was blocked with SeaBlock blocking buffer (Thermo Scientific), probed with the indicated amounts of primary and secondary antibody in SeaBlock, the fluorescence signal detected using the Odyssey Sa imaging system (LiCor) and quantified by densitometry.

Commentary:

… We posit that the request to validate quantitative MS data by Western blotting is no longer justified. In fact, considering that the vast majority of protein identifications claimed from biological samples are still derived from Western blotting, it may be time to "turn the tables" and request that Western blotting results, or at least the assays that support these results, be validated by MS… (86)

2.11. Reduction of labile disulfide bonds followed by SDS-PAGE and in-gel analysis

1 μg ADAM 17 was either i) exposed to mild reducing conditions: 2.5 mM TCEP in PBS for 15 min or 1 μM thioredoxin together 0.1 pM thioredoxin reductase and 200 μM NADPH for 90 min at 37° C, ii) fully-reduced under denaturing conditions (0.1% SDS and 500 μM DTT (dithiothreitol) and heated to 95° C) for 15 min or iii) treated with PBS as a negative control (37° C for 90 min). 2.5 mM Alexa-633-C5-Maleimide (Thermo Scientific) and non-reducing Laemmli SDS loading buffer and were added and the samples separated by molecular weight using SDS-PAGE gels. The signal was detected using the Odyssey Sa imaging system and quantified by densitometry. Total protein was visualised by Coomassie blue staining of the gel.

Chapter III – Quantitation of labile disulfide bond cleavage

3.1. Introduction

Labile disulfide bond reduction is emerging as a key mechanism controlling immune activation and a variety of different diseases as is discussed in *Chapter I – Introduction*. To further the understanding of how labile disulfide bond reduction is used by the immune system and pathogens to modulate protein function, the development of a method that can routinely identify and quantify labile disulfide bond reduction is crucial. By expanding the knowledge on proteins containing labile disulfide bonds and understanding their role in health and disease it will be possible to design new redox drugs for therapy which might provide a handle to manage autoimmune diseases.

The aim of this thesis was to develop a mass spectrometry based method to quantify labile disulfide bond reduction. This will build on a method previously developed by the laboratory which enables the reliable identification of labile disulfide bond containing proteins (26). Quantitation of labile disulfide bond reduction is crucial in order to determine which proteins contain biologically relevant labile disulfide bonds that are reduced to an extent that is likely to affect cellular function. It is anticipated that the majority of a protein has to be in its reduced state for it to have a functional effect. Moreover, quantitation will allow to study the kinetics of labile disulfide bond reduction during immune activation.

To accomplish this, a differential cysteine labelling approach was exploited where cysteines originating from reduced labile disulfide bonds are labelled with alkylation reagent X and all remaining cysteines with reagent Y. To quantify the amount of reduction occurring, label-free area-under-the-curve (AUC) quantitation was carried out to make this method easily accessible to the scientific community, applicable to primary cells and tissues and able to handle unlimited sample numbers.

3.2. Results

To develop a method to quantify labile disulfide bond reduction, standardised conditions with minimal variability are essential. Chemical reduction of 2B4 T cells with TCEP (Tris(2-carboxyethyl)phosphine) was chosen as a model since TCEP reduction was shown to be broadly similar to enzymatic reduction caused by thioredoxin, PDI and gamma-interferon-inducible lysosomal thiol reductase (GILT) (26), but is easier to control.

3.2.1. Labile disulfide bonds are reduced in leukocyte cell surface proteins by TCEP

TCEP reducing conditions were optimised in order to obtain maximal reduction while maintaining high cell viability. To follow labile disulfide bond reduction, cells were labelled with the thiol reactive fluorescent probe Alexa-488-Maleimide before and after TCEP reduction. An increase in Alexa-488-Maleimide labelling, which can be followed by flow cytometry, is indicative of labile disulfide bond reduction as thiol levels increase as a consequence of disulfide bond reduction.

Cells were reduced with different TCEP concentrations ranging from 0 – 5 mM for 15 minutes (Figure 11 A). Maximal reduction was reached with TCEP concentrations ≥ 2 mM (Figure 11 B). Increasing the concentration from 2.5 mM to 5 mM TCEP did not substantially increase the amount of disulfide bond reduction but may put the cells under more stress. If lower concentrations such as 1 mM TCEP were used, the incubation time had to be increased to reach similar levels of reduction as were obtained by 2.5 mM TCEP (Figure 11 D) which might have an effect on the cells. The labelling with Alexa-488-Maleimide could be confirmed to be thiol specific as pre-blocking of free cysteines with $MP_{24}M$ (Methyl-PEG_{24}-Maleimide) after TCEP reduction decreased subsequent labelling with Alexa-488-Maleimide to control level (Figure 11 C).

Therefore, reduction of labile disulfide bonds on 2B4 T cells with 2.5 mM TCEP for 15 min was identified as optimal.

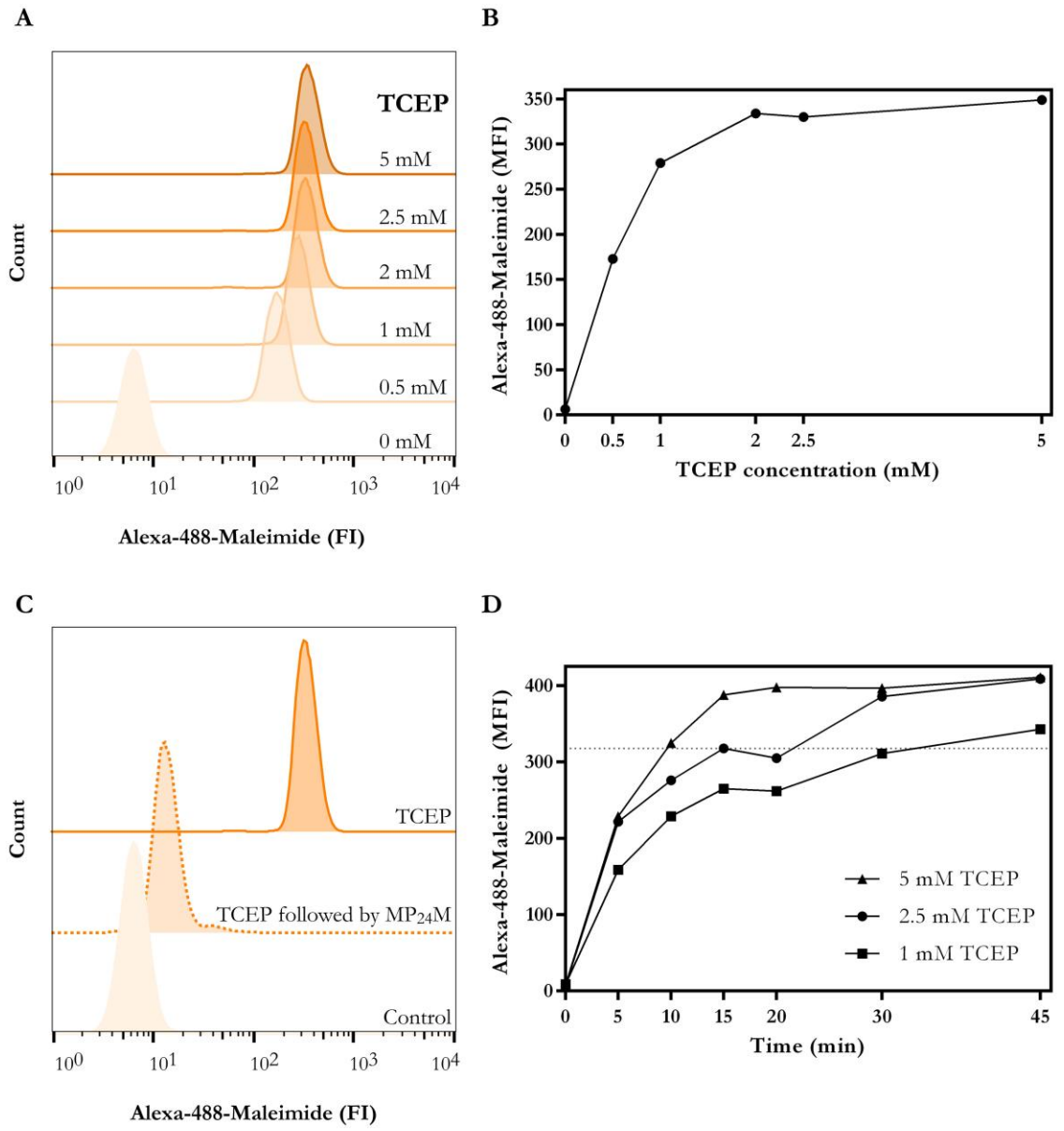

Figure 11: **Labile disulfide bonds are reduced on leukocytes by TCEP.** A) 2B4 T cells were reduced with the indicated TCEP concentrations (0 – 5 mM) for 15 min at room temperature. The cells were then labelled with 25 µM of the fluorescent, thiol reactive Alexa-488-Maleimide and the labelling followed by flow cytometry. B) The median fluorescence intensity (MFI) of the experiment shown in A) is plotted versus the TCEP concentration. C) 2B4 T cells were either incubated with medium (Control), reduced with 2.5 mM TCEP for 15 min (TCEP) or reduced and free thiols blocked with 2.5 mM $MP_{24}M$ for 20 min on ice (TCEP followed by $MP_{24}M$). Samples were then labelled with 25 µM Alexa-488-Maleimide and the fluorescence intensity (FI) plotted as a histogram. D) The reduction of 2B4 T cells with 1 mM (-■-), 2.5 mM (-●-) and 5 mM (-▲-) TCEP over 45 min at room temperature is plotted as the Alexa-488-Maleimide MFI versus time. Cells were gated on size and granularity identify leukocytes for the analysis.

To confirm that the flow cytometry signal obtained from TCEP-reduced, Alexa-488-Maleimide-labelled cells arises from reduced plasma membrane proteins and not intracellular labelling, the cells were analysed by ImageStream. The ImageSteam is an imaging flow cytometer that produces high resolution images of each cell directly in flow which allows to localise fluorescent labels. As shown before, cells are only Alexa-488-Maleimide labelled when reduced with TCEP (Figure 12 A). More importantly, ImageStream analysis showed that the labelling is concentrated on the cell surface which is visible as a green halo around the cell (Figure 12 B). This confirms that the disulfide bonds reduced by TCEP and labelled with Alexa-488-Maleimide are indeed located on the cell surface of leukocytes.

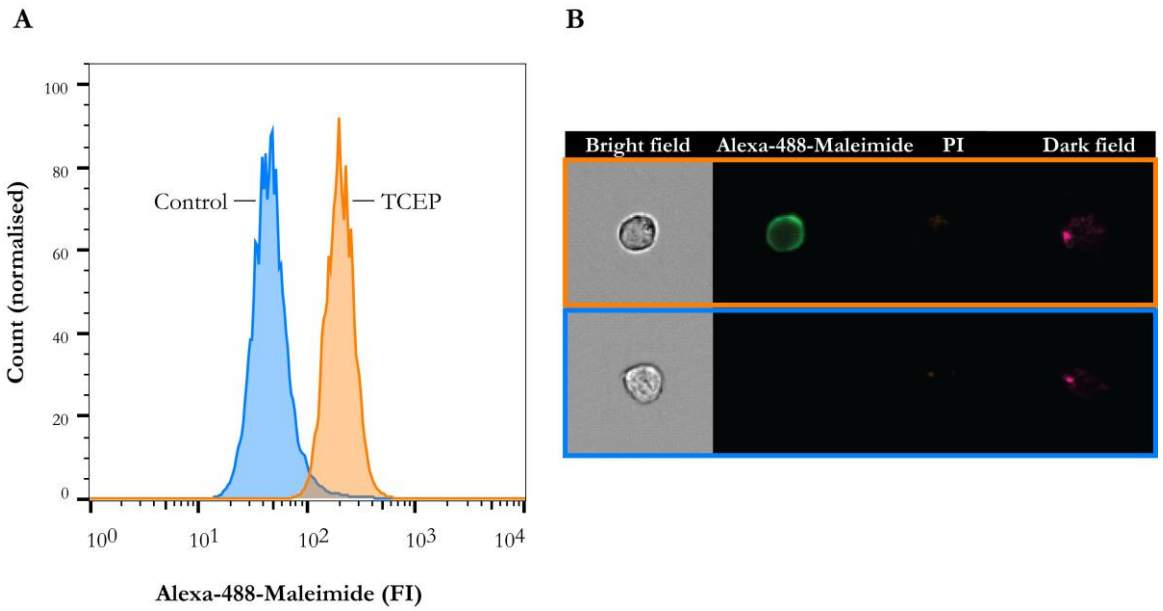

Figure 12: **Labile disulfide bonds are reduced on the leukocyte cell surface by TCEP.** A) Flow cytometry shows that TCEP reduced 2B4 T cells show higher thiol levels compared to control cells. B) Next, the cell surface specific reduction of labile disulfide bonds and thiol labelling with Alelexa-488-Maleimide was investigated. Alexa-488-Maleimide labelling on control and reduced cells was visualised using the ImageStream. The distribution of the dye being most intense on the outline of the cells indicates cell surface labelling of reduced cells. This confirms that the signal obtained by flow cytometry is due to cell surface labelling of reduced disulfide bonds and not due to internal labelling of dead the cells.

Cells were gated on size and granularity and size followed by propidium iodide (PI) exclusion to identify live cells for the analysis.

3.2.2. Quantitation of labile disulfide bond reduction using mass spectrometry

Flow cytometry analysis of labile disulfide bond reduction has provided a reliable and fast tool to globally detect labile disulfide bond reduction. This method is used to assess the redox state of the study system prior to the more expensive and time consuming quantitative analysis of labile disulfide bond reduction using mass spectrometry. To identify the proteins that contain labile disulfide bonds and to quantify the reduction occurring, the Alxa-488-Maleimide label used for flow cytometry detection is exchanged for biotinylated, thiol-reactive labels. This allows to enrich for labile cysteine containing proteins and peptides prior to mass spectrometry analysis to achieve the most complete analysis.

Different approaches were explored to quantify labile disulfide bond reduction, including peptide and protein quantitation strategies (Figure 13 A-C), that are all based on the same principle:

Free cysteines in plasma membrane proteins were blocked with cell impermeable $MP_{24}M$ in a first step to minimise background signal. The cells were then exposed to mild reducing conditions (2.5 mM TCEP for 15 min as was established before) to reduce labile but not structural disulfide bonds. Free cysteines originating from labile disulfide bonds that have been broken by TCEP were then labelled with a biotinylated thiol reactive reagent (MP_2B or IP_2B). This not only allows the identification of the affected cysteines but also to affinity purify proteins and peptides containing labile disulfide bonds. To quantify labile disulfide bond reduction, the remaining cysteines still involved in disulfide bonds were labelled with a further thiol reactive reagent (IAA, IP_2B or ILCB) after full reduction under denaturing conditions. The quantitation principles of the different strategies are explained in further detail in the following sections.

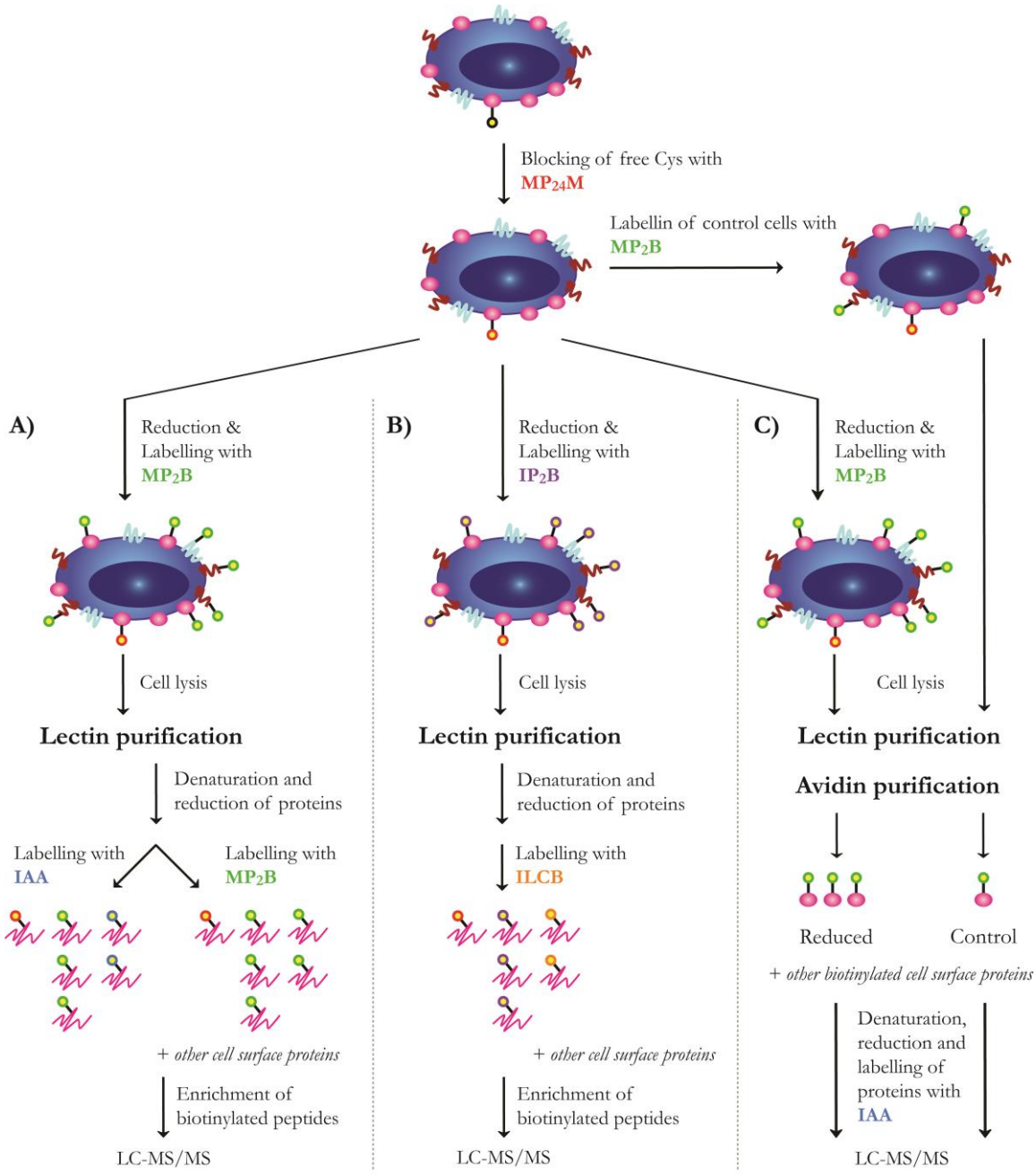

Quantitation of disulfide bond reduction

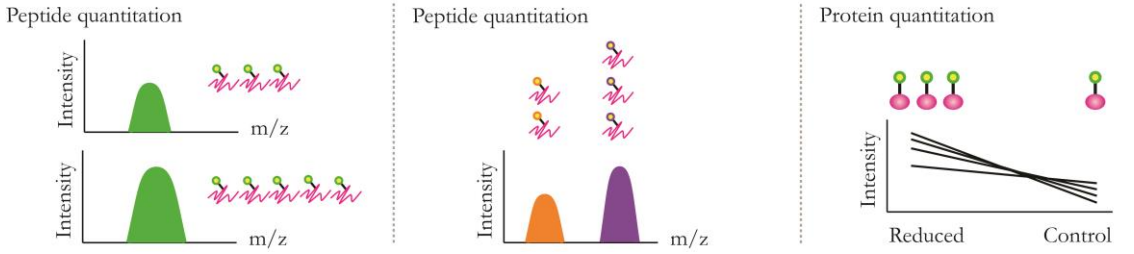

Figure 13: **Differential labelling of cysteines for labile disulfide bond quantitation – three strategies.** Free cysteines on 2B4 T cells were blocked with the cell impermeable, thiol reactive label $MP_{24}M$. Labile disulfide bonds were then reduced with 2.5 mM TCEP for 15 min at room temperature and cysteines previously engaged in labile disulfide bonds labelled with:

A) MP_2B. Cell surface proteins were enriched with lectin beads and proteins fully denatured and reduced. The cysteines of half of the sample were then labelled with IAA (sample) and half with MP_2B (reference). Proteins were then digested with trypsin and biotinylated peptides enriched with monomeric avidin beads prior to LC-MS/MS analysis. Quantitation of disulfide bond reduction is carried out on peptide level. The AUC of each biotinylated peptide is compared between the sample and reference run. The reference AUC serves as the 100 % reference.

B) IP_2B. Cell surface proteins were then enriched with lectin beads, fully denatured and reduced and cysteines labelled with ILCB. All the labile cysteines are labelled with IP_2B, whereas the rest is labelled with ILCB. Biotinylated peptides were enriched and analysed by LC-MS/MS. Labile disulfide bond reduction is quantified by comparing the AUC of peptide X-IP_2B and X-ILCB.

C) After blocking free cysteines, the sample was split in two. Half of the cells were reduced with TCEP whereas the other half was treated with buffer serving as a control. Free cysteines were then labelled with MP_2B and biotinylated cell surface proteins enriched with a tandem lectin-avidin purification method. Labelling of proteins with MP_2B is proportional to disulfide bond reduction and therefore the amount of protein X present in the sample versus the control is indicative of disulfide bond reduction. The proteins were then processed for LC-MS/MS analysis and disulfide bond reduction quantified by protein quantitation.

$MP_{24}M$ (Methyl-PEG24-Maleimide), MP_2B (Maleimide-PEG_2-Biotin), ILCB (N-Iodoacetyl-N-biotinylhexylenediamine), IP_2B ((+)-Biotinyl-iodoacetamidyl-3,6-dioxactanediamine), IAA (iodoacetamide)

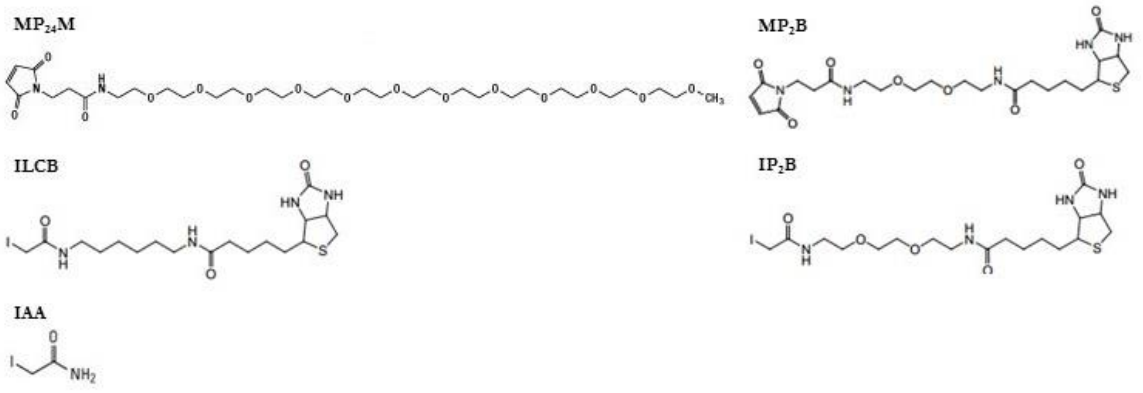

To quantify labile disulfide bond reduction, two different peptide quantitation approaches and a protein quantitation strategy were explored (Figure 13 A-C).

A) Cysteine peptide quantitation between two mass spectrometry runs

The first approach explored bases the quantitation of labile disulfide bond reduction on comparing the amount of biotinylated cysteine-containing peptides after TCEP reduction (sample) to the total amount of the peptide (reference) (Figure 13 A). The AUC for cysteine containing peptides was determined using the software Proteome Discoverer 1.4 (PD1.4) and the ratio between TCEP-reduced and reference sample calculated. This ratio represents the amount of disulfide bond reduction occurring in response to the TCEP treatment. The higher the ratio, the more reduced a labile disulfide bond is. In order to maximise the detection of cysteine containing peptides, biotinylated peptides were enriched prior to LC-MS/MS analysis.

When analysing the data it became apparent that it was difficult to detect the same cysteine-containing peptide in both, the sample and the reference run. Since the mass spectrometer was operated in a top20 acquisition mode, only the 20 most abundant peptides were selected for fragmentation in each duty cycle. Although selected peptides were excluded from subsequent selection for 40 s, less abundant peptides will still not have got selected for fragmentation and thus will not have been identified by search engines. This presented an issue in the more complex reference sample where not all the biotinylated peptides were selected for MS/MS analysis and therefore couldn't be identified by Mascot. PD1.4 analysis depends on the identification of each peptide in both the sample and reference run and could therefore only quantify the reduction of a limited number of labile disulfide bonds. Moreover, the ionisation of peptides is dependent on the abundance of co-eluting peptides which is different for the sample and the reference, potentially introducing a bias.

In summary, the dynamic range limitation of the instrument led to a small number of labile disulfide bonds that could be quantified from each experiment. Moreover, the variation between experiments was too big to draw confident conclusions from the results that were obtained.

B) Cysteine peptide quantitation within a single mass spectrometry run

To avoid the comparison of different mass spectrometry runs to quantify labile disulfide bond reduction, the labelling strategy was adapted to mimic the concept underlying isotopic labelling of peptides (*Appendix - Quantitation methods in proteomics*). Isotopic labels have the same chemical structure but differ in their mass which results in the peptides eluting at the same time but showing a different m/z. In order to be able to enrich for cysteine-containing peptides prior to mass spectrometry analysis the label pair Iodoacetamide-PEG_2-Biotin (IP_2B) and Iodoacetamide-LC-Biotin (ILCB) was chosen for the differential labelling of cysteines (Figure 13 B). The IP_2B-labelled fraction of the peptides represents the labile proportion and the ILCB-labelled fraction the remaining fraction. This allows to deduce what proportion of a labile disulfide bond is reduce. The labels differ in the length of their PEG linker between the iodoacetamide and the biotin moiety and thus add different masses to cysteine-containing peptides which allows to calculate the AUC for each IP_2B and ILCB labelled peptide within a single mass spectrometry run and to quantify the labile disulfide bond reduction.

Data obtained from the differential labelling with IP_2B and ILCB showed that peptides labelled with IP_2B tend to elute later in the gradient compared to when labelled with ILCB. This is not unexpected (although not anticipated) as the chemical properties of the peptide change with the tag. Unfortunately, this means that the peptide elutes in a different peptide context depending on whether it is IP_2B or ILCB labelled which may lead to differences in ionisation efficiencies and selection for fragmentation introducing a bias.

C) SH-IQ

Since peptide based quantitation of labile disulfide bond reduction was hampered by dynamic range and reproducibility issues, the strategy was changed to protein quantitation (Figure 13 C). Protein quantitation is more robust than peptide quantitation as it is based on multiple peptides rather than a single one. This approach compares the amount of biotinylated protein between TCEP-reduced and control sample (Figure 13 C). To do so, biotinylated cell surface proteins were purified by tandem lectin-avidin purification prior to mass spectrometry analysis. Since the biotinylation of reduced protein is directly proportional to labile disulfide bond reduction (Figure 11 D), the relative amount of biotinylated protein in the reduced sample compared to the control is indicative of labile disulfide bond reduction. The more labile a disulfide bond, the more of the protein gets reduced, the more is labelled with MP_2B and the more protein is present after the avidin purification. The identification and quantitation (IQ) of free cysteines (SH) as a measure of labile disulfide bond reduction (SH-IQ) is explained in detail in the following paragraphs.

3.2.3. Tandem lectin-avidin purification maximises the detection of biotinylated cell surface proteins by mass spectrometry

The protein based quantitation of labile disulfide bond reduction (SH-IQ) requires the purification of biotinylated cell surface proteins. The study of plasma membrane proteins by mass spectrometry is challenging due to their association with the cell membrane and their low abundance compared to cytosolic proteins. There are a variety of methods described in the literature to enrich for plasma membrane proteins including membrane fractionation (87, 88), glycoprotein purification (89), labelling of cell surface proteins (90) and labelling of glycol sites in cell surface proteins (91–95) for purification. Labelling of either cell surface proteins with an amine reactive label (Sulfo-NHS-Biotin) or chemical or metabolic labelling of glycoproteins with biocytin hydrazide (BH) (92, 96, 97) or paracetylated N-azidoacetylmannosamine (98) is dependent on affinity purification of tagged proteins based on biotin enrichment. Since SH-IQ already exploits the affinity purification of biotinylated proteins, simple lectin purification was chosen to pre-enrich for glycosylated proteins prior to the biotin enrichment. Solubilisation and purification of plasma membrane proteins was carried out in the presence of the detergent Triton X-100 (TX-100) which was removed prior to mass spectrometry analysis by filter-aided sample preparation (FASP) (99).

Herein it was investigated whether the simple enrichment of biotinylated proteins from whole cell lysate is sufficient to detect a maximum number of biotinylated plasma membrane proteins or whether a preceding lectin purification could improve their detection.

When analysing whole cell lysate by mass spectrometry no plasma membrane proteins and only a few proteins that can associate with the plasma membrane were identified among the 50 most abundant proteins (14 %) due to their low abundance compared to intracellular proteins (Supplementary Table 1). Applying a simple lectin purification allowed the detection of plasma membrane proteins (40 % of the 50 most abundant proteins) through enrichment of glycosylated proteins (plasma membrane proteins are typically glycosylated) (Figure 14 A) (Supplementary Table 2). In both, the whole cell lysate

and the lectin purified fraction the 50 most abundant proteins cover 32 % of the total spectral index (Figure 14 A). The spectral index is the cumulative fragment ion intensity of all identified peptides of a protein (100) and the total spectral index the sum of all the proteins' spectral indexes. The more of the total spectral index a protein or a protein group occupies the more abundant the protein or protein group is in the sample.

The enrichment of cell surface proteins achieved by lectin purification compares to other enrichment methods such: i) Cell fractionation: 66 % cell surface proteins (101), ii) cell surface protein labelling with BH: 95% cell surface glycoproteins (92), iii) cell surface protein labelling with Sulfo-HS-SS-Biotin: 45 % membrane proteins and 24 % plasma membrane proteins (102) or 20 % cell surface proteins (103) and iv) metabolic labelling of glycoproteins: 93 % N-linked glycoproteins (104).

The next step was to assess the efficiency of enriching biotinylated cell surface proteins from either whole cell lysate or the glycoprotein fraction. When biotinylated proteins were purified from whole cell lysate, the 50 most abundant proteins (Supplementary Table 3) covered 39 % of the total spectral index, whereas this marginally increased to 61 % when the sample was pre-purified for cell surface proteins (Figure 14 A). This suggests that the tandem lectin-avidin purified sample is less complex and therefore better data for each protein can be obtained. Indeed, pre-enriching for cell surface proteins improves the detection of cell surface proteins (Supplementary Table 4). 70 % of the 50 most abundant proteins were cell surface proteins when the sample was tandem lectin-avidin purified whereas only 34 % were cell surface proteins when only avidin purified (Figure 14 A). Tandem lectin-avidin purification not only identifies twice as many plasma membrane proteins than simple avidin purification but it also excludes non-specifically MP_2B-labelled intracellular proteins from the experiment as most intracellular proteins are not glycosylated. Furthermore, more unique peptides per protein could be identified in tandem lectin-avidin purified sample on average (24.1 versus 22.1) with higher confidence (Mascot score: 2,481 versus 1,755) and abundance (emPAI: 9.78 versus 3.3) (Table 4).

This effect becomes more noticeable for less abundant proteins, such as semaphorin-4C, where there was no data obtained for biotinylated cell surface proteins enriched from whole lysate (Table 4).

Importantly, it could also be shown that the lectin purification is not introducing any bias towards the subsequent avidin purification. This is shown by a poor correlation (R^2=0.3811) between the protein abundance after lectin purification and tandem lectin-avidin purification (Figure 14 B).

From this data can thus be concluded that tandem lectin-avidin purification maximises the detection of biotinylated cell surface proteins.

Table 4: **Comparison of avidin and tandem lectin-avidin enrichment for selected proteins to assess the purification efficiency of biotinylated cell surface proteins.** Biotinylated cell surface proteins were purified from either 2B4 whole cell lysate by avidin purification or tandem lectin-avidin purification and proteins analysed by mass spectrometry. The data was then searched using the CPF Pipeline (10 ppm precursor tolerance, 0.02 Da fragment tolerance, 2 missed cleavages) and SINQ (FDR 1%) analysis was performed to determine relative protein abundances. For the selected cell surface proteins listed in the table the following information is shown: UniProt accession number, protein description with gene name in brackets, abundance rank (1 indicating the most abundant protein in the sample), Mascot score, molecular weight of the protein in Da, emPAI (exponentially modified protein abundance index), sequence coverage and unique peptide sequences identified.

		Tandem lectin-avidin purification						**Avidin purification**					
Accession	**Description**	**Rank**	**Mascot Score**	**Mass [Da]**	**emPAI**	**Sequence coverage**	**Unique pep. sequences**	**Rank**	**Mascot Score**	**Mass [Da]**	**emPAI**	**Sequence coverage**	**Unique peptides**
S4R1M0	Protein-tyrosine-phosphatase (Ptprc)	1	9863	128489	40.46	0.55	66	1	8292	128489	15.83	0.63	73
E9Q5M7	Integrin alpha-L (Itgal)	2	6004	128233	11.82	0.53	55	5	4631	128233	4.43	0.57	51
Q542I8	Integrin beta (Itgb2)	3	5372	84838	34.63	0.63	46	11	3013	84838	7.62	0.65	45
P43406	Integrin alpha-V (Itgav)	4	3819	115287	16.03	0.51	53	21	2423	115287	3.61	0.53	48
A2APM1	CD44 antigen (Cd44)	7	2887	72043	2.72	0.16	10	30	1876	72043	1.44	0.15	8
O09126	Semaphorin-4D (Sema4d)	27	1207	95579	2.63	0.33	23	224	684	95579	0.83	0.23	14
Q60846	Tumor necrosis factor receptor superfamily member 8 (Tnfrsf8)	38	924	53182	5.46	0.38	17	721	235	53182	0.66	0.18	7
O35598	Disintegrin and metalloproteinase domain-containing protein 10 (Adam10)	95	516	83914	1.08	0.25	12	852	194	83914	0.17	0.08	4
Q9CYA0	Cysteine-rich with EGF-like domain protein 2 (Creld2)	111	467	38194	2.44	0.27	9	345	466	38194	1.41	0.35	8
P01831	Thy-1 membrane glycoprotein (Thy1)	200	306	18069	5.1	0.51	6	451	362	18069	1.48	0.27	4
Q64151	Semaphorin-4C (Sema4c)	452	133	92498	0.23	0.05	4	*not identified*					

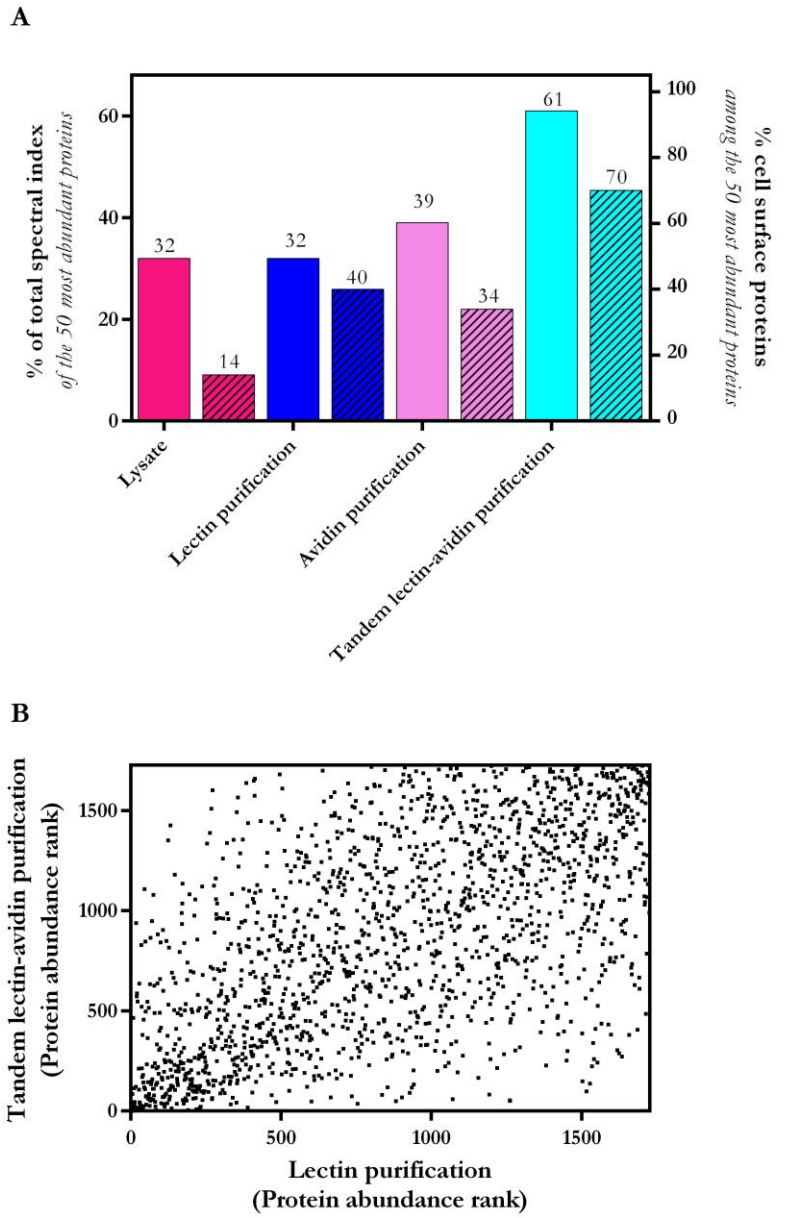

Figure 14: **Efficient enrichment of biotinylated cell surface proteins by tandem lectin-avidin purification.** To assess avidin and tandem lectin-avidin purification efficiencies to enrich for biotinylated cell surface proteins, labile disulfide bonds on 2B4 T cells were reduced with TCEP and cysteines labelled with MP_2B. The lysate was then either directly subjected to avidin purification or a preceding lectin enrichment was carried out to purify biotinylated proteins. A) The % coverage of the total spectral index of the 50 most abundant proteins of either whole cell lysate, the glycoprotein fraction, biotinylated cell surface proteins purified from whole cell lysate or biotinylated cell surface proteins purified from cell surface pre-purified sample (tandem lectin-avidin purification) is represented as solid bars. The number of cell surface proteins and proteins that can localise to the cell surface is represented as hatched bars and is plotted as a % of the parent condition. B) Abundance rank (the protein with the highest abundance is assigned rank 1) plot of proteins in the cell surface fraction (lectin purified sample) versus the abundance rank of the same protein after tandem lectin-avidin purification. There is no linear correlation between the two conditions (R^2=0.3811).

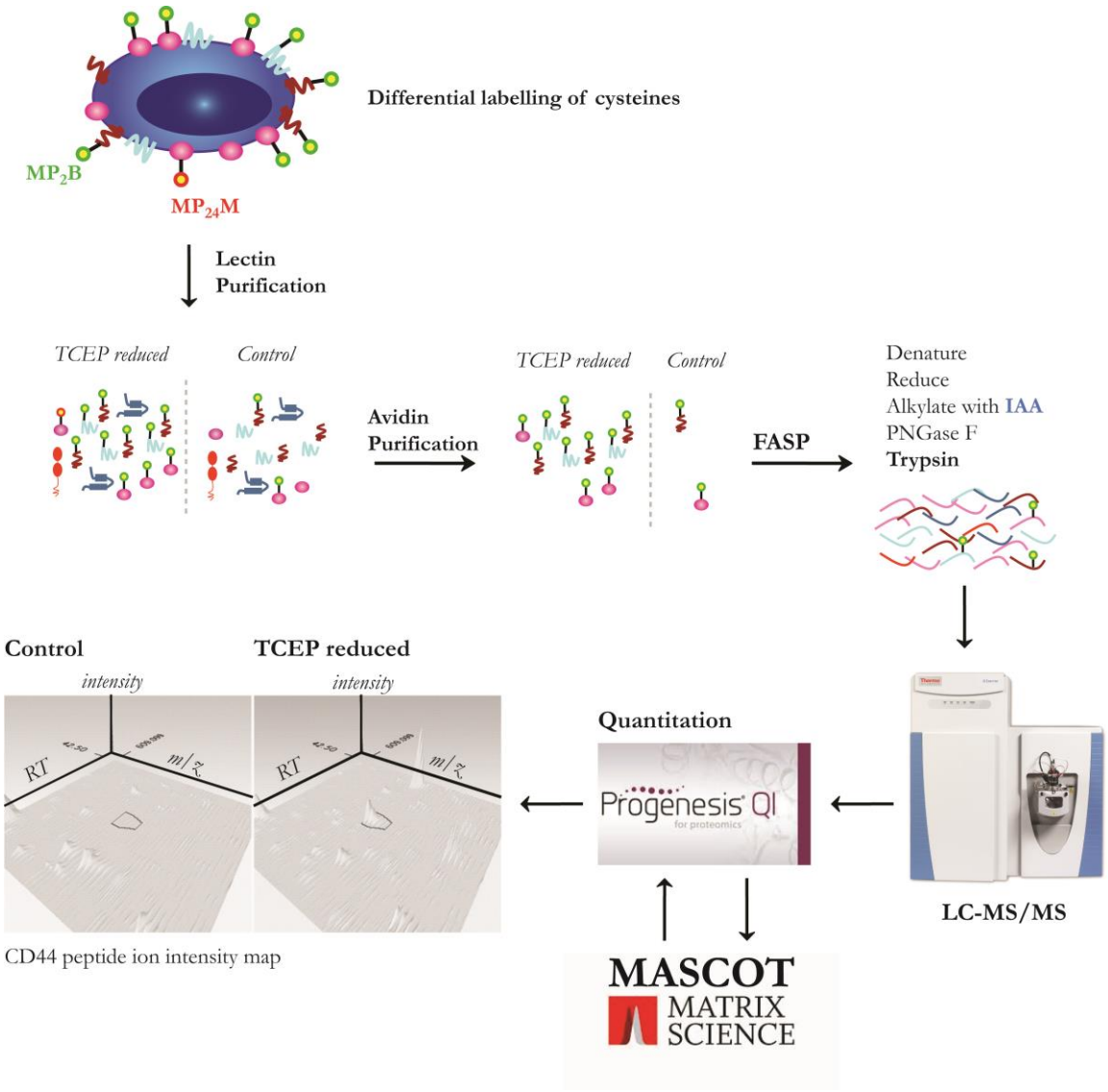

CD44 peptide ion intensity map

Figure 15: **Mass spectrometry workflow for the quantitation of labile disulfide bond reduction.** Cysteines originating from a reduced labile disulfide bond were labelled with MP_2B and biotinylated glycoproteins purified by tandem lectin-avidin purification. The samples were then prepared for mass spectrometry analysis by FASP. The proteins were concentrated on a 10 kDa cut off spin filter, denatured, fully-reduced with TCEP and alkylated with IAA. The sugars were then removed with PNGase F, the remaining detergent washed away, proteins digested with trypsin, peptides desalted on a C18 column and analysed by LC-MS/MS. Protein quantitation was carried out in Progenesis. Ion intensity maps from the different runs were aligned, an aggregate matrix created and searched with Mascot (precursor tolerance 10 ppm, fragment tolerance 0.02 Da, Mascot score ≥ 20). Protein quantitation was carried out on a minimum of two unique peptides per protein by integrating the chromatographic peak areas and calculating the ratios between reduced and control sample. This is illustrated on the example of a CD44 peptide in this figure. The data was normalised using quantile normalisation to compare the data obtained from different mass spectrometry runs and experiments and analysed with the statistical package Limma.

3.2.4. SH-IQ quantifies the reduction of labile disulfide bonds in 32 plasma membrane proteins on leukocytes

To quantify labile disulfide bond reduction in plasma membrane proteins, SH-IQ (differential alkylation of cysteines (Figure 13 C), tandem lectin-avidin purification of biotinylated cell surface proteins, mass spectrometry analysis and label-free quantitation (Figure 15)) was applied.

Label-free quantitation of SH-IQ data using Progenesis QI for Proteomics

The raw data obtained from mass spectrometry analysis was analysed using the software Progenesis QI for Proteomics which quantifies protein abundance by integrating the chromatographic peak areas of unique peptides. In a first step, Progenesis aligns the ion intensity maps (the ion intensity is plotted versus the m/z plotted and retention time) of reduced and control sample. The alignment was then manually reviewed to ensure that like for like peaks were compared and highly reliable results generated. The alignment of ion intensity maps solves the problem of missing data (when there is no MS/MS data collected for a peptide peak in one of the samples) by creating an aggregate data set containing the MS/MS peak information from both runs. After the matrix was searched with Mascot to identify the peptides, the information was re-applied to both ion intensity maps. This means that peaks can be identified although no MS/MS data has been collected for them if they are matched to an identified peak. For quantitation, the relative ion abundance of precursors was compared. A minimum of two unique peptides and a Mascot ion score of 20 was set as a minimum requirement. The Mascot ion score is a probability based score which is reported as $-10*\log_{10}(P)$ where P is the probability that the observed match is a random event. If P is 0.01 then the Mascot ion score is reported as 20.

Quantile normalisation of SH-IQ data

Label-free quantitation involves the parallel processing of samples for mass spectrometry analysis. This introduces technical variation leading to different amounts of sample being injected to the mass

spectrometer. To produce accurate estimates of differences between the runs it is therefore essential to normalise the data.

The raw abundance of each peptide was obtained from Progenesis and transformed to a log_2 scale before normalisation. Log_2 transformation is commonly applied because the data appears near normal distribution and the fold changes are easier to read. A positive 2-fold change (2), for example, appears as 1 when log_2 transformed where a negative 2-fold change (0.5) appears as -1. Quantile normalisation aims at making the data distribution of different datasets identical in statistical terms which is achieved by sorting all the data according to their abundance. The average of the distributions is then set as the reference, meaning that the highest value in all cases will become the mean of all the highest values and so on. Box and whisker plots of unnormalised data show that within an experiment (e.g. Control 1 and TCEP 1) the median of each distribution is similar (Figure 16 A). However, the medians between the experiments slightly differ, especially between the experiments 1 and 3 and 2 and 3. After quantile normalisation, the experimental bias is removed which forces the median of all the data to the same log_2(Intensity) (Figure 16 B).

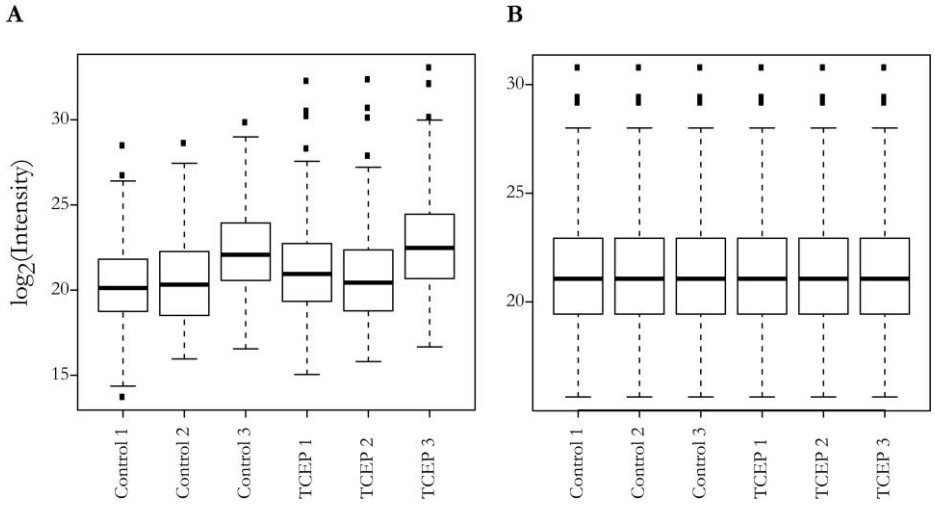

Figure 16: **Normalisation of SH-IQ mass spectrometry data: Box and whisker plots.** The median protein intensity of each experiment is shown as a thick black line (Q2) surrounded by a box representing the first to third quartile (Q1 to Q3) range. The whiskers that extend at both sides of the box indicate the 1.5x interquartile range (IQR = Q3-Q1) from the first and third quartile, respectively. Outliers that are more than 3x IQR below the first quartile or above the third quartile are shown as closed black circles. The distribution of protein intensity before (A) and after (B) quantile normalisation shows the differences in median intensities can be successfully normalised between experiments (1-3) and samples (Control and TCEP-reduced 2B4 T cells).

Statistical analysis of SH-IQ data by Limma

Statistical analysis aims at determining whether the fold change observed is a real signal relative to the variation in the data, whether the change is larger than random noise.

For statistical analysis of SH-IQ data, the abundance of biotinylated cell surface protein in the TCEP sample is expressed relative to the control sample as a fold change, which is a direct readout for labile disulfide bond reduction. The average fold change was then analysed with the linear models for microarray data (Limma) statistical package (75). Limma analysis provides fold changes with P-value. A P-value of 0.02, for example, indicates that if there was no fold change only in 2 % of the experiments would observe the fold change due to a random sampling error.

The normalised average fold changes of proteins quantified in all three biological replicates demonstrates that the majority of proteins does not show any fold change greater or smaller than twofold (Figure 17 A). Moreover, the data demonstrates that the average fold changes observed are independent of protein abundance (Figure 17 B) and that the standard deviation is independent of the average fold change (Figure 17 C). This ensures that neither fold change nor variance are biased by protein abundance.

Figure 17: **SH-IQ: Diagnostic plots.** A) Value-ordered plot of the $\log_2$(Average Fold Change) of proteins in TCEP reduced relative to control sample. This is a direct readout for labile disulfide bond reduction. The higher the $\log_2$(Average Fold Change), the more reduced a protein is. B) MA plot (ratio versus average) shows the $\log_2$(Average Fold Change) plotted against the $\log_2$(Average Abundance). Fold changes that are associated with a P-value < 0.05 are highlighted in red or blue. C) The homogeneity of variance plot shows the $\log_2$(Average Standard Deviation) plotted versus the $\log_2$(Average Fold Change).

Proteins represented were found in three experiments. In order to qualify for quantitation the protein must have ≥ 2 unique peptides per protein with a Mascot score of ≥ 20. Quantitation was carried out by label-free quantitation using the Progenesis software package.

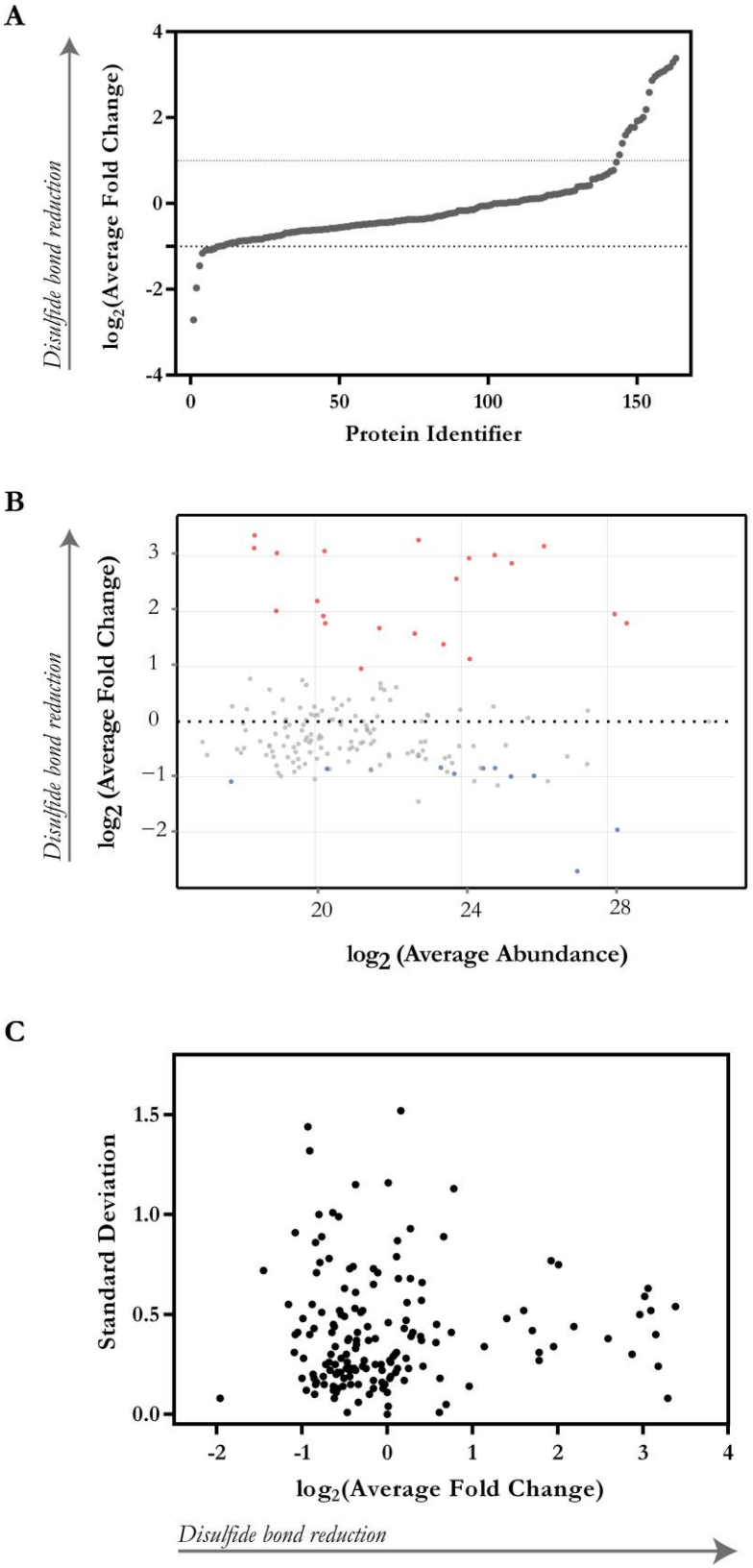
A
Disulfide bond reduction
log2(Average Fold Change)
4
2
0
-2
-4
0
50
100
150
Protein Identifier
B
Disulfide bond reduction
log2 (Average Fold Change)
3
2
1
0
−1
−2
20
24
28
log2 (Average Abundance)
C
Standard Deviation
1.5
1.0
0.5
0.0
-2
-1
0
1
2
3
4
log2(Average Fold Change)
Disulfide bond reduction

Of the 163 proteins that were identified from three SH-IQ experiments (Supplementary Table 5), 32 proteins were significantly (P-value < 0.05) differentially abundant in the TCEP reduced compared to the control sample (Table 5 and Figure 18). It is possible that the analysis of consistently identified proteins misses out on proteins with labile disulfide bonds due to their inconsistent identification. To obtain statistical analysis for those proteins would mean to increase the number of repeats until the protein can be observed at least three times. Of the 32 proteins associated with a P-value < 0.05, 21 proteins are more abundant in the TCEP reduced group meaning that over 50 % of those proteins were reduced by TCEP. This pattern is expected as the reduction of labile disulfide bonds leads to an increase in the number of biotinylated plasma membrane proteins for which SH-IQ enriches in order to quantify labile disulfide bond reduction. However, there shouldn't be any negative fold changes as this would mean that control cells are more reduced than TCEP reduced cells. When looking at the proteins associated with negative fold changes it becomes apparent that 9 of the 11 proteins are intracellular proteins (Table 5). They represent the reproducible CRAPome (contaminant repository for affinity purification (105)) of the purification process.

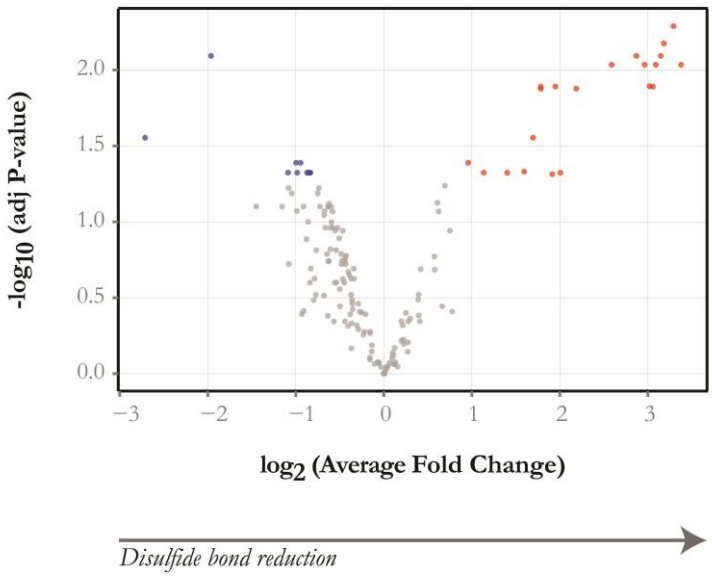

Figure 18: **SH-IQ: Volcano plot.** The $\log_2$(Average Fold Change) is plotted versus the -$\log_{10}$(adj P-value) for each quantified protein. Proteins associated with a P-value < 0.05 are coloured in red when the fold change is positive and in blue when negative. Quantitation was carried out on the 163 proteins present in three biological replicates with ≥ 2 unique peptides per protein and a Mascot score of ≥ 20.

Gene ontology analysis of SH-IQ results

There are freely available online platforms to perform gene ontology (GO) analysis such as www.geneontology.org and www.pantherdb.org. PANTHER (protein annotation through evolutionary relationship) (106) promises to classify proteins based on gene ontology, function and pathways. However, when uploading the SH-IQ dataset to the PANTHER, only 139 out of the 163 UniProt protein accessions were recognised and only 68 proteins were assigned a cellular compartment GO term. This means that only 41 % of the proteins could be assigned to a cellular location which is inadequate. Moreover, a protein can be attributed to more than one subcellular compartment or molecular function which complicates the interpretation of the results. The incomplete GO annotation might be explained by the relatively small size of the *Mus musculus* reference database used by PANTHER that only contains 22,129 of the 46,452 proteins currently deposited in the UniProt database. The GO analysis presented in this thesis was therefore achieved by retrieving the GO annotation of the proteins directly from the UniProt *Mus musculus* database for manual analysis.

124 of the 163 proteins (76 %) consistently identified by SH-IQ are associated with at least one of the following GO terms: cell surface, plasma membrane, extracellular space, extracellular region, integral component of plasma membrane or external side of plasma membrane (Figure 19 A). This proves that the tandem lectin-avidin purification of biotinylated cell surface proteins is indeed efficient.

Power analysis of the SH-IQ dataset

32 of the consistently identified proteins were associated with a P-value <0.05 (Table 5). To reach statistical power it is essential to employ a sufficient number of replicates. The power is defined as 1-β (β is the false-negative rate) and can be understood as the capability of a test to detect a fold change depending on the variance (noise), the number of replicates and the significance α . The power was set to 0.8 meaning that in 4 out of 5 experiments the change in abundance would be detected. With a standard deviation of differences of 0.93, a false-negative rate of 0.05 and a power of 0.8 it is predicted that a minimum fold change of 2.88 can be reliably detected in an SH-IQ experiment with three replicates (Figure 19 B). Indeed, the significant fold changes observed range from 2 to 10-fold. To

detect a smaller fold change, such as 1.5-fold, it would be necessary to increase the sample size to 5 which is consistent with what other research groups have reported for similar experiments (107). This is the reason why proteomic studies cannot identify small fold changes such as 1.5-fold with statistical significance for a typical replicate number of three. However, fold changes smaller than 2 may well be of biological relevance. Protein abundance changes in biological systems can be relatively small. Cell surface protein abundance changes in response to T cell activation, for example, were shown to be smaller than 2-fold for 85 % of the proteins (92). 29 % of the proteins showed a 1.5 to 2-fold change, 56 % stayed unchanged and only 15 % (16 proteins) were shown to increase more than 2-fold in abundance. The data published by this study is based on the analysis of one dataset only. The reason for this might be that the statistical analysis of three biological replicates, which is required by most journals, would be expected to only identify very few proteins associated with as significant fold change, deviating the attention from the intended message.

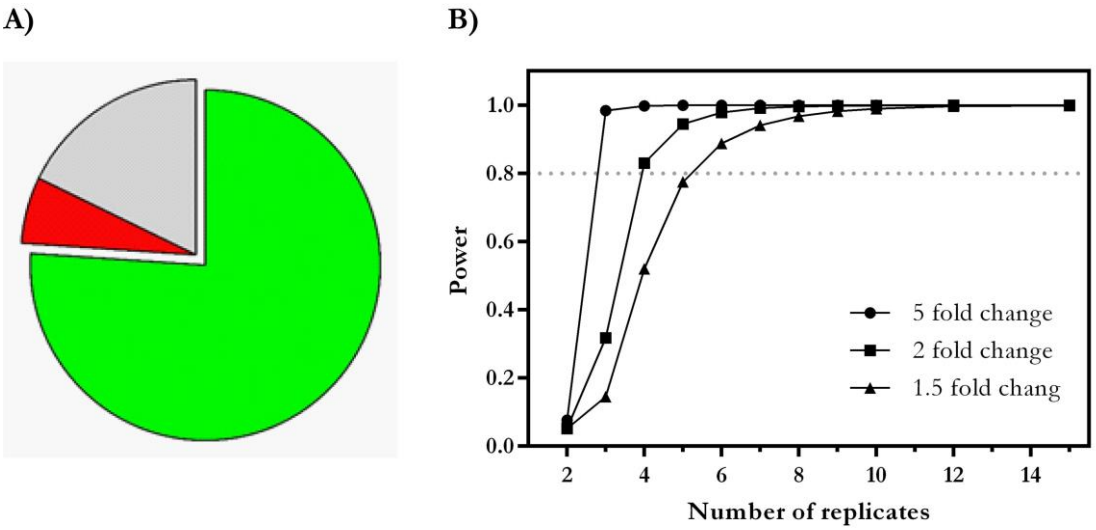

Figure 19: **Gene ontology and power analysis of SH-IQ data.** A) Cellular localisation of the 163 consistently identified proteins from SH-IQ analysis of reduced 2B4 T cells was assigned using the Gene Ontology (GO) terms cell surface, plasma membrane, extracellular space, extracellular region, integral component of plasma membrane or external side of plasma membrane. 76 % of the proteins are cell surface proteins or proteins that can localise to the cell surface (green), 6 % intracellular proteins (red) and 18 % are not associated with either of the GO terms (grey). B) Relationship between power and number of replicates for different fold changes with a standard deviation of 0.93, a significance of 0.05 and a target power of 0.8. To detect a 2-fold change a minimum replicate number of 4 is required whereas a 1.5-fold change requires 6 replicates.

Proteins identified by SH-IQ to contain labile disulfide bonds

Quantitation of labile disulfide bond reduction by SH-IQ allows to identify proteins which are likely to contain labile disulfide bonds that are biologically relevant. This is achieved by ranking the proteins according to their degree of reduction (Table 5). The more reduced a protein is, the more likely it is that this has a functional effect on cellular level. Indeed, when looking at the proteins identified with known labile disulfide bonds (CD44, CD30 and integrin β3 (20, 108–111)), they rank among the 8 most reduced proteins. It is expected that over half of a protein has to be reduced in order to have a significant functional effect on cellular level. Alongside those proteins with known labile disulfide bonds, SH-IQ identified novel cell surface proteins with labile disulfide bonds, including semaphorins, ADAM10 and integrins (Table 5).

Table 5: **Quantitation of labile disulfide bond reduction in leukocyte cell surface proteins after TCEP reduction.** The listed proteins were identified in three biological replicates and their fold change is associated with a P-value that is smaller than 0.05. The average fold change (AFC) was calculated on a minimum of two unique peptides per protein. Limma analysis was used to analyse the difference in protein abundance between control and reduced samples. The P-values were adjusted for multiple testing applying Benjamini-Hochberg correction. Proteins with known labile disulfide bonds are indicated in bold. For the proteins listed in the table the following information is shown: UniProt accession number, gene name, protein description, AFC, $\log_2$(AFC), $\log_2$(Average Abundance), P-value, adjusted P-value and whether the labile disulfide bond has been mapped by Metcalfe *et al.* (26) before.

Accession	Gene Name	Protein Description	Average Fold Change	$\log_2$(AFC)	$\log_2$(Average Abundance)	P-value	Adjusted P-value	Mapped by (26)
Q9CYA0	Creld2	Cysteine-rich with EGF-like domain protein 2	10.39	3.38	18.34	3.92E-04	0.009	NO
Q62469	Itga2	Integrin alpha-2	9.79	3.29	22.83	3.16E-05	0.005	NO
A2APM1	Cd44	**CD44 antigen**	9.08	3.18	26.27	8.20E-05	0.007	YES
Q9QZF2	Gpc1	Glypican-1	8.86	3.15	18.33	2.23E-04	0.008	NO
Q80V42	Cpm	Carboxypeptidase M	8.52	3.09	20.26	4.95E-04	0.009	NO
P35456	Plaur	Urokinase plasminogen activator surface receptor	8.32	3.06	18.96	8.92E-04	0.013	NO
O54890	Itgb3	**Integrin beta-3**	8.11	3.02	24.92	7.84E-04	0.013	YES
Q60846	Tnfrsf8	**Tumor necrosis factor receptor superfamily member 8, CD30**	7.80	2.96	24.22	5.10E-04	0.009	NO
P09055	Itgb1	Integrin beta-1	7.31	2.87	25.39	1.79E-04	0.008	YES
Q6P5F6	Slc39a10	Zinc transporter ZIP10	6.02	2.59	23.87	4.21E-04	0.009	YES
Q8R2Q8	Bst2	Bone marrow stromal antigen 2	4.55	2.19	20.06	1.19E-03	0.013	NO
Q64151	Sema4c	Semaphorin-4C	4.02	2.01	18.94	7.61E-03	0.047	NO
Q542I8	Itgb2	Integrin beta-2	3.86	1.95	28.20	1.03E-03	0.013	YES
Q64697	Ptprcap	Protein tyrosine phosphatase receptor type C-associated protein	3.77	1.92	20.23	9.53E-03	0.049	YES
E9Q5M7	Itgal	Integrin alpha-L	3.44	1.78	28.53	9.61E-04	0.013	YES
O89001	Cpd	Carboxypeptidase D	3.44	1.78	20.28	1.22E-03	0.013	NO
O35598	Adam10	Disintegrin and metalloproteinase domain-containing protein 10	3.24	1.70	21.76	2.75E-03	0.028	YES
P01831	Thy1	Thy-1 membrane glycoprotein	3.02	1.60	22.73	6.01E-03	0.047	YES
Q3TB92	Milr1	Allergin-1	2.64	1.40	23.52	7.67E-03	0.047	NO
O09126	Sema4d	Semaphorin-4D	2.20	1.14	24.23	7.58E-03	0.047	YES
A2AN91	Susd1	Protein Susd1	1.94	0.96	21.26	4.86E-03	0.041	NO

Table 5 continued

Accession	Gene Name	Protein Description	Average Fold Change	log_2(AFC)	log_2(Average Abundance)	P-value	Adjusted P-value	Mapped by (26)
Q61753	Phgdh	D-3-phosphoglycerate dehydrogenase	0.56	-0.83	23.44	8.68E-03	0.047	NO
P97370	Atp1b3	Sodium/potassium-transporting ATPase subunit beta-3	0.56	-0.84	24.93	8.00E-03	0.047	NO
Q03265	Atp5a1	ATP synthase subunit alpha, mitochondrial	0.56	-0.85	24.60	6.68E-03	0.047	NO
D3YU17	Ncln	Nicalin	0.55	-0.86	20.32	8.84E-03	0.047	NO
Q8K297	Colgalt1	Procollagen galactosyltransferase 1	0.55	-0.87	21.53	9.02E-03	0.047	NO
Q9JKR6	Hyou1	Hypoxia up-regulated protein 1	0.52	-0.95	23.81	4.70E-03	0.041	NO
P56480	Atp5b	ATP synthase subunit beta, mitochondrial	0.51	-0.98	25.99	9.00E-03	0.047	NO
Q01965	Ly9	T-lymphocyte surface antigen Ly-9	0.50	-1.00	25.36	5.01E-03	0.041	YES
Q9JLF6	Tgm1	Protein-glutamine gamma-glutamyltransferase K	0.47	-1.09	17.70	7.75E-03	0.047	NO
P38647	Hspa9	Stress-70 protein, mitochondrial	0.26	-1.96	28.28	2.48E-04	0.008	YES
Q9CPN9	2210010C04Rik	Protein 2210010C04Rik	0.15	-2.71	27.18	2.91E-03	0.028	NO

Verification of SH-IQ results by Western blotting

As a proof of concept that the mass spectrometry based SH-IQ results obtained for labile disulfide bond reduction indeed reflect reduction, the results obtained for CD44 were verified by Western blotting. Labile disulfide bond containing proteins were visualised by labelling biotinylated cysteines with a green fluorescent dye. Indeed, only TCEP reduced sample was shown to contain plasma membrane proteins with labile disulfide bonds (A) which is consistent with the results obtained by flow cytometry (Figure 12 A). Moreover, this showed that biotinylated cell surface proteins were efficiently isolated by tandem lectin-avidin purification. CD44 was visualised using a red fluorescent secondary antibody. Reduced CD44, which is biotinylated and therefore enriched by avidin purification, was only found in the TCEP reduced avidin elution fraction but not the control sample avidin elution fraction (Figure 20 B). The fluorescent signal in the TCEP reduced avidin flow-through fraction arises from unreduced CD44. This verifies the results obtained by SH-IQ by showing that reduced CD44 is only present in the reduced but not the control avidin elution fraction which forms the basis for SH-IQ quantitation.

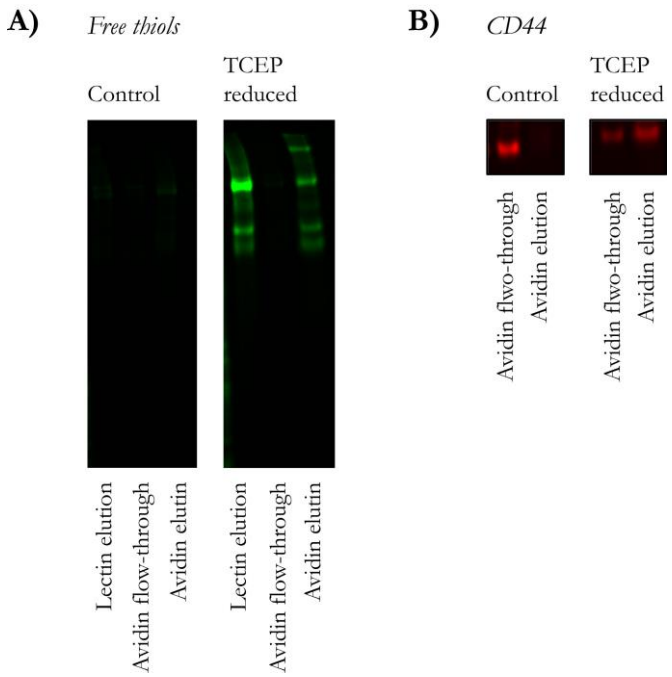

Figure 20: **Verification of SH-IQ by Western blotting.** Free cysteines in control or TCEP reduced 2B4 T cells were labelled with MP_2B and whole cell lysate subjected to tandem lectin-avidin purification. A) The purification of biotinylated cell surface proteins was followed by streptavidinDyLight800 (green) labelling of biotinylated proteins. B) CD44 was visualised using a fluorescent secondary antibody DyLight680 (red) that recognises the primary CD44 antibody. Biotinylated CD44, which indicates a labile disulfide bond reduction, is only present in the TCEP avidin elution fraction.

Fate of reduced plasma membrane proteins

It is unclear at this stage what the fate of reduced plasma membrane proteins is. Preliminary experiments indicate an accelerated turnover and/or shedding of reduced CD44 on 2B4 T cell compared to its native form (Figure 21). If labile disulfide bond reduction can indeed accelerate protein turnover and/or shedding this could allow the cell to not only control protein-protein or protein-ligand interaction through conformational changes but also to modify protein abundance on the cell surface. Moreover, with regards to quantifying labile disulfide bond reduction, this would mean that the amount of reduction occurring could be underestimated for certain proteins due to internalisation and/or shedding of reduced proteins.

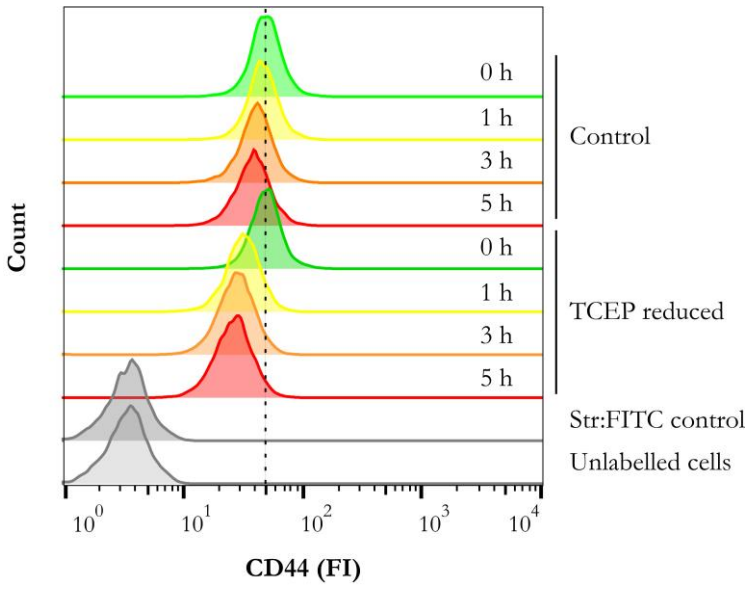

Figure 21: **Internalisation of reduced CD44 is accelerated compared to native CD44.** 2B4 T cells were treated with either medium (DMEM containing 10 % FCS, 100 U/ml penicillin and 100 µg/ml streptomycin) or 2.5 mM TCEP in medium for 15 min. Cells were then washed with medium and incubated with medium containing biotinylated CD44 antibody for up to 5 hours. CD44 internalisation was followed by flow cytometry visualising CD44 cell surface levels with str:FITC. CD44 on TCEP reduced cells is internalised at a faster rate than on control cells.

Summary

This chapter demonstrates the successful development of a mass spectrometry based method to identify proteins with labile disulfide bonds and quantify labile disulfide bond reduction (SH-IQ). The quantitation of labile disulfide bond reduction is crucial in order to identify proteins with labile disulfide bonds whose reduction is likely to be of biological relevance. SH-IQ has revealed 14 novel and 4 known plasma membrane proteins with labile disulfide bonds that are reduced on the leukocyte cell surface upon TCEP reduction (Table 5).

The systematic identification of labile disulfide bonds is not possible with this approach because the sample that is subjected to mass spectrometry analysis is still rather complex. The biotinylated peptides identifying cysteines involved in labile disulfide bonds are likely to be ionised less well than unlabelled peptides due to their big hydrophobic tag and are thus expected to be present in lower amounts. To gain information on labile disulfide bond localisation an additional step would have to be introduced into the method. After the tandem lectin-avidin purification the sample would have to be split in two and one half processed as described before to quantify the reduction and one half of the reduced sample enriched for biotinylated peptides to identify the labile disulfide bonds. The enrichment of biotinylated peptides is a routine procedure in proteomics that would be expected to yield in good results (90, 92). Alternatively, many labile disulfide bonds have already been mapped in the study published by Metcalfe *et al.* (26), including CD44, integrins β1, β2 and β3, semaphorins 4c and 4d and ADAM10 (Table 5), that can be used for cross referencing.

3.3. Discussion

To further the understanding of the role of labile disulfide bonds in the immune system, I have developed a mass spectrometry based method to quantify labile disulfide bond reduction in plasma membrane proteins using a differential cysteine labelling combined with label-free protein quantitation which can be applied to primary samples.

Methods used for cysteine quantitation in intracellular redox proteomics

There have been efforts made to develop a mass spectrometry based method to characterise the intracellular thiol-based redox proteome. To my knowledge, there have been two methods published up to date: OxICAT in 2008 and cysTMTRAQ in 2014 (112, 113). See *Appendix - Quantitation methods in proteomics* for ICAT, TMT and iTRAQ quantitation principles.

OxICAT uses a light ^{12}C-ICAT and a heavy ^{13}C-ICAT to differentially label cysteines. The method has since been successfully applied to study the redox proteome in *E. coli*, *Drosophila melanogaster*, Yeast and *Caenorhabditis elegans* in response to redox stress induced by H_2O_2 or to observe the redox proteome during aging and fasting (112, 114–116). ICAT labels would be ideal to identify and quantify labile disulfide bond reduction since the pair is isotopic, cysteine reactive and biotinylated. However, the labels are vastly expensive at £850 for labelling 10 x 100 µg of sample (compared to £250 for 50 mg MP_2B that allows to label 41 x 1x10^8 cells) making it unsuitable to large scale studies.

cysTMTRAQ is a more recently developed method that allows to label free thiols with cysTMT (up to 6-plex) and peptides for protein-level analysis with iTRAQ (up to 4-plex) tags. Combining cysteine quantitation with protein quantitation allows for the first time to examine redox changes relative to protein abundances. This is a valuable addition to the redox quantitation because it enables the method to distinguish redox effects from protein abundance interferences. In contrast to OxICAT, cyTMTRAQ labelled proteins cannot be affinity purified and must therefore be pre-fractionated prior to LC-MS/MS analysis making the method more time consuming.

Chapter IV – Labile disulfide bonds are cleaved during immune activation

4.1. Introduction

It has previously been reported that when PBMCs (human peripheral blood mononuclear cells) are activated, thiol levels (27) and thioredoxin amounts increase (35). Expanding on this, Pellom *et al.* have recently shown that during acute viral infection thiol levels are increased on antigen-specific effector cells compared to memory cells (38). These observations suggest that activation of immune cells leads to thiol isomerase-mediated reduction of labile disulfide bonds in plasma membrane proteins which can be detected as an increase of thiol levels.

In this chapter I would like to further the understanding of how cell surface thiol levels change during immune activation. Cell-associated antigen presentation in a mixed leukocyte reaction (MLR) was chosen as a model for T cell activation as it is more physiological than the pharmacological activation of T cells through PHA (phytohaemagglutinin), PMA (phorbol 12-myristate 13-acetate), ionomycin or cross linking of the T cell receptor through CD3 antibodies. To investigate the dynamics of labile disulfide bond reduction on the leukocyte cell surface during immune activation, flow cytometry analysis was applied combined with quantitative mass spectrometry to identify the proteins and quantify the reduction occurring using the methods outlined in *Chapter III - Quantitation of labile disulfide bond cleavage*. This will expand the knowledge about labile disulfide bond containing proteins and their reduction during immune activation and allow speculations on the role of labile disulfide bond reduction in immune activation for the first time.

4.2. Results

4.2.1. Reduction of labile disulfide bonds on PBMCs can be followed by flow cytometry

Flow cytometric detection of labile disulfide bond reduction has previously been established using 2B4 T cells (*Chapter III - Quantitation of labile disulfide bond cleavage*). To show that labile disulfide bond reduction can be similarly detected on of a heterogeneous cell population such as PBMCs, cells were labelled with the thiol reactive fluorescent probe Alexa-488-Maleimide before and after TCEP reduction. Indeed, an increase in Alexa-488-Maleimide labelling could be observed as a result of TCEP reduction, indicating labile disulfide bond reduction (Figure 22). The best resolution for detecting changes in thiol levels between reduced and control cells can be obtained with a concentration of 25 μM Alex-488-Maleimide (Figure 22 D) and henceforward used for all experiments.

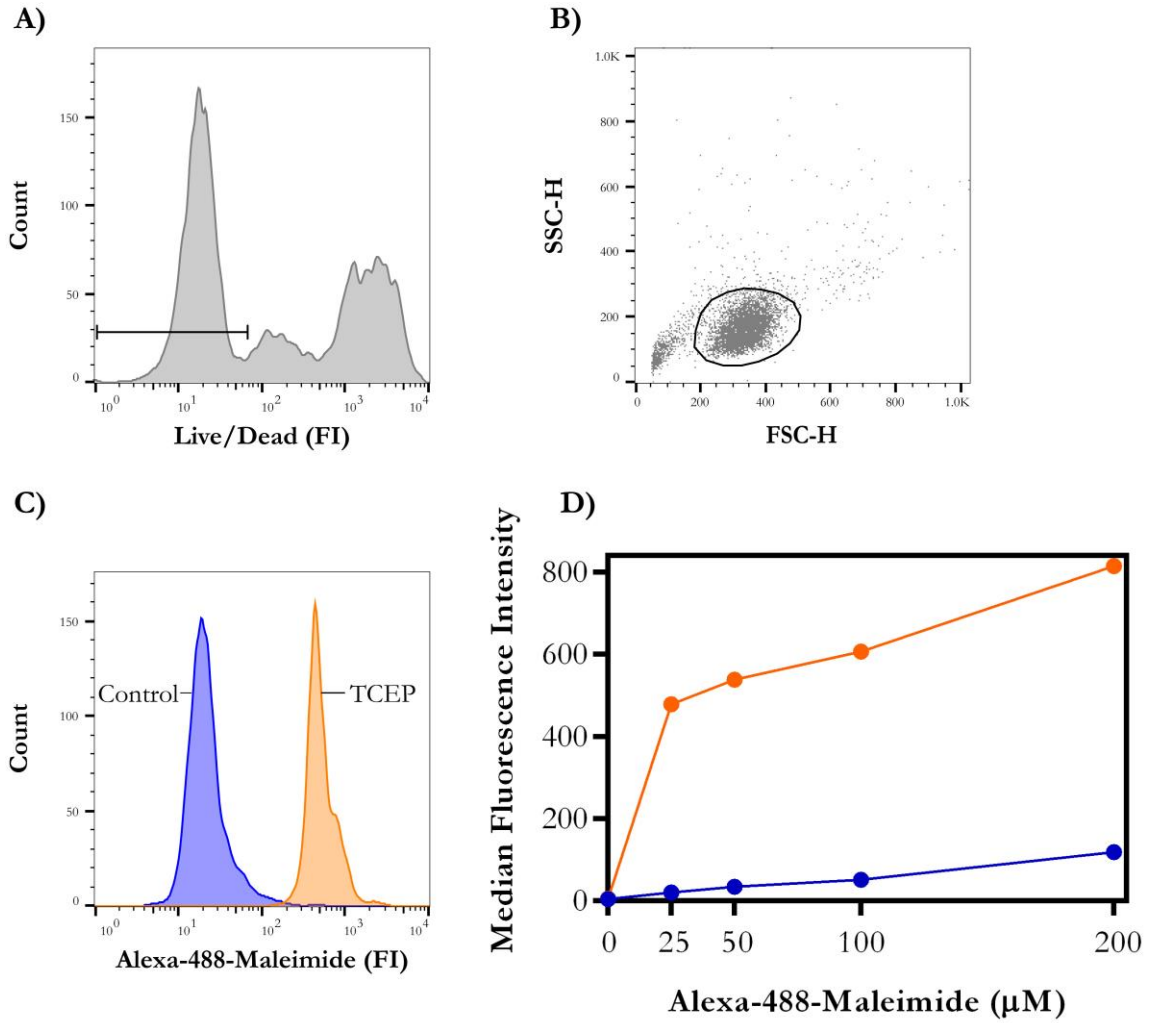

Figure 22: **Labile disulfide bonds are reduced on PBMCs by TCEP.** Panel A) and B) show the gating strategy on the example of control PBMCs. Cells were gated by Live/Dead dye exclusion to identify live cells followed by size (FSC) and granularity (SSC) to identify leukocytes. C) Untreated (control) or TCEP reduced (2.5 mM for 15 min) PBMCs were labelled with 25 µM Alexa-488-Maleimide and the fluorescence plotted as a histogram. The blue line indicates control cells and the orange line TCEP reduced cells. D) The fluorescence intensity of Alexa-488-Maleimide labelled PBMCs is plotted versus the concentration of the Alexa-488-Maleimide label for control (blue line) and TCEP reduced (orange line) cells. The best resolution of the difference between the reduced and control sample can be obtained with 25 µM Alexa-488-Maleimide ($\frac{TCEP\ Alexa-488-Maleimide\ (FI)}{Control\ Alexa-488-Maleimide\ (FI)}$ for different concentrations of Alexa-488-Maleimide: 0 µM=1, ***25 µM=23***, 50 µM=16, 100 µM=12, 200 µM=7). Increasing the concentration of label leads to a decrease in the ratio between the two conditions down to 7 for 200 µM Alexa-488-Maleimide due to an increase in background labelling.

4.2.2. Cell surface thiol levels increase on PBMCs during immune activation

PBMCs were isolated from NC24 leukocyte cones (buffy coat, single donor) and cells from two random donors co-cultured in the presence of IL-2 to facilitate allogenic T cell activation and proliferation. To follow changes in thiol levels on the surface of leukocytes upon activation, samples were removed from the culture over a time course of 96 hours, labelled with Alexa-488-Maleimide and assayed with flow cytometry. This shows a time-dependent increase of thiol levels (Figure 23 C and D), indicating that labile disulfide bonds are reduced as a consequence of immune activation. When the PBMCs of a single donor are cultured separately, no such increase in thiol levels can be observed (Figure 23 D). The increase of thiol levels upon immune activation shows a very similar trend to what Lawrenec *et al.* have shown when PHA activating PBMCs (27). Furthermore, they also observed the initial high levels of cell surface thiols after PBMC isolation. It is unclear why freshly isolated PBMCs have high thiol levels but might be explained by cell stress caused by the isolation process.

This provides further evidence that *in vitro* activation of leukocytes leads to an increase of thiol levels on the cell surface using the more physiological activation of T cells through antigen presentation.

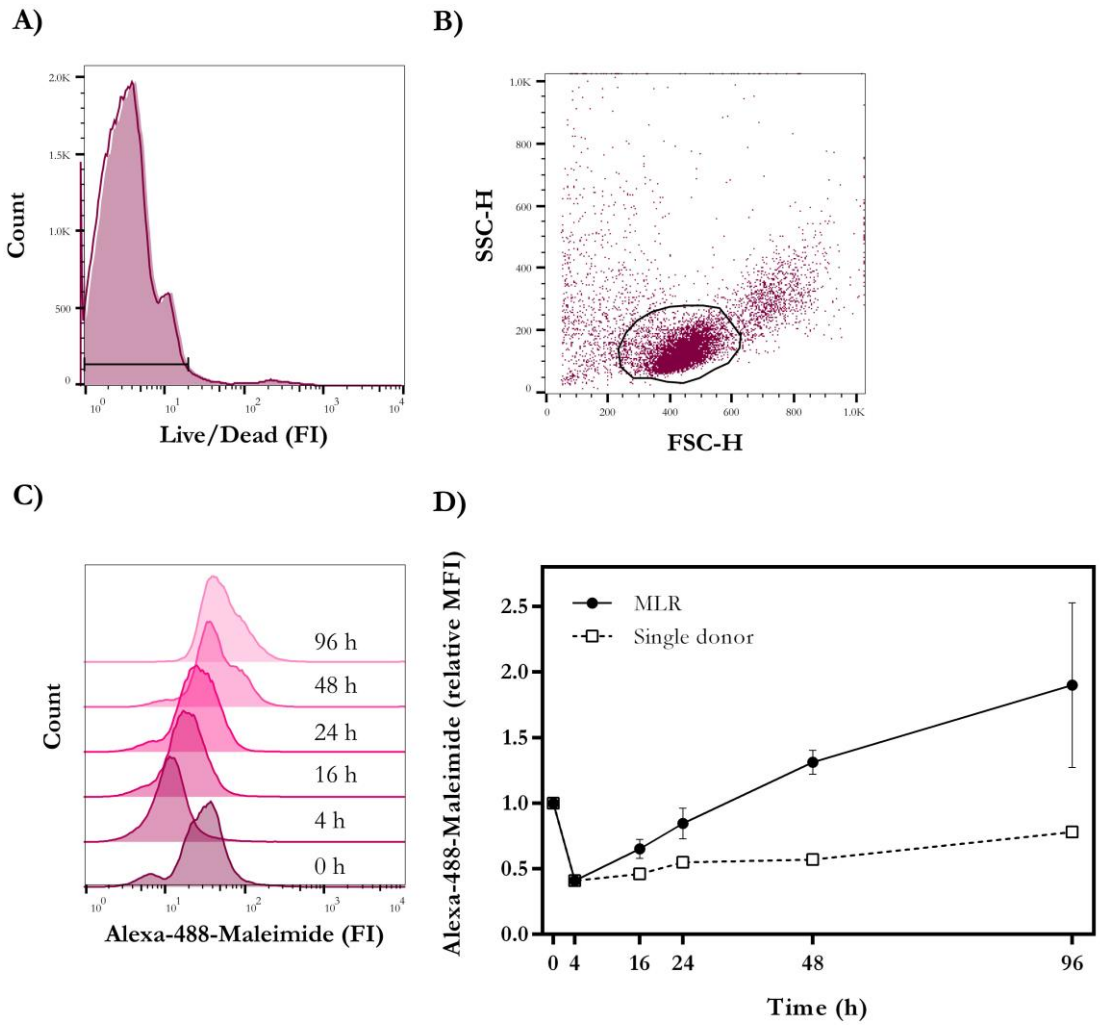

Figure 23: **Thiol levels increase on the leukocyte cell surface during immune activation.** Panels A) and B) show the gating strategy of the experiment on the example of unactivated PBMCs (taken at time point 0 h). A) PBMCs were gated by Live/Dead dye exclusion to identify live cells followed by B) size (FSC) and granularity (SSC) to identify leukocytes which were subsequently analysed for their cell surface thiol levels C) and D). C) Histogram of thiol levels for one representative MLR experiment. Thiol levels increase over time starting from 4 h of incubation. D) Summarises the median fluorescence intensities of four independent MLRs and a single donor relative to time point 0 h. The error bars show the standard deviation (SD) of the mean.

PBMCs of two donors were mixed at a 1:1 ratio with a final concentration of 1-2 x 10^6 cells/ml and were cultured for 96 h in RPMI-1640 containing 10 % FCS and 1-2 % human IL-2.

4.2.3. Cell surface thiol levels are highest on activated T cells

When naïve T cells encounter antigen-presenting cells bearing their cognate antigen, they become activated, start proliferating and acquire effector function (reviewed in (117)). To understand how cell surface thiol levels change during T cell activation, a flow cytometry based assay was performed looking at free thiol on resting and activated T cells. CD69 was used as a T cell activation marker as it is expressed as early as 1 hour after activation.

When activating PBMCs in a MLR, T cell (live Figure 24 A, TCR α/β positive cells, Figure 24 B) activation was detected as early as 4 hours after PBMC co-culture (Figure 24 C). The proportion of activated cells increases from 14 % after 4 hours to 36 % after 96 hours. It is likely that a bigger proportion of T cells is in fact activated, however, cannot be detected in this assay because the sample is taken from the supernatant, excluding T cells from the analysis that have attach to myeloid cells. Flow cytometry being a single cell assay detects the thiol and CD69 level for every single cell in the sample. Interestingly, activated T cells (CD69 high) show a higher time dependent increase in free thiol levels than resting T cells (CD69 low) (Figure 24 D). This suggests that the labile disulfide bond reduction observed is a self-controlled mechanism whereby cells secrete thiol isomerases that reduce their own cell surface and possibly that of directly adjacent cells. Secreted thiol isomerases are probably diluted in the medium and therefore have no effect on distant cells (i.e. resting T cells). Over 30 years ago cell morphology studies of mitogen activated PBMCs have shown that leukocytes contain more microvilli-like membrane extensions when activated (118, 119) which might contribute in the retention of thioredoxin on the surface of activate T cells.

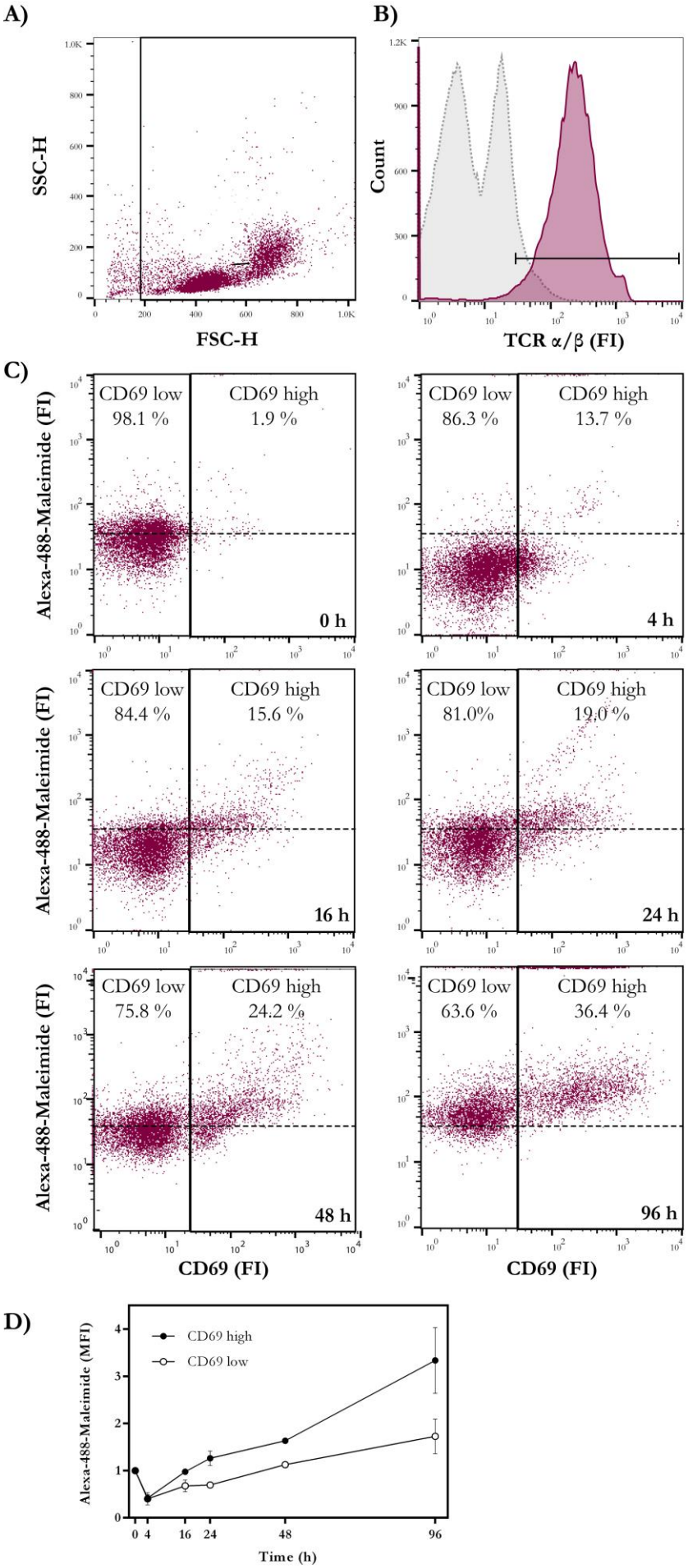

Figure 24: **Cell surface thiol levels are highest on activated T cells.** A) PBMCs taken at time point 0 h were gated for live cells by size (FSC) and for B) T cells by the expression of the TCR α/β chain (TCR α/β stained cells are indicated in purple and the isotype control cells in grey). C) Dot plot of thiol levels and CD69 expression for one representative MLR experiment. The graph in D) summarises the Alexa-488-Maleimide MFI of three independent experiments relative to time point 0 h for CD69 low cells (-○-) and CD69 high cells (-●-). Error bars show SEM.

PBMCs of two donors were mixed at a 1:1 ratio with a final concentration of 1-2 x 10^6 cells/ml and were cultured for 96 h in RPMI-1640 containing 10 % FCS and 1-2 % human IL-2.

4.2.4. Thioredoxin inhibition prevents labile disulfide bond reduction during immune activation

Labile disulfide bonds can be reduced by thiol isomerases such as thioredoxin and protein disulfide isomerase (PDI) family members. In immune activation, lung injury and cancer thiol isomerases are secreted to the cell surface and are likely to cleave labile disulfide bonds which has been observed as an increase in free thiols. PX-12 (1-methylpropyl 2-imidazolyl), an irreversible inhibitor for thioredoxin-1 (120), was tested in a MLR as described previously to assess if this can inhibit labile disulfide bond reduction.

PX-12 prevents adherent cells from attaching to the cell culture flask as can be seen in the FSC vs. SSC by flow cytometry (Figure 25 A). This indicates that inhibition of thioredoxin impairs myeloid cell adhesion. A likely mechanism explaining this phenomenon is through impaired integrins adhesion as disulfide bond reduction is known to be involved in integrin activation (28, 121, 122). Additionally, the phenotype could be caused by thioredoxin reducing labile disulfide bonds in other adhesion molecules leading to a loss of function and impaired adhesion.

The PX-12 treatment does not affect the proportion of activated T cells in MLRs (Figure 25 B), but does lead to lower cell surface thiol levels (Figure 25 C). This proves that the increase of thiol levels detected upon immune activation (Figure 23 D) is at least partially caused by thioredoxin, confirming the effect of bacitracin on thiol isomerases seen by Lawrence *et al.* (27).

SH-IQ was applied to identify the proteins with reduced labile disulfide bonds that cause the increase of thiol levels during immune activation and to quantify the amount of reduction occurring, providing an insight into the kinetics of labile disulfide bond reduction.

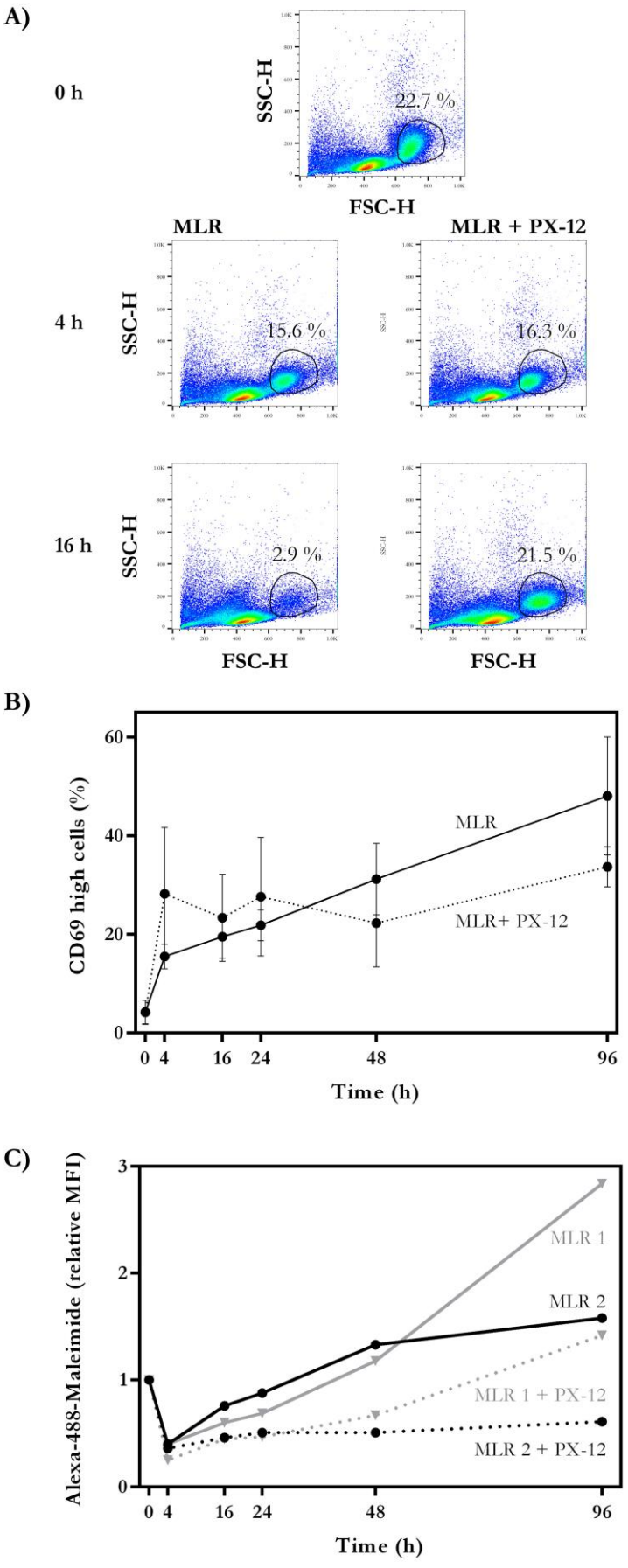

Figure 25: **Thioredoxin inhibition affects labile disulfide bond reduction and cell adhesion during immune activation.**

A) The FSC vs. SSC plots of an ungated MLR show that adherent cells (circular gate) do attach to the cell culture flask over time (the relative number of cells in the gate decreases). However, when PX-12 is added to a MLR, the cells remain in suspension after activation (same relative number of cells is present in the gate after 16 hours as compared to 0 hours). B) T cells (gated for live cells by size and for T cells by the expression of the TCR α/β chain as indicated in Figure 24 A and B) activate similarly in the presence (dotted line) and absence (solid line) of PX-12 but C) T cells treated with PX-12 show lower thiol levels (Alexa-488-Maleimide MFI) compared to control cells. The graph plots the Alexa-488-Maleimide MFI relative to time point 0 hours from two experiments which are indicated in black and grey. PX-12 treated MLRs are indicated with dotted lines. Panel B) represents the average of two experiment with SEM indicated.

Human PBMCs of two donors were mixed at a 1:1 ratio with a final concentration of 1-2 x 10^6 cells/ml and were cultured for 96 h in RPMI-1640 containing 10 % FCS and 1-2 % human IL-2 in the presence of 25 µM PX-12 when indicated.

4.2.5. SH-IQ identifies 29 proteins with labile disulfide bonds that are reduced on PBMCs during immune activation

273 proteins were constantly quantified in two MLRs by SH-IQ. As established during the method development (*Chapter III - Quantitation of labile disulfide bond cleavage*), most proteins are unaffected by the immune activation and show no fold change (log_2(AFC) >-1 and <1) relative to 4 hours after activation which is represented in the value-ordered plot (Figure 26 A). These proteins represent the non-specific background of the experiment.

When plotting the average fold change of all unchanged proteins (Figure 26 A: II = ∑-I-III) versus time, this represents a baseline of proteins that are unaffected by labile disulfide bond reduction (Figure 26 B). In contrast, the average fold change of proteins with labile disulfide bonds increases upon activation (I = minimum two log_2(FC) >1 and minimum one AFC must be composed of both log_2(FC)s >1) (Figure 26 B). There is a group of proteins that show a negative fold change (III = minimum two log_2(FC) <-1 and minimum one AFC must be composed of both log_2(FC)s <-1) (Figure 26 B). There shouldn't be any negative fold change observed in this assay since it records labile disulfide bond reduction which can only lead to an increased fold change per definition. The negative fold changes observed could simply represent experimental noise or indicate shedding or downregulation of reduced proteins. Since over 60 % of the proteins associated with a negative fold change are cell surface proteins or can localise to the cell surface, it seems probable that these proteins are internalised or shed after reduction (Supplementary Table 7). However, further studies are required to conclude about the fate of reduced plasma membrane proteins.

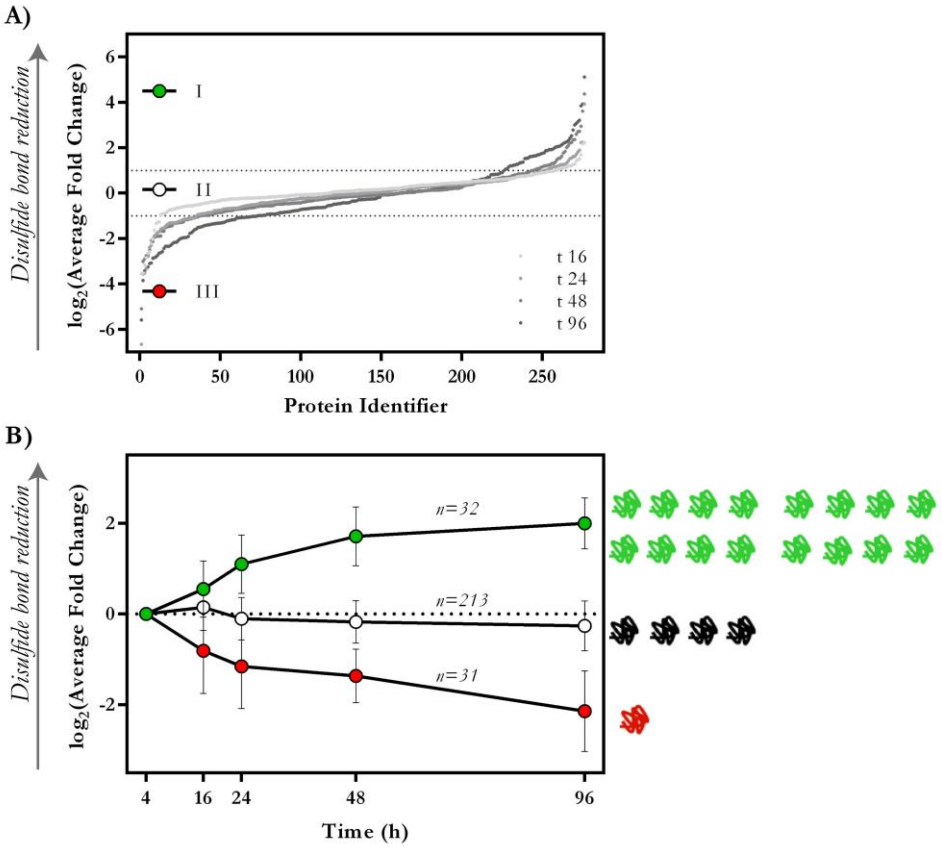

Figure 26: **Diagnostic plots of labile disulfide bond reduction on PBMCs after activation.** A) Value-ordered plot of log_2(Average Fold Change) for each quantified protein at 16 h (-●-), 24 h (-●-), 48 h (-●-) and 96 h (-●-) relative to 4 h. B) The log_2(Average Fold Change) of proteins that do not change in their average abundance (II=∑-I-III, open circles), with labile disulfide bonds that show an increased fold change (I = minimum two log_2(FC) >1 and minimum one FC must be composed of both log_2(FC)s >1, green circles) and proteins with a negative fold change (III = minimum two log_2(FC) <-1 and minimum one FC must be composed of both log_2(FC)s <-1, red circles) are plotted against time (4 h, 16 h, 24 h, 48 h and 96 h). The number of proteins to the side of the plot illustrates the relative abundance at a log_2(FC) of 2, 0 and -2.
The data represents proteins that were identified in two MLRs by SH-IQ (276 proteins, Mascot score ≥ 37) and the SEM is indicated. The data was analysed using Progenesis using the built in normalisation function to normalise peptide intensities to total peptide abundances.

Kinetics of labile disulfide bond reduction

SH-IQ identified proteins with labile disulfide bonds that were reduced during immune activation and quantified their reduction, providing a first insight of what proteins are redox-modulated during immune activation and to what extent. Moreover, quantitation of labile disulfide bond reduction allows to gain an insight into the kinetics of the reaction. Labile disulfide bonds can be reduced at different rates (A-C), meaning that under the same reducing conditions different amounts (a-c) of a specific disulfide bond is reduced after a given time x (Figure 7) (123).

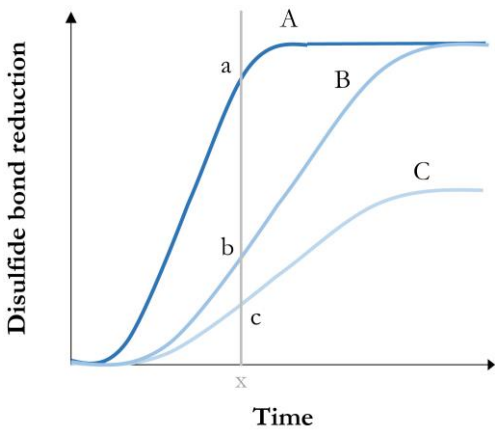

Figure 27: **Schematic of the kinetics of labile disulfide bond reduction.** Proteins A-C contain labile disulfide bonds which are reduced at different rates in a given reducing environment. Therefore, different amounts (a-c) of the labile disulfide bond are reduced after a given time x.

29 leukocyte cell surface proteins were shown to be redox-modulated during immune activation (Figure 28), indicating that labile disulfide bond reduction only affects a small proportion of cell surface proteins. All the redox-modulated proteins identified show continuous reduction of labile disulfide bonds over time but with different kinetics (similar to A-C in Figure 27). The kinetics of labile disulfide bond reduction can be categorised into three groups: A) proteins that get reduced as early as 16 hours after activation (rapid), B and C) proteins that get reduced after 24 hours of activation (intermediate) and D) proteins that are only reduced after 48 hours (slow) (Figure 28 A-D). Proteins found to be rapidly reduced are likely to contain highly labile disulfide bonds or could be preferentially reduced by thiol isomerases. Proteins that were identified to be rapidly reduced during immune activation include the cytokine receptor common gamma chain (CD132) and CD44 which have been previously shown to contain labile disulfide bonds (*Chapter III - Quantitation of labile disulfide bond cleavage* and (19, 20)), illustrating the capacity of the SH-IQ method to confidently detect the reduction of labile disulfide bonds in primary cells. Apart from these known proteins, a number novel cell surface proteins were identified to contain labile disulfide bonds that are reduced during immune activation (Figure 28 A-D). They mainly contain activating signalling molecules (Pcdl1, SLAMF1 and 7) and cell adhesion molecules (Intracellular adhesion molecule 1 (ICAM1), integrin β_7, galectin 3 and 9). This suggests that immune activation leads to the redox regulation of T cell activation and adhesion which could have important implications in controlling the activation of the immune system and immune cell migration. The functional consequences of labile disulfide bond reduction for the individual proteins, however, remain to be studied.

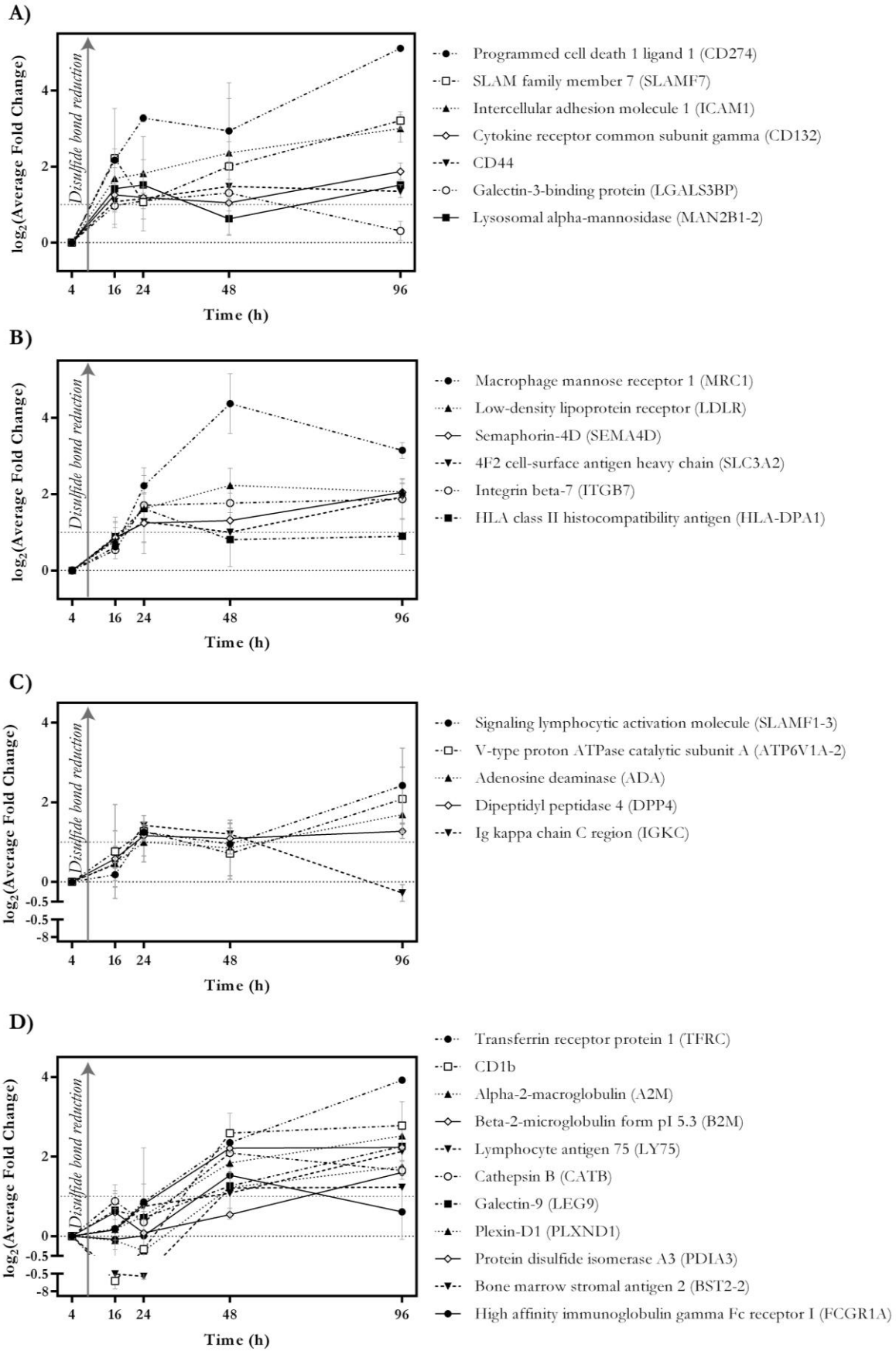
A)
log2(Average Fold Change)
Disulfide bond reduction
Time (h)
Programmed cell death 1 ligand 1 (CD274)
SLAM family member 7 (SLAMF7)
Intercellular adhesion molecule 1 (ICAM1)
Cytokine receptor common subunit gamma (CD132)
CD44
Galectin-3-binding protein (LGALS3BP)
Lysosomal alpha-mannosidase (MAN2B1-2)
B)
Macrophage mannose receptor 1 (MRC1)
Low-density lipoprotein receptor (LDLR)
Semaphorin-4D (SEMA4D)
4F2 cell-surface antigen heavy chain (SLC3A2)
Integrin beta-7 (ITGB7)
HLA class II histocompatibility antigen (HLA-DPA1)
C)
Signaling lymphocytic activation molecule (SLAMF1-3)
V-type proton ATPase catalytic subunit A (ATP6V1A-2)
Adenosine deaminase (ADA)
Dipeptidyl peptidase 4 (DPP4)
Ig kappa chain C region (IGKC)
D)
Transferrin receptor protein 1 (TFRC)
CD1b
Alpha-2-macroglobulin (A2M)
Beta-2-microglobulin form pI 5.3 (B2M)
Lymphocyte antigen 75 (LY75)
Cathepsin B (CATB)
Galectin-9 (LEG9)
Plexin-D1 (PLXND1)
Protein disulfide isomerase A3 (PDIA3)
Bone marrow stromal antigen 2 (BST2-2)
High affinity immunoglobulin gamma Fc receptor I (FCGR1A)

Figure 28: **Kinetics of labile disulfide bond reduction during immune activation.** Proteins with labile disulfide bonds are reduced at different rates during immune activation. Panel A) shows proteins with rapid, B) and C) intermediate and D) with slow labile disulfide bond reduction rates.

Human PBMCs of two donors were mixed at a 1:1 ratio with a final concentration of 1-2 x 10^6 cells/ml and were cultured for 96 h in RPMI-1640 containing 10 % FCS and 1-2 % human IL-2. Samples were taken at the time points indicated and SH-IQ (excluding the blocking of thiols with $MP_{24}M$, Mascot score ≥ 37) was applied to quantify labile disulfide bond reduction. The $\log_2$(Average Fold Change) from two experiments and the SEM is plotted versus time. Only proteins that show at least two twofold average fold change are shown in this figure, detecting 29 proteins with those filtering criteria.

4.2.6. Interesting observation: Thiol levels on splenocytes increase during inflammation

It is clear that free thiols are generated *in vitro* during immune activation (Figure 23) but a key question remaining is to what extent labile disulfide bonds are modified *in vivo*. To address this, SH-IQ was applied to an LPS induced endotoxemia mouse model to follow the modulation of labile disulfide bonds during inflammation.

Splenocytes were harvested from control mice or mice with LPS induced endotoxemia after three hours and the cells prepared for flow cytometry and mass spectrometry analysis (as described in *Chapter III - Quantitation of labile disulfide bond cleavage*) to identify proteins with labile disulfide bonds and quantify their reduction. Flow cytometry analysis of thiol levels demonstrated that splenocytes obtained from mice with LPS induced inflammation contain more free cell surface thiols compared to control cells in one out of three experiments (Figure 29 C, Experiment 1). When no difference in splenocyte cell surface thiol levels could be detected (Figure 29 C, Experiment 2 and 3), control thiol levels were increased. Interestingly, the viability in Experiments 2 and 3 is decreased compared to Experiment 1 (Figure 29, A) and the cells showed an increase in granularity and a decrease in size (Figure 29, B), which is indicative of cells entering apoptosis. This could lead to the release of intracellular thiol isomerases in the control samples, resulting in labile disulfide bond reduction on the cell surface, masking the effect caused by inflammation.

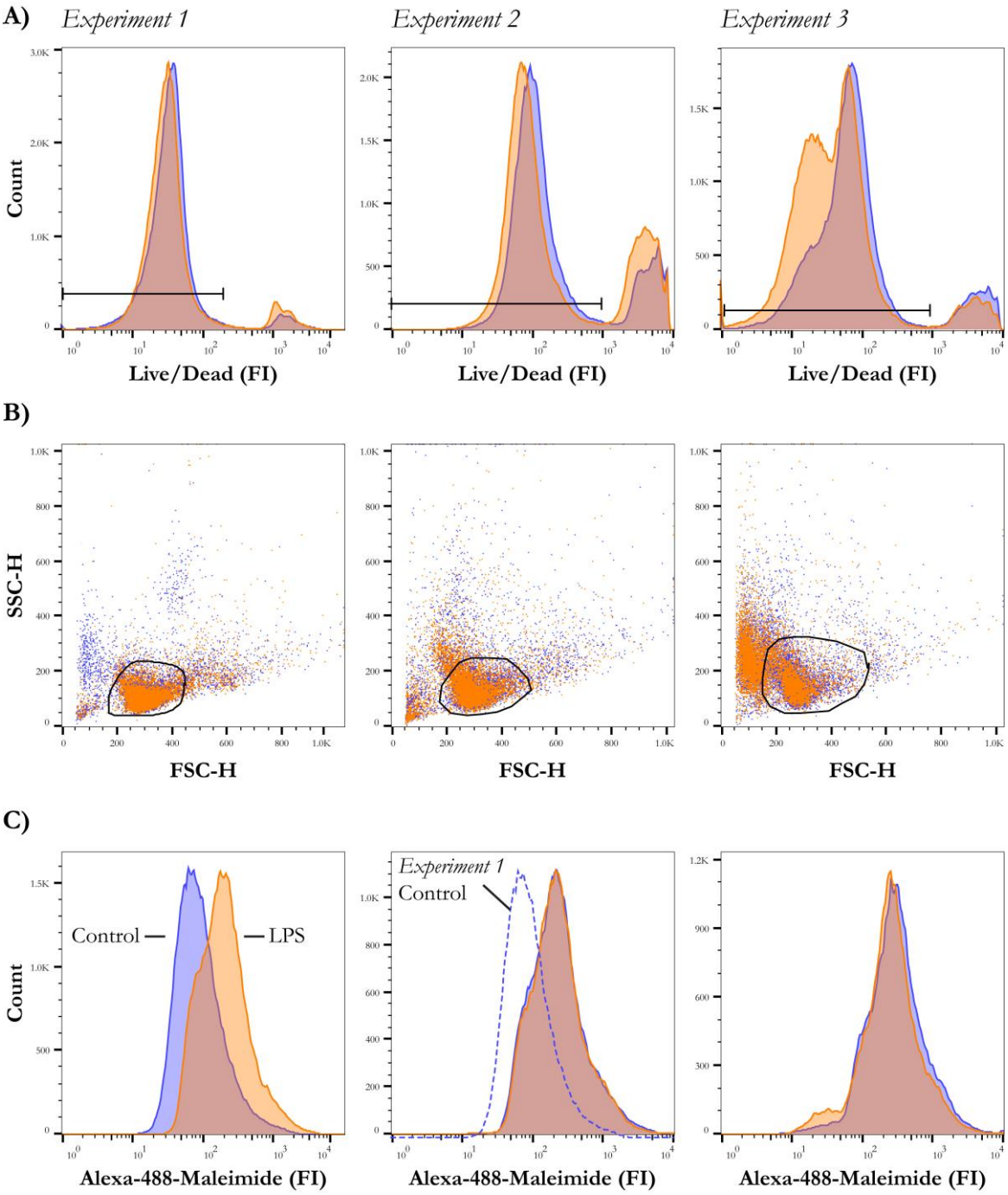

Figure 29: **Labile disulfide bonds are reduced during inflammation.** Splenocytes were isolated from control and LPS-challenged female C57 Bl/6J mice after 3 hours and the cells from three control or LPS-challenged animals pooled. Cells were then labelled with Alexa-488-Maleimide to label free thiols and a Live/Dead dye which labels dead cells. A) Cells were gated on Live/Daed exclusion to identify live cells and B) by size (FSC) and granularity (SSC) for lymphocytes for the analysis. C) Thiol levels were then analysed by following the Alexa-488-Maleimide fluorescenec intensity.

Label-free quantitation using Progenesis QI for Proteomics

Splenocytes from Experiment 1 that showed increased thiol levels after LPS-induced endotoxemia (Figure 29 C) were subjected to SH-IQ to identify the proteins with redox-modulated labile disulfide bonds.

When importing the mass spectrometry data into Progenesis, the ion intensity maps (m/z plotted versus retention time and ion intensity) of the control and LPS sample were too different to confidently align, which is represented as orange or red areas on the ion intensity map (Figure 30 A). This lead to the alignment and comparison of unlike features impairing the quantitation, which is illustrated in the diagnostic value-ordered plot of the fold changes (Figure 30 B). It is expected that the majority of proteins identified will be unchanged in abundance (as established in *Chapter III - Quantitation of labile disulfide bond cleavage*). Progenesis analysis, however, yields in an average twofold change which is indicative of an underlying problem in the data analysis. Therefore, the data analysis strategy was changed to spectral index normalised quantification (SINQ), which relies on the identification of each feature for relative protein quantitation.

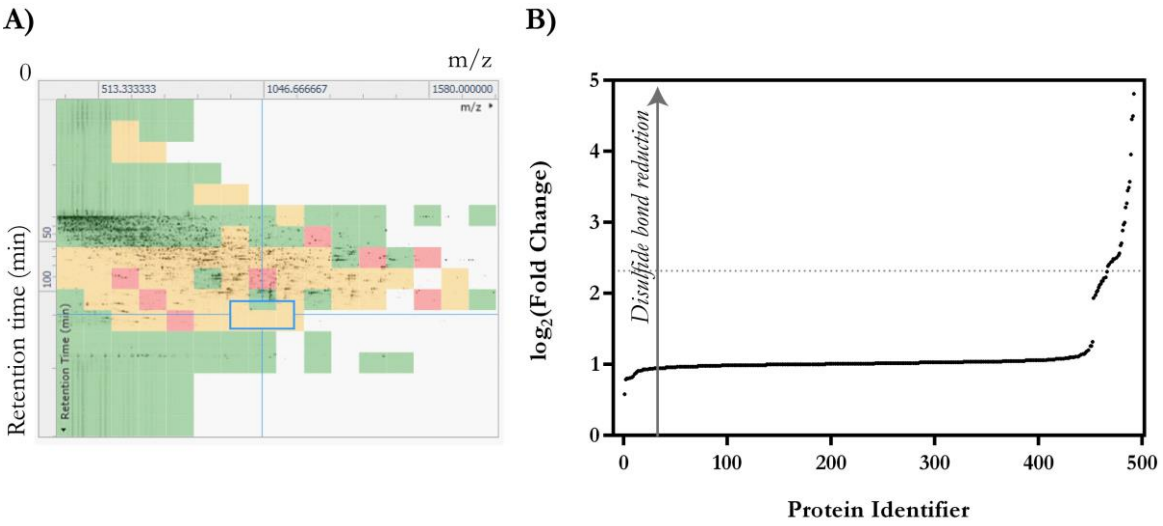

Figure 30: **Progenesis diagnostic plots for the quantitation of labile disulfide bond reduction during inflammation.** Mass spectrometry data was imported into Progenesis for data analysis. A) When aligning the ion intensity maps no good alignment could be achieved which is indicated by orange (OK) and red (Poor) squares in the ion intensity alignment map. Green squares indicate good alignment. B) When plotting the $\log_2$(Fold Change) of proteins in increasing order it shows that the average protein is two-fold more abundant in the LPS sample compared to the control sample.

Label-free quantitation using SINQ

SINQ quantitation solves the problem of the ion intensity map misalignment encountered with Progenesis by only using features that have been identified in both the control and LPS sample. Indeed, this showed the expected data distribution in the value-ordered plot with most proteins unchanged between the conditions and a few indicated to be redox regulated during inflammation which is seen as an increased fold change (Figure 31 A). Since the analysis is performed on one replicate only a fold change cut-off has to be defined instead of using the more robust P-value cut-off. The data is distributed around a mean of 0.19 ($log_2(1.14)=0.19$) with a standard deviation of 1.57 ($log_2(2.97)=1.57$) (Figure 31 B). Therefore, proteins displaying a fold-change greater than 2.3 ($log_2(5)=2.3$) were considered to be redox-modulated.

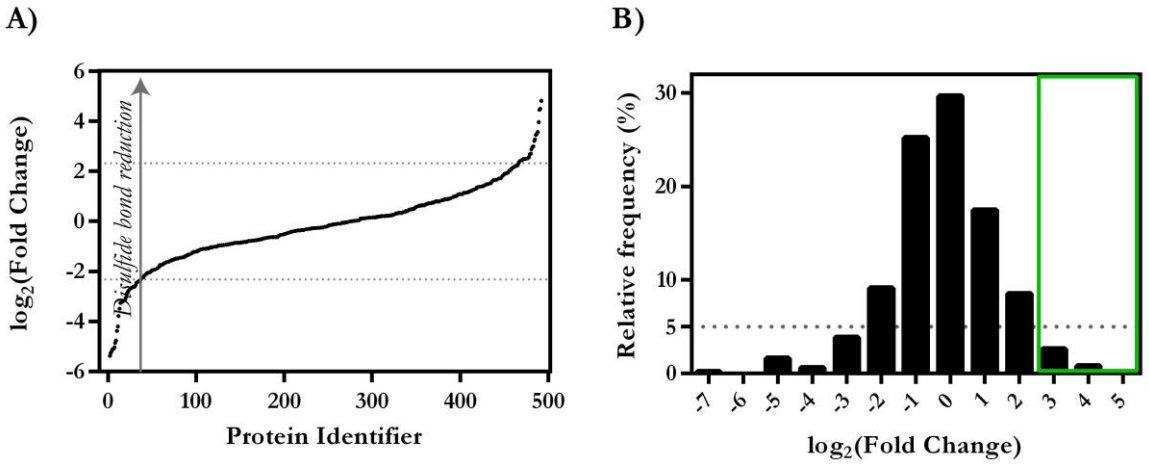

Figure 31: **SINQ diagnostic plots for the quantitation of labile disulfide bond reduction during inflammation.** A) The log_2(Fold Change) of proteins between the control and LPS sample is plotted versus the protein identifier in increasing order. The majority of proteins identified were equally abundant (± 5 fold change) in splenocytes harvested from control and LPS treated mice with only a few proteins showing differential abundance. B) Frequency distribution of the log_2(Fold Change) into bins with width 1. The data is distributed around the mean (0.19) with a standard deviation of 1.57. Therefore, a cut-off fold change of 5 ($log_2(5)=2.3$) was chosen (green box).

SH-IQ identified several proteins to contain labile disulfide bonds that were reduced during inflammation (Table 6). One of those proteins is the cytokine receptor common gamma chain (CD132) which confirms the effectiveness of SH-IQ to confidently identify proteins with labile disulfide bonds from *in vivo* samples. Interestingly, the labile disulfide bond reduction kinetics observed the MLRs seems to apply to this *in vivo* model of inflammation. The *in vitro* data suggests that CD132, SLAMF7, CD44, ICAM1, programmed cell death 1 ligand (CD274) and galectin-3 binding protein are reduced within 12 hours during immune activation (Figure 28 A). Indeed, among the proteins identified after 3 hours of inflammation were CD132 and the SLAMF7 (ICAM1 and CD274 were detected with a twofold change) confirming the early redox-regulation of these proteins *in vivo*. Novel proteins identified include the extracellular space proteins α-2-macroglobulin and cathepsin-O and the plasma membrane proteins semaphorin-4A, lactadherin, receptor-type tyrosine-protein phosphatase α, cytokine-receptor-like factor 2, B- and T-lymphocyte attenuator, SLAMF5, Fc receptor-like protein 5, signalling lymphocytic activation molecule and tumour necrosis factor receptor superfamily member 18.

To ensure that the increase of thiol levels observed during inflammation is caused by the reduction of labile disulfide bonds and is not an artefact of different cell composition in the spleen of healthy and LPS-challenged mice, splenocytes were stained for T cells, B cells, DCs and macrophages and analysed by flow cytometry. The results show that there is no difference in cell type composition between LPS and control splenocytes (Figure 32).

When SH-IQ was applied to splenocytes obtained from Experiment 2 and 3 where no difference in thiol levels could be observed between healthy and LPS-challenged mice by flow cytometry analysis (Figure 29 C), the mass spectrometry analysis indeed reflected this by only identifying one protein to contain a labile disulfide bond, CD274 (Supplementary Table 6).

Table 6: **Quantitation of labile disulfide bond reduction in splenocyte cell surface proteins during inflammation.** Labile disulfide bond reduction was quantified in a mouse model of LPS-induced inflammation using SINQ (10 ppm precursor tolerance, 0.02 Da fragment tolerance, 2 missed cleavages, 1% FDR). For the cell surface proteins listed in the table the following information is shown: UniProt accession number, gene name, protein description, fold change and log_2(Fold Change). The listed proteins are representative of one experiment (Experiment 1). Cell surface proteins are indicated in black, intracellular proteins in grey and proteins with known labile disulfide bonds bold.

Accession	Gene Name	Protein description	Fold change	log_2(FC)
Q61838	A2m	Alpha-2-macroglobulin	28.05	4.81
P63037	Dnaja1	DnaJ homolog subfamily A member 1	22.63	4.50
Q8BM88	Ctso	Cathepsin O	21.86	4.45
Q62178	Sema4a	Semaphorin-4A	15.56	3.96
Q9DB20	Atp5o	ATP synthase subunit O, mitochondrial	11.88	3.57
P21956-2	Mfge8	Isoform 2 of Lactadherin	11.24	3.49
P34902	Il2rg	**Cytokine receptor common subunit gamma (CD132)**	10.93	3.45
P62852	Rps25	40S ribosomal protein S25	9.65	3.27
Q91V35	Ptpra	Receptor-type tyrosine-protein phosphatase	9.25	3.21
Q8CII9-2	Crlf2	Cytokine receptor-like factor 2	8.00	3.00
Q7TSA3-3	Btla	B- and T-lymphocyte attenuator	7.84	2.97
A0A075B5Y3	Ighv1-80	Protein Ighv1-80	7.41	2.89
Q18PI6	Cd84	SLAM family member 5	6.54	2.71
Q5SYH2	Tmem199	Transmembrane protein 199	6.41	2.68
A0A075B677	Igkv4-53	Protein Igkv4-53	5.90	2.56
Q3U1J4	Ddb1	DNA damage-binding protein 1	5.78	2.53
O09046-2	Il4i1-2	L-amino-acid oxidase	5.70	2.51
Q8BHK6-4	Slamf7	SLAM family member 7	5.66	2.50
P12265	Gusb	Beta-glucuronidase	5.66	2.50
Q9R0P6	Sec11a	Signal peptidase complex catalytic subunit SEC11A	5.62	2.49
Q68SN8	Fcrl5	Fc receptor-like protein 5	5.62	2.49
Q00PI9	Hnrnpul2	Heterogeneous nuclear ribonucleoprotein U-like protein 2	5.46	2.45
A0A075B5M1	Igkv4-63	Protein Igkv4-63	5.46	2.45
Q9QUM4-2	Slamf1	Signaling lymphocytic activation molecule	5.31	2.41
Q8VEB4	Pla2g15	Group XV phospholipase A2	5.31	2.41
O35714-2	Tnfrsf18	**Tumor necrosis factor receptor superfamily member 18, CD30**	5.21	2.38

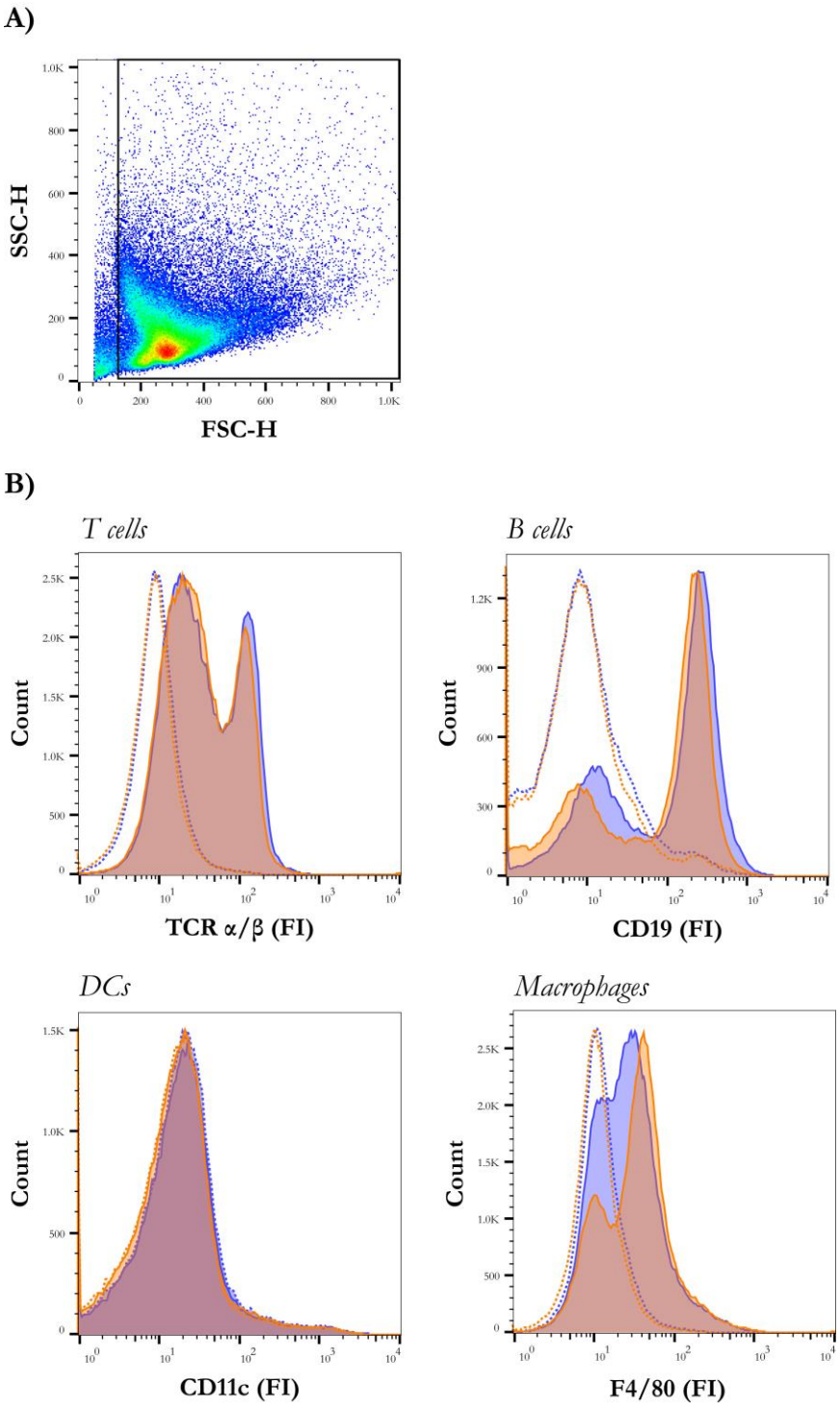

Figure 32: **Splenocyte cell type composition is unchanged after immunisation with LPS.** A) Splenocytes were gated by size (FSC) and granularity (SSC) to exclude dead cells. B) The histograms in B represent the cell type composition of control (indicated in blue) and LPS splenocytes (indicated in orange). An overlap of the curves indicates similar frequencies of the respective cell type. The antibody stainings indicated on the X-axis are represented with solid lines and the respective isotype controls with dotted lines. There is no obvious difference in the splenocyte cell composition between healthy and LPS-challenged mice.

4.3. Discussion

The development of a mass spectrometry based method able to identify plasma membrane proteins with labile disulfide bonds and to quantify their reduction (*Chapter III - Quantitation of labile disulfide bond cleavage*) has provided a valuable tool to study the redox plasma membrane proteome. Although an increase in thiol levels following immune activation was first observed about 20 years ago, this could not be linked to specific proteins until now. This chapter presents the first identification of proteins that are affected by changes in the redox environment following immune activation.

The results show that several cell surface proteins contain labile disulfide bonds that are reduced to a significant extent during immune activation (Figure 28, Table 5). Amongst other proteins, SH-IQ identified CD44 and CD132 which both contain labile disulfide bonds whose reduction inhibits their function (19, 20). Their identification further increases the confidence in the SH-IQ method to confidently identify labile disulfide bond containing proteins *in vitro*. However, there is a concern that the method could be picking up on protein abundance changes induced by T cell activation. Wollscheid *et al.* have examined the cell surface proteome of Jurkat T cells in response to CD3/CD28 co-stimulation after 24 hours (92). They detected the strong upregulation of the T cell activation marker CD69 and the downregulation of the TCR as would be expected. Furthermore, the data showed the differential abundance of an additional 45 proteins in response to activation with only 16 proteins changing in their abundance more than twofold. The smallest fold change SH-IQ can confidently identify when analysing three independent experiments is twofold. Therefore, the protein abundance fold change would have to be greater than two to marginally influence the SH-IQ results. None of the proteins with an increased abundance after T cell activation were identified as containing a labile disulfide bond in this experiment, confirming that the detection of labile disulfide bond cleavage by SH-IQ is independent of protein abundance changes induced by T cell activation.

Labile disulfide bond reduction in different proteins has shown different kinetics (Figure 28). To understand if the rate of disulfide bond reduction is dependent on protein abundance, the results have been compared to the cell surface protein atlas (CSPA) (124). If there was a correlation between abundance and rate of reduction, a highly abundant protein would get reduced before a low abundant protein according to the hypergeometric distribution (The hypergeometric distribution is a discrete probability distribution that describes the probability of *k* successes (reduction of protein A) in *n* draws (10 cycles of thiol isomerase reduction), without replacement (once a disulfide bond is reduced it cannot be reduced again), from a finite population of size *N* (total number of proteins A and B) that contains exactly *K* successes (total number of protein A), wherein each draw is either a success or a failure. $P(X=k)=\frac{\binom{K}{k}\binom{N-K}{n-k}}{\binom{N}{n}}$), regardless of how labile the disulfide bonds are. The CSPA is a collection of 41 human and 31 mouse cell surface proteomes that not only contains information on what proteins are present on the cell surface of a specific cell type but more importantly also about their abundance. The data obtained in this chapter was compared to the Jurkat T cell data in the CSPA. The 254 cell surface proteins identified in the MLR have been ranked from 1 to 254 with increasing abundance. ICAM1 and CD132 with highly labile disulfide bonds are ranked 35 and 76. Signalling lymphocytic activation molecule 1 (CD150), semaphorin-4D (CD100) and 4F2 (CD98) with less labile disulfide bonds are ranked 129, 90 and 105, indicating higher abundances than both ICAM1 and CD132. This illustrates that disulfide bond reduction is probably independent of protein abundance. Factors that may contribute to the kinetics of disulfide bond reduction are disulfide bond configuration, accessibility and thiol isomerase specificity.

It was then further investigated whether labile disulfide bond reduction is occurring *in vivo* when the immune system is challenged. The quantitative analysis of labile disulfide bond reduction was hampered by poor cell viability. Nevertheless, the experiment with high cell viability showed that a number of plasma membrane proteins is redox-controlled during inflammation. Some of the proteins identified to contain labile disulfide bonds (Table 6) partially overlap with proteins identified in the *in vitro* model (Figure 28) and others are novel candidates.

Chapter V – Labile disulfide bonds in ADAM17 and gp130

5.1. Introduction

The reduction of labile disulfide bonds by thiol isomerase enzymes is a way of post-translationally controlling plasma membrane protein function. There is evidence that the cleavage of such functional disulfide bonds leads to conformational changes altering protein function. An example of this is the plant peptidyl-prolyl cis-trans isomerase (AtFKBP13) that loses its peptidyl-prolyl isomerase activity upon thioredoxin reduction. The change in conformation upon labile disulfide bond reduction was captured by crystallising the oxidised and reduced form of the AtFKBP13 (PDB codes 1Y0O and 1U79 for oxidised and reduced AtFKBP13, respectively) (125). Another example of a protein where oxidised and reduced states differ in structure is plasminogen (PDB: 4DUR) (126). Interestingly, the reduced disulfide bond between Cys462 and Cys541 is present in the labile -/+RHHook in the oxidised molecule. It is likely that labile disulfide bond reduction in other proteins similarly affects their structure and function.

Both, ADAM17 (a disintegrin and metalloproteinase 17) and gp130 (glycoprotein 130) are plasma membrane proteins that were identified in screens to identify proteins with labile disulfide bonds (26). The objective of this chapter was to identify the labile disulfide bonds in ADAM17 and gp130 by mass spectrometry applying a differential cysteine labelling technique that uses the isotope pair NEM and d5NEM and to investigate the functional consequences of labile disulfide bond reduction. If these proteins indeed contain labile disulfide bonds, their function could be redox-regulated allowing the cells to post-translationally control their activity.

5.1.1. ADAM17

ADAMs are a family of transmembrane proteins that contain a metalloproteinase domain that can be involved in ectodomain shedding of plasma membrane proteins (127). They share a common multidomain structure that contains an N-terminal catalytic metalloproteinase (MP) domain that is followed by a disintegrin (DS), a cysteine-rich (Cys) and a trans-membrane (TM) domain (Figure 33).

ADAM17 or tumor necrosis factor-α converting enzyme (TACE) activity has been shown to be redox sensitive, H_2O_2 activating and PDI and DTT inactivating the protein (128). ADAM17 possesses 16 disulfide bonds that can potentially be modulated by thiol isomerases or reducing agents. The location of the susceptible disulfide bond(s) has been mapped to the DS and/or Cys domains using antibodies. The antibody specific for the membrane proximal domain (DS+Cys) no longer bound to ADAM17 after reduction, indicating a conformational change mediated by labile disulfide bond reduction (129). Moreover, PDI could be shown to induce a rearrangement of disulfide bonds in the Cys domain, leading to a conformational change within the domain (Figure 43) (130). Therefore, it was suggested that labile disulfide bond reduction in the DS and/or Cys domains leads to ADAM17 entering a closed, inactive conformation in which the metalloproteinase domain is inaccessible for substrates (Figure 33 A). The role of the three disulfide bonds in the catalytic MP domain, however, haven't been studied yet. It is possible that the reduction of a labile disulfide bond in the catalytic MP domain leads to a conformational change rendering ADAM17 inactive (Figure 33 B).

ADAM17 is involved in the shedding of the cytokine TNFα, the cytokine receptors TNF-R and IL-6R and the adhesion molecules L-selectin and ICAM-1 (131). TNFα is produced as a transmembrane protein that is released by ADAM17 to induce signalling through TNF receptor. It is thought that only soluble TNFα possesses pro-inflammatory activity but not membrane bound protein as transmembrane TMFα protects mice against inflammation (132). IL-6 signalling has been shown to be affected by ADAM17-dependent IL-6Rα shedding (133). Soluble IL-6Ra can then induce trans-signalling on cells that don't express IL-6Rα themselves but the common signalling receptor gp130. Furthermore, ADAM17 is involved in the shedding of the cell adhesion molecule L-selectin (134) which controls the adhesion and migration of activated lymphocytes (135).

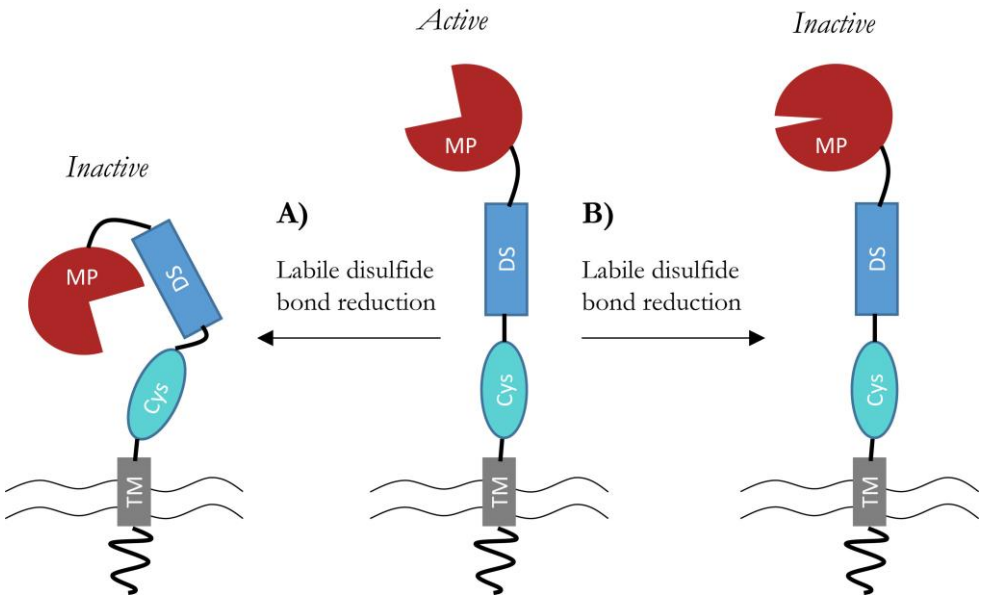

Figure 33: **ADAM17 activity is redox-controlled.** ADAM17 labile disulfide bond reduction was shown to inhibit shedding of substrates such as L-selectin (136). A) Based on antibody-mapping it was proposed that the inhibition is caused by labile disulfide bond reduction in the DS and/or Cys domain leading to a closed, inactive conformation of ADAM17. B) However, it is also possible that the reduction of a labile disulfide bond in the metalloproteinase domain causes a structural change in the catalytic site directly inactivating ADAM17.

ADAM17 domains from N- to C-terminus: MP: metalloproteinase domain, DS: disintegrin domain, Cys: cysteine-rich domain, TM: trans-membrane domain.

5.1.2. Gp130 and IL-6 signalling

There are good data showing that CD132, the common gamma chain of several cytokine receptors, contains a labile disulfide bond which when reduced prevents IL-2 signalling [14]. This implies that CD132-mediated cytokine signalling may be regulated by redox changes during the immune response. Indeed, it was shown in this thesis that CD132 is redox-controlled during immune activation (Figure 28 A, *Chapter IV – Labile disulfide bonds are cleaved during immune activation*).

Gp130, the shared signalling subunit for the IL-6 family of cytokines, was identified alongside CD132 in screens of proteins with labile disulfide bonds (26), suggesting that this family of cytokine receptors may also be redox regulated.

Gp130 is the shared receptor for IL-6 type of cytokines that include IL-6, IL-11, IL-27, LIF (leukemia inhibitory factor), OSM (oncostatin M), CTNF (ciliary neurotrophic factor), CT-1 (cardiotrophin 1) and CLC (cardiotrophin-like cytokine) (137, 138). Like other shared cytokine receptors (*Appendix – Shared cytokine receptors*), cytokine specificity is mediated by the α (IL-6Rα, IL-11Rα) or β (OSMRβ, LIFRβ) receptor. The α receptors and LIFRβ are non-signalling whereas gp130 and OSMRβ are signal transducing receptors.

IL-6 type of cytokines are helix-bundle cytokines that contain 4 α helixes A, B, C and D that are oriented up, up, down, down. For IL-6 to induce signalling through gp130, a hexameric complex consisting of two gp130/IL-6Rα/IL-6 trimers has to assemble. In a first step, IL-6 engages with IL-6Rα that then bind to gp130 (Figure 34) (139). Neither IL-6 nor IL-6Rα alone have a measurable affinity to gp130. There are 20 two-fold contact interfaces in the hexameric complex, four between gp130 and IL-6, four between gp130 and IL-6Rα and two between IL-6Rα and IL-6. It is hypothesised that labile disulfide bond reduction in gp130 prevents gp130 binding to IL-6Rα/IL-6 and thereby inhibits the formation of the functional, hexameric signalling complex (Figure 34).

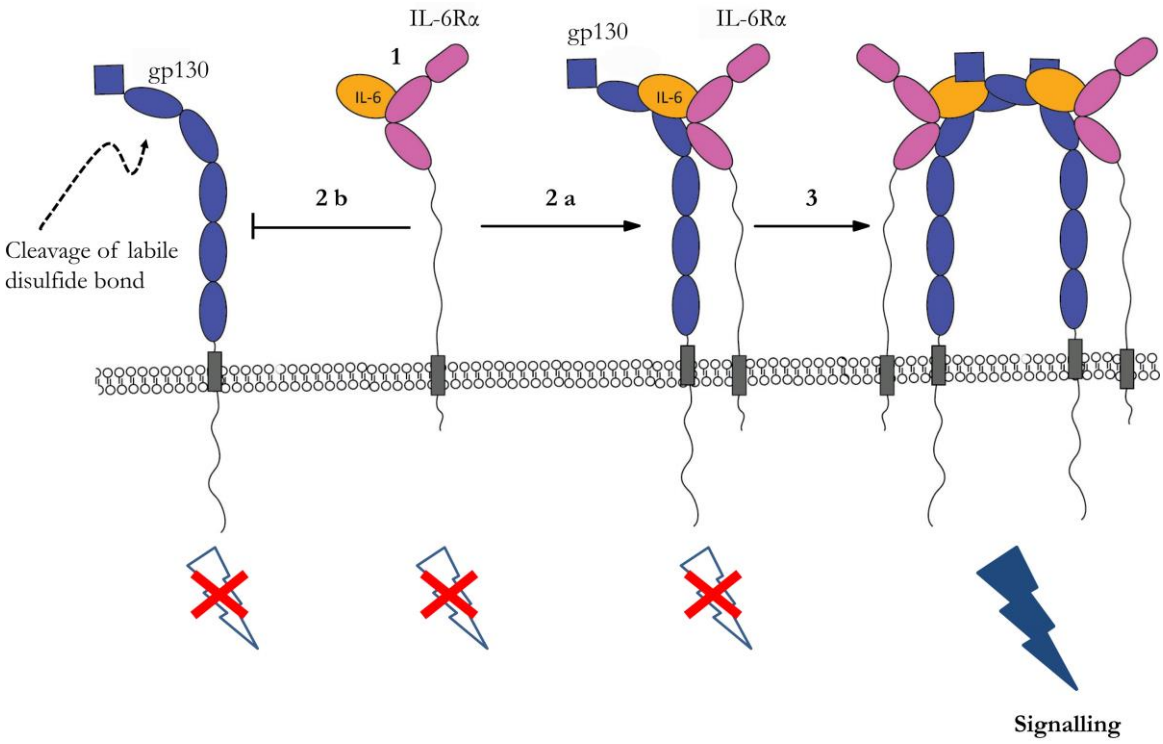

Figure 34: **IL-6 signalling complex formation and functional implication of redox modulation.** In a first step, IL-6 binds to IL-6Rα (1) which then bind to gp130 (2 a). The gp130/IL-6Rα/IL-6 trimer then has to form a dimer with another trimer to form the hexameric, functional signalling complex (3). It is hypothesised that IL-6 signalling can be inhibited by the cleavage of a labile disulfide bond in the shared cytokine receptor gp130 preventing the assembly of the functional signalling complex (2 b).

Once the hexameric signalling complex is formed, the intracellular gp130 tails are brought into close proximity which leads to the activation of the constitutively associated JAKs (Janus kinases). IL-6 signals through three cascades JAK-STAT, Ras-Raf-MEK-Erk and PI3K/Akt with JAK-STAT being the most prominent among them. Activation of JAK leads to the phosphorylation of gp130 and the recruitment of STAT3 (signal transducer and activator of transcription) which becomes phosphorylated by JAK. Once phosphorylated, STAT3 dimerises and translocates to the nucleus where it regulates transcription of target genes (Figure 35) (140). Moreover, SHP-2 is recruited to phosphorylated gp130 in a JAK-dependent manner. Phosphorylated SHP-2 then binds GRB2 (growth-factor-receptor-bound-protein) (141) and recruits SOS to the receptor complex which then activates the Ras-Raf-MEK-Erk cascade (Figure 35).

While gp130 is ubiquitously expressed, the IL-6Rα is only present on a restricted number of cell types such as T cells, B cells, monocytes, macrophages, neutrophils and hepatocytes. For signal transduction, the IL-6Rα can either be membrane bound or soluble, classifying the signalling into classical and trans-signalling.

IL-6 is a pro-inflammatory cytokine that promotes acute-phase protein production and expansion and activation of T cells and differentiation of B cells. Moreover, IL-6 is implicated in the pathogenesis of various inflammatory diseases such as Crohn's disease, Parkinson and rheumatoid arthritis (142) in which IL-6 serum levels are increased. IL-6 has also been found to be upregulated in tumours which might promote tumour growth and survival. This makes IL-6 signalling an interesting research target with the aim of treating inflammatory diseases and cancer.

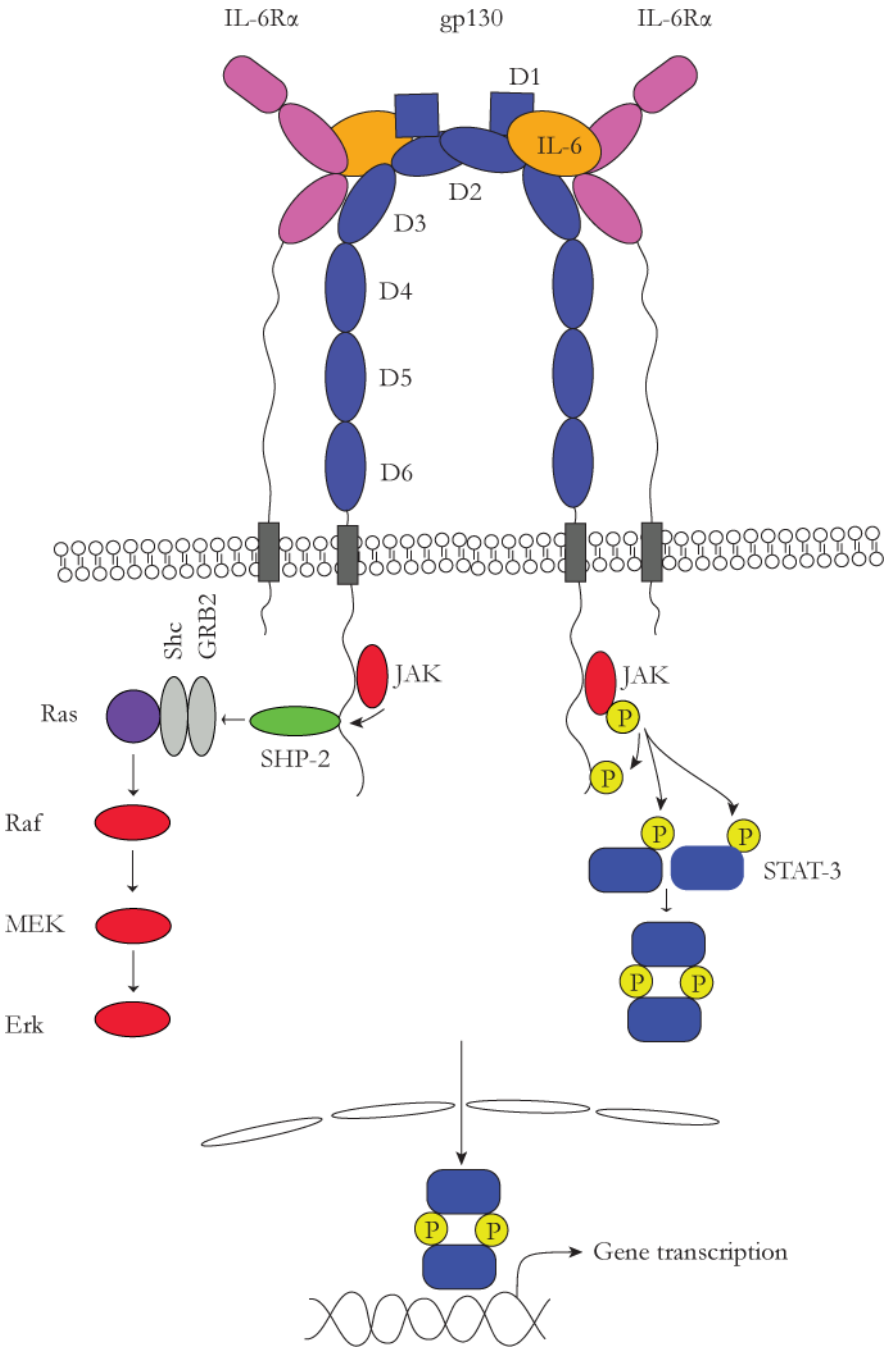

Figure 35: **Major IL-6 signalling cascades through JAK-STAT and Ras-Raf-MEK-Erk.** Gp130 is a transmembrane glycoprotein with one Ig-like domain (D1), two cytokine-binding homology domains (D2-D3) and three fibronectin-type III domains (D4-D6) in the extracellular portion (138). The N-terminal domains D1 and D2, which are needed for ligand binding (139), possesses eight cysteines that are linked via disulfide bonds (143). The gp130 intracellular tails are brought into close proximity in the hexameric signalling complex, allowing trans-phosphorylation of tyrosine residues on gp130 by the associated JAKs (144). Tyrosine phosphorylation creates docking sites for STATs and SHP-2. Once STATs are phosphorylated they dimerize and translocate into the nucleus where they are responsible for transcription of target genes. SHP-2, on the other hand, activates the Ras-Raf-MEK-Erk signalling cascade.

5.2. Results

5.2.1. Free cysteines are formed upon ADAM17 reduction with TCEP and thioredoxin

To investigate whether ADAM17 contains labile disulfide bonds, recombinant human ADAM17 was exposed to different reducing conditions (TCEP, thioredoxin and complete reduction under denaturing conditions), free cysteines labelled with the thiol reactive Alexa-633-C5-Maleimide fluorophore, analysed by gel electrophoresis and fluorescence detected with the infrared imaging system Odyssey Sa.

Native ADAM17 (51 kDa) contains 32 disulfide-bonded cysteines and was thus not labelled with the thiol reactive Alexa-633-C5-Maleimide dye and not be visible in the infrared image as a consequence (Figure 36 A, Control). Coomassie blue staining of the protein gels confirmed the presence of native ADAM17 in the control sample (Figure 36 B, Control).

When ADAM17 was exposed to mild reducing conditions such as 2.5 mM TCEP for 15 min, ADAM17 was labelled with Alexa-633-C5-Maleimide and appears at a molecular weight of approximately 60 kDa in the infrared scan (Figure 36 A, TCEP). Reduction of each disulfide bond leads to the addition of two Alexa-633-C5-Maleimide labels to ADAM17 and increase the molecular weight by 2.6 kDa (1.3 kDa per Alexa-633-C5-Maleimide label). The mass shift observed corresponds to the addition of 10 kDa in form of the Alexa-633-C5-Maleimide label which translates to the reduction of three to four disulfide bonds.

Thioredoxin reduction (1 µM TRX for 90 min at 37° C) of ADAM17 had a similar effect (Figure 36 A, TRX). To keep thioredoxin in its reduced state, capable of continuously reducing ADAM17, NADPH and thioredoxin reductase were added to the system to recycle oxidised thioredoxin (Figure 3). Thioredoxin appears at a molecular weight of 17 kDa (14 kDa plus 2.6 kDa Alexa-633-C5-Maleimide as it contains two Cys) and thioredoxin reductase at around 75 kDa (55-67 kDa, plus 3.9 kDa Alexa-633-C5-Maleimide as it contains three Cys) in the infrared image (Figure 36 A, TRX and TRX control).

Fully-reduced (500 µM DTT in 0.1 % SDS, 95° C for 15 min) ADAM17 shows a major band around 90 kDa in the infrared scan, corresponding to the reduction of all 16 disulfide bonds and a second band around 60 kDa, corresponding to the reduction of three to four disulfide bonds (Figure 36 A, Fully-reduced).

This indicates that there are likely to be one to four labile disulfide bonds in ADAM17 that are reduced by mild reducing conditions.

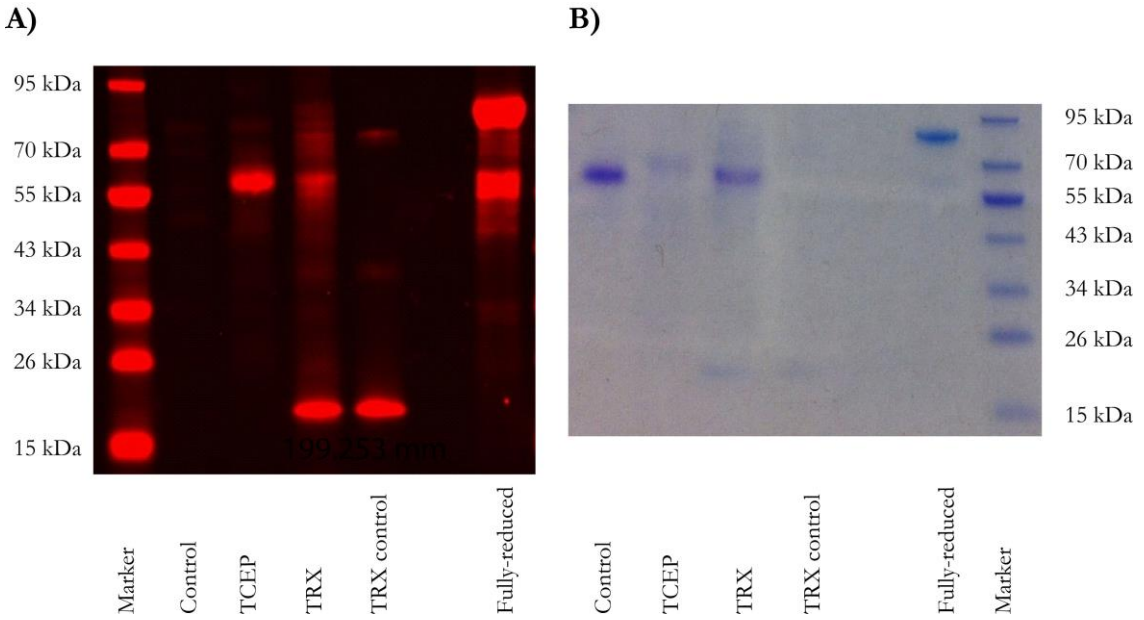

Figure 36: **ADAM17 labile disulfide bond reduction followed by SDS-PAGE.** 1 µg recombinant human ADAM17 (51 kDa, 32 disulfide-bonded cysteines) was exposed to different reducing conditions, free cysteines labelled with 2.5 mM Alexa-633-C5-maleimide fluorophore (1.3 kDa) and subjected to non-reducing SDS-PAGE. A) Free cysteines were imaged in the 700 nm channel on the LiCor stystem. No free cysteines can be detected in native ADAM17 (control). Fully-reduced (500 µM DTT in 0.1 % SDS, 95° C for 15 min) ADAM17 runs at a molecular weight of about 90 kDa, corresponding to ADAM17 labelled with 32 Alexa-633-C5-Maleimide labels, and at 60 kDa which represents partially reduced ADAM17. When ADAM17 is exposed to mild reducing conditions (2.5 mM TCEP or 1 µM thioredoxin together 0.1 pM thioredoxin reductase and 200 µM NADPH), a partial reduction of the protein can be observed (TCEP and TRX). The band at around 17 kDa in the TRX and TRX control corresponds to TRX (contains two Cys) and the faint band at around 75 kDa to TRX reductase (contains three Cys). This assay shows that one to four labile disulfide bonds are present in ADAM17. B) Coomassie blue staining of the protein gel confirms the presence of ADAM17 in all conditions (Control, TCEP, TRX and fully-reduced but not in the TRX control).

5.2.2. Labile disulfide bond is located in the ADAM17 metalloproteinase domain

To identify the labile disulfide bond in ADAM17, differential labelling of cysteines with isotope pair NEM and d5NEM combined with mass spectrometry analysis was carried out. Labelled peptides have almost identical retention times and thus identical ionisation efficiencies, allowing the calculation and comparison of peak intensities using MaxQant. As described before, ADAM17 was reduced with either TCEP or thioredoxin or was treated with buffer as a control and the redox state kinetically trapped by alkylating free cysteines with NEM instead of Alexa-633-C5-Maleimide. The protein was then denatured, fully reduced, all remaining cysteines labelled with d5NEM and the peptides analysed by mass spectrometry. The cysteines that were involved in a labile disulfide bond that was reduced will carry the NEM modification, whereas the remaining cysteines will be d5NEM modified. This allows the quantitation of the degree of reduction by calculating the ratio of NEM to d5NEM labelled peptide. A structural disulfide bond will not be NEM labelled and therefore show a low NEM/d5NEM ratio, whereas a labile disulfide bond will be NEM labelled and thus show a higher NEM/d5NEM ratio.

The NEM/d5NEM ratio of cysteine-containing peptides in TECP or thioredoxin reduced sample is expressed relative to the respective NEM/d5NEM ratio observed in the control. Only one peptide (*EADLVTTHELGHNFGAEHDPDGLAE-Cys423*-APNEDQGGK) displays an increased NEM/d5NEM ratio after TCEP and thioredoxin reduction (20-fold and 3-fold, respectively) compared to the average ratios observed for TCEP and thioredoxin reduced peptides (3-fold and 1.3-fold, respectively) (Figure 37). This indicates that cysteine 423 is involved in a labile disulfide bond that is reduced by TCEP and thioredoxin. Only a few cysteines contained in the disintegrin and cysteine-rich domains could be unambiguously quantified because many of them are contained in peptides with multiple cysteines. Nevertheless, there is no indication that any of these cysteines that are found in multiple cysteine containing peptides are involved in labile disulfide bonds as their cumulative NEM/d5NEM ratio is indistinguishable from the TCEP or thioredoxin average NEM/d5NEM ratio. A TCEP reduced labile disulfide bond would be expected to show at least a 10-fold higher NEM/d5NEM ratio relative to the control based on results obtained from ADAM17 and CD44 using this differential NEM/d5NEM cysteine labelling technique. The multi cysteine-containing peptide would therefore still be represented with an at least 5-fold change assuming one labile cysteine in the peptide sequence.

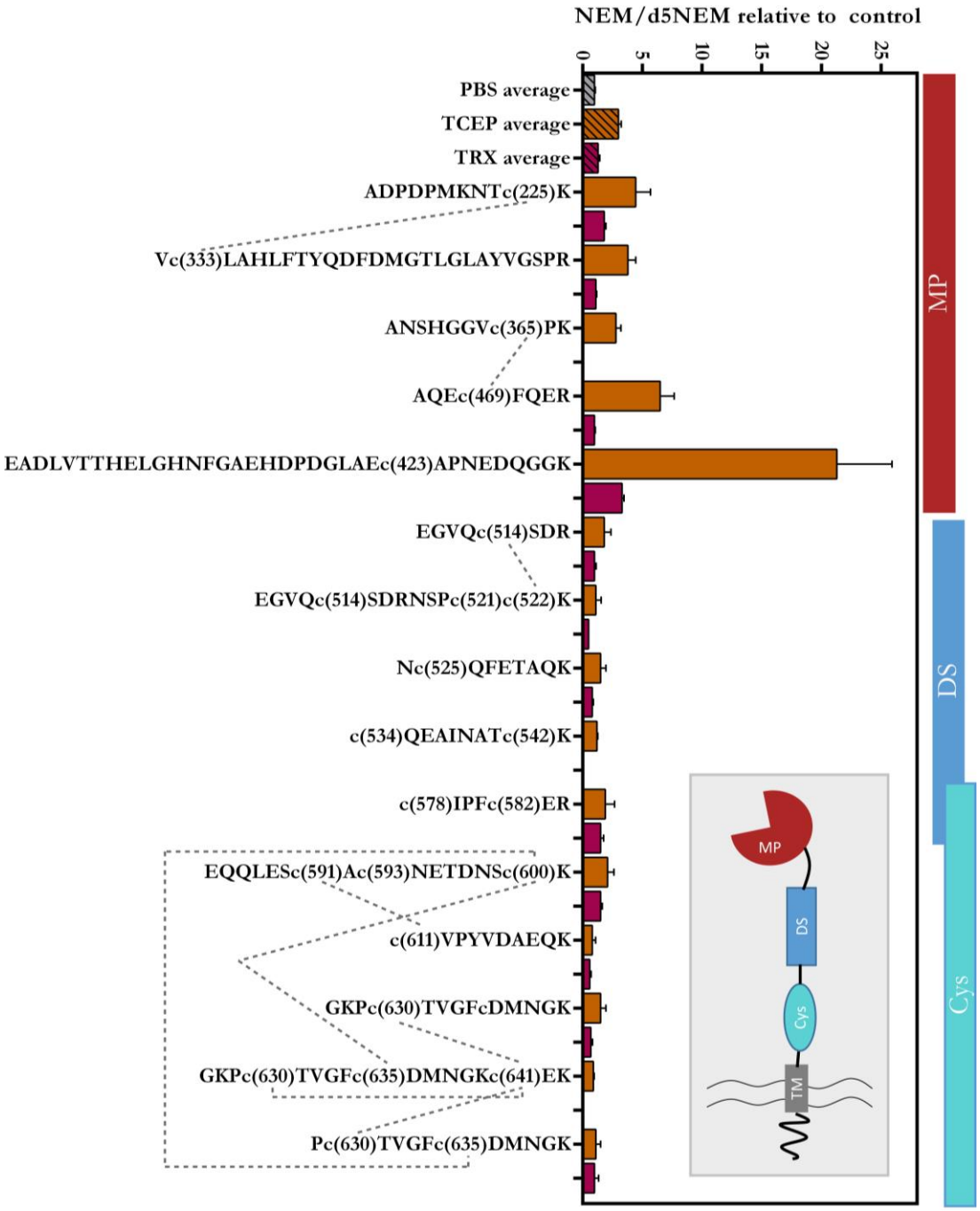

Figure 37: **Labile disulfide bond is located in the ADAM17 metalloproteinase domain.** To identify the labile disulfide bond(s) in ADAM17, the protein was reduced, labile cysteines labelled with NEM, fully denatured and reduced, the remaining cysteines labelled with d5NEM and the sample prepared for mass spectrometry analysis. The data was then analysed with MaxQuant (quantitation of NEM/d5NEM-peptides based on MS1 peak apex intensities). The graph shows the ratio of NEM to d5NEM abundance for the indicated cysteine-peptides normalised to the control. The disulfide bond between cysteine 423 and cysteine 453 was identified as a labile disulfide bond since cysteine 423 showed a 20-fold and 3-fold higher ratio compared to the control when reduced with 2.5 mM TCEP (orange bars) or 1µM thioredoxin together 0.1 pM thioredoxin reductase and 200 µM NADPH (purple bars), respectively. Each peptide was identified in 2-7 experiments. The error bars indicate SEM. Disulfide bonds between cysteines are indicated with dotted lines.

Structural analysis of the metalloproteinase domain disulfide bonds using the Disulfide Bond Analysis Tool from the P.J. Hogg laboratory (145) revealed that the disulfide bond between cysteine 423 and cysteine 453 is the most solvent accessible disulfide bond, which is a key factor determining disulfide bond reactivity (Figure 38 B). Furthermore, the labile disulfide bond between cysteine 423 and cysteine 453 is located in the catalytic domain of ADAM17 (Figure 38 A), linking a loop (red) to an α-helix. The reduction of this disulfide bond could lead to the release of the loop which might unfold into the catalytic domain blocking its access for substrates which could explain why ADAM17 shedding activity is negatively regulated by reducing conditions and thiol isomerases (129). The implications of this are discussed later in this chapter.

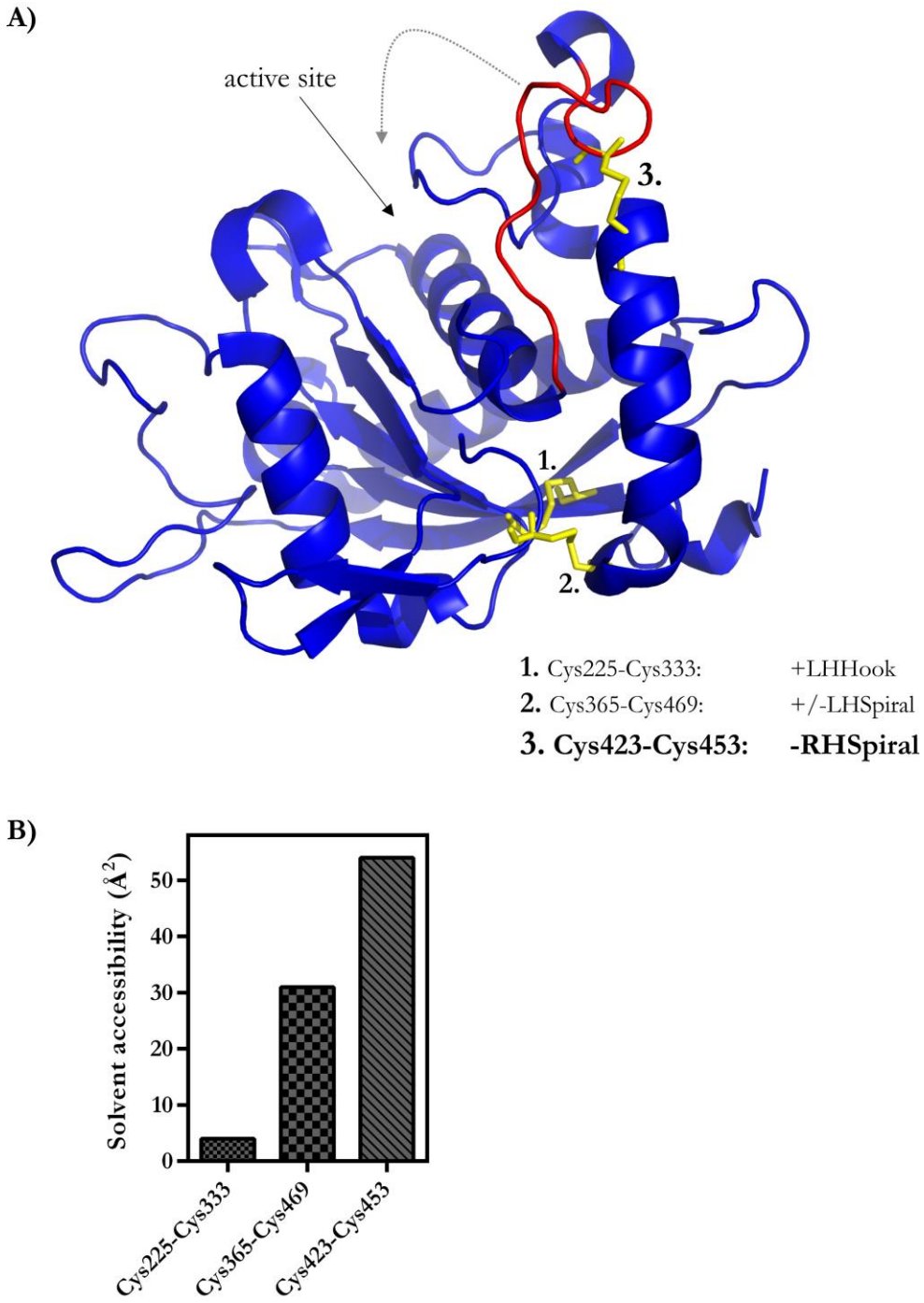

Figure 38: **Structural analysis of ADAM17 metalloproteinase domain.** A) ADAM17 possesses three disulfide bonds in the catalytic domain (Cys228-Cys333, Cys365-Cys469 and Cys423-Cys453) that are represented as yellow sticks. The labile disulfide bond between cysteine 423 and cysteine 453 (3.) links a loop (indicated in red) to an α-helix structure. Reduction of this disulfide bond could lead to the loop folding into the active site blocking ADAM17 function. PDB: 3EWJ, the inhibitor is removed from the structure for clarity reasons. B) Bioinformatic analysis of the catalytic domain disulfide bonds illustrates that Cys423-Cys453 shows the highest solvent accessibility with 54 Å² compared to 4 and 31 Å² for Cys225-Cys333 and Cys365-Cys469, respectively. This is the only parameter that indicates a labile disulfide bond in the catalytic domain. Neither of the disulfide bond configurations, dihedral strain energies nor Cα- Cα' distances points towards a labile disulfide bond.

5.2.3. Structural analysis of gp130 reveals potential labile disulfide bonds

Gp130 possesses four disulfide bonds that are located in the N-terminal domains D1 and D2: Cys6-Cys32, Cys26-Cys81, Cys112-Cys122 and Cys150-Cys160 (Figure 39 A). Both, gp130 D1 and D2 interact with IL-6 and/or IL6Rα in the hexameric gp130-IL-6Rα-IL-6 signalling complex (139). Disruption of any of those protein-protein interfaces could lead to the disintegration of the complex or prevent complex formation. It is therefore predicted that the reduction of a labile disulfide bond in gp130 D1 or D2 could lead to such a conformational change in gp130 affecting the signalling complex assembly (Figure 34).

Bioinformatics analysis of the disulfide bond properties (145) of monomeric gp130 (PDB: 3L5H) and gp130 in the hexameric signalling complex with IL-6Rα and IL-6 (PDB: 1P9M) showed that the disulfide bond between Cys6 and Cys32 is highly solvent accessible with 78 $Å^2$ in monomeric gp130 and 44 $Å^2$ in gp130 in the signalling complex (compared to 19 $Å^2$ in average structural disulfide bonds) (Figure 39 B). Although the disulfide bond is solvent accessible it does not display any of the other characteristics of labile disulfide bonds such as a short Cα-Cα' distance, high strain energy or labile structural configuration. On the contrary, Cys112-Cys122 shows a low solvent accessibility but it adopts the labile -RHStaple conformation and has a short Cα-Cα' distance. This makes Cys6-Cys32 and Cys112-Cys122 likely candidates for labile disulfide bonds that can respond to redox changes in the extracellular environment.

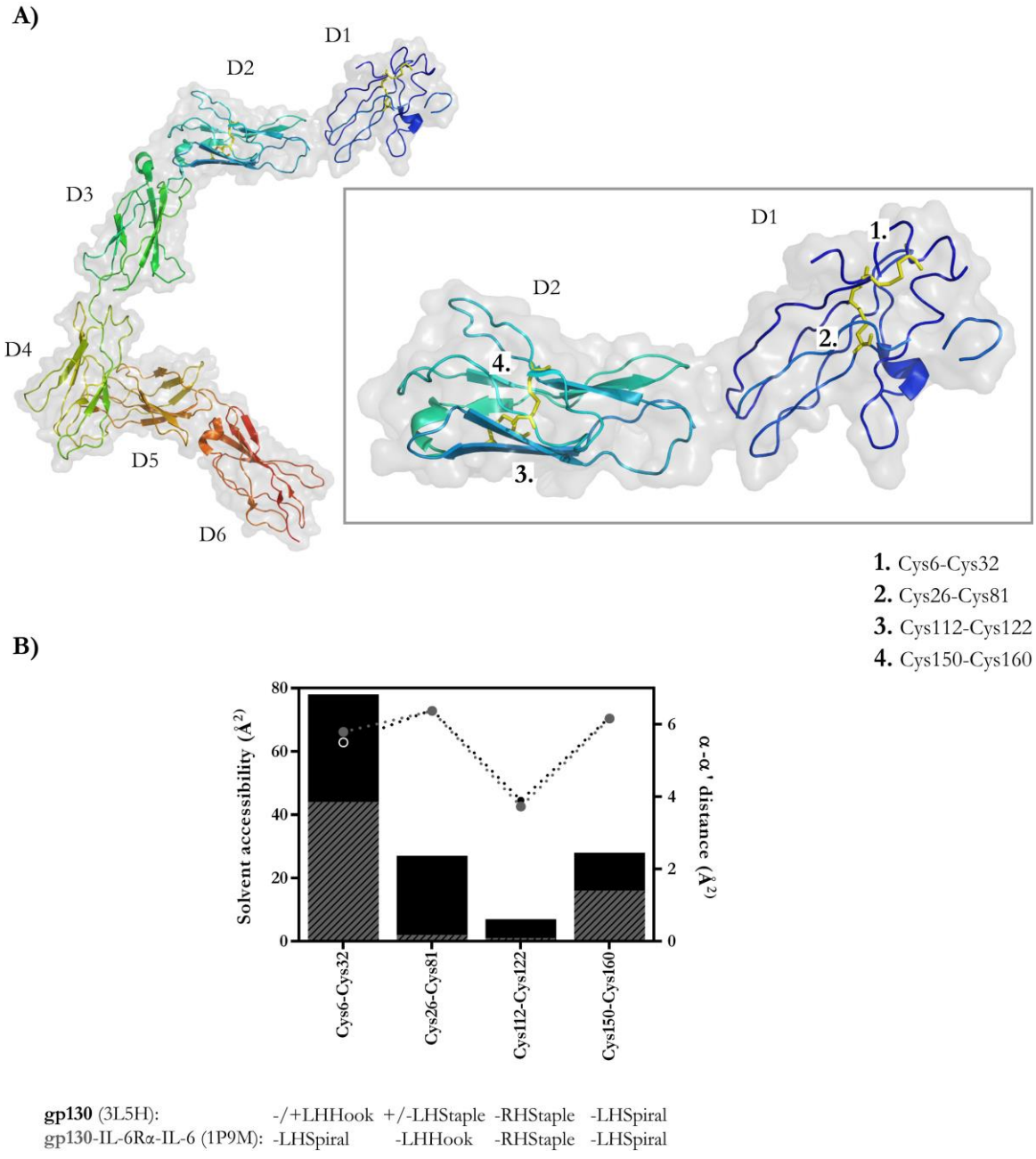

Figure 39: **Structural analysis of gp130 disulfide bonds.** A) Structural representation of gp130 ectodomain in the absence of IL-6 and IL-Rα (PDB: 3L5H). The four disulfide bonds (indicated in yellow sticks) in gp130 are located in D1 (Cys6-Cys32 and Cys26-Cys81) and D2 (Cys112-Cys122, Cys150-Cys160) which are both involved in IL-6 and/or IL-6Rα binding. B) Cys6-Cys32 is the only disulfide bond in gp130 that is solvent accessible with 78 Å² for monomeric gp130 (PDB: 3L5H) and 44 Å² for gp130 in the hexameric signalling complex (PDB: 1P9M). Solvent accessibility (bars) is shown on the left Y-axis and the Cα-Cα' distance (symbols) on the right Y-axis. Monomeric gp130 is indicated in black and gp130 in the hexameric complex in hatched. The disulfide bond Cys112-Cys122 shows a short Cα-Cα' distance and the labile signature configuration -RHStaple.

5.2.4. IL-6 induces tyrosine phosphorylation of STAT3

To investigate whether IL-6 signalling through gp130 is redox regulated, the strictly IL-6 dependent plasma cell line INA-6 has been chosen to study this (73). Due to the cells' dependency on IL-6, the JAK-mediated STAT3 phosphorylation is a direct readout of IL-6 signalling through gp130.

To determine the optimal IL-6 concentration that induces tyrosine phosphorylation of STAT3 in INA-6 cells, immunoblotting was used. No tyrosine phosphorylation is observed in unstimulated cells (Figure 40 A, 0 U/ml IL-6). After 15 min of IL-6 stimulation, STAT3 phosphorylation was induced by 30 U/ml IL-6 and increased in a dose dependent manner to maximal levels at 75-100 U/ml IL-6 (Figure 40 A). Higher concentrations did not further increase STAT3 phosphorylation (Figure 40 B).

100 U/ml IL-6 have therefore been chosen for all further experiments as it yields in maximal STAT3 phosphorylation in INA-6 cells after 15 min of stimulation.

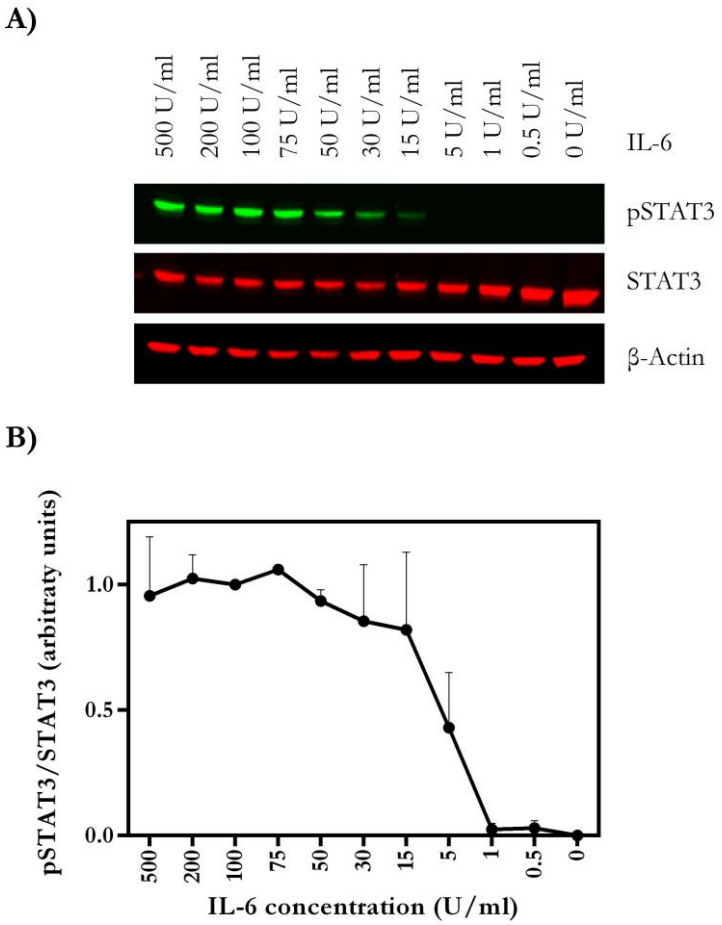

Figure 40: **Dose-dependent phosphorylation of STAT3 by IL-6.** INA-6 cells were treated with increasing concentrations of IL-6 (0 U/ml to 500 U/ml) for 15 min at 37° C. A) Lysate was resolved by SDS-PAGE and immunoblotted with antibodies specific to pSTAT3, STAT3 and β-Actin. B) The results are quantified by densitometry (Odyssey SA) calculating the ratio between pSTAT3 and STAT3. The error bars indicate SEM of two independent experiments. One of two experiments with similar results is represented in A).

5.2.5. IL-6 signalling is inhibited by thioredoxin through the JAK-STAT3 but not the Ras-Raf-MEK-Erk pathway

The next step was to assess if reducing conditions can inhibit IL-6 signalling through gp130 in INA-6 cells.

INA-6 cells were starved of exogenous IL-6, pre-incubated in the presence of either 2.5 mM TCEP (15 min) or 1 μM thioredoxin (90 min), washed and stimulated with 100 U/ml IL-6 over 30 minutes. STAT-3 phosphorylation was followed by immunoblotting and fluorescent intensity ratios of pSTAT3 to STAT3 calculated. IL-6 activates the STAT3 signalling pathway in a time-dependent manner with maximal STAT3 phosphorylation after 15 minutes (Figure 41 A). When exposing the cells to the chemical reductant TCEP, STAT3 phosphorylation occurs at the same rate as in the control. However, the enzyme thioredoxin inhibits STAT3 phosphorylation by half. These results are consistent with the observation that the enzymes thioredoxin, PDI and GLT can reduce gp130 but not TCEP (26).

That only thioredoxin but not TCEP inhibits IL-6 mediated STAT3 signalling might indicate that the labile disulfide bond whose reduction leads to the functional effect is not solvent accessible and can thus only be cleaved by thioredoxin. The bioinformatic analysis has resulted in two possible labile disulfide bonds, one of which being solvent accessible but not showing the labile configuration (Cys6-Cys32) and one not being solvent accessible but displaying the labile configuration -RHStaple (Cys112-Cys122). It is therefore likely that the labile disulfide bond whose reduction results in the observed functional effect is Cys112-Cys122.

To show that thioredoxin treatment of INA-6 cells does not generally affect protein phosphorylation, the IL-6 independent phosphorylation of constitutively phosphorylated Erk1/2 was studied (73). The lysate of control and reduced INA-6 cells was immunoblotted for Erk1/2 and pErk1/2. Both, control and reduced INA-6 cells show the same levels of pErk1/2 throughout the time-course (Figure 41 B). This confirms that IL-6 independen Erk1/2 signalling is not affected by thioredoxin.

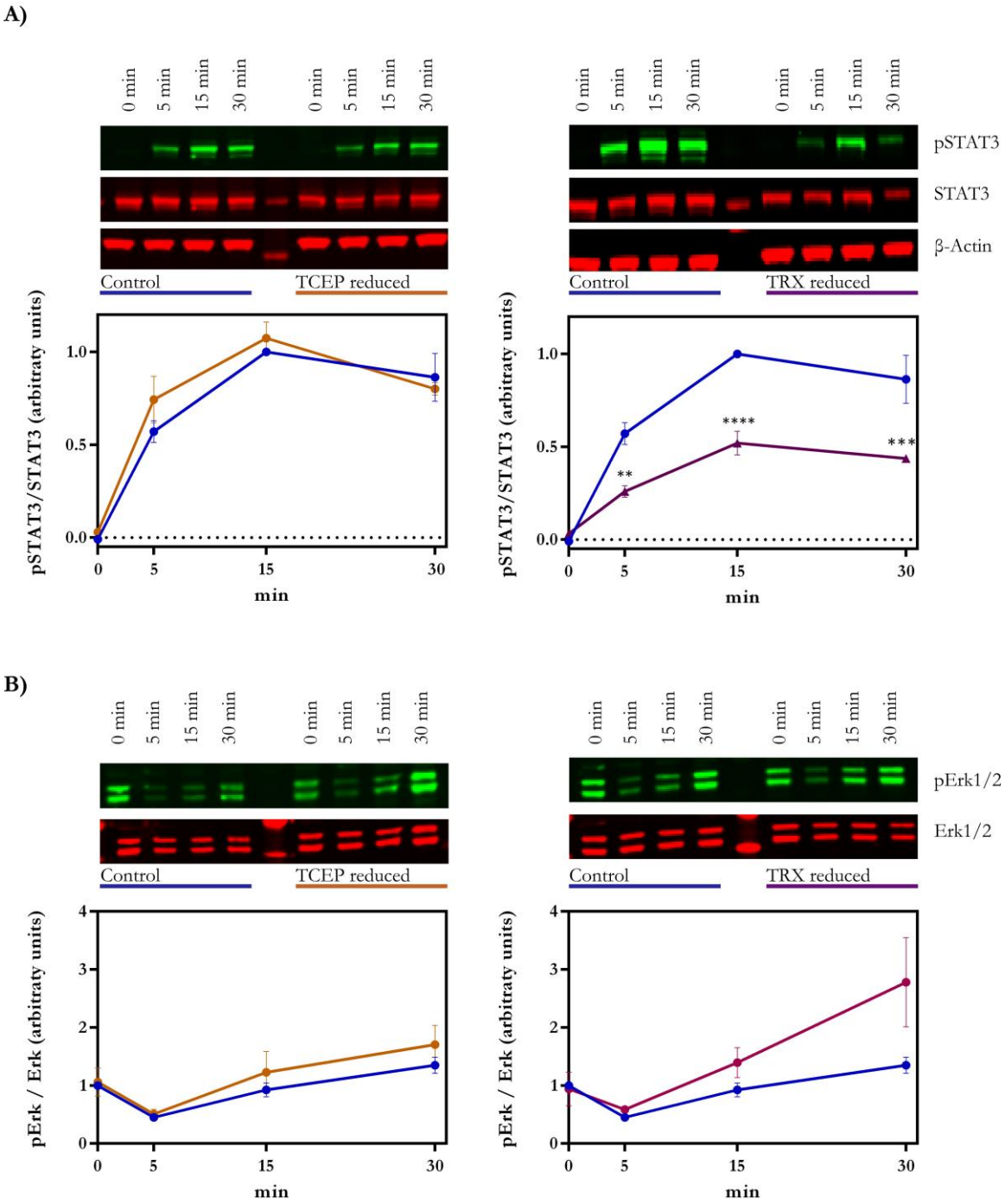

Figure 41: **IL-6 signalling through JAK-STAT but not Ras-Raf-MEK-Erk is inhibited by thioredoxin.** INA-6 cells were stimulated with 100 U/ml IL-6 over 30 min in the presence or absence of reducing conditions (pre-incubated with 2.5 mM TCEP for 15 min or 1 µM thioredoxin together 0.1 pM thioredoxin reductase and 200 µM NADPH for 90 min). The lysate was resolved on SDS-PAGE and immunoblotted with specific antibodies to A) pSTAT3, STAT3 and βActin or B) pErk1/2 and Erk1/2. The results from three independent experiments were quantified by calculating the fluorescence ratios between either phosphorylated/unphosphorylated STAT3 or Erk1/2. The error bars indicate the SEM, the data was analysed using a two-way ANOVA and statistical significance between control and reduced samples indicated with asterisks. ** P <0.01, *** P <0.001 and **** P <0.0001

5.2.6. Thioredoxin inhibits IL-6 induced STAT3 phosphorylation in a time-dependent manner

I showed that the reduction of 2B4 T cells with TCEP leads to an increase of cell surface thiol levels (Figure 12). A similar effect was observed on INA-6 cells when reducing the cells with thioredoxin. Thiol levels increased in a time-dependent manner which is inversely proportional to IL-6 induced STAT3 phosphorylation (Figure 42 A and B). The longer the cells were exposed to thioredoxin, the less STAT3 was phosphorylated by 100 U/ml IL-6 in 15 min. After 90 min of thioredoxin reduction only half of the initial STAT3 is phosphorylated which is in agreement with the results obtained in the time course experiment before (Figure 40 A).

These results show that INA-6 cells have to be exposed to 1 µM thioredoxin for at least 90 min to reduce STAT3 phosphorylation by half. It is likely that reduction of other plasma membrane protein by thioredoxin takes a similar amount of time until enough of the protein is reduced to exhibit a functional effect.

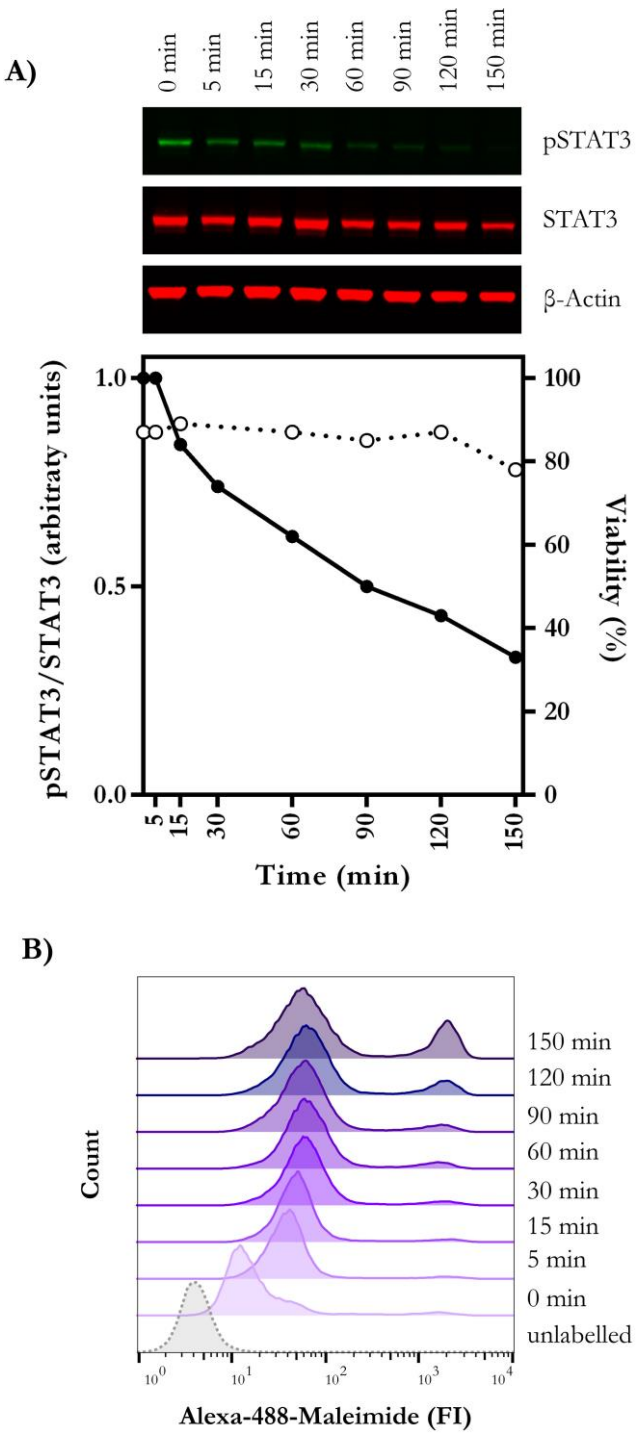

Figure 42: **Labile disulfide bonds are reduced on leukaemia cells by thioredoxin in a time-dependent manner.** INA-6 cells were reduced with 1 µM thioredoxin together 0.1 pM thioredoxin reductase and 200 µM NADPH over 150 min at 37° C. A) The cells were then stimulated with 100 U/ml IL-6 for 15 min. The lysate was resolved by gel electrophoresis and immunoblotted with antibodies specific to pSTAT3, STAT3 and βActin. B) After thioredoxin reduction, the cells were labelled with 25 µM of the fluorescent thiol reactive label Alexa-488-Maleimide and analysed by flow cytometry.

5.3. Discussion

5.3.1. ADAM17

ADAM17 activity has been shown to be inhibited by PDI and the labile disulfide bond(s) involved mapped to the non-catalytic domains using antibodies (128). Düsterhöft *et al.* showed that PDI induces a rearrangement of disulfide bonds in the ADAM17 membrane proximal cysteine-rich domain which leads to a conformational change within the domain (130). They propose that disulfide bonds Cys600-Cys630 and Cys635-641 in the cysteine-rich domain rearrange to Cys635-Cys641 and Cys600-Cys630 under reducing conditions, leading to a closed, inactive conformation of ADAM17 (Figure 33 A). The N-terminal part of the cysteine-rich domain, however, doesn't seem to change structurally between the native and reduced protein (Figure 43) (130) and it is therefore difficult to see how the rearrangement of the disulfide bonds in the C-terminal part of the cysteine-rich domain could influence the orientation of the N-terminally adjacent catalytic domain. Since the ADAM17 membrane proximal domain has been shown to be involved in substrate binding (146–148), it is more likely that the rearrangement of disulfide bonds in this domain affects substrate recognition rather than protein shedding activity.

In this study I have identified a labile disulfide bond that is reduced in the catalytic domain of ADAM17 by TCEP and thioredoxin (Figure 38 C, Cys423-Cys453). The reduction of the disulfide bond Cys423-Cys453 could lead to the release of the loop that it anchors to an α-helix (Figure 38 A), allowing it to fold into the active site inhibiting ADAM17 catalytic function. I therefore propose that ADAM17 inhibition through labile disulfide bond reduction is caused by a conformational change in the catalytic domain (Figure 33 B) rather than the formation of a closed conformation (Figure 33 A). However, it may well be possible that ADAM17 reduction impairs both substrate shedding and recognition.

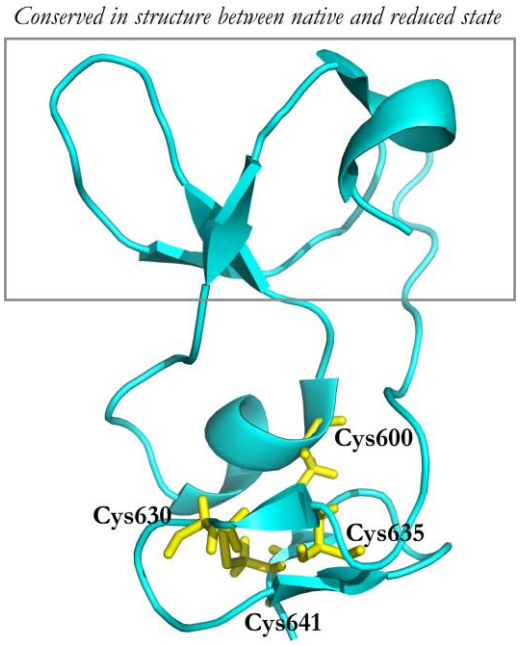

Figure 43: **Reduced ADAM17 cysteine-rich domain structure.** Structure of the reduced ADAM17 cysteine-rich domain with disulfide bonds Cys630-Cys641 and Cys600-Cys635 indicated in yellow (PDB: 2M2F). The structure of the native and reduced ADAM17 cysteine-rich domain is conserved in the N-terminal part of the domain (contained in the grey box) but not the rest of the domain (130). The disulfide bonds Cys600-Cys630 and Cys630-641 present in native ADAM17 have been found to rearrange to Cys630-Cys641 and Cys600-Cys635 under reducing conditions, leading to the observed conformational changes in the C-terminal part of the cysteine-rich domain.

Although the identification of a labile disulfide bond in the ADAM17 catalytic domain is in contrast to what Willems *et al. (128)* suggested, it cannot be excluded by the antibody-based assay they performed. They assume that the antibodies used to detect the catalytic and non-catalytic domains only bind to the native (oxidised) but not the reduced form of the protein. However, it is possible that the antibody specific for the catalytic domain recognises an epitope facing away from Cys423-Cys453 and thus might not be sensitive to the reduction in this part of the domain. To answer this it would be necessary to map the epitope of the antibody as it is unknown.

ADAM17 is upregulated in most tumour cells and has been shown to be involved in ErB and pro-ErbB ligand shedding (149) which is implicated in the growth of many tumours (150). Therefore, inhibiting ADAM17 catalytic function by redox regulation could provide a novel target for cancer therapy.

5.3.2. Gp130

As a major acute phase regulator, IL-6 expression has to be tightly regulated and is only present at very low levels under physiological conditions. Dysregulation of IL-6 signalling is associated with inflammatory diseases such as rheumatoid arthritis, inflammatory bowel disease, multiple sclerosis and cancer (151) which are generally characterised by elevated IL-6 levels (152). Inhibiting IL-6 signalling, therefore presents a target to control those chronic inflammatory diseases.

In this chapter it could be shown that IL-6 signalling through gp130 is redox regulated by thioredoxin which inhibits IL-6 induced STAT3 signalling on leukaemia cells (INA-6). Chemical reduction with TCEP, on the other hand, had no effect on IL-6 mediated STAT3 signalling through gp130. This is consistent with the observation that LIF-mediated STAT3 signalling through gp130 is not affected the reducing environment generated by N-acetylcysteine (153). This could indicate that that the labile disulfide bond affected by thioredoxin is not solvent accessible and therefore not affected by chemical reduction. Bioinformatics analysis has identified two potential labile disulfide bonds based on high solvent accessibility (Cys6-Cys32) and labile -RHStaple configuration (Cys112-Cys122). Based on this it is likely that thioredoxin reduces the less solvent accessible -RHStaple disulfide bond Cys112-Cys122 because it would be expected that the solvent accessible Cys6-Cys32 would be affected by both enzymatic and chemical reduction. This illustrates that thiol isomerases might be able to access disulfide bonds that are not exposed to the surface providing a negative cross-talk mechanism for cytokine signalling.

Chapter VI – Discussion

6.1. Quantitative analysis of labile disulfide bond reduction using mass spectrometry

It has been known for about two decades that immune activation leads to an increase of cell surface thiols on leukocytes through labile disulfide bond reduction catalysed by thiol isomerases (27). Since then, the observation that free thiols increase upon immune activation and the involvement of thiol isomerases in this process have been confirmed by different research groups (30, 154, 155). All these studies make qualitative statements of over-all labile disulfide bond reduction in plasma membrane proteins but are not capable of allowing an insight into what proteins are affected and to what extent. To understand the role of labile disulfide bond reduction and its consequences it is crucial to identify proteins affected. This will help to develop an understanding of how cells use the post-translational modification of labile disulfide bonds to control plasma membrane protein function and how this is involved in regulating cellular responses.

Post-translational modifications can affect protein conformation, activity, stability, cellular location or a combination of these parameters. The best studied post-translational modifications are probably phosphorylation and ubiquitination. Although the identification of post-translational modification sites has become routine, it is still challenging to quantify the degree of modification. Most studies aim for relative quantitation comparing post-translational modification between health and disease. Since the identification and quantitation of post-translational modifications relies on a single peptide MS/MS spectrum rather than multiple as in protein quantitation, peptide quantitation is substantially more difficult than protein quantitation. To identify and quantify post-translational modifications, a high mass accuracy and resolution is required. Hybrid quadrupole-Orbitrap mass spectrometers such as the QExactive combine the high-resolution of the quadrupole with the high accuracy of the Orbitrap analyser for maximal sensitivity and accuracy. However, further enrichment of proteins and peptides is required for robust identification and quantitation of post-translational modifications. This can be achieved by affinity enrichment (e.g. antibody, IMAC) or chromatographic separation (e.g. TiO_2) and reverse phase liquid chromatography to increase the level of sensitivity. Quantitation is best achieved by comparing the peptide peaks (on MS or MS/MS level) between the conditions generating the area-

under-the-curve which directly relates to the abundance of the peptide (156, 157). To circumvent differences in ionization efficiencies and MS-detector responses between samples, quantitation of post-translational modifications is generally carried out on labelled sample. Differential isotopic or isobaric labelling introduces a specific mass tag that can be distinguished by the mass spectrometer on MS or MS/MS level (*Appendix - Quantitation methods in proteomics*).

The robust, label-free method to quantify labile disulfide bond reduction that I have developed in this thesis (*Chapter III - Quantitation of labile disulfide bond cleavage*) now allows the study of labile disulfide bond reduction in virtually any system of interest, including primary cells and tissues. Quantitation of labile disulfide bond reduction is crucial in determining which proteins are likely to be functionally affected. It is expected that only proteins reduced to a major extent affect cellular function. Indeed, proteins with known labile disulfide bonds such as CD132 and CD44 were shown to be highly reduced. I have used this method to identify proteins with labile disulfide bonds that are reduced during immune activation providing the first evidence that adhesion and cell signalling are redox-regulated in plasma membrane proteins during immune activation (*Chapter IV - Labile disulfide bonds are cleaved during immune activation*). Furthermore, the data showed that labile disulfide bonds are specifically cleaved on activated T cells but not on resting T cells which is in agreement with the observation that thioredoxin expression is increased in activated T cells (154). This indicates that labile disulfide bond reduction is a local phenomenon which can be used to control cellular activity.

Interestingly, a number of different thiol isomerase enzymes are secreted from activated immune cells including endoplasmic reticulum resident proteins, PDIs and thioredoxin domain-containing proteins (Figure 44) (158). Secretion can be detected as early as 8 hours after activation with no further accumulation of proteins over the following 8 hours. The constant levels of thiol isomerases after 8 hours of activation could either represent a balance between secretion and turn-over or an initial secretion and maintained protein levels. If thiol isomerases are rapidly turned over in the extracellular space this would mean that 'fresh', reduced thioredoxin is constantly available that can reduce labile disulfide bonds over extended periods of time. If the thioredoxin levels are constant, however, this would require the recycling of thioredoxin from its oxidised back to its reduced state for thioredoxin to catalyse more than one disulfide bond cleavage which is carried out by thioredoxin reductase utilising NADPH as electron donors (Figure 3). It is unclear which scenario is more likely since nothing is known about thiol isomerase's half-life in different cellular compartments apart from that thioredoxin has a half-life of less than 1 hour in the plasma (159). This might not be representative as small proteins such as thiol isomerases, are constantly filtered out of the blood by the kidney.

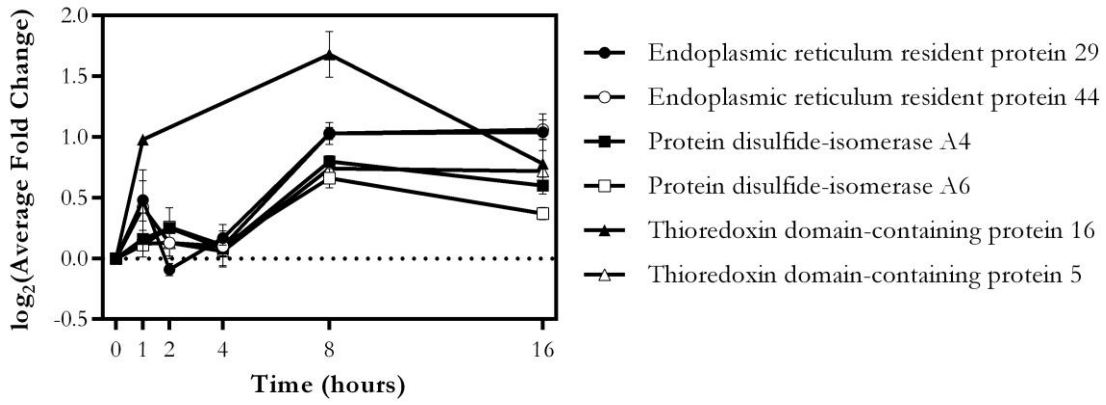

Figure 44: **Immune cells secrete thiol isomerases upon activation.** Macrophages were activated with LPS and the relative abundance of secreted proteins relative to unstimulated cells determined by mass spectrometry. The data acquired by Meissner *et al.* was analysed to gain information on thiol isomerase secretion upon activation. Endoplasmic reticulum resident proteins 29 and 44, protein disulfide isomerase A4 and A6 and thioredoxin domain-containing protein 16 and 5 accumulate in the supernatant of activated cells. The log_2(Average Fold Changes) are plotted versus time with the SEM indicated.
Analysis of data from supplementary database S1 (www.sciencemag.org/cgi/content/full/340/6131/475/DC1) (158).

6.2. Labile disulfide bonds are reduced in many different cell surface proteins

To understand how cells use the post-translational modification of labile disulfide bonds to control plasma membrane protein function to modulate cellular responses it is crucial to identify the key players. This allows one to speculate how redox-control of these proteins could affect cellular function during immune activation. In this section a selection of proteins that have been identified to contain labile disulfide bonds that are reduced to a substantial extent during immune activation (*Chapter IV - Labile disulfide bonds are cleaved during immune activation*) are discussed.

6.2.1. ICAM-1

ICAM-1 (intracellular adhesion molecule 1) is a plasma membrane protein composed of five immunoglobulin superfamily domains, a transmembrane domain and a short cytoplasmic tail. It can bind two leukocyte integrins, integrin $\alpha_L\beta_2$ (LFA-1) and $\alpha_M\beta_2$ via its N-terminal domains 1 and 3, respectively. Binding of ICAM-1 to $\alpha_L\beta_2$ mediates leukocyte adhesion and has been implicated in providing a co-stimulatory signal for naïve T cells but not (or only limited) activated T cells (160–162). This discrepancy in signalling function in naïve and activated T cells could be elicited by redox regulation of ICAM-1 in activated T cells. It has been shown that thiol isomerases modulate the redox cell surface proteome during immune activation by reducing labile disulfide bonds in plasma membrane proteins (27). I showed that a labile disulfide bond in ICAM-1 is indeed reduced during immune activation (Figure 28) supporting this hypothesis. Labile disulfide bond reduction in ICAM-1 might lead to a conformational change in the protein that ablates integrin $\alpha_L\beta_2$ binding and subsequent T cell co-stimulation which might provide a negative-feedback mechanism to prevent over-activation of T cells.

6.2.2. Integrins

Integrins are heterodimeric cell adhesion proteins composed of an α- and β-subunit binding to extracellular matrix proteins or counter receptors on other cells (163). Their activation has been proposed to be triggered by 'inside-out' signalling (164) which leads to conformational changes in the extracellular domain rendering the integrin active. Alternatively, redox research in platelets is suggesting that the active, open conformation of integrins is reached by disulfide bond isomerisation and/or reduction (Figure 45). It has been shown that the most abundant platelet integrin (integrin $\alpha_{IIb}\beta_3$) is activated by reducing condition leading to increased binding of its ligands fibrinogen, fibronectin and von Willebrand factor leading to thrombus formation (28). Integrin β3 contains 56 highly conserved cysteines forming 28 disulfide bonds. Disruption of only a single disulfide bond (Cys560-Cys583) in the epidermal growth factor domain (121) has been shown to lead to constitutively activated integrin $\alpha_{IIb}\beta_3$ (108). When integrin β_3 forms a complex with integrin α_v instead (integrin $\alpha_v\beta_3$), activity is additionally regulated by Cys523-Cys544 disulfide bond reduction (110). Integrin $\alpha_V\beta_3$ has been shown to associate PDI and to be PDI-dependent for activation (165). A further integrin that is implicated to be redox regulated is integrin α_4 (53). Integrin $\alpha_4\beta_7$ adhesion to its ligand MAdCAM-1 under low affinity and to a lesser extent high affinity conditions have been indicated to be affected by disulfide bond disruption in integrin α_4 affecting $\alpha_4\beta_7$-mediated rolling and cell adhesion (110).

Taken together, integrin activation seems to be controlled by thiol isomerases making them a potential therapeutic target. PDI inhibition, for example, has been shown to block thrombus formation (166). It is likely that other integrin-mediated events such as leukocyte migration can be controlled in a similar way.

In this thesis I identified both the known redox-regulated integrins β_3 and β_7 and the novel integrins α_2, α_L, β_1 and β_2. This illustrates that integrin activation is likely to be generally redox-controlled.

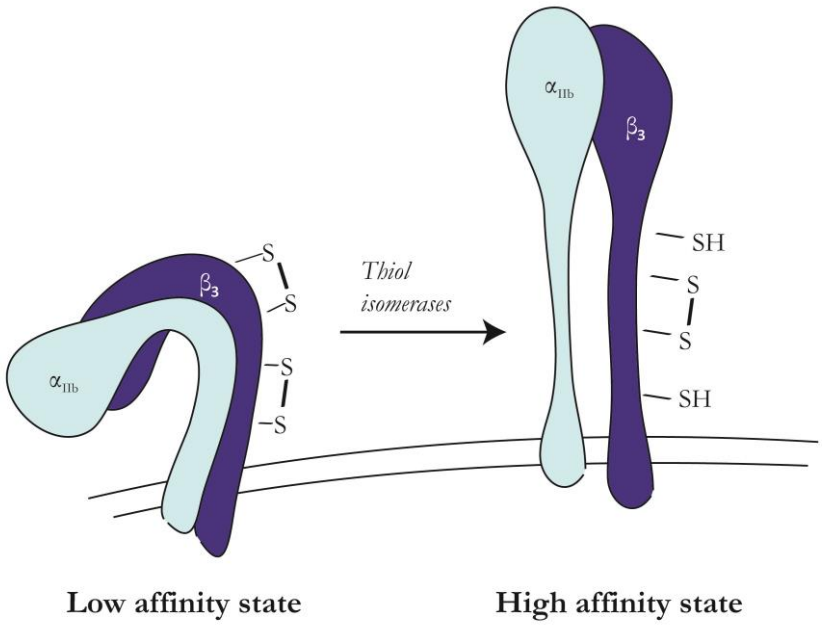

Figure 45: **Redox regulation of integrin $\alpha_{IIb}\beta_3$ activation on platelets.** Integrin $\alpha_{IIb}\beta_3$ has a low affinity for its ligands fibrinogen, fibronectin and von Willebrand factor in its oxidised, low affinity state. To reach its high affinity state, integrin $\alpha_{IIb}\beta_3$ needs to be activated by reducing conditions that lead to disulfide bond isomerisation and/or reduction.

6.2.3. Tumor necrosis factor receptor superfamily member 8 (CD30)

CD30 is a member of the tumor necrosis factor superfamily which is implicated in regulating the immune response by controlling the T helper cell population (167, 168). Although the exact mechanism of CD30-CD30 ligand (CD30L) interaction is still poorly understood, it has been observed that this balance is disrupted in different cancers by increased levels of soluble CD30 which blocks the CD30-CD30L interaction (169). CD30-CD30L interaction can further be regulated by thioredoxin. Thioredoxin reduces a labile disulfide bond in CD30, leading to a conformational change in the ligand binding site resulting in impaired binding to CD30L (111). This mechanism is likely to be exploited by various tumours as they show upregulated thioredoxin expression (170–177).

The combination of increased levels of thioredoxin and sCD30 in tumours might contribute to the higher frequencies of regulatory T cells which can supress self-antigen reactive T cells (178, 179) allowing tumour evasion (180). This suggests a possible therapeutic route by restoring CD30 signalling in cancer cells by inhibiting thioredoxin-mediated reduction of CD30. As a consequence, natural regulatory T cell levels would recover allowing cytotoxic T cells to recognise and kill the tumour.

6.2.4. CD44

CD44 is an adhesion receptor that is associated with leukocyte adhesion and migration (181). Its major ligand is the extracellular matrix component hyaluronic acid which is implicated in leukocyte migration into inflamed tissues. Dysregulation of CD44 is implicated in different diseases such as rheumatoid arthritis (182), lupus nephritis (183) and cancer (183) in which CD44 is up-regulated.

Rheumatoid arthritis severity can be reduced by CD44 antibodies that either cause CD44 shedding from the leukocyte cell surface or inhibit substrate binding leading to impaired leucocyte recruitment to the site of inflammation (184, 185). Similarly, inhibition of hyaluronic acid-CD44 interaction by i) small hyaluronic acid competitors, ii) soluble hyaluronic acid-binding proteins, iii) antibodies blocking hyaluronic acid-CD44 binding and iv) the inhibition of the post-transcriptional expression of CD44 are potential targets for cancer therapy . These examples illustrate the therapeutic potential of inhibiting CD44-haluronic acid binding in different diseases.

CD44 is upregulated and maintained on activated T cells (186, 187) whereas hyaluronic acid binding is only transient (188). This suggests that CD44-haluronic acid binding is ablated independently of receptor expression. T cell activation leads to an increased expression of thioredoxin and an increase of free cell surface thiols which is caused by thiol isomerase-mediated reduction of labile disulfide bonds (27, 154). Interestingly, I identified CD44 labile disulfide bond reduction upon T cell activation (*Chapter IV - Labile disulfide bonds are cleaved during immune activation*) which suggests that the CD44-hyaluronic acid binding is redox regulated. This hypothesis is further supported by the observation that CD44 no longer binds to hyaluronic acid after treatment with reducing agents such as thioredoxin (20). Moreover, Kellett-Clarke *et al.* identified the labile disulfide bond (Cys77-Cys99) in CD44 (20) applying the differential NEM/d5NEM alkylation strategy developed in this thesis (*Chapter V – Labile disulfide bonds in ADAM17 and gp130).*

CD44 is potentially not only involved in the hyaluronic acid-mediated recruitment of leukocytes to inflamed tissues but also in activation, differentiation and homeostasis of T cells (189, 190). CD44 was shown to signal via the PI3K/Akt pathway upon hyaluronic acid binding promoting survival and cell growth (191). Furthermore, hyaluronic acid signalling through CD44 is suggested to induce FoxP3 in

regulatory T cells which leads to an increase of IL-2 IL-10 and TGF-β1 production (192, 193). Redox regulation of CD44-hyaluronic acid binding thus offers a novel mechanism to regulate leukocyte migration and T cell activation, differentiation and homeostasis.

6.3. Implications of labile disulfide bond reduction in disease

Hypothesis: Labile disulfide bond reduction prevents over-activation of the immune system.

The redox control of plasma membrane proteins during immune activation seems to mainly affect activating molecules (CD132, gp130) and adhesion molecules (integrins, ICAM1, CD44). The signalling through activating molecules is switched-off when the receptors are reduced (i.e. gp130 (*Chapter V – Labile disulfide bonds in ADAM17 and gp130*) and CD132 (19)) and immune cell migration is inhibited under reducing conditions (194).

Therefore, I propose that immune cells use labile disulfide bond reduction to prevent over-activation of the immune system and excessive accumulation of leukocytes in sites of inflammation. This is crucial because although accumulation and activation of leukocytes is required for efficient pathogen elimination, uncontrolled infiltration is associated with chronic auto inflammatory diseases. Labile disulfide bond reduction might be the key to orchestrate the immune response in a way that the right response takes place at the right location at the right time.

Does the loss of redox control of immune cells lead to auto inflammatory diseases?

It would be interesting to apply the newly developed SH-IQ method to samples obtained from chronic inflammatory diseases such as inflammatory bowel disease or rheumatoid arthritis to elucidate how the redox control of plasma membrane proteins is affected in these conditions compared to the healthy state. It is possible that the redox-control is failing in auto inflammatory diseases, leading to the constitutive activation of the immune system and accumulation of immune cells in sites of inflammation. If that should be true it would provide a new handle for the treatment of inflammatory diseases by thioredoxin administration to restore the natural redox balance.

Indeed, it has been recently shown that administration of thioredoxin protects mice from LPS-induced endotoxic shock (159) through impaired leukocyte recruitment (195). Furthermore, it was

shown that LPS induced neutrophil adhesion to epithelial cells which can be inhibited by thioredoxin (195).

Thioredoxin levels are increased in patients with acute lung injury (196) which is likely to reflect the secretion of thiol isomerases upon immune cell activation. It would be interesting to see if the redox balance is disturbed in chronic lung conditions such as asthma. Interestingly, lung infiltration and inflammation in OVA-induced chronic asthma and influenza-induced pneumonia can be inhibited by thioredoxin (194, 197). Migration of immune cells is clearly inhibited in the presence of thioredoxin confirming that adhesion molecules are targeted by thioredoxin by inhibiting the interaction with their cognate ligand.

Is labile disulfide bond reduction exploited by tumour cells to evade immune surveillance?

The redox balance has been shown to be altered in tumours. Thioredoxin, thioredoxin reductase (170, 198) and PDI (199) secretion are increased which may lead to inhibition of immune cells, allowing the cancer cells to evade immune detection and killing. As a consequence, removing the cancer's control over the immune system by inhibiting thiol isomerases could restore the natural redox balance allowing detection and killing of tumour cells.

Furthermore, it has been shown that tumour cells use the reduction of labile disulfide bonds in plasma membrane proteins to their advantage as has been shown on the example of MICA (major histocompatibility complex class I homologue) (49). MICA is recognised by the NKG2D receptor, leading to tumour rejection. To evade this, tumour cells shed MICA from the cell surface in a disulfide bond reduction-dependent manner (200, 201). This knowledge could be used to inhibit disulfide bond reduction in MICA by antibodies targeting thiol isomerases in the tumour microenvironment or stabilising MICA which would be expected to promote tumour rejection (Figure 46).

Redox drugs

There are a few thioredoxin system inhibitors targeting either thioredoxin or thioredoxin reductase approved for cancer treatment or are undergoing clinical trials (202). One of them is the thioredoxin inhibitor PX-12 which entered a phase Ib (203) and more recently phase II trial for pancreatic cancer (204). Standardized uptake values of fluorodeoxyglucose PET-CT (Positron emission tomography–computed tomography) oncology imaging decreased for 5 out of 15 patients, 2 remained unchanged and 8 increased. A decrease in standardized uptake values in a PET-CT scan is indicative of tumour regression. There is no data presented on how the standardised uptake values increased prior PX-12 treatment, which makes it difficult to assess the success of the treatment. However, it indicates that PX-12 may have a positive effect in cancer treatment since there is a tendency of decreased PET-CT standardised uptake units in 1/3 of the patients. The study discarded PX-12 as a cancer drug, partially because no decrease in thioredoxin levels could be detected. It is not clear why they were expecting a decrease of thioredoxin levels upon PX-12 inhibition.

Potential of novel, redox-based drugs for cancer therapy

Conventional cancer therapy treatments fall into two main categories i) cytotoxic chemotherapy and ii) immunotherapy. The most successful treatment is cytotoxic chemotherapy which is based on the higher toxicity of the drugs for tumour cells compared to normal cells due to their higher metabolic rate. However, cytotoxic chemotherapy is not tumour specific and therefore results in significant toxic side effects in healthy tissues, presenting a problem when long-term chemo therapy is required due to relapse. Moreover, not all cancer types respond well to chemotherapy. Advances in immunotherapy, which targets cancer specific features, has provided a novel way of delivering cytotoxicity to the target cell type. This has been proven to be successful if the cancer cells display a unique feature that distinguishes them from healthy cells. The tyrosine kinase inhibitor Imatinib, for example, is used successfully to treat chronic myelogenous leukaemia which is associated with BCR/ABL expression. BCR/ABL is the result of a gene translocation event, creating a constitutively active tyrosine kinase. Imatinib binds to the BCR/ABL ATP binding site, stabilising its inactive form and thereby inhibits activation. Yet, not every tumour type is associated with specific mutations that can be targeted and cancer cells can develop resistance to treatment by mutations of the target protein. Using targets such as over-expressed cell surface proteins leads to off-target effects as those features are also present on healthy cells.

It has been shown that the tumour redox environment is altered and thioredoxin secretion increased. If it can be shown that this leads to the cancer specific reduction of plasma membrane proteins, this could be a novel, distinguishing feature between cancer and normal cells. Antibodies specific for the reduced conformation of plasma membrane proteins could serve as targeting vehicles of cytotoxic drugs to tumours (Figure 46). This would minimise the exposure of healthy tissue to the toxin and therefore minimise unintended side effects. Furthermore, NK cells could be recruited to tumours using bispecific antibodies for NK cells and reduced cancer plasma membrane proteins inducing antibody-dependent cell cytotoxicity for tumour clearance. Another use of redox-specific cancer antibodies could be the coupling to IL-2. By targeting IL-2 to the cancer microenvironment it is expected that immune cells are activated better, improving cytotoxicity. Although, if leukocyte IL-2 signalling through CD132 is inhibited in the tumour microenvironment through CD132 reduction, crosslinking of reduced

CD132 on immune cells might be necessary to restore cytotoxicity (Figure 46). Moreover, cancer survival or migration that depends on plasma membrane proteins that contain labile disulfide bonds could be controlled by antibodies coupled to a thiol isomerase by generating a local reducing environment (Figure 46).

Up to date there has been no systematic screen of tumours to study their cell surface redox proteome due to the lack of a suitable method. With SH-IQ I present a method that allows the systematic identification of redox-modulated tumour cell surface proteins which is essential to design antibodies to target drugs, immune cells or cytokines to the tumour microenvironment. Moreover, the identification of cancer-related proteins that are redox controlled could allow the inhibition of redox control though small molecule thiol isomerase inhibitors or antibodies.

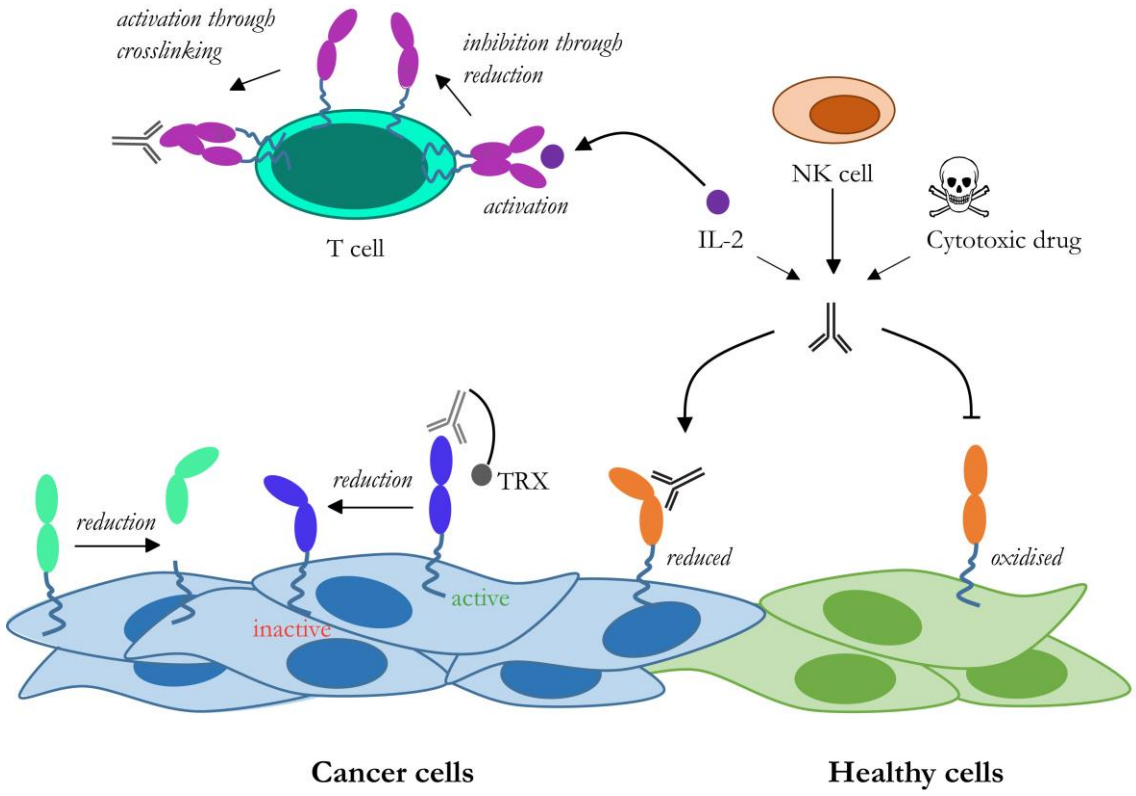

Figure 46: **Redox and cancer therapy.** Thioredoxin secretion is increased in cancer cells, generating a reducing extracellular environment. The cancer specific reduction of plasma membrane proteins (indicated in orange) could be a distinguishing feature between cancer and healthy cells. This could allow the targeted delivery of cytotoxic drugs, NK cells or IL-2 by antibodies specific for the reduced conformation of the protein to cancer cells. IL-2 signalling on T cells was shown to be inhibited by reducing conditions and might thus be impaired in the tumour microenvironment. Crosslinking of the reduced IL-2 receptor might be able to restore signalling (indicated in purple). Moreover, the function of proteins with labile disulfide bonds could be controlled by either i) antibodies that are coupled to a thiol isomerase and induce labile disulfide bond cleavage (indicated in blue) or ii) by preventing the reduction of labile disulfide bonds by either inhibiting thiol isomerases or stabilising the oxidised form of the protein (indicated in aquamarine, i.e. MICA).

Bibliography

1. International Human Genome Sequencing Consortium (2004) Finishing the euchromatic sequence of the human genome. *Nature* 431, 931–945

2. Jensen, O. N. (2004) Modification-specific proteomics: characterization of post-translational modifications by mass spectrometry. *Curr. Opin. Chem. Biol.* 8, 33–41

3. Mondo, J., Wyman, J., and Changeux, J. (1965) On the nature of allosteric transitions: a plausible model. *J. Mol. Biol.* 12, 88–118

4. Zhou, B., Baldus, I. B., Li, W., Edwards, S. A., and Gräter, F. (2014) Identification of allosteric disulfides from prestress analysis. *Biophys. J.* 107, 672–681

5. Schmidt, B., Ho, L., and Hogg, P. J. (2006) Allosteric disulfide bonds. *Biochemistry* 45, 7429–7433

6. Wouters, M. A., Lau, K. K., and Hogg, P. J. (2004) Cross-strand disulphides in cell entry proteins: poised to act. *BioEssays* 26, 73–79

7. Azimi, I., Wong, J. W. H., and Hogg, P. J. (2011) Control of mature protein function by allosteric disulfide bonds. *Antioxidants Redox Signal.* 14, 113–126

8. Wells, J. A., and Powers, D. B. (1986) In vivo formation and stability of engineered disulfide bonds in subtilisin. *J. Biol. Chem.* 261, 6564–6570

9. Jones, D. T., Taylor, W. R., and Thornton, J. M. (1992) The rapid generation of mutation data matrices from protein sequences. *Comput. Appl. Biosci. CABIOS* 8, 275–282

10. Gonnet, G., Cohen, M., and Benner, S. (1992) Exhaustive matching of the entire protein sequence database. *Science* 256, 1443–1445

11. Wong, J. W. H., Ho, S. Y. W., and Hogg, P. J. (2011) Disulfide bond acquisition through eukaryotic protein evolution. *Mol. Biol. Evol.* 28, 327–334

12. Butera, D., Cook, K. M., Chiu, J., Wong, J. W. H., and Hogg, P. J. (2014) Control of blood proteins by functional disulfide bonds. *Blood* 123, 2000–2007

13. Ferrari, D. M., and Soling, H. D. (1999) The protein disulphide-isomerase family: unravelling a string of folds. *Biochem. J.* 339, 1–10

14. Freedman, R. B., Hirst, T. R., and Tuite, M. F. (1994) Protein disulphide isomerase: building bridges in protein folding. *Trends Biochem. Sci.* 19, 331–336

15. Turano, C., Coppari, S., Altieri, F., and Ferraro, A. (2002) Proteins of the PDI family: Unpredicted non-ER locations and functions. *J. Cell. Physiol.* 193, 154–163

16. Teasdale, R. D., and Jackson, M. R. (1996) Signal-mediated sorting of membrane proteins between the endoplasmic reticulum and the golgi apparatus. *Annu. Rev. cell Dev. Biol.* 12, 27–54

17. Farrah, T., Deutsch, E. W., Omenn, G. S., Campbell, D. S., Sun, Z., Bletz, J. A., Mallick, P., Katz, J. E., Malmström, J., Ossola, R., Watts, J. D., Lin, B., Zhang, H., Moritz, R. L., and Aebersold, R. (2011) A high-confidence human plasma proteome reference set with estimated concentrations in PeptideAtlas. *Mol. & Cell. Proteomics* 10, M110.006353

18. Fernandes, P. A., and Ramos, M. J. (2004) Theoretical insights into the mechanism for thiol/disulfide exchange. *Chemistry* 10, 257–266

19. Metcalfe, C., Cresswell, P., and Barclay, N. A. (2012) Interleukin-2 signalling is modulated by a labile disulfide bond in the CD132 chain of its receptor. *Open Biol. J.*, 110036

20. Kellett-Clark, H., Stegmann, M., Banerji, S., Jackson, D. G., Metcalfe, C., and Barclay, A. N. (2015) CD44 Binding to Hyaluronic Acid is Redox Regulated by a Labile Disulfide Bond in the Hyaluronic Acid Binding Site. *PLoS ONE*, e0138137

21. Azimi, I., Matthias, L. J., Center, R. J., Wong, J. W. H., and Hogg, P. J. (2010) Disulfide bond that constrains the HIV-1 gp120 V3 domain is cleaved by thioredoxin. *J. Biol. Chem.* 285, 40072–40080

22. Go, E. P., Zhang, Y., Menon, S., and Desaire, H. (2011) Analysis of the disulfide bond arrangement of the HIV-1 envelope protein CON-S gp140 ΔCFI shows variability in the V1 and V2 regions. *J. proteome Res.* 10, 578–591

23. Ou, W., and Silver, J. (2006) Role of protein disulfide isomerase and other thiol-reactive proteins in HIV-1 envelope protein-mediated fusion. *Virology* 350, 406–417

24. Auwerx, J., Isacsson, O., Söderlund, J., Balzarini, J., Johansson, M., and Lundberg, M. (2009) Human glutaredoxin-1 catalyzes the reduction of HIV-1 gp120 and CD4 disulfides and its inhibition reduces HIV-1 replication. *Int. J. Biochem. & Cell Biol.* 41, 1269–1275

25. Gallina, A., Hanley, T. M., Mandel, R., Trahey, M., Broder, C. C., Viglianti, G. A., and Ryser, H. J.-P. (2002) Inhibitors of protein-disulfide isomerase prevent cleavage of disulfide bonds in receptor-bound glycoprotein 120 and prevent HIV-1 entry. *J. Biol. Chem.* 277, 50579–50588

26. Metcalfe, C., Cresswell, P., Ciaccia, L., Thomas, B., and Barclay, A. N. (2011) Labile disulfide bonds are common at the leucocyte cell surface. *Open Biol.* 1, 110010

27. Lawrence, D. A., Song, R., and Weber, P. (1996) Surface thiols of human lymphocytes and their changes after in vitro and in vivo activation. *J. Leukoc. Biol.* 60, 611–618

28. Essex, D. W. (2009) Redox control of platelet function. *Antioxidants & redox Signal.* 11, 1191–1225

29. Burke-Gaffney, A., Callister, M. E. J., and Nakamura, H. (2005) Thioredoxin: friend or foe in human disease? *Trends Pharmacol. Sci.* 26, 398–404

30. Angelini, G., Gardella, S., Ardy, M., Ciriolo, M. R., Filomeni, G., Di Trapani, G., Clarke, F., Sitia, R., and Rubartelli, A. (2002) Antigen-presenting dendritic cells provide the reducing extracellular microenvironment required for T lymphocyte activation. *Proc. Natl. Acad. Sci. United States Am.* 99, 1491–1496

31. Tate, S. S., and Meister, A. (1985) gamma-Glutamyl transpeptidase from kidney. *Methods Enzymol.* 113, 400–419

32. Yan, Z., Garg, S., Kipnis, J., and Banerjee, R. (2009) Extracellular redox modulation by regulatory T cells. *Nat. Chem. Biol.* 5, 721–723

33. Yan, Z., Garg, S. K., and Banerjee, R. (2010) Regulatory T cells interfere with glutathione metabolism in dendritic cells and T cells. *J. Biol. Chem.* 285, 41525–41532

34. Sido, B., Lasitschka, F., Giese, T., Gassler, N., Funke, B., Schröder-Braunstein, J., Brunnemer, U., Meuer, S. C., and Autschbach, F. (2008) A prominent role for mucosal cystine/cysteine metabolism in intestinal immunoregulation. *Gastroenterology* 134, 179–191

35. Castellani, P., Angelini, G., Delfino, L., Matucci, A., and Rubartelli, A. (2008) The thiol redox state of lymphoid organs is modified by immunization: role of different immune cell populations. *Eur. J. Immunol.* 38, 2419–2425

36. Francisco, V., Neves, B. M., Cruz, M. T., Gonçalo, M., Figueiredo, A., Duarte, C. B., and Lopes, M. C.

(2010) Effect of lipopolysaccharide, skin sensitizers and irritants on thioredoxin-1 expression in dendritic cells: relevance of different signalling pathways. *Arch. Dermatol. Res.* 302, 271–282

37. Sahaf, B., Heydari, K., Herzenberg, L. A., and Herzenberg, L. A. (2003) Lymphocyte surface thiol levels. *Proc. Natl. Acad. Sci. United States Am.* 100, 4001–4005

38. Pellom, S. T., Michalek, R. D., Crump, K. E., Langston, P. K., Juneau, D. G., and Grayson, J. M. (2013) Increased Cell Surface Free Thiols Identify Effector CD8(+) T Cells Undergoing T Cell Receptor Stimulation. *PLoS ONE,* e81134

39. Fenouillet, E., Barbouche, R., and Jones, I. M. (2007) Cell entry by enveloped viruses: redox considerations for HIV and SARS-coronavirus. *Antioxidants Redox Signal.* 9, 1009–1034

40. Grove, J., and Marsh, M. (2011) The cell biology of receptor-mediated virus entry. *J. cell Biol.* 195, 1071–1082

41. Ashkenazi, A., Viard, M., Wexler-Cohen, Y., Blumenthal, R., and Shai, Y. (2011) Viral envelope protein folding and membrane hemifusion are enhanced by the conserved loop region of HIV-1 gp41. *FASEB J.* 25, 2156–2166

42. Matthias, L. J., Azimi, I., Tabrett, C. A., and Hogg, P. J. (2010) Reduced monomeric CD4 is the preferred receptor for HIV. *J. Biol. Chem.* 285, 40793–40799

43. Stegmann, M., Metcalfe, C., and Barclay, A. N. (2013) Immunoregulation through membrane proteins modified by reducing conditions induced by immune reactions. *Eur. J. Immunol.* 43, 15–21

44. Fraser, J., Boo, I., Poumbourios, P., and Drummer, H. E. (2011) Hepatitis C virus (HCV) envelope glycoproteins E1 and E2 contain reduced cysteine residues essential for virus entry. *J. Biol. Chem.* 286, 31984–31992

45. Jain, S., McGinnes, L. W., and Morrison, T. G. (2007) Thiol/disulfide exchange is required for membrane fusion directed by the Newcastle disease virus fusion protein. *J. Virol.* 81, 2328–2339

46. Jain, S., McGinnes, L. W., and Morrison, T. G. (2008) Overexpression of thiol/disulfide isomerases enhances membrane fusion directed by the Newcastle disease virus fusion protein. *J. Virol.* 82, 12039–12048

47. Butera, D., Cook, K. M., Chiu, J., Wong, J. W. H., and Hogg, P. J. (2014) Control of blood proteins by

functional disulfide bonds. *Blood* 123, 2000–2007

48. Cook, K. M., and Hogg, P. J. (2013) Post-translational control of protein function by disulfide bond cleavage. *Antioxidants & redox Signal.* 18, 1987–2015

49. Hogg, P. J. (2013) Targeting allosteric disulphide bonds in cancer. *Nat. Rev. Cancer* 13, 425–431

50. Hogg, P. J. (2009) Contribution of allosteric disulfide bonds to regulation of hemostasis. *J. Thromb. Haemost.* 7 Suppl 1, 13–16

51. Chen, V. M., and Hogg, P. J. (2006) Allosteric disulfide bonds in thrombosis and thrombolysis. *J. Thromb. Haemost.* 4, 2533–2541

52. Hogg, P. (2003) Disulfide bonds as switches for protein function. *Trends Biochem. Sci.*, 210–214

53. Laragione, T., Bonetto, V., Casoni, F., Massignan, T., Bianchi, G., Gianazza, E., and Ghezzi, P. (2003) Redox regulation of surface protein thiols: Identification of integrin alpha-4 as a molecular target by using redox proteomics. *Proc. Natl. Acad. Sci. United States Am.* 100, 14737–14741

54. Yue, X., Schunter, A., and Hummon, A. B. (2015) Comparing multistep immobilized Metal affinity chromatography and multistep TiO2 methods for phosphopeptide enrichment. *Anal. Chem.* 87, 8837–8844

55. Udeshi, N. D., Svinkina, T., Mertins, P., Kuhn, E., Mani, D. R., Qiao, J. W., and Carr, S. A. (2013) Refined preparation and use of anti-diglycine remnant (K-ε-GG) antibody enables routine quantification of 10,000s of ubiquitination sites in single proteomics experiments. *Mol. & Cell. Proteomics* 12, 825–831

56. Wagner, S. A., Beli, P., Weinert, B. T., Nielsen, M. L., Cox, J., Mann, M., and Choudhary, C. (2011) A proteome-wide, quantitative survey of in vivo ubiquitylation sites reveals widespread regulatory roles. *Mol. & Cell. Proteomics* 10, M111.013284

57. Henriksen, P., Wagner, S. A., Weinert, B. T., Sharma, S., Bacinskaja, G., Rehman, M., Juffer, A. H., Walther, T. C., Lisby, M., and Choudhary, C. (2012) Proteome-wide analysis of lysine acetylation suggests its broad regulatory scope in Saccharomyces cerevisiae. *Mol. & Cell. Proteomics* 11, 1510–1522

58. Shevchenko, G., Musunuri, S., Wetterhall, M., and Bergquist, J. (2012) Comparison of extraction methods for the comprehensive analysis of mouse brain proteome using shotgun-based mass spectrometry. *J. proteome Res.* 11, 2441–2451

59. Liebler, D. C., and Ham, A.-J. L. (2009) Spin filter-based sample preparation for shotgun proteomics. *Nat. methods* 6, 785–786–785; author reply 786

60. Wiśniewski, J. R., Zougman, A., Nagaraj, N., and Mann, M. (2009) Universal sample preparation method for proteome analysis. *Nat. methods* 6, 359–362

61. Brocchieri, L., and Karlin, S. (2005) Protein length in eukaryotic and prokaryotic proteomes. *Nucleic acids Res.* 33, 3390–3400

62. Olsen, J. V., Ong, S.-E., and Mann, M. (2004) Trypsin cleaves exclusively C-terminal to arginine and lysine residues. *Mol. & Cell. Proteomics* 3, 608–614

63. Keller, A., Purvine, S., Nesvizhskii, A. I., Stolyar, S., Goodlett, D. R., and Kolker, E. (2002) Experimental protein mixture for validating tandem mass spectral analysis. *Omics : J. Integr. Biol.* 6, 207–212

64. Steen, H., and Mann, M. (2004) The ABC's (and XYZ's) of peptide sequencing. *Nat. Rev. Mol. cell Biol.* 5, 699–711

65. Ong, S.-E., Blagoev, B., Kratchmarova, I., Kristensen, D. B., Steen, H., Pandey, A., and Mann, M. (2002) Stable isotope labeling by amino acids in cell culture, SILAC, as a simple and accurate approach to expression proteomics. *Mol. & Cell. Proteomics* 1, 376–386

66. Gygi, S. P., Rist, B., Gerber, S. A., Turecek, F., Gelb, M. H., and Aebersold, R. (1999) Quantitative analysis of complex protein mixtures using isotope-coded affinity tags. *Nat. Biotechnol.* 17, 994–999

67. Ross, P. L., Huang, Y. N., Marchese, J. N., Williamson, B., Parker, K., Hattan, S., Khainovski, N., Pillai, S., Dey, S., Daniels, S., Purkayastha, S., Juhasz, P., Martin, S., Bartlet-Jones, M., He, F., Jacobson, A., and Pappin, D. J. (2004) Multiplexed protein quantitation in Saccharomyces cerevisiae using amine-reactive isobaric tagging reagents. *Mol. & Cell. Proteomics* 3, 1154–1169

68. Thompson, A., Schäfer, J., Kuhn, K., Kienle, S., Schwarz, J., Schmidt, G., Neumann, T., Johnstone, R., Mohammed, A. K. A., and Hamon, C. (2003) Tandem mass tags: a novel quantification strategy for comparative analysis of complex protein mixtures by MS/MS. *Anal. Chem.* 75, 1895–1904

69. Dayon, L., Hainard, A., Licker, V., Turck, N., Kuhn, K., Hochstrasser, D. F., Burkhard, P. R., and Sanchez, J. C. (2008) Relative quantification of proteins in human cerebrospinal fluids by MS/MS using 6-plex isobaric tags. *Anal. Chem.* 80, 2921–2931

70. Hebert, A. S., Merrill, A. E., Bailey, D. J., Still, A. J., Westphall, M. S., Strieter, E. R., Pagliarini, D. J., and Coon, J. J. (2013) Neutron-encoded mass signatures for multiplexed proteome quantification. *Nat. methods* 10, 332–334

71. Altelaar, A. F. M., Frese, C. K., Preisinger, C., Hennrich, M. L., Schram, A. W., Timmers, H. T. M., Heck, A. J. R., and Mohammed, S. (2013) Benchmarking stable isotope labeling based quantitative proteomics. *J. proteomics* 88, 14–26

72. Wild, M. K., Cambiaggi, A., Brown, M. H., Davies, E. A., Ohno, H., Saito, T., and van der Merwe, P. A. (1999) Dependence of T cell antigen recognition on the dimensions of an accessory receptor-ligand complex. *J. Exp. Med.* 190, 31–41

73. Burger, R., Guenther, A., Bakker, F., Schmalzing, M., Bernand, S., Baum, W., Duerr, B., Hocke, G. M., Steininger, H., Gebhart, E., and Gramatzki, M. (2001) Gp130 and ras mediated signaling in human plasma cell line INA-6: a cytokine-regulated tumor model for plasmacytoma. *Hematol. J.* 2, 42–53

74. Bolstad, B. M., Irizarry, R. A., Astrand, M., and Speed, T. P. (2003) A comparison of normalization methods for high density oligonucleotide array data based on variance and bias. *Bioinformatics* 19, 185–193

75. Smyth, G. K. (2004) Linear models and empirical bayes methods for assessing differential expression in microarray experiments. *Stat. Appl. Genet. Mol. Biol.* 3, Article3

76. Hochberg, Y., and Benjamini, Y. (1990) More powerful procedures for multiple significance testing. *Stat. Med.* 9, 811–818

77. Trudgian, D. C., Thomas, B., McGowan, S. J., Kessler, B. M., Salek, M., and Acuto, O. (2010) CPFP: a central proteomics facilities pipeline. *Bioinformatics* 26, 1131–1132

78. MacLean, B., Eng, J. K., Beavis, R. C., and McIntosh, M. (2006) General framework for developing and evaluating database scoring algorithms using the TANDEM search engine. *Bioinformatics* 22, 2830–2832

79. Geer, L. Y., Markey, S. P., Kowalak, J. A., Wagner, L., Xu, M., Maynard, D. M., Yang, X., Shi, W., and Bryant, S. H. (2004) Open mass spectrometry search algorithm. *J. proteome Res.* 3, 958–964

80. Trudgian, D. C., Ridlova, G., Fischer, R., Mackeen, M. M., Ternette, N., Acuto, O., Kessler, B. M., and Thomas, B. (2011) Comparative evaluation of label-free SINQ normalized spectral index quantitation in the central proteomics facilities pipeline. *Proteomics* 11, 2790–2797

81. Cox, J., and Mann, M. (2008) MaxQuant enables high peptide identification rates, individualized p.p.b.-range mass accuracies and proteome-wide protein quantification. *Nat. Biotechnol.* 26, 1367–1372

82. Dupont, W. D., and Plummer, W. D. (1990) Power and sample size calculations. A review and computer program. *Control. Clin. trials* 11, 116–128

83. Dupont, W. D., and Plummer, W. D. (1998) Power and sample size calculations for studies involving linear regression. *Control. Clin. trials* 19, 589–601

84. Laemmli, U. K. (1970) Cleavage of structural proteins during the assembly of the head of bacteriophage T4. *Nature* 227, 680–685

85. Towbin, H., Staehelin, T., and Gordon, J. (1979) Electrophoretic transfer of proteins from polyacrylamide gels to nitrocellulose sheets: procedure and some applications. *Proc. Natl. Acad. Sci. United States Am.*, 4350–4354

86. Aebersold, R., Burlingame, A. L., and Bradshaw, R. A. (2013) Western blots versus selected reaction monitoring assays: time to turn the tables? *Mol. & Cell. Proteomics* 12, 2381–2382

87. Foster, L. J., Zeemann, P. A., Li, C., Mann, M., Jensen, O. N., and Kassem, M. (2005) Differential expression profiling of membrane proteins by quantitative proteomics in a human mesenchymal stem cell line undergoing osteoblast differentiation. *Stem cells* 23, 1367–1377

88. Jeong, J. A., Ko, K.-M., Park, H. S., Lee, J., Jang, C., Jeon, C.-J., Koh, G. Y., and Kim, H. (2007) Membrane proteomic analysis of human mesenchymal stromal cells during adipogenesis. *Proteomics* 7, 4181–4191

89. Zielinska, D. F., Gnad, F., Wiśniewski, J. R., and Mann, M. (2010) Precision mapping of an in vivo N-glycoproteome reveals rigid topological and sequence constraints. *Cell* 141, 897–907

90. Chen, W.-N. U., Yu, L.-R., Strittmatter, E. F., Thrall, B. D., Camp, D. G., and Smith, R. D. (2003) Detection of in situ labeled cell surface proteins by mass spectrometry: application to the membrane subproteome of human mammary epithelial cells. *Proteomics* 3, 1647–1651

91. Schiess, R., Mueller, L. N., Schmidt, A., Mueller, M., Wollscheid, B., and Aebersold, R. (2009) Analysis of cell surface proteome changes via label-free, quantitative mass spectrometry. *Mol. & Cell. Proteomics* 8, 624–638

92. Wollscheid, B., Bausch-Fluck, D., Henderson, C., O'Brien, R., Bibel, M., Schiess, R., Aebersold, R., and

Watts, J. D. (2009) Mass-spectrometric identification and relative quantification of N-linked cell surface glycoproteins. *Nat. Biotechnol.* 27, 378–386

93. Zeng, Y., Ramya, T. N. C., Dirksen, A., Dawson, P. E., and Paulson, J. C. (2009) High-efficiency labeling of sialylated glycoproteins on living cells. *Nat. methods* 6, 207–209

94. Ramya, T. N. C., Weerapana, E., Cravatt, B. F., and Paulson, J. C. (2013) Glycoproteomics enabled by tagging sialic acid- or galactose-terminated glycans. *Glycobiology* 23, 211–221

95. Deeb, S. J., Cox, J., Schmidt-Supprian, M., and Mann, M. (2014) N-linked glycosylation enrichment for in-depth cell surface proteomics of diffuse large B-cell lymphoma subtypes. *Mol. & Cell. Proteomics* 13, 240–251

96. Bayer, E. A., Ben-Hur, H., and Wilchek, M. (1988) Biocytin hydrazide - a selective label for sialic acids, galactose, and other sugars in glycoconjugates using avidin-biotin technology. *Anal. Biochem.* 170, 271–281

97. Zhang, H., Li, X.-J., Martin, D. B., and Aebersold, R. (2003) Identification and quantification of N-linked glycoproteins using hydrazide chemistry, stable isotope labeling and mass spectrometry. *Nat. Biotechnol.* 21, 660–666

98. Laughlin, S. T., and Bertozzi, C. R. (2009) Imaging the glycome. *Proc. Natl. Acad. Sci. United States Am.* 106, 12–17

99. Manza, L. L., Stamer, S. L., Ham, A.-J. L., Codreanu, S. G., and Liebler, D. C. (2005) Sample preparation and digestion for proteomic analyses using spin filters. *Proteomics* 5, 1742–1745

100. Griffin, N. M., Yu, J., Long, F., Oh, P., Shore, S., Li, Y., Koziol, J. A., and Schnitzer, J. E. (2010) Label-free, normalized quantification of complex mass spectrometry data for proteomic analysis. *Nat. Biotechnol.* 28, 83–89

101. Lund, R., Leth-Larsen, R., Jensen, O. N., and Ditzel, H. J. (2009) Efficient isolation and quantitative proteomic analysis of cancer cell plasma membrane proteins for identification of metastasis-associated cell surface markers. *J. proteome Res.* 8, 3078–3090

102. Ozlü, N., Qureshi, M. H., Toyoda, Y., Renard, B. Y., Mollaoglu, G., Ozkan, N. E., Bulbul, S., Poser, I., Timm, W., Hyman, A. A., Mitchison, T. J., and Steen, J. A. (2014) Quantitative comparison of a human cancer cell surface proteome between interphase and mitosis. *EMBO J.*, 251–265

103. Niehage, C., Steenblock, C., Pursche, T., Bornhäuser, M., Corbeil, D., and Hoflack, B. (2011) The cell surface proteome of human mesenchymal stromal cells. *PloS one* 6, e20399

104. Autelitano, F., Loyaux, D., Roudières, S., Déon, C., Guette, F., Fabre, P., Ping, Q., Wang, S., Auvergne, R., Badarinarayana, V., Smith, M., Guillemot, J.-C., Goldman, S. A., Natesan, S., Ferrara, P., and August, P. (2014) Identification of novel tumor-associated cell surface sialoglycoproteins in human glioblastoma tumors using quantitative proteomics. *PloS one* 9, e0110316

105. Mellacheruvu, D., Wright, Z., Couzens, A. L., Lambert, J.-P., St-Denis, N. A., Li, T., Miteva, Y. V., Hauri, S., Sardiu, M. E., Low, T. Y., Halim, V. A., Bagshaw, R. D., Hubner, N. C., Al-Hakim, A., Bouchard, A., Faubert, D., Fermin, D., Dunham, W. H., Goudreault, M., Lin, Z.-Y., Badillo, B. G., Pawson, T., Durocher, D., Coulombe, B., Aebersold, R., Superti-Furga, G., Colinge, J., Heck, A. J. R., Choi, H., Gstaiger, M., Mohammed, S., Cristea, I. M., Bennett, K. L., Washburn, M. P., Raught, B., Ewing, R. M., Gingras, A.-C., and Nesvizhskii, A. I. (2013) The CRAPome: a contaminant repository for affinity purification-mass spectrometry data. *Nat. methods* 10, 730–736

106. Mi, H., Muruganujan, A., Casagrande, J. T., and Thomas, P. D. (2013) Large-scale gene function analysis with the PANTHER classification system. *Nat. Protoc.* 8, 1551–1566

107. Karp, N. A., and Lilley, K. S. (2005) Maximising sensitivity for detecting changes in protein expression: experimental design using minimal CyDyes. *Proteomics* 5, 3105–3115

108. Sun, Q.-H., Liu, C.-Y., Wang, R., Paddock, C., and Newman, P. J. (2002) Disruption of the long-range GPIIIa Cys(5)-Cys(435) disulfide bond results in the production of constitutively active GPIIb-IIIa (alpha(IIb)beta(3)) integrin complexes. *Blood* 100, 2094–2101

109. Mor-Cohen, R., Rosenberg, N., Landau, M., Lahav, J., and Seligsohn, U. (2008) Specific cysteines in beta 3 are involved in disulfide bond exchange-dependent and -independent activation of alpha IIb beta 3. *J. Biol. Chem.* 283, 19235–19244

110. Mor-Cohen, R., Rosenberg, N., Einav, Y., Zelzion, E., Landau, M., Mansour, W., Averbukh, Y., and Seligsohn, U. (2012) Unique disulfide bonds in epidermal growth factor (EGF) domains of beta 3 affect structure and function of alpha IIb beta 3 and alpha v beta 3 Integrins in different manner. *J. Biol. Chem.* 287, 8879–8891

111. Schwertassek, U., Balmer, Y., Gutscher, M., Weingarten, L., Preuss, M., Engelhard, J., Winkler, M., and

Dick, T. P. (2007) Selective redox regulation of cytokine receptor signaling by extracellular thioredoxin-1. *EMBO J.* 26, 3086–3097

112. Leichert, L. I., Gehrke, F., Gudiseva, H. V., Blackwell, T., Ilbert, M., Walker, A. K., Strahler, J. R., Andrews, P. C., and Jakob, U. (2008) Quantifying changes in the thiol redox proteome upon oxidative stress in vivo. *Proc. Natl. Acad. Sci. United States Am.* 105, 8197–8202

113. Parker, J., Balmant, K., Zhu, F., Zhu, N., and Chen, S. (2015) cysTMTRAQ-An integrative method for unbiased thiol-based redox proteomics. *Mol. & Cell. Proteomics* 14, 237–242

114. Menger, K. E., James, A. M., Cochemé, H. M., Harbour, M. E., Chouchani, E. T., Ding, S., Fearnley, I. M., Partridge, L., and Murphy, M. P. (2015) Fasting, but not aging, dramatically alters the redox status of cysteine residues on proteins in drosophila melanogaster. *Cell reports* 11, 1856–1865

115. Brandes, N., Reichmann, D., Tienson, H., Leichert, L. I., and Jakob, U. (2011) Using quantitative redox proteomics to dissect the yeast redoxome. *J. Biol. Chem.* 286, 41893–41903

116. Kumsta, C., Thamsen, M., and Jakob, U. (2011) Effects of oxidative stress on behavior, physiology, and the redox thiol proteome of Caenorhabditis elegans. *Antioxidants & redox Signal.* 14, 1023–1037

117. Smith-Garvin, J. E., Koretzky, G. A., and Jordan, M. S. (2009) T cell activation. *Annu. Rev. Immunol.* 27, 591–619

118. Patarroyo, M., Yogeeswaran, G., Biberfeld, P., Klein, E., and Klein, G. (1982) Morphological changes, cell aggregation and cell membrane alterations caused by phorbol 12,13-dibutyrate in human blood lymphocytes. *Int. J. cancer. J. Int. du Cancer* 30, 707–717

119. Cuschieri, A., and Mughal, S. (1985) Surface morphology of mitogen-activated human lymphocytes and their derivatives in vitro. *J. Anat.* 140, 93–104

120. Baker, A. F., Dragovich, T., Tate, W. R., Ramanathan, R. K., Roe, D., Hsu, C.-H., Kirkpatrick, D. L., and Powis, G. (2006) The antitumor thioredoxin-1 inhibitor PX-12 (1-methylpropyl 2-imidazolyl disulfide) decreases thioredoxin-1 and VEGF levels in cancer patient plasma. *J. Lab. Clin. Med.* 147, 83–90

121. Kamata, T., Ambo, H., Puzon-McLaughlin, W., Tieu, K. K., Handa, M., Ikeda, Y., and Takada, Y. (2004) Critical cysteine residues for regulation of integrin alphaIIb beta3 are clustered in the epidermal growth factor domains of the beta3 subunit. *Biochem. J.* 378, 1079–1082

122. Kim, C., Ye, F., and Ginsberg, M. H. (2011) Regulation of integrin activation. *Annu. Rev. cell Dev. Biol.* 27, 321–345

123. Chang, J. Y. (1997) A two-stage mechanism for the reductive unfolding of disulfide-containing proteins. *J. Biol. Chem.* 272, 69–75

124. Bausch-Fluck, D., Hofmann, A., Bock, T., Frei, A. P., Cerciello, F., Jacobs, A., Moest, H., Omasits, U., Gundry, R. L., Yoon, C., Schiess, R., Schmidt, A., Mirkowska, P., Härtlová, A., Van Eyk, J. E., Bourquin, J.-P., Aebersold, R., Boheler, K. R., Zandstra, P., and Wollscheid, B. (2015) A mass spectrometric-derived cell surface protein atlas. *PloS one* 10, e0121314

125. Gopalan, G., He, Z., Balmer, Y., Romano, P., Gupta, R., Héroux, A., Buchanan, B. B., Swaminathan, K., and Luan, S. (2004) Structural analysis uncovers a role for redox in regulating FKBP13, an immunophilin of the chloroplast thylakoid lumen. *Proc. Natl. Acad. Sci. United States Am.* 101, 13945–13950

126. Butera, D., Wind, T., Lay, A. J., Beck, J., Castellino, F. J., and Hogg, P. J. (2014) Characterization of a reduced form of plasma plasminogen as the precursor for angiostatin formation. *J. Biol. Chem.* 289, 2992–3000

127. Edwards, D. R., Handsley, M. M., and Pennington, C. J. The ADAM metalloproteinases.

128. Wang, Y., Herrera, A. H., Li, Y., Belani, K. K., and Walcheck, B. (2009) Regulation of mature ADAM17 by redox agents for L-selectin shedding. *J. Immunol.*, 2449–57

129. Willems, S., Tape, C., Stanley, P., Taylor, N., Mills, I., Neal, D., McCafferty, J., and Murphy, G. (2010) Thiol isomerases negatively regulate the cellular shedding activity of ADAM17. *Biochem. J.* 428, 439–450

130. Düsterhöft, S., Jung, S., Hung, C.-W., Tholey, A., Sönnichsen, F. D., Grötzinger, J., and Lorenzen, I. (2013) Membrane-proximal domain of a disintegrin and metalloprotease-17 represents the putative molecular switch of its shedding activity operated by protein-disulfide isomerase. *J. Am. Chem. Soc.* 135, 5776–5781

131. Scheller, J., Chalaris, A., Garbers, C., and Rose-John, S. (2011) ADAM17: a molecular switch to control inflammation and tissue regeneration. *Trends Immunol.* 32, 380–387

132. Alexopoulou, L., Kranidioti, K., Xanthoulea, S., Denis, M., Kotanidou, A., Douni, E., Blackshear, P. J., Kontoyiannis, D. L., and Kollias, G. (2006) Transmembrane TNF protects mutant mice against intracellular bacterial infections, chronic inflammation and autoimmunity. *Eur. J. Immunol.* 36, 2768–2780

133. Chalaris, A., Rabe, B., Paliga, K., Lange, H., Laskay, T., Fielding, C. A., Jones, S. A., Rose-John, S., and Scheller, J. (2007) Apoptosis is a natural stimulus of IL6R shedding and contributes to the proinflammatory trans-signaling function of neutrophils. *Blood* 110, 1748–1755

134. Li, Y., Brazzell, J., Herrera, A., and Walcheck, B. (2006) ADAM17 deficiency by mature neutrophils has differential effects on L-selectin shedding. *Blood* 108, 2275–2279

135. Venturi, G. M., Tu, L., Kadono, T., Khan, A. I., Fujimoto, Y., Oshel, P., Bock, C. B., Miller, A. S., Albrecht, R. M., Kubes, P., Steeber, D. A., and Tedder, T. F. (2003) Leukocyte migration is regulated by L-selectin endoproteolytic release. *Immunity* 19, 713–724

136. Bennett, T. A., Edwards, B. S., Sklar, L. A., and Rogelj, S. (2000) Sulfhydryl regulation of L-selectin shedding: phenylarsine oxide promotes activation-independent L-selectin shedding from leukocytes. *J. Immunol.* 164, 4120–4129

137. Boulanger, M. J., Bankovich, A. J., Kortemme, T., Baker, D., and Garcia, K. C. (2003) Convergent mechanisms for recognition of divergent cytokines by the shared signaling receptor gp130. *Mol. Cell* 12, 577–589

138. Wang, X., Lupardus, P., Laporte, S. L., and Garcia, K. C. (2009) Structural biology of shared cytokine receptors. *Annu. Rev. Immunol.* 27, 29–60

139. Boulanger, M. J., Chow, D., Brevnova, E. E., and Garcia, K. C. (2003) Hexameric structure and assembly of the interleukin-6/IL-6 alpha-receptor/gp130 complex. *Science* 300, 2101–2104

140. Heinrich, P. C., Behrmann, I., Haan, S., Hermanns, H. M., Müller-Newen, G., and Schaper, F. (2003) Principles of interleukin (IL)-6-type cytokine signalling and its regulation. *Biochem. J.* 374, 1–20

141. Schaper, F., Gendo, C., Eck, M., Schmitz, J., Grimm, C., Anhuf, D., Kerr, I. M., and Heinrich, P. C. (1998) Activation of the protein tyrosine phosphatase SHP2 via the interleukin-6 signal transducing receptor protein gp130 requires tyrosine kinase Jak1 and limits acute-phase protein expression. *Biochem. J.* 335, 557–565

142. Ataie-Kachoie, P., Pourgholami, M. H., and Morris, D. L. (2013) Inhibition of the IL-6 signaling pathway: A strategy to combat chronic inflammatory diseases and cancer. *Cytokine Growth Factor Rev.* 24, 163–173

143. Bazan, J. F. (1990) Structural design and molecular evolution of a cytokine receptor superfamily. *Proc. Natl. Acad. Sci. United States Am.* 87, 6934–6938

144. Xu, Y., Kershaw, N. J., Luo, C. S., Soo, P., Pocock, M. J., Czabotar, P. E., Hilton, D. J., Nicola, N. A., Garrett, T. P. J., and Zhang, J.-G. (2010) Crystal structure of the entire ectodomain of gp130: insights into the molecular assembly of the tall cytokine receptor complexes. *J. Biol. Chem.* 285, 21214–21218

145. Wong, J. W. H., and Hogg, P. J. (2010) Analysis of disulfide bonds in protein structures. *J. Thromb. haemostasis: JTH* 8, 2345

146. Reddy, P., Slack, J. L., Davis, R., Cerretti, D. P., Kozlosky, C. J., Blanton, R. A., Shows, D., Peschon, J. J., and Black, R. A. (2000) Functional analysis of the domain structure of tumor necrosis factor-alpha converting enzyme. *J. Biol. Chem.* 275, 14608–14614

147. Janes, P. W., Saha, N., Barton, W. A., Kolev, M. V., Wimmer-Kleikamp, S. H., Nievergall, E., Blobel, C. P., Himanen, J.-P., Lackmann, M., and Nikolov, D. B. (2005) Adam meets Eph: an ADAM substrate recognition module acts as a molecular switch for ephrin cleavage in trans. *Cell* 123, 291–304

148. Lorenzen, I., Lokau, J., Düsterhöft, S., Trad, A., Garbers, C., Scheller, J., Rose-John, S., and Grötzinger, J. (2012) The membrane-proximal domain of A Disintegrin and Metalloprotease 17 (ADAM17) is responsible for recognition of the interleukin-6 receptor and interleukin-1 receptor II. *FEBS Lett.* 586, 1093–1100

149. Rodland, K. D., Bollinger, N., Ippolito, D., Opresko, L. K., Coffey, R. J., Zangar, R., and Wiley, H. S. (2008) Multiple mechanisms are responsible for transactivation of the epidermal growth factor receptor in mammary epithelial cells. *J. Biol. Chem.* 283, 31477–31487

150. Kenny, P. A., and Bissell, M. J. (2007) Targeting TACE-dependent EGFR ligand shedding in breast cancer. *J. Clin. Investig.* 117, 337–345

151. Neurath, M., and Finotto, S. (2011) IL-6 signaling in autoimmunity, chronic inflammation and inflammation-associated cancer. *Cytokine Growth Factor Rev.* 22, 83–89

152. Rose-John, S., Waetzig, G. H., Scheller, J., Grötzinger, J., and Seegert, D. (2007) The IL-6/sIL-6R complex as a novel target for therapeutic approaches. *Expert Opin. Ther. targets* 11, 613–624

153. Kurdi, M., and Booz, G. W. (2007) Evidence that IL-6-type cytokine signaling in cardiomyocytes is inhibited by oxidative stress: parthenolide targets JAK1 activation by generating ROS. *J. Cell. Physiol.* 212, 424–431

154. Castellani, P., Angelini, G., Delfino, L., Matucci, A., and Rubartelli, A. (2008) The thiol redox state of

lymphoid organs is modified by immunization: role of different immune cell populations. *Eur. J. Immunol.* 38, 2419–2425

155. Pellom, S. T., Michalek, R. D., Crump, K. E., Langston, P. K., Juneau, D. G., and Grayson, J. M. (2013) Increased cell surface free thiols identify effector CD8+ T cells undergoing T cell receptor stimulation. *PloS one* 8, e81134

156. Bondarenko, P. V., Chelius, D., and Shaler, T. A. (2002) Identification and relative quantitation of protein mixtures by enzymatic digestion followed by capillary reversed-phase liquid chromatography-tandem mass spectrometry. *Anal. Chem.* 74, 4741–4749

157. Chelius, D., and Bondarenko, P. V. (2002) Quantitative profiling of proteins in complex mixtures using liquid chromatography and mass spectrometry. *J. proteome Res.* 1, 317–323

158. Meissner, F., Scheltema, R. A., Mollenkopf, H.-J., and Mann, M. (2013) Direct proteomic quantification of the secretome of activated immune cells. *Science* 340, 475–478

159. Ikuta, S., Chuang, V. T. G., Ishima, Y., Nakajou, K., Furukawa, M., Watanabe, H., Maruyama, T., and Otagiri, M. (2010) Albumin fusion of thioredoxin--the production and evaluation of its biological activity for potential therapeutic applications. *J. Control. Release : Off. J. Control. Release Soc.* 147, 17–23

160. Fischer, H., Gjörloff, A., Hedlund, G., Hedman, H., Lundgren, E., Kalland, T., Sjögren, H. O., and Dohlsten, M. (1992) Stimulation of human naive and memory T helper cells with bacterial superantigen. Naive CD4+45RA+ T cells require a costimulatory signal mediated through the LFA-1/ICAM-1 pathway. *J. Immunol.* 148, 1993–1998

161. Damle, N. K., Klussman, K., Linsley, P. S., and Aruffo, A. (1992) Differential costimulatory effects of adhesion molecules B7, ICAM-1, LFA-3, and VCAM-1 on resting and antigen-primed CD4+ T lymphocytes. *J. Immunol.* 148, 1985–1992

162. Dubey, C., Croft, M., and Swain, S. L. (1995) Costimulatory requirements of naive CD4+ T cells. ICAM-1 or B7-1 can costimulate naive CD4 T cell activation but both are required for optimum response. *J. Immunol.* 155, 45–57

163. Humphries, J. D., Byron, A., and Humphries, M. J. (2006) Integrin ligands at a glance. *J. cell Sci.* 119, 3901–3903

164. Abram, C. L., and Lowell, C. A. (2009) The ins and outs of leukocyte integrin signaling. *Annu. Rev. Immunol.* 27, 339–362

165. Swiatkowska, M., Szymański, J., Padula, G., and Cierniewski, C. S. (2008) Interaction and functional association of protein disulfide isomerase with αvβ3 integrin on endothelial cells. *FEBS J.* 275, 1813–1823

166. Jasuja, R., Passam, F. H., Kennedy, D. R., Kim, S. H., van Hessem, L., Lin, L., Bowley, S. R., Joshi, S. S., Dilks, J. R., Furie, B., Furie, B. C., and Flaumenhaft, R. (2012) Protein disulfide isomerase inhibitors constitute a new class of antithrombotic agents. *J. Clin. Investig.* 122, 2104–2113

167. Pellegrini, P., Berghella, A. M., Contasta, I., and Adorno, D. (2003) CD30 antigen: not a physiological marker for TH2 cells but an important costimulator molecule in the regulation of the balance between TH1/TH2 response. *Transpl. Immunol.* 12, 49–61

168. Zeiser, R., Nguyen, V. H., Hou, J.-Z., Beilhack, A., Zambricki, E., Buess, M., Contag, C. H., and Negrin, R. S. (2007) Early CD30 signaling is critical for adoptively transferred CD4+CD25+ regulatory T cells in prevention of acute graft-versus-host disease. *Blood* 109, 2225–2233

169. Hargreaves, P. G., and Al-Shamkhani, A. (2002) Soluble CD30 binds to CD153 with high affinity and blocks transmembrane signaling by CD30. *Eur. J. Immunol.* 32, 163–173

170. Lincoln, D. T., Ali Emadi, E. M., Tonissen, K. F., and Clarke, F. M. (2003) The thioredoxin-thioredoxin reductase system: over-expression in human cancer. *Anticancer. Res.* 23, 2425–2433

171. Kakolyris, S., Giatromanolaki, A., Koukourakis, M., Powis, G., Souglakos, J., Sivridis, E., Georgoulias, V., Gatter, K. C., and Harris, A. L. (2001) Thioredoxin expression is associated with lymph node status and prognosis in early operable non-small cell lung cancer. *Clin. Cancer Res.* 7, 3087–3091

172. Raffel, J., Bhattacharyya, A. K., Gallegos, A., Cui, H., Einspahr, J. G., Alberts, D. S., and Powis, G. (2003) Increased expression of thioredoxin-1 in human colorectal cancer is associated with decreased patient survival. *J. Lab. Clin. Med.* 142, 46–51

173. Li, J., Cheng, Z.-J., Liu, Y., Yan, Z.-L., Wang, K., Wu, D., Wan, X.-Y., Xia, Y., Lau, W. Y., Wu, M.-C., and Shen, F. (2015) Serum thioredoxin is a diagnostic marker for hepatocellular carcinoma. *Oncotarget* 6, 9551–9563

174. Welsh, S. J., Bellamy, W. T., Briehl, M. M., and Powis, G. (2002) The redox protein thioredoxin-1 (Trx-

1) increases hypoxia-inducible factor 1alpha protein expression: Trx-1 overexpression results in increased vascular endothelial growth factor production and enhanced tumor angiogenesis. *Cancer Res.* 62, 5089–5095

175. Powis, G., Mustacich, D., and Coon, A. (2000) The role of the redox protein thioredoxin in cell growth and cancer. *Free. Radic. Biol. & Med.* 29, 312–322

176. Rubartelli, A., Bajetto, A., Allavena, G., Wollman, E., and Sitia, R. (1992) Secretion of thioredoxin by normal and neoplastic cells through a leaderless secretory pathway. *J. Biol. Chem.* 267, 24161–24164

177. Chaiswing, L., Bourdeau-Heller, J. M., Zhong, W., and Oberley, T. D. (2007) Characterization of redox state of two human prostate carcinoma cell lines with different degrees of aggressiveness. *Free. Radic. Biol. & Med.* 43, 202–215

178. Shevach, E. M. (2002) CD4+ CD25+ suppressor T cells: more questions than answers. *Nat. Rev. Immunol.* 2, 389–400

179. Zou, W. (2005) Immunosuppressive networks in the tumour environment and their therapeutic relevance. *Nat. Rev. Cancer* 5, 263–274

180. Zou, W. (2006) Regulatory T cells, tumour immunity and immunotherapy. *Nat. Rev. Immunol.* 6, 295–307

181. Ponta, H., Sherman, L., and Herrlich, P. A. (2003) CD44: from adhesion molecules to signalling regulators. *Nat. Rev. Mol. cell Biol.* 4, 33–45

182. Haynes, B. F., Hale, L. P., Patton, K. L., Martin, M. E., and McCallum, R. M. (1991) Measurement of an adhesion molecule as an indicator of inflammatory disease activity. Up-regulation of the receptor for hyaluronate (CD44) in rheumatoid arthritis. *Arthritis Rheum.* 34, 1434–1443

183. Yung, S., and Chan, T. M. (2012) The Role of Hyaluronan and CD44 in the Pathogenesis of Lupus Nephritis. *Autoimmune Dis.* 2012,

184. Mikecz, K., Dennis, K., Shi, M., and Kim, J. H. (1999) Modulation of hyaluronan receptor (CD44) function in vivo in a murine model of rheumatoid arthritis. *Arthritis Rheum.* 42, 659–668

185. Mikecz, K., Brennan, F. R., Kim, J. H., and Glant, T. T. (1995) Anti-CD44 treatment abrogates tissue oedema and leukocyte infiltration in murine arthritis. *Nat. Med.* 1, 558–563

186. DeGrendele, H. C., Kosfiszer, M., Estess, P., and Siegelman, M. H. (1997) CD44 activation and associated primary adhesion is inducible via T cell receptor stimulation. *J. Immunol.* 159, 2549–2553

187. Baaten, B. J. G., Li, C.-R., Deiro, M. F., Lin, M. M., Linton, P. J., and Bradley, L. M. (2010) CD44 regulates survival and memory development in Th1 cells. *Immunity* 32, 104–115

188. Lesley, J., Howes, N., Perschl, A., and Hyman, R. (1994) Hyaluronan binding function of CD44 is transiently activated on T cells during an in vivo immune response. *J. Exp. Med.* 180, 383–387

189. Baaten, B. J. G., Tinoco, R., Chen, A. T., and Bradley, L. M. (2012) Regulation of antigen-experienced T cells: lessons from the quintessential memory marker CD44. *Front. Immunol.* 3, 1–12

190. Baaten, B. J., Li, C.-R., and Bradley, L. M. (2010) Multifaceted regulation of T cells by CD44. *Commun. & Integr. Biol.* 3, 508–512

191. Bourguignon, L. Y. W., Peyrollier, K., Xia, W., and Gilad, E. (2008) Hyaluronan-CD44 interaction activates stem cell marker Nanog, Stat-3-mediated MDR1 gene expression, and ankyrin-regulated multidrug efflux in breast and ovarian tumor cells. *J. Biol. Chem.* 283, 17635–17651

192. Bollyky, P. L., Lord, J. D., Masewicz, S. A., Evanko, S. P., Buckner, J. H., Wight, T. N., and Nepom, G. T. (2007) Cutting edge: high molecular weight hyaluronan promotes the suppressive effects of CD4+CD25+ regulatory T cells. *J. Immunol.* 179, 744–747

193. Bollyky, P. L., Falk, B. A., Long, S. A., Preisinger, A., Braun, K. R., Wu, R. P., Evanko, S. P., Buckner, J. H., Wight, T. N., and Nepom, G. T. (2009) CD44 costimulation promotes FoxP3+ regulatory T cell persistence and function via production of IL-2, IL-10, and TGF-beta. *J. Immunol.* 183, 2232–2241

194. Furukawa, M., Tanaka, R., Chuang, V. T. G., Ishima, Y., Taguchi, K., Watanabe, H., Maruyama, T., and Otagiri, M. (2011) Human serum albumin-thioredoxin fusion protein with long blood retention property is effective in suppressing lung injury. *J. Control. Release : Off. J. Control. Release Soc.* 154, 189–195

195. Nakamura, H., Herzenberg, L. A., Bai, J., Araya, S., Kondo, N., Nishinaka, Y., and Yodoi, J. (2001) Circulating thioredoxin suppresses lipopolysaccharide-induced neutrophil chemotaxis. *Proc. Natl. Acad. Sci. United States Am.* 98, 15143–15148

196. Callister, M. E., Burke-Gaffney, A., Quinlan, G. J., Nicholson, A. G., Florio, R., Nakamura, H., Yodoi, J., and Evans, T. W. (2006) Extracellular thioredoxin levels are increased in patients with acute lung injury. *Thorax*

61, 521–527

197. Tanaka, R., Ishima, Y., Enoki, Y., Kimachi, K., Shirai, T., Watanabe, H., Chuang, V. T. G., Maruyama, T., and Otagiri, M. (2014) Therapeutic impact of human serum albumin-thioredoxin fusion protein on influenza virus-induced lung injury mice. *Front. Immunol.* 5, 1–10

198. Berggren, M., Gallegos, A., Gasdaska, J. R., Gasdaska, P. Y., Warneke, J., and Powis, G. (1996) Thioredoxin and thioredoxin reductase gene expression in human tumors and cell lines, and the effects of serum stimulation and hypoxia. *Anticancer. Res.* 16, 3459–3466

199. Goplen, D., Wang, J., Enger, P. Ø., Tysnes, B. B., Terzis, A. J. A., Laerum, O. D., and Bjerkvig, R. (2006) Protein disulfide isomerase expression is related to the invasive properties of malignant glioma. *Cancer Res.* 66, 9895–9902

200. Kaiser, B. K., Yim, D., Chow, I.-T., Gonzalez, S., Dai, Z., Mann, H. H., Strong, R. K., Groh, V., and Spies, T. (2007) Disulphide-isomerase-enabled shedding of tumour-associated NKG2D ligands. *Nature* 447, 482–486

201. Huergo-Zapico, L., Gonzalez-Rodriguez, A., Contesti, J., Gonzalez, E., Lopez-Soto, A., Ferdinandez-Guizan, A., Acebes-Huerta, A., de Los Toyos, J., Lopez-Larrea, C., Groh, V., Spies, T., and Gonzalez, S. (2012) Expression of ERp5 and GRP78 on the membrane of chronic lymphocytic leukemia cells: association with soluble MICA shedding. *Cancer Immunol. Immunother.* 61, 1201–1210

202. Tonissen, K. F., and Di Trapani, G. (2009) Thioredoxin system inhibitors as mediators of apoptosis for cancer therapy. *Mol. Nutr. & Food Res.* 53, 87–103

203. Powis, G., and Kirkpatrick, D. L. (2007) Thioredoxin signaling as a target for cancer therapy. *Curr. Opin. Pharmacol.* 7, 392–397

204. Ramanathan, R. K., Abbruzzese, J., Dragovich, T., Kirkpatrick, L., Guillen, J. M., Baker, A. F., Pestano, L. A., Green, S., and Von Hoff, D. D. (2011) A randomized phase II study of PX-12, an inhibitor of thioredoxin in patients with advanced cancer of the pancreas following progression after a gemcitabine-containing combination. *Cancer Chemother. Pharmacol.* 67, 503–509

205. Krüger, M., Moser, M., Ussar, S., Thievessen, I., Luber, C. A., Forner, F., Schmidt, S., Zanivan, S., Fässler, R., and Mann, M. (2008) SILAC mouse for quantitative proteomics uncovers kindlin-3 as an essential

factor for red blood cell function. *Cell* 134, 353–364

206. Sury, M. D., Chen, J.-X., and Selbach, M. (2010) The SILAC fly allows for accurate protein quantification in vivo. *Mol. & Cell. Proteomics* 9, 2173–2183

207. Zhang, R., Sioma, C. S., Wang, S., and Regnier, F. E. (2001) Fractionation of isotopically labeled peptides in quantitative proteomics. *Anal. Chem.* 73, 5142–5149

208. Choe, L., D'Ascenzo, M., Relkin, N. R., Pappin, D., Ross, P., Williamson, B., Guertin, S., Pribil, P., and Lee, K. H. (2007) 8-plex quantitation of changes in cerebrospinal fluid protein expression in subjects undergoing intravenous immunoglobulin treatment for Alzheimer's disease. *Proteomics* 7, 3651–3660

209. Pichler, P., Köcher, T., Holzmann, J., Mazanek, M., Taus, T., Ammerer, G., and Mechtler, K. (2010) Peptide labeling with isobaric tags yields higher identification rates using iTRAQ 4-plex compared to TMT 6-plex and iTRAQ 8-plex on LTQ Orbitrap. *Anal. Chem.* 82, 6549–6558

210. Ow, S. Y., Salim, M., Noirel, J., Evans, C., Rehman, I., and Wright, P. C. (2009) iTRAQ underestimation in simple and complex mixtures: "the good, the bad and the ugly". *J. proteome Res.* 8, 5347–5355

211. Ting, L., Rad, R., Gygi, S. P., and Haas, W. (2011) MS3 eliminates ratio distortion in isobaric multiplexed quantitative proteomics. *Nat. methods* 8, 937–940

212. Merrill, A. E., Hebert, A. S., MacGilvray, M. E., Rose, C. M., Bailey, D. J., Bradley, J. C., Wood, W. W., El Masri, M., Westphall, M. S., Gasch, A. P., and Coon, J. J. (2014) NeuCode labels for relative protein quantification. *Mol. & Cell. Proteomics* 13, 2503–2512

213. Hebert, A. S., Merrill, A. E., Stefely, J. A., Bailey, D. J., Wenger, C. D., Westphall, M. S., Pagliarini, D. J., and Coon, J. J. (2013) Amine-reactive neutron-encoded labels for highly plexed proteomic quantitation. *Mol. & Cell. Proteomics* 12, 3360–3369

214. Mallick, P., Schirle, M., Chen, S. S., Flory, M. R., Lee, H., Martin, D., Ranish, J., Raught, B., Schmitt, R., Werner, T., Kuster, B., and Aebersold, R. (2007) Computational prediction of proteotypic peptides for quantitative proteomics. *Nat. Biotechnol.* 25, 125–131

215. Rappsilber, J., Ryder, U., Lamond, A. I., and Mann, M. (2002) Large-scale proteomic analysis of the human spliceosome. *Genome Res.* 12, 1231–1245

216. Ishihama, Y., Oda, Y., Tabata, T., Sato, T., Nagasu, T., Rappsilber, J., and Mann, M. (2005) Exponentially modified protein abundance index (emPAI) for estimation of absolute protein amount in proteomics by the number of sequenced peptides per protein. *Mol. & Cell. Proteomics* 4, 1265–1272

217. Wang, X., Rickert, M., and Garcia, K. C. (2005) Structure of the quaternary complex of interleukin-2 with its alpha, beta, and gammac receptors. *Science* 310, 1159–1163

218. Puck, J. M., Deschênes, S. M., Porter, J. C., Dutra, A. S., Brown, C. J., Willard, H. F., and Henthorn, P. S. (1993) The interleukin-2 receptor gamma chain maps to Xq13.1 and is mutated in X-linked severe combined immunodeficiency, SCIDX1. *Hum. Mol. Genet.* 2, 1099–1104

219. Niemela, J. E., Puck, J. M., Fischer, R. E., Fleisher, T. A., and Hsu, A. P. (2000) Efficient detection of thirty-seven new IL2RG mutations in human X-linked severe combined immunodeficiency. *Clin. Immunol.* 95, 33–38

220. Hansen, G., Hercus, T. R., McClure, B. J., Stomski, F. C., Dottore, M., Powell, J., Ramshaw, H., Woodcock, J. M., Xu, Y., Guthridge, M., McKinstry, W. J., Lopez, A. F., and Parker, M. W. (2008) The structure of the GM-CSF receptor complex reveals a distinct mode of cytokine receptor activation. *Cell* 134, 496–507

Abbreviations

ACN	Acetonitrile
ADAM	A disintegrin and metalloproteinase
AFC	Average fold change
AMBIC	Amoniumbicarbonate
Aa	Amino acids
C, Cys	Cysteine
G, Gly	Glycine
N, Asn	Asparagine
Q, Gln	Glutamine
M, Met	Methionine
P, Pro	Proline
AUC	Area-under-the-curve
BH	Biocytin hydrazide
CD	Cluster of differentiation
CSPA	Cell surface protein atlas
d1/X	Dilution 1/X
d5	Deuterium
DC	Dendritic cell
DSE	Dihedral strain energy
DTT	Dithiothreitol

ER	Endoplasmic reticulum
FA	Formic acid
FASP	Filter-aided sample preparation
FDR	False discovery rate
emPAI	Exponentially modified protein abundance index
FI	Fluorescence intensity
g	Gravity
GILT	Gamma-interferon-inducible lysosomal thiol reductase
GO	Gene ontology
gp	Glycoprotein
GSH	Glutathione
HCV	Hepatitis C virus
HIV	Human immune deficiency virus
IAA	Iodoacetamide
ICAM	Intracellular adhesion molecule
IL	Interleukin
ILCB	N-Iodoacetyl-N-biotinylhexylenediamine
IMAC	Immobilised metal affinity chromatography
IP_2B	(+)-Biotinyl-iodoacetamidyl-3,6-dioxactanediamine
LC-MS/MS	Liquid chromatography-tandem mass spectrometry

LCMV	Lymphocytic choriomeningitis virus
Limma	Linear models for microarray
LPS	Lipopolysaccharide
MFI	Median fluorescence intensity
MLR	Mixed leukocyte reaction
MP_2B	Maleimide-PEG_2-Biotin
$MP_{24}M$	Methyl-PEG_{24}-Maleimide
m/z	mass/charge
NADPH	Nicotinamide adenine dinucleotide phosphate
NEM	N-ethylmaleimide
PDB	Protein Data Bank
PBS	Phosphate buffered saline
PBMCs	Peripheral blood mononuclear cells
PHA	Phytohaemagglutinin
PMA	Phorbol 12-myristate 13-acetate
PDI	Protein disulfide isomerase
PEP	Posterior error probability
ppm	Parts per million
PSM	Peptide spectrum match
PTM	Post-translational modification

PX-12	1-methylpropyl 2-imidazolyl
-SH	Thiol
SH-IQ	Thiol identification and quantitation
SINQ	Spectral index normalised quantification
SEM	Standard error of the mean
SD	Standard deviation
SDS	Sodium dodecyl sulfate
TCEP	Tris(2-carboxyethyl)phosphine hydrochloride
TiO_2	Titanium dioxide
TRX	Thioredoxin
TX-100	Triton X-100

Appendix

1. Supplementary tables

Supplementary Table 1: **50 most abundant proteins identified from leukocyte whole cell lysate.** Samples were prepared for mass spectrometry analysis and the results searched using the CPF Pipeline (10 ppm precursor tolerance, 0.02 Da fragment tolerance, 2 missed cleavages). SINQ (FDR 1%) analysis was performed to determine relative protein abundances. For the cell surface proteins listed in the table the following information is shown: Abundance rank (1 indicating the most abundant protein in the sample), UniProt accession number, gene name, Mascot score, emPAI (exponentially modified protein abundance index), molecular weight of the protein in Da, sequence coverage and unique peptide sequences identified.

Abundance Rank	Accession	Gene	Description	Mascot Score	emPAI	Mass (Da)	Sequence Coverage	Unique peptides
1	P17742	Ppia	Peptidyl-prolyl cis-trans isomerase A	878	62.49	18131	0.65	9
2	S4R1W1	Gm3839	Glyceraldehyde-3-phosphate dehydrogenase	219	4.77	18776	0.52	7
3	P18760	Cfl1	Cofilin-1	219	4.77	18776	0.52	7
4	P06151	Ldha	L-lactate dehydrogenase A chain	584	4.89	40075	0.42	12
5	P35700	Prdx1	Peroxiredoxin-1	283	7.17	22390	0.49	8
6	P26350	Ptma	Prothymosin alpha	793	20.11	12247	0.23	6
7	P10126	Eef1a1	Elongation factor 1-alpha 1	709	2.74	50424	0.36	11
8	P14131	Rps16	40S ribosomal protein S16	189	3.12	16549	0.38	6
9	P58252	Eef2	Elongation factor 2	1394	6.99	96222	0.5	35
10	P62962	Pfn1	Profilin-1	458	29.22	15119	0.72	8
11	O55142	Rpl35a	60S ribosomal protein L35a	458	29.22	15119	0.72	8
12	P63017	Hspa8	Heat shock cognate 71 kDa protein	1623	9.41	71055	0.49	25
13	P63038	Hspd1	60 kDa heat shock protein, mitochondrial	1462	13.11	61088	0.68	27
14	P62908	Rps3	40S ribosomal protein S3	355	12.96	26828	0.65	14
15	P14148	Rpl7	60S ribosomal protein L7	242	2.33	31457	0.27	8
16	P17182	Eno1	Alpha-enolase	1082	8.95	47453	0.56	20
17	P34884	Mif	Macrophage migration inhibitory factor	79	1.09	12667	0.17	2
18	Q6ZWN5	Rps9	40S ribosomal protein S9	133	4.28	22635	0.39	8

Supplementary Table 1continued

19	P61255	Rpl26	60S ribosomal protein L26	60	1.29	17020	0.17	3
20	P62270	Rps18	40S ribosomal protein S18					
21	P41105	Rpl28	60S ribosomal protein L28	166	2.28	15781	0.23	4
22	P10853	Hist1h2bf	Histone H2B type 1-F/J/L					
23	Q03265	Atp5a1	ATP synthase subunit alpha, mitochondrial	1118	8.24	59830	0.5	24
24	P11499	Hsp90ab1	Heat shock protein HSP 90-beta	1924	9.32	83571	0.51	18
25	P61358	Rpl27	60S ribosomal protein L27	163	4.94	15788	0.33	5
26	P99027	Rplp2	60S acidic ribosomal protein P2	402	23.31	11644	0.81	6
27	Q91V55	Rps5	40S ribosomal protein S5	268	2.95	20572	0.37	5
28	Q64433	Hspe1	10 kDa heat shock protein, mitochondrial	194	4.42	10956	0.37	4
29	P62082	Rps7	40S ribosomal protein S7					
30	Q6ZWZ6	Rps12	40S ribosomal protein S12	111	1.57	14905	0.32	3
31	P62259	Ywhae	14-3-3 protein epsilon	520	8.56	29326	0.53	11
32	P47963	Rpl13	60S ribosomal protein L13	199	2.2	24348	0.26	6
33	P60867	Rps20	40S ribosomal protein S20	107	1	13478	0.19	2
34	Q9D1R9	Rpl34	60S ribosomal protein L34	86	2.97	13513	0.28	4
35	P14211	Calr	Calreticulin	233	1.43	48136	0.27	8
36	P97351	Rps3a	40S ribosomal protein S3a	456	9.56	30094	0.49	13
37	Q9CZN7	Shmt2	Serine hydroxymethyltransferase	687	5.4	56237	0.45	18
38	P62702	Rps4x	40S ribosomal protein S4, X isoform	503	8.17	29807	0.42	10
39	P51881	Slc25a5	ADP/ATP translocase 2	318	4.53	33138	0.41	6
40	P62900	Rpl31	60S ribosomal protein L31	84	0.87	14987	0.17	2
41	P62204	Calm1	Calmodulin	275	2.69	21603	0.34	6
42	P62806	Hist1h4a	Histone H4	170	4.16	11360	0.43	4
43	P63101	Ywhaz	14-3-3 protein zeta/delta	407	7.98	27925	0.5	8
44	P84099	Rpl19	60S ribosomal protein L19	192	1.24	23347	0.19	4

Supplementary Table 1continued

Abundance Rank	Accession	Gene	Description	Mascot Score	emPAI	Mass (Da)	Sequence Coverage	Unique peptides
45	P62852	Rps25	40S ribosomal protein S25	127	1.77	13791	0.16	3
46	P17918	Pcna	Proliferating cell nuclear antigen	327	2.67	29108	0.34	7
47	P62245	Rps15a	40S ribosomal protein S15a	87	2.08	12417	0.22	3
48	P62751	Rpl23a	60S ribosomal protein L23a	178	1.22	17684	0.21	3
49	P25444	Rps2	40S ribosomal protein S2	423	5.05	31497	0.38	10
50	P62830	Rpl23	60S ribosomal protein L23	269	5.51	14970	0.38	4

Supplementary Table 2: **50 most abundant proteins identified after lectin purification.** 2B4 T cells were reduced with TCEP and free cysteines labelled with MPB. The sample was then enriched for glycosylated proteins with lectin beads and prepared for mass spectrometry analysis. The results were searched using the CPF Pipeline (10 ppm precursor tolerance, 0.02 Da fragment tolerance, 2 missed cleavages). SINQ (FDR 1%) analysis was performed to determine relative protein abundances. For the cell surface proteins listed in the table the following information is shown: Abundance rank (1 indicating the most abundant protein in the sample), UniProt accession number, gene name, Mascot score, emPAI (exponentially modified protein abundance index), molecular weight of the protein in Da, sequence coverage and unique peptide sequences identified.

Abundance Rank	Protein	Gene	Description	Mascot Score	emPAI	Mass	Sequence Coverage	Unique peptides
1	P01831	Thy1	Thy-1 membrane glycoprotein	1039	8.22	18297	0.55	9
2	P06800	Ptprc	Receptor-type tyrosine-protein phosphatase C	7279	8.39	130199	0.54	59
3	P10404	Hspa9	MLV-related proviral Env polyprotein	4015	4.82	70709	0.48	19
4	P10126	Eef1a1	Elongation factor 1-alpha 1	2325	2.3	50424	0.39	12
5	S4R1W1	Gm3839	Glyceraldehyde-3-phosphate dehydrogenase	1668	8.17	38914	0.51	15
6	P38647	Hspa9	Stress-70 protein, mitochondrial	4770	11.96	73701	0.58	35
7	Q62351	Tfrc	Transferrin receptor protein 1	2882	5.61	86076	0.4	29
8	P26350	Ptma	Prothymosin alpha	1005	9.93	12247	0.23	6
9	P99027	Rplp2	60S acidic ribosomal protein P2	552	11.19	11644	0.92	8
10	P51881	Slc25a5	ADP/ATP translocase 2	542	2.46	33138	0.29	5
11	P18760	Cfl1	Cofilin-1	326	1.1	25074	0.27	5
12	P63017	Hspa8	Heat shock cognate 71 kDa protein	2595	6.94	71055	0.5	24
13	P24668	M6pr	Cation-dependent mannose-6-phosphate receptor	516	2.67	31666	0.4	9
14	P48962	Slc25a4	ADP/ATP translocase 1	351	2.1	33111	0.32	6
15	P20029	Hspa5	78 kDa glucose-regulated protein	2923	5.87	72492	0.46	27
16	Q8VEM8	Slc25a3	Phosphate carrier protein, mitochondrial	588	2.07	40167	0.26	9

Supplementary Table 2 continued

Abundance Rank	Protein	Gene	Description	Mascot Score	emPAI	Mass	Sequence Coverage	Unique peptides
17	P14131	Rps16	40S ribosomal protein S16	199	3.76	16549	0.42	6
18	P62962	Pfn1	Profilin-1	566	7.96	15119	0.63	7
19	E9Q5M7	Itgal	Integrin alpha-L	2967	2.73	129487	0.44	37
20	P17742	Ppia	Peptidyl-prolyl cis-trans isomerase A	775	5.29	18131	0.61	8
21	P35980	Rpl18	60S ribosomal protein L18	216	0.99	21688	0.25	4
22	P35700	Prdx1	Peroxiredoxin-1	317	2.77	22390	0.43	7
23	Q64433	Hspe1	10 kDa heat shock protein, mitochondrial	268	4.22	10956	0.53	5
24	Q03265	Atp5a1	ATP synthase subunit alpha, mitochondrial	1583	3.54	59830	0.44	20
25	P11835	Itgb2	Integrin beta-2	2360	5.07	88031	0.53	34
26	Q9JKR6	Hyou1	Hypoxia up-regulated protein 1	3422	4.86	111340	0.58	42
27	P11942	Cd3g	T-cell surface glycoprotein CD3 gamma chain	346	1.97	20450	0.32	6
28	P47911	Rpl6	60S ribosomal protein L6	602	3.27	33546	0.34	12
29	Q61753	Phgdh	D-3-phosphoglycerate dehydrogenase	1314	2.97	57347	0.36	18
30	P08113	Hsp90b1	Endoplasmin	1787	2.84	92703	0.39	26
31	O08573-2	Lgals9	Isoform Short of Galectin-9	814	3.05	40281	0.34	9
32	P16045	Lgals1	Galectin-1	448	5.93	15198	0.53	6
33	P01851		T-cell receptor beta-2 chain C region					
34	P10852	Slc3a2	4F2 cell-surface antigen heavy chain	2047	5.54	62315	0.44	25
35	P14148	Rpl7	60S ribosomal protein L7	233	1.24	32564	0.2	7
36	P61358	Rpl27	60S ribosomal protein L27	144	1.55	15788	0.21	3
37	Q9JJI8	Rpl38	60S ribosomal protein L38	186	4.72	8256	0.5	4
38	P99024	Tubb5	Tubulin beta-5 chain	3401	17.77	50095	0.71	4
39	P62751	Rpl23a	60S ribosomal protein L23a	195	1.85	17684	0.27	4
40	P56480	Atp5b	ATP synthase subunit beta, mitochondrial	2570	5.97	56265	0.6	21

Supplementary Table 2 continued

41	P05064	Aldoa	Fructose-bisphosphate aldolase A	1153	5.02	39787	0.57	13
42	P60843	Eif4a1	Eukaryotic initiation factor 4A-I	1310	4.06	46353	0.41	14
43	P17182	Eno1	Alpha-enolase	1573	4.27	47453	0.47	15
44	P06151	Ldha	L-lactate dehydrogenase A chain	624	2.08	40075	0.34	10
45	P18572	Bsg	Basigin	727	2.07	29941	0.5	9
46	P84099	Rpl19	60S ribosomal protein L19	275	0.61	23347	0.13	2
47	Q9CZN7	Shmt2	Serine hydroxymethyltransferase	964	3.08	56237	0.43	16
48	Q9D8E6	Rpl4	60S ribosomal protein L4	819	2.29	47409	0.38	14
49	P61255	Rpl26	60S ribosomal protein L26	184	1.92	17248	0.32	5
50	P21995	Emb	Embigin	804	3.95	37554	0.38	11

Supplementary Table 3: **SH-IQ: 50 most abundant proteins identified after avidin purification.** 2B4 T cells were reduced with TCEP and free cysteines labelled with MPB. The sample was then enriched for biotinylated proteins with avidin beads and prepared for mass spectrometry analysis. The results were searched using the CPF Pipeline (10 ppm precursor tolerance, 0.02 Da fragment tolerance, 2 missed cleavages). SINQ (FDR 1%) analysis was performed to determine relative protein abundances. For the cell surface proteins listed in the table the following information is shown: Abundance rank (1 indicating the most abundant protein in the sample), UniProt accession number, gene name, Mascot score, emPAI (exponentially modified protein abundance index), molecular weight of the protein in Da, sequence coverage and unique peptide sequences identified.

Abundance Rank	Accession	Gene	Description	Score	emPAI	Mass	Sequence coverage	Unique peptides
1	P63017	Hspa8	Heat shock cognate 71 kDa protein	5994	24.62	70827	0.66	33
2	P99027	Rplp2	60S acidic ribosomal protein P2	1256	35.85	11644	0.96	10
3	P06800	Ptprc	Receptor-type tyrosine-protein phosphatase C	8292	15.83	128489	0.63	73
4	P63038	Hspd1	60 kDa heat shock protein, mitochondrial	6210	62.51	60917	0.77	49
5	P27773	Pdia3	Protein disulfide-isomerase A3	2948	15.41	56643	0.67	40
6	P11499	Hsp90ab1	Heat shock protein HSP 90-beta	5430	14.84	83229	0.62	34
7	P10126	Eef1a1	Elongation factor 1-alpha 1	2970	9.52	50082	0.77	26
8	P35700	Prdx1	Peroxiredoxin-1	836	9.9	22162	0.68	13
9	P56480	Atp5b	ATP synthase subunit beta, mitochondrial	3205	8.73	56265	0.66	24
10	Q6ZWZ6	Rps12	40S ribosomal protein S12	441	5.03	14505	0.58	7
11	P06151	Ldha	L-lactate dehydrogenase A chain	1464	7.98	39733	0.71	18
12	P11835	Itgb2	Integrin beta-2	3013	7.62	84838	0.65	45
13	P47962	Rpl5	60S ribosomal protein L5	1258	5.99	34379	0.4	13
14	Q99MN9	Pccb	Propionyl-CoA carboxylase beta chain, mitochondrial	2625	6.12	58372	0.58	25
15	E9Q5M7	Itgal	Integrin alpha-L	4631	4.43	128233	0.57	51
16	Q91ZA3	Pcca	Propionyl-CoA carboxylase alpha chain, mitochondrial	3406	6.62	79871	0.6	39

Supplementary Table 3 continued

17	Q9CPQ1	Cox6c	Cytochrome c oxidase subunit 6C	146	3.5	8464	0.26	3
18	Q03265	Atp5a1	ATP synthase subunit alpha, mitochondrial	2719	6.22	59716	0.65	31
19	P20029	Hspa5	78 kDa glucose-regulated protein	3411	6.8	72377	0.5	35
20	Q8VEM8	Slc25a3	Phosphate carrier protein, mitochondrial	847	2.55	39711	0.27	9
21	Q61937	Npm1	Nucleophosmin	1268	2.81	32540	0.37	9
22	P17751	Tpi1	Triosephosphate isomerase	1007	3.75	32171	0.45	11
23	P18760	Cfl1	Cofilin-1	379	1.91	18548	0.54	6
24	Q61753	Phgdh	D-3-phosphoglycerate dehydrogenase	2048	5.35	56549	0.46	24
25	Q99LP6	Grpel1	GrpE protein homolog 1, mitochondrial	511	5.77	24292	0.67	13
26	P10639	Txn	Thioredoxin	317	4.28	11668	0.49	6
27	Q6ZWX6	Eif2s1	Eukaryotic translation initiation factor 2 subunit 1	1341	8.28	36085	0.7	19
28	Q8BG32	Psmd11	26S proteasome non-ATPase regulatory subunit 11	1309	6.29	47407	0.6	27
29	Q9Z0N1	Eif2s3x	Eukaryotic translation initiation factor 2 subunit 3, X-linked	1031	2.07	51033	0.44	15
30	P17918	Pcna	Proliferating cell nuclear antigen	753	4.7	28766	0.59	10
31	G3UX26	Vdac2	Voltage-dependent anion-selective channel protein 2 (Fragment)	992	5.46	30427	0.57	13
32	Q8R180	Ero1l	ERO1-like protein alpha	1312	3.75	54050	0.5	22
33	P58252	Eef2	Elongation factor 2	3078	4.91	95253	0.59	42
34	P16045	Lgals1	Galectin-1	511	6.23	14856	0.61	7
35	P08003	Pdia4	Protein disulfide-isomerase A4	2092	6.54	71938	0.47	33
36	P14685	Psmd3	26S proteasome non-ATPase regulatory subunit 3	1046	2.39	60680	0.47	21
37	P09528	Fth1	Ferritin heavy chain	384	3.8	21053	0.46	10
38	P38647	Hspa9	Stress-70 protein, mitochondrial	3491	9.47	73416	0.63	39
39	P62908	Rps3	40S ribosomal protein S3	607	3.48	26657	0.46	10
40	Q99JI4	Psmd6	26S proteasome non-ATPase regulatory subunit 6	1463	6.35	45507	0.59	25
41	P26516	Psmd7	26S proteasome non-ATPase regulatory subunit 7	877	2.61	36517	0.5	12
42	Q9WVJ2	Psmd13	26S proteasome non-ATPase regulatory subunit 13	1421	4.21	42782	0.48	17

Supplementary Table 3 continued

Abundance Rank	Accession	Gene	Description	Score	emPAI	Mass	Sequence coverage	Unique peptides
43	P63325	Rps10	40S ribosomal protein S10	412	2.4	18904	0.42	6
44	P47955	Rplp1	60S acidic ribosomal protein P1	255	2.1	11468	0.67	3
45	P09103	P4hb	Protein disulfide-isomerase	1408	3.38	57023	0.53	24
46	P67778	Phb	Prohibitin	647	3.3	29802	0.64	13
47	P60867	Rps20	40S ribosomal protein S20	313	1.08	13364	0.24	3
48	P51881	Slc25a5	ADP/ATP translocase 2	828	3.6	32910	0.47	9
49	P99024	Tubb5	Tubulin beta-5 chain	3228	12.16	49639	0.72	5
49	P99024	Tubb5	Tubulin beta-5 chain	3228	12.16	49639	0.72	5
50	S4R1W1	Gm3839	Glyceraldehyde-3-phosphate dehydrogenase					

Supplementary Table 4: **SH-IQ: 50 most abundant proteins identified after tandem lectin-avidin purification.** 2B4 T cells were reduced with TCEP and free cysteines labelled with MPB. The sample was then enriched for biotinylated glycoproteins by tandem lectin-avidin purification and prepared for mass spectrometry analysis. The results were searched using the CPF Pipeline (10 ppm precursor tolerance, 0.02 Da fragment tolerance, 2 missed cleavages). SINQ (FDR 1%) analysis was performed to determine relative protein abundances. For the cell surface proteins listed in the table the following information is shown: Abundance rank (1 indicating the most abundant protein in the sample), UniProt accession number, gene name, Mascot score, emPAI (exponentially modified protein abundance index), molecular weight of the protein in Da, sequence coverage and unique peptide sequences identified.

Abundance Rank	Accession	Gene	Description	Score	emPAI	Mass	Sequence coverage	Unique peptides
1	P06800	Ptprc	Receptor-type tyrosine-protein phosphatase C	9863	40.46	128489	0.55	66
2	P11835	Itgb2	Integrin beta-2	5372	34.63	84838	0.63	46
3	E9Q5M7	Itgal	Integrin alpha-L	6004	11.82	128233	0.53	55
4	P15379-10	Cd44	Isoform 8 of CD44 antigen	2887	2.72	72043	0.16	10
5	P43406	Itgav	Integrin alpha-V	3819	16.03	115287	0.51	53
6	P10852	Slc3a2	4F2 cell-surface antigen heavy chain	2121	10.41	62201	0.39	24
7	Q62351	Tfrc	Transferrin receptor protein 1	1779	8.12	85677	0.43	27
8	P38647	Hspa9	Stress-70 protein, mitochondrial	3752	29.51	73416	0.58	40
9	P99027	Rplp2	60S acidic ribosomal protein P2	694	78.25	11644	0.95	9
10	O54890	Itgb3	Integrin beta-3	2419	6.97	86681	0.47	30
11	P10126	Eef1a1	Elongation factor 1-alpha 1	756	3.12	50082	0.39	13
12	P35700	Prdx1	Peroxiredoxin-1	498	31.15	18858	0.53	11
13	P56382	Atp5e	ATP synthase subunit epsilon, mitochondrial	52	1.16	5834	0.15	1
14	P10404	1 SV	MLV-related proviral Env polyprotein	2170	8.42	69569	0.43	16
15	P09055	Itgb1	Integrin beta-1	2265	7.58	88173	0.45	33
16	P56480	Atp5b	ATP synthase subunit beta, mitochondrial	1984	12.51	56265	0.47	20

Supplementary Table 4 continued

Abundance Rank	Accession	Gene	Description	Score	emPAI	Mass	Sequence coverage	Unique peptides
17	Q03265	Atp5a1	ATP synthase subunit alpha, mitochondrial	1290	6.83	59716	0.45	21
18	Q3TB92	Milr1	Allergin-1	1032	30.26	27349	0.53	11
19	O08573-2	Lgals9	Isoform Short of Galectin-9	708	3.66	39882	0.3	9
20	P20029	Hspa5	78 kDa glucose-regulated protein	1899	6.59	72377	0.48	27
21	P48962	Slc25a4	ADP/ATP translocase 1	282	3.19	32883	0.33	4
22	D3YZZ5	Tmed7	Protein Tmed7	311	2.06	25185	0.24	6
23	P04223-2	H2-K1	Isoform 2 of H-2 class I histocompatibility antigen, K-K alpha chain	709	4.71	40604	0.39	9
24	Q8C129	Lnpep	Leucyl-cystinyl aminopeptidase	2543	6.55	117229	0.4	37
25	P06151	Ldha	L-lactate dehydrogenase A chain	526	2.69	39733	0.28	9
26	P27773	Pdia3	Protein disulfide-isomerase A3	1020	7.06	56643	0.45	23
27	P63017	Hspa8	Heat shock cognate 71 kDa protein	1688	8.07	70827	0.52	25
28	P16045	Lgals1	Galectin-1	466	7.95	14856	0.45	5
29	G3UX26	Vdac2	Voltage-dependent anion-selective channel protein 2 (Fragment)	526	3.02	30427	0.39	8
30	Q8VEM8	Slc25a3	Phosphate carrier protein, mitochondrial	337	1.58	39711	0.22	7
31	P01831	Thy1	Thy-1 membrane glycoprotein	306	5.1	18069	0.51	6
32	P01851	1 SV	T-cell receptor beta-2 chain C region	2170	8.42	69569	0.43	16
33	P11499	Hsp90ab1	Heat shock protein HSP 90-beta	2017	6.75	83229	0.43	16
34	Q9DB20	Atp5o	ATP synthase subunit O, mitochondrial	525	8.15	23349	0.53	8
35	P42932	Cct8	T-complex protein 1 subunit theta	1139	6.89	59518	0.44	22
36	Q8C145	Slc39a6	Zinc transporter ZIP6	972	1.28	86326	0.13	12
37	Q01965	Ly9	T-lymphocyte surface antigen Ly-9	1168	2.2	73096	0.32	16
38	P14426	H2-D1	H-2 class I histocompatibility antigen, D-K alpha chain	631	2.59	40594	0.3	4
39	Q6ZWZ6	Rps12	40S ribosomal protein S12	166	2.6	14505	0.34	4
40	P97370	Atp1b3	Sodium/potassium-transporting ATPase subunit beta-3	149	0.56	31755	0.18	3

Supplementary Table 4 continued

41	P08113	Hsp90b1	Endoplasmin	987	1.93	92418	0.32	18
42	P51881	Slc25a5	ADP/ATP translocase 2	345	3.84	32910	0.31	4
43	Q02242	Pdcd1	Programmed cell death protein 1	651	3.38	31822	0.32	8
44	Q61753	Phgdh	D-3-phosphoglycerate dehydrogenase	811	3.9	56549	0.37	17
45	P24668	M6pr	Cation-dependent mannose-6-phosphate receptor	304	1.47	31152	0.3	6
46	Q6P5F6	Slc39a10	Zinc transporter ZIP10	518	1.23	94335	0.17	14
47	P11370	Fv4	Retrovirus-related Env polyprotein from Fv-4 locus	806	1.01	74406	0.17	4
48	Q62179	Sema4b	Semaphorin-4B	819	1.68	91335	0.25	5
49	Q61543	Glg1	Golgi apparatus protein 1	2049	4.58	132265	0.35	36
50	Q80V42	Cpm	Carboxypeptidase M	773	3.07	50524	0.35	14

Supplementary Table 5: **Quantitation of labile disulfide bond reduction in leukocyte cell surface proteins after TCEP reduction.** The listed 163 proteins have been identified in three biological replicates. The average fold change (AFC) has been calculated on a minimum of two unique peptides per protein. Limma analysis was used to analyse the differential protein abundance between control and reduced samples. The P-values were adjusted for multiple testing applying Benjamini-Hochberg correction. Cell surface proteins are indicated in black, intracellular proteins in grey and proteins with known labile disulfide bonds bold. For the cell surface proteins listed in the table the following information is shown: UniProt accession number, gene name, gene description, AFC, $\log_2$(AFC), $\log_2$(Average abundance), P-value and adjusted P-value.

Accession	Gene Name	Protein Description	Average Fold Change	$\log_2$(AFC)	$\log_2$(Average Abundance)	P-value	Adjusted P-value
Q9CYA0	Creld2	Cysteine-rich with EGF-like domain protein 2	10.39	3.38	18.34	3.92E-04	0.009
Q62469	Itga2	Integrin alpha-2	9.79	3.29	22.83	3.16E-05	0.005
A2APM1	Cd44	CD44 antigen	9.08	3.18	26.27	8.20E-05	0.007
Q9QZF2	Gpc1	Glypican-1	8.86	3.15	18.33	2.23E-04	0.008
Q80V42	Cpm	Carboxypeptidase M	8.52	3.09	20.26	4.95E-04	0.009
P35456	Plaur	Urokinase plasminogen activator surface receptor	8.32	3.06	18.96	8.92E-04	0.013
O54890	Itgb3	Integrin beta-3	8.11	3.02	24.92	7.84E-04	0.013
Q60846	Tnfrsf8	Tumor necrosis factor receptor superfamily member 8, CD30	7.80	2.96	24.22	5.10E-04	0.009
P09055	Itgb1	Integrin beta-1	7.31	2.87	25.39	1.79E-04	0.008
Q6P5F6	Slc39a10	Zinc transporter ZIP10	6.02	2.59	23.87	4.21E-04	0.009
Q8R2Q8	Bst2	Bone marrow stromal antigen 2	4.55	2.19	20.06	1.19E-03	0.013
Q64151	Sema4c	Semaphorin-4C	4.02	2.01	18.94	7.61E-03	0.047
Q542I8	Itgb2	Integrin beta	3.86	1.95	28.20	1.03E-03	0.013
Q64697	Ptprcap	Protein tyrosine phosphatase receptor type C-associated protein	3.77	1.92	20.23	9.53E-03	0.049
E9Q5M7	Itgal	Integrin alpha-L	3.44	1.78	28.53	9.61E-04	0.013
O89001	Cpd	Carboxypeptidase D	3.44	1.78	20.28	1.22E-03	0.013
O35598	Adam10	Disintegrin and metalloproteinase domain-containing protein 10	3.24	1.70	21.76	2.75E-03	0.028
P01831	Thy1	Thy-1 membrane glycoprotein	3.02	1.60	22.73	6.01E-03	0.047
Q3TB92	Milr1	Allergin-1	2.64	1.40	23.52	7.67E-03	0.047
O09126	Sema4d	Semaphorin-4D	2.20	1.14	24.23	7.58E-03	0.047

Supplementary Table 5 continued

A2AN91	Susd1	Protein Susd1	1.94	0.96	21.26	4.86E-03	0.041
Q91VK1	Bzw2	Basic leucine zipper and W2 domain-containing protein 2	1.71	0.78	18.22	2.53E-01	0.389
P16045	Lgals1	Galectin-1	1.68	0.75	19.65	4.21E-02	0.114
Q8K094	Pvr	Poliovirus receptor	1.62	0.69	21.79	1.17E-02	0.058
Q61503	Nt5e	5'-nucleotidase	1.59	0.66	19.76	2.28E-01	0.361
Q02242	Pdcd1	Programmed cell death protein 1	1.54	0.62	22.22	2.59E-02	0.085
Q8BMS1	Hadha	Trifunctional enzyme subunit alpha, mitochondrial	1.53	0.61	21.80	1.75E-02	0.075
Q3U0X8	Cd96	T-cell surface protein tactile	1.49	0.58	18.75	1.03E-01	0.207
P24668	M6pr	Cation-dependent mannose-6-phosphate receptor	1.49	0.57	21.90	7.16E-02	0.169
P04202	Tgfb1	Transforming growth factor beta-1	1.34	0.42	20.50	1.01E-01	0.205
P51881	Slc25a5	ADP/ATP translocase 2	1.33	0.41	21.58	3.25E-01	0.452
Q07797	Lgals3bp	Galectin-3-binding protein	1.32	0.40	20.93	2.86E-01	0.413
P48962	Slc25a4	ADP/ATP translocase 1	1.32	0.40	19.12	1.76E-01	0.302
P35330	Icam2	Intercellular adhesion molecule 2	1.31	0.39	22.06	1.93E-01	0.325
P01735	4 SV	T-cell receptor beta chain V region 86T1	1.23	0.30	20.73	3.06E-01	0.433
Q60943	Il17ra	Interleukin-17 receptor A	1.21	0.28	17.73	3.31E-01	0.453
P28843	Dpp4	Dipeptidyl peptidase 4	1.21	0.27	24.88	5.03E-01	0.622
Q9QUM4-2	Slamf1	Isoform Short of Signaling lymphocytic activation molecule	1.21	0.27	19.98	6.07E-01	0.717
Q8K4F0	Cd226	CD226 antigen	1.19	0.25	19.59	2.66E-01	0.398
Q9JJF9	Sppl2a	Signal peptide peptidase-like 2A	1.17	0.23	18.13	5.19E-01	0.636
P04235	Cd3d	T-cell surface glycoprotein CD3 delta chain	1.17	0.22	20.59	4.76E-01	0.597
P35951	Ldlr	Low-density lipoprotein receptor	1.16	0.22	23.97	3.59E-01	0.480
P35564	Canx	Calnexin	1.15	0.20	20.19	4.89E-01	0.608
P10852-2	Slc3a2	Isoform 2 of 4F2 cell-surface antigen heavy chain	1.15	0.20	27.47	3.25E-01	0.452
P19001	Krt19	Keratin, type I cytoskeletal 19	1.11	0.16	18.87	8.49E-01	0.898
Q91WD0-2	Gpr108	Isoform 2 of Protein GPR108	1.09	0.13	19.89	7.45E-01	0.838
Q64735-2	Cr1l	Isoform 2 of Complement component receptor 1-like protein	1.09	0.12	23.07	5.60E-01	0.676
Q8R5L1	C1qbp	Complement component 1 Q subcomponent-binding protein, mitochondrial	1.09	0.12	20.07	8.03E-01	0.865
Q80VP8	Tmem106c	Transmembrane protein 106C	1.08	0.11	20.00	8.07E-01	0.865
Q8VD58	Evi2b	Protein EVI2B	1.08	0.11	23.09	6.49E-01	0.756

Supplementary Table 5 continued

Accession	Gene Name	Protein Description	Average Fold Change	log_2(AFC)	log_2(Average Abundance)	P-value	Adjusted P-value
Q9EQH2	Erap1	Endoplasmic reticulum aminopeptidase 1	1.07	0.10	21.11	6.19E-01	0.726
Q99JY0	Hadhb	Trifunctional enzyme subunit beta, mitochondrial	1.07	0.09	21.70	6.86E-01	0.788
B1AQR8	Lgals9	Galectin	1.05	0.07	25.83	7.70E-01	0.848
P23242	Gja1	Gap junction alpha-1 protein	1.03	0.04	20.48	8.40E-01	0.895
Q9CYN9	Atp6ap2	Renin receptor	1.03	0.04	19.20	8.59E-01	0.904
P07356	Anxa2	Annexin A2	1.02	0.03	19.75	8.97E-01	0.925
P70289	Ptprv	Receptor-type tyrosine-protein phosphatase V	1.02	0.03	20.40	8.93E-01	0.925
P51863	Atp6v0d1	V-type proton ATPase subunit d 1	1.01	0.01	21.30	9.53E-01	0.977
P24161	Cd247	T-cell surface glycoprotein CD3 zeta chain	1.01	0.01	20.71	9.90E-01	0.997
P22646	Cd3e	T-cell surface glycoprotein CD3 epsilon chain	1.01	0.01	22.92	9.80E-01	0.996
S4R1M0	Ptprc	Receptor-type tyrosine-protein phosphatase C	1.00	0.00	30.79	1.00E+00	1.000
Q8VE99	Ccdc115	Coiled-coil domain-containing protein 115	1.00	0.00	19.18	9.84E-01	0.996
P67778	Phb	Prohibitin	0.98	-0.03	18.03	8.67E-01	0.905
P28658	Atxn10	Ataxin-10	0.96	-0.05	20.71	7.63E-01	0.846
Q8K201	Kct2	Keratinocyte-associated transmembrane protein 2	0.96	-0.06	19.68	7.80E-01	0.853
Q9ET30	Tm9sf3	Transmembrane 9 superfamily member 3	0.96	-0.06	19.30	7.58E-01	0.846
O35114	Scarb2	Lysosome membrane protein 2	0.95	-0.07	21.40	7.44E-01	0.838
Q9EPS3	Glce	D-glucuronyl C5-epimerase	0.93	-0.11	19.18	7.94E-01	0.862
P01851	1 SV	T-cell receptor beta-2 chain C region	0.91	-0.14	21.43	5.34E-01	0.650
F8VQJ3	Lamc1	Laminin subunit gamma-1	0.91	-0.14	21.61	6.01E-01	0.715
Q68FM6	Elfn2	Protein phosphatase 1 regulatory subunit 29	0.90	-0.16	21.43	4.12E-01	0.530
Q9D771	Tmem206	Transmembrane protein 206	0.90	-0.16	21.12	7.08E-01	0.807
Q91VD9	Ndufs1	NADH-ubiquinone oxidoreductase 75 kDa subunit, mitochondrial	0.90	-0.16	18.10	4.25E-01	0.541
A2A7A7	H6pd	GDH/6PGL endoplasmic bifunctional protein	0.90	-0.16	19.64	6.79E-01	0.785
Q99KF1	Tmed9	Transmembrane emp24 domain-containing protein 9	0.87	-0.21	21.51	2.77E-01	0.406
Z4YK56	AU040320	Protein AU040320	0.86	-0.22	18.91	4.13E-01	0.530
P01734	4 SV	T-cell receptor beta chain V region 3H.25	0.85	-0.23	19.89	4.39E-01	0.555
Q8VDL4-3	Adpgk	Isoform 3 of ADP-dependent glucokinase	0.84	-0.25	20.12	2.62E-01	0.395

Supplementary Table 5 continued

Q80XN0	Bdh1	D-beta-hydroxybutyrate dehydrogenase, mitochondrial	0.83	-0.27	19.25	2.56E-01	0.390
P17439	Gba	Glucosylceramidase	0.82	-0.29	20.17	3.92E-01	0.511
P17918	Pcna	Proliferating cell nuclear antigen	0.82	-0.29	19.78	2.14E-01	0.346
Q9QYJ0	Dnaja2	DnaJ homolog subfamily A member 2	0.81	-0.31	20.10	3.62E-01	0.480
Q3TAA8	Pigu	Phosphatidylinositol glycan anchor biosynthesis class U protein	0.79	-0.34	19.74	1.23E-01	0.237
Q920A5	Scpep1	Retinoid-inducible serine carboxypeptidase	0.79	-0.34	19.89	9.82E-02	0.203
Q3U0P5	Entpd6	Ectonucleoside triphosphate diphosphohydrolase 6, isoform CRA_a	0.78	-0.35	21.61	2.40E-01	0.376
Q7JCZ1	mt-Co2	Cytochrome c oxidase subunit 2	0.78	-0.36	18.50	2.14E-01	0.346
Q8HWA3	Ulbp1	Protein Ulbp1	0.78	-0.36	23.02	1.98E-01	0.327
Q3TDQ1	Stt3b	Dolichyl-diphosphooligosaccharide--protein glycosyltransferase subunit STT3B	0.78	-0.37	20.99	3.46E-01	0.466
Q3UHN9	Ndst1	Bifunctional heparan sulfate N-deacetylase/N-sulfotransferase 1	0.77	-0.37	16.92	5.68E-01	0.680
G5E902	Slc25a3	MCG10343, isoform CRA_b	0.77	-0.37	22.89	1.24E-01	0.237
O89051	Itm2b	Integral membrane protein 2B	0.77	-0.37	21.32	1.76E-01	0.302
Q3U9G9	Lbr	Lamin-B receptor	0.77	-0.38	19.85	2.79E-01	0.406
Q8C7U7	Galnt6	Polypeptide N-acetylgalactosaminyltransferase 6	0.76	-0.39	21.25	1.14E-01	0.224
Q8BVE3	Atp6v1h	V-type proton ATPase subunit H	0.76	-0.40	19.55	1.07E-01	0.214
E9Q557	Dsp	Desmoplakin	0.76	-0.40	21.53	3.70E-01	0.486
Q60767	Ly75	Lymphocyte antigen 75	0.74	-0.43	25.22	6.97E-02	0.167
Q8BMT4-2	Nrros	Isoform 2 of Negative regulator of reactive oxygen species	0.74	-0.43	18.75	8.87E-02	0.190
Q9CRT8	Xpot	Exportin-T	0.74	-0.44	19.14	7.43E-02	0.173
Q792Z1	Try10	MCG140784	0.74	-0.44	24.34	3.27E-01	0.452
Q91YQ5	Rpn1	Dolichyl-diphosphooligosaccharide--protein glycosyltransferase subunit 1	0.74	-0.44	23.95	8.08E-02	0.181
Q61074	Ppm1g	Protein phosphatase 1G	0.73	-0.45	18.75	1.40E-01	0.251
Q3UXS0	Scamp3	Secretory carrier-associated membrane protein 3	0.72	-0.46	19.42	1.27E-01	0.238
O88325	Naglu	Alpha-N-acetylglucosaminidase	0.72	-0.47	21.02	4.10E-02	0.114
Q9CPQ3	Tomm22	Mitochondrial import receptor subunit TOM22 homolog	0.72	-0.47	20.17	7.92E-02	0.181
Q9JJZ2	Tuba8	Tubulin alpha-8 chain	0.72	-0.48	18.06	8.97E-02	0.190
P53986	Slc16a1	Monocarboxylate transporter 1	0.72	-0.48	20.67	6.64E-02	0.163
P68368	Tuba4a	Tubulin alpha-4A chain	0.71	-0.50	20.94	2.26E-01	0.361
Q60932-2	Vdac1	Isoform Mt-VDAC1 of Voltage-dependent anion-selective channel protein 1	0.71	-0.50	17.87	1.57E-01	0.277

Supplementary Table 5 continued

Accession	Gene Name	Protein Description	Average Fold Change	log_2(AFC)	log_2(Average Abundance)	P-value	Adjusted P-value
Q9WU60	Atrn	Attractin	0.70	-0.51	21.15	4.81E-02	0.129
O35604	Npc1	Niemann-Pick C1 protein	0.70	-0.52	22.95	3.80E-02	0.109
D3YTP0	Steap3	Metalloreductase STEAP3 (Fragment)	0.69	-0.54	18.83	1.39E-01	0.251
Q8VBZ3	Clptm1	Cleft lip and palate transmembrane protein 1 homolog	0.69	-0.54	22.67	6.13E-02	0.154
Q3U1J4	Ddb1	DNA damage-binding protein 1	0.68	-0.55	19.47	4.21E-02	0.114
Q8BYI8-2	Kiaa1467	Isoform 2 of Uncharacterized protein KIAA1467	0.68	-0.56	19.86	1.40E-01	0.251
P97350	Pkp1	Plakophilin-1	0.67	-0.57	17.97	3.33E-01	0.453
Q91UZ6	D17H6S56E-5	DNA segment, Chr 17, human D6S56E 5, isoform CRA_c	0.67	-0.58	22.54	3.80E-02	0.109
Q8BL63	Pigk	GPI-anchor transamidase	0.67	-0.58	20.34	2.62E-02	0.085
P27046	Man2a1	Alpha-mannosidase 2	0.66	-0.60	22.02	3.27E-02	0.100
P70168	Kpnb1	Importin subunit beta-1	0.66	-0.60	22.83	2.22E-02	0.079
Q3V3R1	Mthfd1l	Monofunctional C1-tetrahydrofolate synthase, mitochondrial	0.66	-0.61	18.66	5.85E-02	0.151
Q8K2C7-2	Os9	Isoform 2 of Protein -9	0.66	-0.61	17.04	3.82E-02	0.109
P99027	Rplp2	60S acidic ribosomal protein P2	0.65	-0.62	22.82	1.82E-02	0.076
Q91XA2	Golm1	Golgi membrane protein 1	0.65	-0.62	22.84	8.11E-02	0.181
Q9D8L3	Ssr4	Signal sequence receptor, delta	0.65	-0.63	22.03	1.98E-02	0.079
Q9CY50	Ssr1	Translocon-associated protein subunit alpha	0.65	-0.63	23.68	2.13E-02	0.079
Q9QY81	Nup210	Nuclear pore membrane glycoprotein 210	0.65	-0.63	26.90	8.24E-02	0.182
Q9DBH5	Lman2	Vesicular integral-membrane protein VIP36	0.64	-0.64	18.86	2.91E-01	0.415
Q99KV1	Dnajb11	DnaJ homolog subfamily B member 11	0.64	-0.65	19.25	6.69E-02	0.163
P01849	Tcra	T-cell receptor alpha chain C region	0.63	-0.66	23.56	3.66E-02	0.109
P62814	Atp6v1b2	V-type proton ATPase subunit B, brain isoform	0.63	-0.67	20.05	2.45E-02	0.085
Q9D1D4	Tmed10	Transmembrane emp24 domain-containing protein 10	0.62	-0.68	23.03	2.83E-02	0.091
Q5XJY5	Arcn1	Coatomer subunit delta	0.62	-0.68	19.54	1.80E-01	0.306
Q99LL3	Chst12	Carbohydrate sulfotransferase 12	0.61	-0.72	20.91	2.24E-02	0.079
Q9D1K2	Atp6v1f	V-type proton ATPase subunit F	0.60	-0.74	19.40	1.29E-02	0.060
O54734	Ddost	Dolichyl-diphosphooligosaccharide--protein glycosyltransferase 48 kDa subunit	0.59	-0.75	23.75	1.47E-02	0.065
O09159	Man2b1	Lysosomal alpha-mannosidase	0.59	-0.77	19.73	6.10E-02	0.154

Supplementary Table 5 continued

Q62351	Tfrc	Transferrin receptor protein 1	0.59	-0.77	27.45	1.74E-01	0.302
P11942	Cd3g	T-cell surface glycoprotein CD3 gamma chain	0.58	-0.79	21.78	1.25E-01	0.237
O55029	Copb2	Coatomer subunit beta'	0.58	-0.80	18.94	1.99E-01	0.327
G3UYZ1	Igsf8	Immunoglobulin superfamily member 8	0.56	-0.83	19.56	9.85E-02	0.203
Q61753	Phgdh	D-3-phosphoglycerate dehydrogenase	0.56	-0.83	23.44	8.68E-03	0.047
E9Q0F0	Krt78	Protein Krt78	0.56	-0.84	24.53	1.37E-01	0.251
P97370	Atp1b3	Sodium/potassium-transporting ATPase subunit beta-3	0.56	-0.84	24.93	8.00E-03	0.047
Q03265	Atp5a1	ATP synthase subunit alpha, mitochondrial	0.56	-0.85	24.60	6.68E-03	0.047
D3YU17	Ncln	Nicalin	0.55	-0.86	20.32	8.84E-03	0.047
P09405	Ncl	Nucleolin	0.55	-0.86	20.39	3.19E-02	0.100
Q8K297	Colgalt1	Procollagen galactosyltransferase 1	0.55	-0.87	21.53	9.02E-03	0.047
Q9Z2K1	Krt16	Keratin, type I cytoskeletal 16	0.54	-0.88	21.54	4.95E-02	0.130
Q3TTY5	Krt2	Keratin, type II cytoskeletal 2 epidermal	0.53	-0.91	23.62	2.49E-01	0.386
Q921V5	Mgat2	Alpha-1,6-mannosyl-glycoprotein 2-beta-N-acetylglucosaminyltransferase	0.53	-0.91	19.43	2.23E-02	0.079
P17809	Slc2a1	Solute carrier family 2, facilitated glucose transporter member 1	0.52	-0.93	18.99	2.73E-01	0.405
Q9JKR6	Hyou1	Hypoxia up-regulated protein 1	0.52	-0.95	23.81	4.70E-03	0.041
P56480	Atp5b	ATP synthase subunit beta, mitochondrial	0.51	-0.98	25.99	9.00E-03	0.047
Q64518-2	Atp2a3	Isoform SERCA3A of Sarcoplasmic/endoplasmic reticulum calcium ATPase 3	0.50	-0.99	19.06	2.50E-02	0.085
Q01965	Ly9	T-lymphocyte surface antigen Ly-9	0.50	-1.00	25.36	5.01E-03	0.041
Q8VCS3	Fam20b	Glycosaminoglycan xylosylkinase	0.48	-1.05	19.99	1.47E-02	0.065
P04104	Krt1	Keratin, type II cytoskeletal 1	0.47	-1.08	24.36	8.76E-02	0.190
P20029	Hspa5	78 kDa glucose-regulated protein	0.47	-1.08	26.37	1.26E-02	0.060
Q9JLF6	Tgm1	Protein-glutamine gamma-glutamyltransferase K	0.47	-1.09	17.70	7.75E-03	0.047
Q6GQT9	Nomo1	Nodal modulator 1	0.45	-1.16	25.00	2.14E-02	0.079
P07724	Alb	Serum albumin	0.37	-1.45	22.83	2.06E-02	0.079
P38647	Hspa9	Stress-70 protein, mitochondrial	0.26	-1.96	28.28	2.48E-04	0.008
Q9CPN9	2210010C04Rik	Protein 2210010C04Rik	0.15	-2.71	27.18	2.91E-03	0.028

Supplementary Table 6: **Analysis of splenocyte control experiments.** Labile disulfide bond reduction was quantified by SINQ on splenocytes obtained from a mouse model of LPS-induced inflammation that didn't show any difference of thiol cell surface levels by flow cytometry compared to the control (Experiment 2 and Experiment 3). The listed proteins show proteins that were identified in both experiments with their respective log_2(Fold Change), UniProt accession, gene name and protein description.

			Experiment 2	Experiment 3
Accession	**Gene Name**	**Protein Description**	**log_2(Fold Change)**	**log_2(Fold Change)**
Q9EP73	Cd274	Programmed cell death 1 ligand 1	4.29	2.72
Q80UR4	Prss34	Mast cell protease-11	-2.53	-3.22
P01750	1 SV	Ig heavy chain V region 102	-3.19	2.78
P01750	1 SV	Ig heavy chain V region 102	-3.19	-2.76
Q9Z2K1	Krt16	Keratin, type I cytoskeletal 16	-3.31	2.49
A0A075B5V8	Ighv1-47	Protein Ighv1-47	-4.89	2.73
Q3UV17	Krt76	Keratin, type II cytoskeletal 2 oral	-6.89	2.84

Supplementary Table 7: **Kinetics of labile disulfide bond reduction during immune activation.** Labile disulfide bond reduction during immune activation was quantified in a MLR using SH-IQ (Mascot score ≥ 37, ≥ 2 unique peptides). The data was analysed using Progenesis using the built in normalisation function to normalise peptide intensities to total peptide abundances and represents proteins that were constantly identified in two MLRs. For the proteins listed in the table the following information is shown: Gene name, protein description, the FC for each experiment (MLR1 and MLR2) at the different time points relative to t4, the AFC and the SEM. Proteins highlighted in green have at least two log_2(AFC) >1 and a minimum of one of those AFC must be composed of both log_2(FC)s >1. Proteins highlighted in red have at least two log_2(AFC) <-1 and a minimum of one of those AFC must be composed of both log_2(FC)s <-1.

Gene name	Protein description	MLR1 t16	MLR2 t16	AFC t16	SEM t16	MLR1 t24	MLR2 t24	AFC t24	SEM t24	MLR1 t48	MLR2 t48	AFC t48	SEM t48	MLR1 t96	MLR2 t96	AFC t96	SEM t96
CD44	CD44 antigen	0.48	1.68	1.08	0.60	1.19	1.13	1.16	0.03	0.82	2.13	1.48	0.65	1.18	1.52	1.35	0.17
MAN2B1-2	Lysosomal alpha-mannosidase	1.48	1.36	1.42	0.06	2.42	0.62	1.52	0.90	0.14	1.12	0.63	0.49	1.48	1.56	1.52	0.04
KRT13-3	Keratin, type I cytoskeletal 13	2.50	-4.00	-0.75	3.25	2.58	1.88	2.23	0.35	3.12	4.11	3.61	0.49	0.80	2.30	1.55	0.75
CTSB	Cathepsin B	1.07	0.69	0.88	0.19	0.42	0.29	0.35	0.07	1.60	2.59	2.09	0.50	1.43	1.87	1.65	0.22
ITGB7	Integrin beta-7	0.77	0.30	0.54	0.23	0.73	2.69	1.71	0.98	1.31	2.22	1.77	0.46	1.33	2.41	1.87	0.54
HSPA5	78 kDa glucose-regulated protein	-0.70	0.76	0.03	0.73	0.95	0.39	0.67	0.28	1.45	1.64	1.55	0.10	1.52	2.33	1.92	0.40
SEMA4D	Semaphorin-4D	1.26	0.47	0.86	0.40	2.04	0.44	1.24	0.80	1.31	1.32	1.31	0.00	2.27	1.83	2.05	0.22
LDLR-2	Low-density lipoprotein receptor	0.43	1.12	0.78	0.35	1.23	2.01	1.62	0.39	1.78	2.68	2.23	0.45	1.73	2.39	2.06	0.33
ATP6V1A	V-type proton ATPase catalytic subunit A	-0.42	1.93	0.76	1.18	1.03	1.51	1.27	0.24	0.07	1.35	0.71	0.64	1.28	2.89	2.08	0.80
B2M	Beta-2-microglobulin form pI 5.3	0.56	-0.25	0.16	0.41	2.14	-0.51	0.81	1.32	2.57	1.84	2.21	0.36	2.57	1.90	2.23	0.34
SLAMF1	Isoform 3 of Signaling lymphocytic activation molecule	-0.14	0.49	0.18	0.31	1.08	1.43	1.25	0.18	1.20	0.71	0.95	0.25	1.48	3.35	2.42	0.94
A2M	Alpha-2-macroglobulin	0.09	0.24	0.17	0.07	1.60	-0.58	0.51	1.09	1.50	2.19	1.84	0.34	3.77	1.28	2.52	1.24
CD1B	T-cell surface glycoprotein CD1b	-0.09	-7.01	-3.55	3.46	2.11	-2.77	-0.33	2.44	2.10	3.09	2.59	0.50	3.38	2.18	2.78	0.60
ICAM1	Intercellular adhesion molecule 1	1.05	2.34	1.69	0.64	1.46	2.18	1.82	0.36	2.06	2.67	2.36	0.30	2.64	3.36	3.00	0.36
MRC1	Macrophage mannose receptor 1	0.61	0.62	0.62	0.01	2.23	2.21	2.22	0.01	3.59	5.16	4.37	0.79	3.36	2.95	3.15	0.21
SLAMF7	SLAM family member 7	1.97	2.47	2.22	0.25	1.83	0.31	1.07	0.76	0.22	3.80	2.01	1.79	2.98	3.45	3.21	0.23
TFRC	Transferrin receptor protein 1	0.95	-0.57	0.19	0.76	1.31	0.41	0.86	0.45	2.34	2.35	2.35	0.01	3.98	3.86	3.92	0.06

Supplementary Table 7 continued

Gene name	Protein description	MLR1 t16	MLR2 t16	AFC t16	SEM t16	MLR1 t24	MLR2 t24	AFC t24	SEM t24	MLR1 t48	MLR2 t48	AFC t48	SEM t48	MLR1 t96	MLR2 t96	AFC t96	SEM t96
CD274	Programmed cell death 1 ligand 1	0.80	3.53	2.17	1.36	4.02	3.81	3.92	0.10	1.68	4.21	2.94	1.27	5.10	5.12	5.11	0.01
IGKC	Ig kappa chain C region	0.55	0.34	0.44	0.10	1.42	1.43	1.42	0.00	0.92	1.48	1.20	0.28	-0.07	-0.49	-0.28	0.21
LGALS3BP	Galectin-3-binding protein	0.38	1.55	0.97	0.58	0.89	1.31	1.10	0.21	1.45	1.16	1.31	0.14	0.06	0.57	0.31	0.25
KRT4	Keratin, type II cytoskeletal 4	0.65	0.42	0.53	0.12	2.92	-1.34	0.79	2.13	2.53	2.89	2.71	0.18	0.03	2.12	1.08	1.04
BST2-2	Bone marrow stromal antigen 2	0.16	-1.19	-0.51	0.67	-2.65	-0.45	-1.55	1.10	0.59	1.83	1.21	0.62	1.01	1.46	1.23	0.22
HLA-DQB1	HLA class II histocompatibility antigen, DQ beta 1 chain	1.17	0.66	0.92	0.26	1.90	0.77	1.34	0.57	1.50	0.99	1.24	0.25	1.24	1.23	1.24	0.00
DPP4	Dipeptidyl peptidase 4	1.28	-0.12	0.58	0.70	1.66	0.65	1.16	0.51	1.46	0.72	1.09	0.37	1.09	1.45	1.27	0.18
HLA-DRB1	HLA class II histocompatibility antigen, DRB1-4 beta chain	1.62	0.68	1.15	0.47	2.36	0.75	1.55	0.81	3.99	1.48	2.73	1.25	2.49	0.24	1.37	1.12
ADA	Adenosine deaminase	0.89	0.03	0.46	0.43	1.50	0.51	1.00	0.50	1.55	0.15	0.85	0.70	1.21	2.17	1.69	0.48
HLA-DPB1	HLA class II histocompatibility antigen, DP beta 1 chain	1.23	0.68	0.95	0.28	1.42	0.84	1.13	0.29	-1.63	1.43	-0.10	1.53	2.25	1.20	1.73	0.53
PLXND1	Plexin-D1	-0.32	0.09	-0.11	0.20	-0.89	0.14	-0.37	0.51	0.99	1.46	1.22	0.23	1.82	1.69	1.75	0.07
IL2RG	Cytokine receptor common subunit gamma	0.85	1.67	1.26	0.41	0.62	1.76	1.19	0.57	0.19	1.91	1.05	0.86	2.08	1.65	1.87	0.22
SLC3A2	4F2 cell-surface antigen heavy chain	0.21	1.40	0.81	0.59	0.82	1.74	1.28	0.46	-0.03	2.04	1.00	1.03	1.56	2.29	1.93	0.37
LY75	Lymphocyte antigen 75	0.42	-0.10	0.16	0.26	2.22	-0.71	0.75	1.47	1.73	0.43	1.08	0.65	2.70	1.56	2.13	0.57
LGALS9	Isoform Short of Galectin-9	0.16	1.14	0.65	0.49	-0.01	0.93	0.46	0.47	0.77	1.76	1.26	0.49	2.49	2.04	2.26	0.23
KRT31	Keratin, type I cuticular Ha1	2.76	0.21	1.48	1.28	-1.29	-1.34	-1.31	0.02	-0.12	-0.85	-0.48	0.37	-0.96	-5.21	-3.08	2.13
THBS1	Thrombospondin-1	-0.73	0.22	-0.26	0.47	-0.95	-0.12	-0.53	0.42	-3.00	-0.87	-1.94	1.07	-3.55	-2.17	-2.86	0.69
GPR56-2	G-protein coupled receptor 56	-0.72	-0.44	-0.58	0.14	-0.47	-0.91	-0.69	0.22	-1.68	-0.59	-1.13	0.55	-3.12	-2.17	-2.64	0.48
CLU-4	Clusterin	-0.08	-0.28	-0.18	0.10	0.00	-1.08	-0.54	0.54	-0.95	-1.72	-1.33	0.38	-2.19	-2.29	-2.24	0.05
CTSZ	Cathepsin Z	-1.33	-0.13	-0.73	0.60	-0.78	-1.11	-0.94	0.17	-1.27	-0.74	-1.01	0.27	-2.18	-1.96	-2.07	0.11
TUBA4A-2	Tubulin alpha-4A chain	-1.38	0.16	-0.61	0.77	-2.11	-0.05	-1.08	1.03	-1.72	-0.21	-0.97	0.76	-1.05	-1.65	-1.35	0.30
PLXDC2	Plexin domain-containing protein 2	0.60	-5.08	-2.24	2.84	1.04	-5.84	-2.40	3.44	-1.36	2.67	0.66	2.02	-0.66	-1.67	-1.16	0.50
SIRPB1	Signal-regulatory protein beta-1 isoform 3	-2.44	0.64	-0.90	1.54	-2.33	-1.12	-1.73	0.61	-1.66	-0.06	-0.86	0.80	-1.38	-0.77	-1.07	0.31

Supplementary Table 7 continued

NDUFS8	NADH dehydrogenase [ubiquinone] iron-sulfur protein 8, mitochondrial	-0.37	-2.31	-1.34	0.97	-0.28	-0.12	-0.20	0.08	-4.44	-1.35	-2.90	1.55	-0.20	-0.49	-0.34	0.15
4 SV	Uncharacterized protein	-1.14	-0.26	-0.70	0.44	0.24	-2.46	-1.11	1.35	-2.97	-2.55	-2.76	0.21	1.48	-2.06	-0.29	1.77
CTSC	Dipeptidyl peptidase 1	0.78	-4.07	-1.64	2.42	-0.23	-3.94	-2.08	1.86	-0.34	0.76	-0.91	0.55	-5.66	-2.01	-3.84	1.83
STT3B	Dolichyl-diphosphooligosaccharide--protein glycosyltransferase subunit STT3B	-0.64	-5.03	-2.84	2.20	-0.75	-5.88	-3.31	2.57	-0.87	-0.30	-0.58	0.28	-0.33	-6.51	-3.42	3.09
ITGB3	Integrin beta-3	-0.25	-0.25	-0.25	0.00	-1.94	-0.65	-1.30	0.64	-2.27	-1.54	-1.91	0.36	-3.61	-3.03	-3.32	0.29
HRNR	Hornerin	2.05	-3.95	-0.95	3.00	1.19	-0.59	0.30	0.89	-1.05	-4.97	-3.01	1.96	-1.46	-5.03	-3.25	1.78
FCGRT	IgG receptor FcRn large subunit p51	-1.34	-2.71	-2.02	0.69	3.02	-4.03	-0.51	3.53	-1.25	-2.54	-1.90	0.65	-1.56	-4.63	-3.10	1.54
ITGA2B-2	Integrin alpha-IIb	-0.51	0.02	-0.25	0.26	1.20	-0.68	0.26	0.94	-3.01	-1.99	-2.50	0.51	-3.08	-2.61	-2.84	0.23
S100A9	Protein S100-A9	-1.84	-4.47	-3.16	1.32	-1.69	-1.93	-1.81	0.12	-1.86	-1.47	-1.67	0.19	-0.20	-5.26	-2.73	2.53
GP1BA	Platelet glycoprotein Ib alpha chain	-0.03	-0.31	-0.17	0.14	-0.06	-0.39	-0.22	0.17	-2.49	-1.76	-2.13	0.37	-2.20	-2.94	-2.57	0.37
PLD4	Phospholipase D4	-0.62	0.55	-0.04	0.59	-0.15	-0.50	-0.32	0.18	-2.03	-1.32	-1.68	0.36	-2.33	-2.52	-2.43	0.09
TLR2	Toll-like receptor 2	-1.00	0.29	-0.36	0.64	-1.76	-0.75	-1.25	0.50	-1.23	-1.29	-1.26	0.03	-2.28	-2.41	-2.34	0.07
PTPRCAP	Protein tyrosine phosphatase receptor type C-associated protein	0.01	-0.41	-0.20	0.21	0.72	-3.37	-1.33	2.05	-0.22	-3.57	-1.90	1.68	-0.07	-4.61	-2.34	2.27
RAB27A	Ras-related protein Rab-27A	-1.17	-1.40	-1.29	0.12	-1.45	-2.54	-2.00	0.55	-1.88	-0.67	0.65	0.61	-3.77	-0.84	-2.31	1.47
APMAP	Adipocyte plasma membrane-associated protein	-0.51	0.50	0.00	0.50	-1.68	-0.60	-1.14	0.54	-1.42	-1.19	-1.30	0.11	-2.08	-1.85	-1.96	0.11
CECR1	Adenosine deaminase CECR1	-0.87	1.08	0.10	0.98	-1.11	-1.62	-1.37	0.26	-1.24	-1.80	-1.52	0.28	-2.63	-1.28	-1.95	0.67
RPL4	60S ribosomal protein L4	-0.25	0.21	-0.02	0.23	-0.04	-2.34	-1.19	1.15	0.01	-2.28	-1.13	1.15	-0.51	-3.32	-1.91	1.41
ERLIN2	Erlin-2 (Fragment)	-0.81	0.05	-0.38	0.43	-1.54	-1.35	-1.45	0.09	-0.56	-1.55	-1.06	0.50	-0.68	-2.82	-1.75	1.07
MMRN1	Multimerin-1	-0.83	0.46	-0.19	0.65	-1.04	0.05	-0.50	0.55	-1.96	-1.79	-1.88	0.08	-2.06	-1.27	-1.67	0.39
ATP2A3	Isoform SERCA3A of Sarcoplasmic/endoplasmic reticulum calcium ATPase 3	-0.91	-4.38	-2.64	1.73	-0.26	-1.91	-1.08	0.83	-1.17	-1.01	-1.09	0.08	-0.98	-2.23	-1.60	0.62
CPVL	Probable serine carboxypeptidase CPVL	-0.86	0.67	-0.10	0.76	-0.84	-1.60	-1.22	0.38	-1.02	-1.60	-1.31	0.29	-1.44	-1.55	-1.50	0.06
SUN2	Isoform 2 of SUN domain-containing protein 2	-0.92	0.59	-0.17	0.76	0.03	-0.16	-0.06	0.09	-1.15	-1.43	-1.29	0.14	-1.26	-1.52	-1.39	0.13

Supplementary Table 7 continued

Gene name	Protein description	MLR1 t16	MLR2 t16	AFC t16	SEM t16	MLR1 t24	MLR2 t24	AFC t24	SEM t24	MLR1 t48	MLR2 t48	AFC t48	SEM t48	MLR1 t96	MLR2 t96	AFC t96	SEM t96
UQCRC2	Cytochrome b-c1 complex subunit 2, mitochondrial	-0.32	-4.83	-2.58	2.26	-0.54	-6.50	-3.52	2.98	0.28	-0.30	-0.01	0.29	0.10	-2.24	-1.07	1.17

2. Quantitation methods in proteomics

2.1. SILAC

In SILAC, the 'heavy' isotopes is biologically incorporated by uptake of amino acids by the cells from the medium. Typical amino acids chosen for SILAC are leucine or lysine and arginine so that all peptides will contain at least one labelled amino acid after a tryptic digest. Two cell populations are grown in medium either containing either the 'light' (e.g. $^{12}C_6$ leucine) or 'heavy' (e.g. $^{13}C_6$ leucine) version of the amino acids. After several cell divisions, all the proteins will contain this particular amino acid. SILAC was successfully incorporated into higher organisms such as mice (205) and flies (206) by feeding them with labelled food. SILAC method benefits from the fact that the label is incorporated at the earliest stage possible of the experiment. Thus, the samples can be combined directly after harvesting the cells and variation arising from sample preparation and purification is eliminated. The limitation of this method, however, is that it depends on endogenous labelling which is not applicable when studying primary tissue/cell samples. Moreover, it is limited to studying three conditions at the same time.

2.2. ICAT

ICAT was the first commercially available isotope coded tagging system for comparing the amount of protein between two samples. ICATs are thiol reactive iodoacetamide derivatives linked to a biotin tag by a linker originally containing eight ^{2}D (deuterium). The biotin tag allows the sample to be enriched for biotinylated peptides and thus reducing the sample complexity. The relative abundance of peptides is determined measuring the peak ratios. A few years later it has been shown, that deuterium containing peptides lute earlier in reverse phase chromatography than their 'normal' analogues because deuterium is more polar than hydrogen (207). This problem has been solved my modifying the linker using nine ^{13}C instead. ICAT has been further improved by introducing an acid-cleavable site into the reagent which allows the removal of the biotin moiety prior to LC-MS/MS. This reduces the overall size of the tag enabling the analysis of larger peptides and it reduces tag fragmentation which improves the quality of the MS/MS and thus leads to an increase of protein identification. ICAT quantitation is

limited to proteins that contain a cysteine residue and to two conditions. Moreover, the cost of the reagent is rather high compared to other stable isotope labelling methods.

2.3. iTRAQ and TMT

The previously discussed isotopic tagging methods SILAC and ICAT produce peptides with a particular mass variation that elute at the same time in the reverse phase chromatography. Quantitation of peptides is carried out on the precursor level. These methods are limited in the multiplex numbers (three for SILAC and two for ICAT) which has been substantially increased by introducing isobaric tags. Isobaric tags (iTRAQ and TMT) are identical in mass and are only distinguishable by their fragmentation pattern (reporter ions). Isobaric tags consist of an amine reactive group (N-hydroxy-succinimide, NHS) that covalently binds to free amines of peptides, a balancer and a reporter. The total weight of the balancer and the reporter group is always the same but the individual weight changes. Therefore, when the reporter ion is released in MS/MS fragmentation and can be correlated to a particular sample source. As discussed before, the charge of a peptide is found on the most basic part of the peptide. In iTRAQ or TMT labelled peptides this is the label. As a result, the reporter signal is relatively high compared to the fragment ion signal. This results in a decrease in identification of PSMs and therefore a slightly lower identification of proteins when compared to SILAC.

iTRAQ initially has been designed for simultaneous analysis of four samples but is meanwhile available as an 8-plex kit (208). The total mass of the balance and reporter group for the 4-plex and 8-plex version is 145 Da and 305 Da respectively. The m/z of the reporter fragment ions is 113, 114, 115, 116, 117, 118, 119, and 121. Their abundance is directly proportional to the abundance of each tagged peptide. Because the number of atoms is increased from the 4-plex to the 8-plex label, this can lead to a more complex fragmentation pattern with competing unwanted daughter ions and may lead to a decrease in the number of peptide spectral matches, unique peptides and proteins (209). TMT labels omit this problem by having an identical chemical structure and only varying the numbers and

combinations of ^{13}C and ^{15}N isotopes in the reporter and linker region. TMTs exist as 2-plex, 6-plex and 10-plex kits. The drawback of isobaric tagging is that it suffers from dynamic range suppression caused by co-isolation of precursor ions which decreases the quantitative accuracy (210). This can be solved by a double isolation where the MS/MS spectrum is used for identification and the MS3 spectrum for quantification (211).

2.4. NeuCode

In 2013, the lab of Joshua J. Coon introduced a novel way of protein quantification called neutron encoding (NeuCode) (70). This method exploits subtle mass differences caused by variations in nuclear binding energy in stable isotopes. This mass defect is caused because nuclear binding energy (the energy that is required to break down the nucleus into its nucleons) is different for each isotope for every element. Therefore, mass defects can be introduced with many different elements such as the elements contained in amino acids: $^{12}C/^{13}C$ (+3.3 mDa), $^{1}H/^{2}H$ (+6.3 mDa), $^{16}O/^{18}O$ (+4.2 mDa), $^{14}N/^{15}N$ (-3.0 mDa) and $^{32}S/^{34}S$ (-4.2 mDa). This would theoretically allow 39 isotopologues of the amino acid lysine with a mass range of 38.5 mDa. However, these isotopologues are only separated by ~1 mDa which cannot be resolved by today's mass spectrometers. With a resolving power of 240,000 a mass difference of 36 mDa, at 480,000 a mass difference of 18 and 12 mDa and at 960,000 a mass difference of 6 mDa could be distinguished (separated at full with at 10% of full peak height). Applying this strategy to SILAC metabolically integrating NeuCode lysine that this allows 3-plex NeuCode SILAC with a 480,000 resolving power MS1 scan (70) and 6-plex NeuCode SILAC at 960,000 (212). NeuCode SILAC compares to traditional SILAC in overall MS/MS spectra collected, and mass accuracy. The benefit of NeuCode SILAC is that it produced considerably more unique peptide spectral matches (PSMs). Due to NeuCode SILAC peptides appearing at very close m/z spacing, both isotopologues are isolated at the same time (which is not the case in traditional SILAC). This eliminates redundant peptide identification and therefore allows increased sampling depth that is comparable to unlabelled sample. When comparing a 4-plex NeuCode SILAC and TMT labelling, NeuCode SILAC produced a

wider dynamic range in protein abundance measurements which provides a solution to the dynamic range suppression in isobaric tagging caused by co-isolation of precursor peptides.

NeuCode can also be applied to chemical amine labelling (in which an amine reactive NHS ester is coupled to $_{acetyl}$Arg-$_{acetyl}$Lys-Gly apanning a mass range of 37.9 mDa (213)) when metabolic incorporation of the label is not feasible. Given that at a resolution of 480,000 12 mDa can be distinguished this allows 4-plex NeuCode labelling. This strategy offers comparable precision and accuracy to traditional SILAC. The current tag, however, reduces the number of peptides identified compared to unlabelled sample. This can be explained by the fact that the tag is relatively big and it contains amine bonds that can get fragmented. This then leads to an increase in spectral complexity. This can be avoided by introducing a small molecule as a tag.

2.5. Label-free quantitation

Quantitative mass spectrometry methods based on stable isotope or NeuCode labelling will always be restricted by the number of tags available and/or the resolution of the mass spectrometer. Label-free quantitation is cost effective, can be applied to primary cell and tissue samples, has a high percentage of identified PSMs and can analyse any number of samples.

There are two different types of label-free quantitation, area under the curve (AUC) and spectral counting methods.

AUC methods involves the integrated signal intensity measurement of chromatographic peak areas for a given peptide in MS1. The AUC has been shown to be linearly proportional to the peptide concentration in the range of 10 fmol – 1000 pmol (156, 157). Although this conceptually simple, reproducibility (minimise sample preparation variations) and accurate detection between individual sample runs has to be ensured. This means that the individual samples have to be processed in parallel and run on the mass spectrometer in consecutive order to avoid technical variations. To compare peak intensities between mass spectrometry runs, software is used to either pair peaks based on their identity (ProteomeDiscoverer 1.4, Thermo) or chromatographic alignment of m/z retention times (Progenesis QI for Proteomics). To obtain accurate quantitation normalisation of the data is required which accounts for loading differences and instrument variations between samples. This is generally done by either normalising to the total ion current or a set of house-keeping proteins that are known to be unchanged in the conditions studied. A statistical approach (quantile normalisation) can be taken as well in which it is assumed that the data is normally distributed when transformed to $\log_2$.

Spectral counting methods on the other hand are based on the observation that more abundant peptides are selected for fragmentation more often and therefore will produce higher abundance MS/MS spectra. In data-dependent acquisition (DDA), which is the standard mode in shotgun proteomics, the MS/MS abundance is proportional amount of precursor. Different spectral counting methods have emerged over the years all with the aim to increase accuracy. The protein abundance index (PAI) is an estimation of protein abundance in a sample. (214). It is defined as the number of observed peptides in the experiment divided by the number of observable tryptic peptides within a

given mass range (215). The PAI has later been exponentially modified (emPAI) which is proportional to the amount of protein (216). A shortcoming of this method is the physiochemical incoherence of peptides which introduced variability and bias in measurements. In 2007, this has been addressed in absolute protein expression (APEX) which is a modified spectral counting technique that takes into consideration the number of observed peptide mass spectra for a protein and the probability of the peptides being detected by the instrument machine learning algorithm. Spectral counting has also been modified to take into account that the length of a protein will affect the number of spectral counts. This normalised spectral abundance factor (NSAF) presents an improved measure for protein abundance. Combining peptide count, spectral count and fragment ion intensity from each MS2 spectrum later gave rise to a normalised spectral index SI_N (100).

AUC methods are more accurate and precise than the spectral counting methods emPAI, NSAF and SINQ (80). Comparing the spectral counting methods, SINQ outperforms emPAI and NSAF with a higher accuracy (80). Progenesis QI for Proteomics (PQIP) is highly dependent on chromatographic reproducibility to confidently align the m/z features. It is therefore of utmost importance that the samples to be compared are run on the same column back to back to minimise systemic variation. Complying with these guidelines, AUC quantitation using PQIP for data analysis is an accurate method for relative protein quantitation that allows easy review of peptides used for quantitation.

3. Shared cytokine receptors

Cytokines are small molecules that control the immune response by regulating proliferation, differentiation and other cellular functions. Cytokines interact with their cell surface receptor and induce signalling to enable cell-cell communication. This can be autocrine (on the same cell) or paracrine (on cells in the close proximity). Shared cytokine receptors are polyspecific meaning that they can bind to different cytokines. There are three different types of shared cytokine receptors i) the common gamma chain (γ_c), ii) the common beta chain (β_c) and iii) gp130. Shared cytokine receptors show a modular architecture of the extracellular proportion which is composed of at least one cytokine-binding homology region (CHR). The CHR includes two fibronectin type II domains containing 4 and 2 cysteines forming disulfide bonds in the N-terminal and C-terminal domain respectively. Moreover, the C-terminal domain contains a conserved Trp-Ser-X-Trp-Ser motif. The common γ chain is composed of one and common β chain of two CHR modules. gp130 contains one CHR domain an N-terminal Ig-like domain and a membrane-proximal fibronectin type III domain.

The γ_c recognises IL-2, IL-4, IL-7, IL-9, IL-15 and IL-21 depending on the ligand-specific α and/or β receptor partner. IL-2 and IL-15 are recognised by a heterotrimer that is composed of γ_c /IL-2Rβ/IL-2Rα or IL-15Rα. The other cytokines that signal through γ_c are recognised by a heterodimer of γ_c and the cytokine specific α receptor. IL-4Rα and IL-7Rα are shared between IL-4 and IL-13 and IL-7 and TSLRP, respectively. The IL-13 recognition additionally requires IL-13Rα and TSLP (thymic stromal-derived lymphopoietin) TLSPR. Mutations in several residues in the γ_c, including Cys160-Cys209, have been shown to abolish the cytokine-dependent signalling causing X-linked severe combined immunodeficiency disease (X-SCID) (217–219). Interestingly, IL-2 signalling through γ_c can also be redox-regulated by reducing a labile disulfide bond (Cys183 –Cys232 in mouse) (19) which potentially ablates the signalling of several cytokine receptor complexes that include the γ_c.

The β_c recognises IL-3, IL-5 and GM-CSF in complex with a ligand-specific α subunit (IL-3Rα, IL-5Rα or GM-CSFRα). In contrast to the other shared cytokine receptors, β_c signalling seems to be mediated by two hexamers (β_c/cytokine/Rα) forming a dodecamer. This is suggested by crystal contacts between two β_c/GM-CSF/GMRα hexamers and that mutation of the contact site ablates the GM-CSF induced signalling (220).

Cytokine binding mediates clustering of the extracellular cytokine receptor domains initiating the activation of constitutively associated Janus kinase (Jak) family kinases. This then leads to the phosphorylation of the cytokine receptors which serves as a docking site for secondary signalling molecule. The major cascades activated are JAK-STAT, RAS-RAF-MAP and PI3 kinase.

4. Papers

4.1. Immunoregulation through membrane proteins modified by reducing conditions induced by immune reactions.

(43)

Stegmann M, Metcalfe C, Barclay AN

Abstract

Selected disulfide bonds in membrane proteins are labile and are thus susceptible to changes in redox potential and/or the presence of thiol isomerase enzymes. Modification of these disulfide bonds can lead to conformational changes of the protein that in turn may alter protein activity and function. This occurs in the entry of several enveloped viruses into their host cells, e.g. HIV, hepatitis C virus and Newcastle disease virus. Labile disulfide bonds are also important in platelet activation, cytokine signalling and in a variety of diseases including cancer and arthritis. In this review we will concentrate on recent advances in understanding the conditions that lead to disulfide bond reduction in membrane proteins and their effects in regulating immune function.

4.2. CD44 binding to hylaruonic acid is redox regulated by a labile disulfide bond in the hylaruonic acid binding site.

(20)

Kellett-Clarke H, **Stegmann M**, Barclay AN and Metcalfe C

Abstract

CD44 is the primary leukocyte cell surface receptor for hyaluronic acid (HA), a component 11 of the extracellular matrix. Enzymatic post translational cleavage of labile disulfide bonds is a 12 mechanism by which proteins are structurally regulated by imparting an allosteric change and 13 altering activity. We have identified one such disulfide bond in CD44 formed by Cys77 and 14 Cys97 that stabilises the HA binding groove. This bond is labile on the surface of leukocytes 15 treated with chemical and enzymatic reducing agents. Analysis of CD44 crystal structures 16 reveal the disulfide bond to be solvent accessible and in the –LH hook configuration 17 characteristic of labile disulfide bonds. Kinetic trapping and binding experiments on CD44-Fc 18 chimeric proteins show the bond is preferentially reduced over the other disulfide bonds in 19 CD44 and reduction inhibits the CD44-HA interaction. Furthermore cells transfected with CD44 20 no longer adhere to HA coated surfaces after pre-treatment with reducing agents. The 21 implications of CD44 redox regulation are discussed in the context of immune function, disease 22 and therapeutic strategies.

European Journal of Immunology

Review

Immunoregulation through membrane proteins modified by reducing conditions induced by immune reactions

Monika Stegmann, Clive Metcalfe and A. Neil Barclay

Oxford Molecular Pathology Institute, Sir William Dunn School of Pathology, University of Oxford, South Parks Road, Oxford, United Kingdom

Selected disulfide bonds in membrane proteins are labile and are thus susceptible to changes in redox potential and/or the presence of thiol isomerase enzymes. Modification of these disulfide bonds can lead to conformational changes of the protein that in turn may alter protein activity and function. This occurs in the entry of several enveloped viruses into their host cells, e.g. HIV, hepatitis C virus and Newcastle disease virus. Labile disulfide bonds are also important in platelet activation, cytokine signalling and in a variety of diseases including cancer and arthritis. In this review we will concentrate on recent advances in understanding the conditions that lead to disulfide bond reduction in membrane proteins and their effects in regulating immune function.

Keywords: Disulfide redox · Immunoregulation · Membrane protein · Virus fusion

Labile disulfide bonds

A role in regulating membrane protein function

Cysteine is a unique aa in that it contains a sulfydryl group (–SH) that can covalently bond with a sulfydryl group of a separate cysteine residue to form a disulfide bond. Disulfide bonds can form between cysteines within the same polypeptide chain (intramolecular disulfide bond) or between cysteines on different polypeptide chains (intermolecular disulfide bond). The formation of disulfide bonds requires oxidation of the constituent cysteine residues. Once formed disulfide bonds are not chemically inert, they can be reduced back to their constituent cysteine residues. Although disulfide bonds are clearly important structurally, there is increasing evidence that they can be reduced under certain physiological conditions and that this can affect the activity of the protein itself with downstream functional consequences. In this review we discuss how these redox events may be important in regulating the immune system and we review recent data on the characterisation of membrane proteins that contain labile disulfide bonds.

Correspondence: Dr. A. Neil Barclay
e-mail: neil.barclay@path.ox.ac.uk

Structure and modification

The disulfide bonds formed between cysteine residues in proteins play an important structural role such as stabilising Ig-like domains in the harsh extracellular environment by bridging the beta sheets at the core of the fold, stabilising dimer formation for example, bridging between the light and heavy chains of Ig. Some disulfide bonds have a catalytic role notably in thioredoxin and protein disulfide isomerases (PDIs). In addition other disulfide bonds can be reduced and these can lead to changes in protein structure and have been termed 'allosteric'. The disulfide bonds themselves are heterogeneous in geometry and this is discussed in detail by Schmidt et al. [1] who studied the geometry of about 7000 disulfide bonds from known structures. In this review we use term labile to describe those disulfide bonds that can be reduced under physiological conditions. It seems likely that they will cause conformational changes but, in the absence of such data, we use the simple term 'labile' meaning easy to break. Recent screening studies have shown that a surprisingly large number of different

membrane proteins have labile disulfide bonds that can be reduced by mild reducing conditions in vitro and that many are reduced in vivo during inflammation [2]. The proteins identified include integrins, adhesion proteins, cytokine and chemokine receptors, Ag receptors and transporters.

PDI is an enzyme involved in catalysing disulfide bond formation, reduction and isomerization [3–5]. As a member of the thioredoxin superfamily, it contains regions with high aa sequence identity to the thioredoxin active site, which is comprised of a double-cysteine motif (CXXC, C refers to cysteine and X any aa). Disulfide bond reduction by PDI and thioredoxin superfamily members is a catalytic process where one molecule of enzyme can reduce many disulfide bonds. However co-enzymes such as thioredoxin reductase are needed to supply electrons to PDI to allow continuous turnover. This is controlled by the NADPH pathway [6].

Reducing conditions at the cell surface and extracellularly

The cytoplasm of cells is maintained under reducing conditions that are highly controlled, for example, in disease situations and in processes such as the oxidative burst. This area is beyond the scope of this review and is extensively reviewed elsewhere [7]. The extracellular space is generally oxidising but decreases in redox potential occur in inflammation and immune activation. For example, activation of DCs leads to the production of free extracellular cysteine [8], in vivo immunisation leads to increased free thiol production and induction of thioredoxin expression in lymphoid organs [9] and levels of extracellular thioredoxin are increased in lung injury [10]. Enzymes such as the PDI members are generally associated with the ER where they assist in the proper folding of proteins but they are also found in other locations such as the cell surface, the extracellular space, the cytosol and the nucleus [4]. Localisation of PDI and related proteins on the cell surface or the extracellular space can cause the reduction of labile disulfide bonds in membrane proteins, which may be important for viral infection, disease or cell signalling [4, 5]. Thus the presence of thioredoxin and PDI provides the mechanism to alter disulfide bonds in membrane proteins as discussed later in a variety of different situations.

Viruses

HIV

Enveloped viruses infect host cells by firstly binding to specific host cell receptors and then fusing with the host cell membrane. Virus-cell membrane fusion is a consequence of conformational changes in the envelope (ENV) proteins. These changes can be triggered by acidification, as in influenza virus infection [11], or by rearrangement of disulfide bonds by PDI family members as shown in HIV and other viruses such as, HCV, Newcastle disease virus and rotavirus as discussed in this and subsequent sections.

HIV is a major human pathogen that causes Acquired Immune Deficient Syndrome (AIDS). During HIV entry into the host cell, HIV ENV gp 120 (gp120) binds the CD4 receptor on T cells or macrophages [12]. HIV uptake can be blocked by preventing disulfide bond reduction by several agents including the PDI inhibitor bacitracin, the membrane-impermeable sulfhydryl reagent 5,5'-dithiobis (2-nitrobenzoic acid) (DTNB) and Abs against PDI (reviewed in [13]). Various disulfide bonds in gp120 have been implicated as being labile using thioredoxin, PDI and glutaredoxin [14–17]. A recent comparison of PDI, thioredoxin and DTT indicates reduction to some extent of five disulfide bonds in gp120 [18, 19], and complexes of PDI and gp120 have been identified [16]. It is proposed that the conformational change that occurs due to disulfide bond reduction leads to structural changes in gp41 which, in turn lead to the fusion of the viral envelope with the host cell [20].

CD4, the receptor for HIV, also contains a labile disulfide bond in domain 2 of the four extracellular Ig-like domains [21]. There is evidence that CD4 may exist as disulfide-linked multimers on the T- and myeloid-cell surfaces and that multimer formation increases upon activation of a myeloid cell line with PMA [22]. It is proposed that HIV has a preference for binding to the monomeric, reduced form of CD4 [23]. Interestingly thioredoxin but not PDI was effective in reducing the labile disulfide bond of CD4 whereas PDI is clearly involved in HIV uptake [13]. The role of disulfide exchange in the various stages of HIV uptake and shedding together with possibilities for therapy has been extensively studied and is reviewed in [13].

HCV

HCV, which primarily infects the liver, is the causative agent of hepatitis C. In severe cases patients develop chronic liver infections and subsequent liver cirrhosis, carcinoma, hepatitis and liver failure [24]. Entry of HCV is a slow and complex multistep process that involves initial attachment of the virion to the host cell, interaction of the envelope proteins with the host cell surface receptors and subsequent internalisation by membrane fusion (reviewed in [25]). The two viral envelope proteins E1 and E2 are expressed as inactive precursors [26] which associate as large covalent complexes [27]. The two envelope proteins E1 and E2, contain 8 and 18 cysteine residues, respectively [28]. Alkylation of free cysteine residues on viral particles containing E1 and E2 has been shown to block the uptake of the virus [28]. This process, however, could not be rescued by addition of reducing agents as is the case for other retroviruses [28]. Recent mutagenesis studies on E2 showed that all nine disulfide pairs were strictly required for infection. The role of cysteines is complex as mutagenesis of individual cysteines had differential effects on assembly with E1 and binding to the tetraspanin membrane protein CD81 [29].

Newcastle disease virus

Newcastle disease virus infection is extremely rare in humans and usually only occurs in people in close contact with infected birds. Entry into the host cell is mediated by viral haemagglutinin neuraminidase (HN) and fusion (F) gp attachment to the host cell. Free thiols in the F gp, which are required for virus entry into the cell [30], are only present after binding of the virus to the target cell surface [31]. This suggests that labile disulfide bonds are reduced before major conformational changes in the F protein occur and before activation by HN. How the appearance of free thiols influences F protein activation or conformational changes is as yet unknown [30]. The enzyme responsible for catalysing the reduction of disulfide bonds in F protein is likely to be PDI due to the observation that membrane-impermeable inhibitors of PDI (DTNB, bacitracin and anti-PDI Ab) could suppress the formation of free thiols and inhibit virus entry [30]. Further support for this is the observation that over-expression of PDI resulted in significantly increased cell–cell fusion mediated by F and HN proteins [32].

Other viruses

Labile disulfide bonds are likely to be important in other viruses. For instance in the rotaviruses that are a major cause of diarrhoea, in addition to proteolytic cleavage of the surface proteins, labile disulfide bonds are implicated in virus entry by the blocking of virus uptake by reagents such as DTNB, bacitracin and Abs to PDI [33]. DTNB also inhibited the uptake of the Sindbis alphavirus that causes fever in humans and, interestingly, virus fusion could be enhanced by exogenous reducing agent [34]. Although the SARS (severe acute respiratory syndrome) coronavirus contains free cysteine and labile disulfides, cysteine blocking reagents such as DTNB and bacitracin had no effect on virus uptake [35].

The extracellular redox state affects immune regulation, disease and clotting

Immune regulation

A reducing environment is important in the generation of immune responses as naive T cells do not express a cystine transporter and require a source of extracellular cysteine. X_C^- is a major transporter for cystine that is comprised of a common CD98 chain and a specific chain for cysteine, xCT. The DCs provide the source of cysteine for T cells. Although it was originally thought that, on activation, DCs secrete thioredoxin that in turn can reduce cystine to cysteine (Fig. 1) [8], further analysis suggests this is not the main cysteine source for T cells [36]. Blocking the X_C^- transporter, for example, prevents cysteine accumulation in DCs indicating the importance of cystine uptake by the DCs and secretion of cysteine [36]. When Tregs act on DCs, this process is inhibited [36]. This

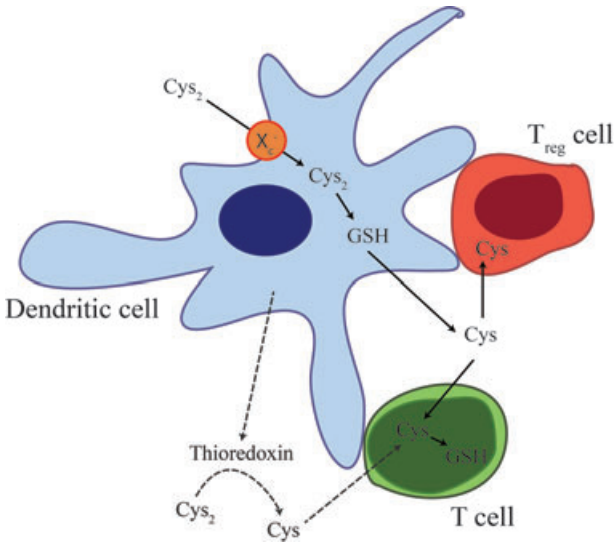

Figure 1. Tregs can limit redox changes. Resting T cells require a source of extracellular cysteine (Cys) as they lack the cystine (Cys_2) transporter X_C^- [8, 36, 37]. This transporter is, however, expressed by DCs meaning that these cells can generate glutathione (GSH) (cystine is rate-limiting for glutathione production); this, in turn, leads to the secretion of Cys that can be utilised by T cells. Thioredoxin secretion from DCs can be induced by activation but in the absence of a source of electrons, which are required for conversion of cysteine from cystine by thioredoxin, may not be a major source of extracellular Cys for T cells. The interaction of Tregs with DCs leads to inhibition of extracellular Cys [37].

inhibition depends on cell contact between the DC and the Treg and the modulation of glutathione metabolism in the DC [37].

The importance of the cystine transporter system for the immune system is illustrated in the gut, where lamina propria macrophages in mice do not normally express the X_C^- transporter which is, in contrast, expressed in peripheral blood monocytes. Gut lamina propria macrophages are therefore unable to take up cystine and hence cannot provide cysteine for the neighbouring T cells [38]. This may be important for maintaining an environment in the healthy gut that is more tolerant than that found in inflammatory bowel disease, a disease state in which there is increased expression of the X_C^- transporter and higher T-cell activity [38].

In addition to the metabolic effects of cystine transport and reduction, the reducing environment has effects on membrane and secreted proteins. This is illustrated by the breadth of membrane proteins on leukocytes that have labile disulfide bonds that are susceptible to the reducing conditions that are typical of both T-cell activation and innate activation in an LPS model of inflammation [2]. In one case a labile disulfide bond was identified in CD132 (see Fig. 2), the common gamma chain of several cytokine receptors, which on reduction prevented IL-2 signalling [39]. Signalling of other cytokine receptors seems likely to be affected [40] with possible additional effects on cytokines as well as IL-4 has a labile disulfide that leads to loss of activity upon reduction [41]. The implication is that the effects of the pro-inflammatory cytokines may be ameliorated by the redox changes resulting from

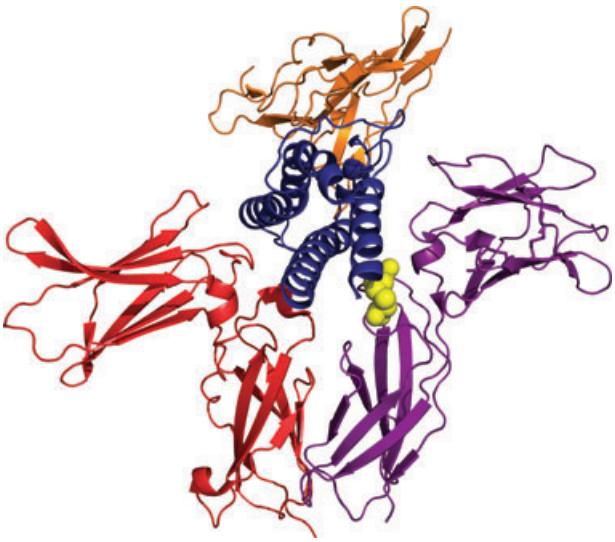

Figure 2. One of the disulfide bonds in CD132 is labile and lies at the interface with IL-2. Crystal structure of the IL-2/IL-2 receptor complex (PDB code 2ERJ). The labile disulfide bond (yellow spheres) in CD132 (purple) is in direct contact with the cytokine, IL-2 (blue). The IL-2 receptor alpha chain (CD25) is shown in orange and the beta chain (CD122) is shown in red.

the inflammatory response itself – a feedback control mechanism. It seems likely that other cytokine/chemokine interactions are affected by redox conditions. For example, thioredoxin affects the chemokine-induced chemotaxis of eosinophils although the molecular basis for this is unclear [42]. A different type of cytokine is the high mobility group box 1 (HMGB1) that is both a nuclear protein that regulates transcription and a secreted protein demonstrating extracellular inflammatory cytokine activity. The latter activity is dependent on one free cysteine and a disulfide bond that can be reduced by mild reducing conditions [43].

Redox changes, such as secretion of thioredoxin, occur to balance ROS production. For example, the induction of IL-1β processing in monocytes involves firstly an ROS response and then an anti-oxidant response but studies with inhibitors show that both are necessary for production of IL-1β [44]. As the effects of ROS on the immune system have recently been reviewed [45], this shall not be discussed further here.

Cancer

An important aspect of cancer resistance to chemotherapy is the up-regulation of anti-oxidant systems such as the cysteine/cystine redox cycle, PDI, thioredoxin, glutathione [46] and the X_C^- cystine transporter [47]. A possible link to the cell surface is indicated by a CD44 variant (CD44v) that interacts with the xCT component of the cysteine transporter; ablation of CD44v leads to inhibition of xCT and subsequent suppression of tumour growth [48].

The analysis of differential expression of proteins in invasive glioma cells and angiogenic glioma cells revealed that PDI is overexpressed in the invasive phenotype [49]. Interestingly, PDI was found in the tumour periphery but not in the angiogenic core. This led to the hypothesis that PDI has a functional role in glioma cell migration, which is supported by the observation that tumour cell migration is inhibited by bacitracin, a non-selective PDI inhibitor, and by a PDI Ab [49]. PDI can reduce disulfide bonds in many proteins, but one class of particular interest with respect to cancer is the metalloproteinase family of enzymes that can modulate the extracellular environment and is important in metastasis; PDI had recently been shown to regulate the activity and secretion of MMP-9 [50]. A key element in these enzymes is that the catalytic site contains a Zn ion coordinated to histidine residues and one cysteine; the site is in an inactive state until the cysteine coordination is broken – the 'Cys Switch' – by changes in the conformation of the protein that exposes the Zn ion to solvent [51, 52]. The potential for redox involvement in the immune regulation of cancer is large as illustrated by recent data indicating that chronic lymphocytic leukemia cells have high levels of surface PDI and thioredoxin that are associated with receptors for TNF, and blocking PDI and thioredoxin activity inhibits the production of the autocrine TNF [53].

Rheumatoid arthritis

Rheumatoid arthritis is a chronic inflammatory disease that is triggered by both environmental and genetic factors. A link between rheumatoid arthritis regulation and the ROS system is provided by the finding that neutrophil cytosolic factor 1 (Ncf1) is a regulator of rheumatoid arthritis [54]. Ncf1, is a component of the NADPH oxidase complex which catalyses the reduction of oxygen to ROS (reviewed in [55–57]). With regard to membrane proteins in particular, a decreased level of ROS has been shown to increase the number of reduced thiol groups (–SH) on the T-cell surface [58]. This resulted in increased activation and proliferation of T cells, as well as arthritis incidence and severity [58].

Platelet activation is associated with redox changes at the cell surface

Platelets are involved in haemostasis, wound healing and atherosclerosis. There are extensive data to suggest that platelet activation is associated with an increase in the extracellular redox potential and several PDI family members come to the cell surface [59–61]. A key protein that can be modulated by reduction is the fibrinogen receptor, integrin $\alpha_{IIb}\beta_3$. This is the most abundant integrin on the platelet surface and its activation leads to increased binding of adhesive ligands such as fibrinogen, fibronectin and von Willebrand factor which in turn promote thrombus formation [59]. The β subunit of $\alpha_{IIb}\beta_3$ contains 56 highly conserved cysteine residues which all form disulfide bonds [62]. Interestingly, the active state of $\alpha_{IIb}\beta_3$ seems to be attained by the reduction of cysteines within the EGF-like domains $\alpha_{IIb}\beta_3$ [63]. Mutagenesis of a single disulfide in the β_3 chain leads to constitutively active $\alpha_{IIb}\beta_3$ [64] whereas a more extensive mutagenesis

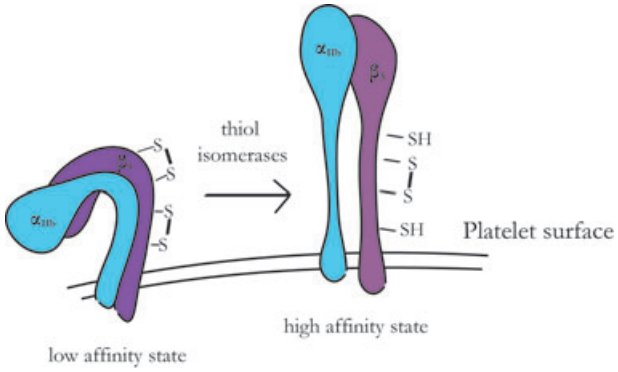

Figure 3. Scheme showing the redox regulation of the $\alpha_{IIb}\beta_3$ integrin on platelets. The resting state of $\alpha_{IIb}\beta_3$ has a low affinity for fibrinogen, $\alpha_{IIb}\beta_3$ being present in its oxidized state. The high affinity state is reached by reducing disulfide bonds on $\alpha_{IIb}\beta_3$.

of specific disulfide bonds in β_3 gave differential affects on the function of α_{IIb} and α_V integrins [65]. Integrins are unusual in containing disulfide bonds not only in the extracellular domains but also in their intracellular part and mutagenesis of the latter can also affect ligand binding [66]. The binding capacity of integrins can be modulated by various stimuli and the underlying concept is that the disulfide bonds maintain the integrin in a less active form (Fig. 3). This is evidenced by the finding that cysteine mutations and the addition of reducing agents result in increased ligand binding [67–69] and, more recently, a PDI inhibitor was shown to block thrombus formation [70]. In addition to the fibrinogen receptor integrin $\alpha_{IIb}\beta_3$, other platelet surface proteins are known to have increased levels of free thiols, such as the $P2Y_{12}$ ADP receptor, gp Ib adhesion receptor α (GPIbα) and the gp VI collagen receptor (GPVI) on platelet activation [59]. Thus, redox changes at the surface of platelets seem likely to be important in regulating clotting.

Concluding remarks

Although the role of disulfide bonds in stabilising protein structures is well known, we have only recently started to understand the role of redox labile disulfide bonds. By changing from an oxidized to a reduced state, these bonds can control protein function. Labile disulfide bonds in membrane proteins play a key role in a number of viral infections, as well as in rheumatoid arthritis, cancer, platelet activation and cytokine signalling. Given the large numbers of membrane proteins with labile disulfides, it is likely that they may be important in immune responses, a variety of diseases and inflammation. These molecular mechanisms could be important for therapy based on four types of strategy: (i) prevention of the reduction of labile disulfide bonds by Abs that block PDI access to specific targets; (ii) the use of small molecular inhibitors or Abs to target specific PDIs; (iii) targeting the pathways that lead to activation of the cell surface PDIs; and (iv) targeting the transporters involved in the redox system.

Acknowledgements: This work was supported by the Medical Research Council (reference G9826026). MS was supported by a Scatcherd European Scholarship. We are grateful for helpful comments from Marion H. Brown and Lisa-Marie Holbrook.

Conflict of interest: The authors declare no financial or commercial conflicts of interest.

References

1 **Schmidt, B., Ho, L. and Hogg, P. J.**, Allosteric disulfide bonds. *Biochemistry* 2006. **45**: 7429–7433.

2 **Metcalfe, C., Cresswell, P., Ciaccia, L., Thomas, B. and Barclay, A. N.**, Labile disulfide bonds are common at the leucocyte cell surface. *Open Biol.* 2011. **1**: 110010–110010.

3 **Freedman, R. B., Hirst, T. R. and Tuite, M. F.**, Protein disulphide isomerase: building bridges in protein folding. *Trends Biochem. Sci.* 1994. **19**: 331–336.

4 **Benham, A. M.**, The protein disulfide isomerase family: key players in health and disease. *Antioxid. Redox Signal.* 2012. **16**: 781–789.

5 **Hatahet, F. and Ruddock, L. W.**, Protein disulfide isomerase: a critical evaluation of its function in disulfide bond formation. *Antioxid. Redox Signal.* 2009. **11**: 2807–2850.

6 **Arner, E. S. and Holmgren, A.**, Physiological functions of thioredoxin and thioredoxin reductase. *Eur. J. Biochem.* 2000. **267**: 6102–6109.

7 **Kemp, M., Go, Y. M. and Jones, D. P.**, Nonequilibrium thermodynamics of thiol/disulfide redox systems: a perspective on redox systems biology. *Free Radic. Biol. Med.* 2008. **44**: 921–937.

8 **Angelini, G., Gardella, S., Ardy, M., Ciriolo, M. R., Filomeni, G., Di Trapani, G., Clarke, F. et al.**, Antigen-presenting dendritic cells provide the reducing extracellular microenvironment required for T lymphocyte activation. *Proc. Natl. Acad. Sci. USA* 2002. **99**: 1491–1496.

9 **Castellani, P., Angelini, G., Delfino, L., Matucci, A. and Rubartelli, A.**, The thiol redox state of lymphoid organs is modified by immunization: role of different immune cell populations. *Eur. J. Immunol.* 2008. **38**: 2419–2425.

10 **Callister, M. E., Burke-Gaffney, A., Quinlan, G. J., Nicholson, A. G., Florio, R., Nakamura, H., Yodoi, J. et al.**, Extracellular thioredoxin levels are increased in patients with acute lung injury. *Thorax* 2006. **61**: 521–527.

11 **Colman, P. M. and Lawrence, M. C.**, The structural biology of type I viral membrane fusion. *Nature Rev. Mol. Cell Biol.* 2003. **4**: 309–319.

12 **Wyatt, R. and Sodroski, J.**, The HIV-1 envelope glycoproteins: fusogens, antigens, and immunogens. *Science* 1998. **280**: 1884–1888.

13 **Fenouillet, E., Barbouche, R. and Jones, I. M.**, Cell entry by enveloped viruses: redox considerations for HIV and SARS-coronavirus. *Antioxid. Redox Signal.* 2007. **9**: 1009–1034.

14 **Azimi, I., Matthias, L. J., Center, R. J., Wong, J. W. H. and Hogg, P. J.**, Disulfide bond that constrains the HIV-1 gp120 V3 domain is cleaved by thioredoxin. *J. Biol. Chem.* 2010. **285**: 40072–40080.

15 **Go, E. P., Zhang, Y., Menon, S. and Desaire, H.**, Analysis of the disulfide bond arrangement of the HIV-1 envelope protein CON-S gp140 DeltaCFI shows variability in the V1 and V2 regions. *J. Prot. Res.* 2011. **10**: 578–591.

16 **Ou, W. and Silver, J.**, Role of protein disulfide isomerase and other thiol-reactive proteins in HIV-1 envelope protein-mediated fusion. *Virology* 2006. **350**: 406–417.

17 **Auwerx, J., Isacsson, O., S√∂derlund, J., Balzarini, J., Johansson, M. and Lundberg, M.**, Human glutaredoxin-1 catalyzes the reduction of HIV-1 gp120 and CD4 disulfides and its inhibition reduces HIV-1 replication. *Int. J. Biochem. Cell Biol.* 2009. **41**: 1269–1275.

18 **Reiser, K., Francois, K. O., Schols, D., Bergman, T., Jornvall, H., Balzarini, J., Karlsson, A. et al.**, Thioredoxin-1 and protein disulfide isomerase catalyze the reduction of similar disulfides in HIV gp120. *Int. J. Biochem. Cell Biol.* 2012. **44**: 556–562.

19 **Papandreou, M. J., Barbouche, R., Guieu, R., Rivera, S., Fantini, J., Khrestchatisky, M., Jones, I. M. et al.**, Mapping of domains on HIV envelope protein mediating association with calnexin and protein-disulfide isomerase. *J. Biol. Chem.* 2010. **285**: 13788–13796.

20 **Ashkenazi, A., Viard, M., Wexler-Cohen, Y., Blumenthal, R. and Shai, Y.**, Viral envelope protein folding and membrane hemifusion are enhanced by the conserved loop region of HIV-1 gp41. *FASEB J.* 2011. **25**: 2156–2166.

21 **Matthias, L. J., Yam, P. T. W., Jiang, X.-M., Vandegraaff, N., Li, P., Poumbourios, P., Donoghue, N. et al.**, Disulfide exchange in domain 2 of CD4 is required for entry of HIV-1. *Nat. Immunol.* 2002. **3**: 727–732.

22 **Lynch, G. W., Sloane, A. J., Raso, V., Lai, A. and Cunningham, A. L.**, Direct evidence for native CD4 oligomers in lymphoid and monocytoid cells. *Eur. J. Immunol.* 1999. **29**: 2590–2602.

23 **Matthias, L. J., Azimi, I., Tabrett, C. A. and Hogg, P. J.**, Reduced monomeric CD4 is the preferred receptor for HIV. *J. Biol. Chem.* 2010. **285**: 40793–40799.

24 **Hoofnagle, J. H.**, Course and outcome of hepatitis C. *Hepatology* 2002. **36**: S21–S29.

25 **Zeisel, M. B., Barth, H., Schuster, C. and Baumert, T. F.**, Hepatitis C virus entry: molecular mechanisms and targets for antiviral therapy. *Front. Biosci.* 2009. **14**: 3274–3285.

26 **Bartosch, B. and Cosset, F. L.**, Cell entry of hepatitis C virus. *Virology* 2006. **348**: 1–12.

27 **Vieyres, G., Thomas, X., Descamps, V. R., Duverlie, G., Patel, A. H. and Dubuisson, J.**, Characterization of the envelope glycoproteins associated with infectious hepatitis C virus. *J. Virol.* 2010. **84**: 10159–10168.

28 **Fraser, J., Boo, I., Poumbourios, P. and Drummer, H. E.**, Hepatitis C virus (HCV) envelope glycoproteins E1 and E2 contain reduced cysteine residues essential for virus entry. *J. Biol. Chem.* 2011. **286**: 31984–31992.

29 **McCaffrey, K., Boo, I., Tewierek, K., Edmunds, M. L., Poumbourios, P. and Drummer, H. E.**, Role of conserved cysteine residues in hepatitis C virus glycoprotein e2 folding and function. *J. Virol.* 2012. **86**: 3961–3974.

30 **Jain, S., McGinnes, L. W. and Morrison, T. G.**, Thiol/disulfide exchange is required for membrane fusion directed by the Newcastle disease virus fusion protein. *J. Virol.* 2007. **81**: 2328–2339.

31 **Jain, S., McGinnes, L. W. and Morrison, T. G.**, Role of thiol/disulfide exchange in newcastle disease virus entry. *J. Virol.* 2009. **83**: 241–249.

32 **Jain, S., McGinnes, L. W. and Morrison, T. G.**, Overexpression of thiol/disulfide isomerases enhances membrane fusion directed by the Newcastle disease virus fusion protein. *J. Virol.* 2008. **82**: 12039–12048.

33 **Calderon, M. N., Guerrero, C. A., Acosta, O., Lopez, S. and Arias, C. F.**, Inhibiting rotavirus infection by membrane-impermeant thiol/disulfide exchange blockers and antibodies against protein disulfide isomerase. *Intervirology* 2012. **55**: 451–464.

34 **Abell, B. A. and Brown, D. T.**, Sindbis virus membrane fusion is mediated by reduction of glycoprotein disulfide bridges at the cell surface. *J. Virol.* 1993. **67**: 5496–5501.

35 **Lavillette, D., Barbouche, R., Yao, Y., Boson, B., Cosset, F. L., Jones, I. M. and Fenouillet, E.**, Significant redox insensitivity of the functions of the SARS-CoV spike glycoprotein: comparison with HIV envelope. *J. Biol. Chem.* 2006. **281**: 9200–9204.

36 **Yan, Z., Garg, S. K., Kipnis, J. and Banerjee, R.**, Extracellular redox modulation by regulatory T cells. *Nat. Chem. Biol.* 2009. **5**: 721–723.

37 **Yan, Z., Garg, S. K. and Banerjee, R.**, Regulatory T cells interfere with glutathione metabolism in dendritic cells and T cells. *J. Biol. Chem.* 2010. **285**: 41525–41532.

38 **Sido, B., Lasitschka, F., Giese, T., Gassler, N., Funke, B., Schr√∂der-Braunstein, J., Brunnemer, U. et al.**, A prominent role for mucosal cystine/cysteine metabolism in intestinal immunoregulation. *Gastroenterology* 2008. **134**: 179–191.

39 **Metcalfe, C., Cresswell, P. and Barclay, A. N.**, Interleukin-2 signalling is modulated by a labile disulfide bond in the CD132 chain of its receptor. *Open Biology* 2012. **2**: 110036–110036.

40 **Wang, X., Lupardus, P., Laporte, S. L. and Garcia, K. C.**, Structural biology of shared cytokine receptors. *Annu. Rev. Immunol.* 2009. **27**: 29–60.

41 **Curbo, S., Gaudin, R. l., Carlsten, M., Malmberg, K.-J., Troye-Blomberg, M., Ahlborg, N., Karlsson, A. et al.**, Regulation of interleukin-4 signaling by extracellular reduction of intramolecular disulfides. *Biochem. Biophys. Res. Commun.* 2009. **390**: 1272–1277.

42 **Kobayashi, N., Yamada, Y., Ito, W., Ueki, S., Kayaba, H., Nakamura, H., Yodoi, J. et al.**, Thioredoxin reduces C-C chemokine-induced chemotaxis of human eosinophils. *Allergy* 2009. **64**: 1130–1135.

43 **Yang, H., Lundback, P., Ottosson, L., Erlandsson-Harris, H., Venereau, E., Bianchi, M. E., Al-Abed, Y. et al.**, Redox modification of cysteine residues regulates the cytokine activity of high mobility group box-1 (HMGB1). *Mol. Med.* 2012. **18**: 250–259.

44 **Tassi, S., Carta, S., Vene, R., Delfino, L., Ciriolo, M. R. and Rubartelli, A.**, Pathogen-induced interleukin-1beta processing and secretion is regulated by a biphasic redox response. *J. Immunol.* 2009. **183**: 1456–1462.

45 **Kesarwani, P., Murali, A. K., Al-Khami, A. A. and Mehrotra, S.**, Redox regulation of T-cell function: from molecular mechanisms to significance in human health and disease. *Antioxid. Redox Signal.* 2012.

46 **Vene, R., Castellani, P., Delfino, L., Lucibello, M., Ciriolo, M. R. and Rubartelli, A.**, The cystine/cysteine cycle and GSH are independent and crucial antioxidant systems in malignant melanoma cells and represent druggable targets. *Antioxid. Redox Signal.* 2011. **15**: 2439–2453.

47 **Lo, M., Ling, V., Wang, Y. Z. and Gout, P. W.**, The xc- cystine/glutamate antiporter: a mediator of pancreatic cancer growth with a role in drug resistance. *Br. J. Cancer* 2008. **99**: 464–472.

48 **Ishimoto, T., Nagano, O., Yae, T., Tamada, M., Motohara, T., Oshima, H., Oshima, M. et al.**, CD44 variant regulates redox status in cancer cells by stabilizing the xCT subunit of system xc(-) and thereby promotes tumor growth. *Cancer Cell* 2011. **19**: 387–400.

49 **Goplen, D., Wang, J., Enger, P. Ò., Tysnes, B. B., Terzis, A. J. A., Laerum, O. D. and Bjerkvig, R.**, Protein disulfide isomerase expression is related to the invasive properties of malignant glioma. *Cancer Res.* 2006. **66**: 9895–9902.

50 **Khan, M. M., Simizu, S., Suzuki, T., Masuda, A., Kawatani, M., Muroi, M., Dohmae, N. et al.**, Protein disulfide isomerase-mediated disulfide bonds regulate the gelatinolytic activity and secretion of matrix metalloproteinase-9. *Exp. Cell Res.* 2012. **318**: 904–914.

51 **Van Wart, H. E. and Birkedal-Hansen, H.**, The cysteine switch: a principle of regulation of metalloproteinase activity with potential applicability to the entire matrix metalloproteinase gene family. *Proc. Natl. Acad. Sci. USA* 1990. **87**: 5578–5582.

52 **Tallant, C., Marrero, A. and Gomis-Ruth, F. X.**, Matrix metalloproteinases: fold and function of their catalytic domains. *Biochim. Biophys. Acta* 2010. **1803**: 20–28.

53 **Soderberg, A., Hossain, A. and Rosen, A.**, A protein-disulfide isomerase/thioredoxin-1 complex is physically attached to exofacial membrane TNF-receptors: overexpression in chronic lymphocytic leukemia cells. *Antioxid. Redox Signal.* 2012.

54 **Olofsson, P., Holmberg, J., Tordsson, J., Lu, S., Akerstr√∂m, B. and Holmdahl, R.**, Positional identification of Ncf1 as a gene that regulates arthritis severity in rats. *Nat. Genet.* 2003. **33**: 25–32.

55 **Hultqvist, M., Olsson, L. M., Gelderman, K. A. and Holmdahl, R.**, The protective role of ROS in autoimmune disease. *Trends Immunol.* 2009. **30**: 201–208.

56 **Olsson, L. M., Nerstedt, A., Lindqvist, A. K., Johansson, S. C., Medstrand, P., Olofsson, P. and Holmdahl, R.**, Copy number variation of the gene NCF1 is associated with rheumatoid arthritis. *Antioxid. Redox Signal.* 2012. **16**: 71–78.

57 **Hultqvist, M., Olofsson, P., Gelderman, K. A., Holmberg, J. and Holmdahl, R.**, A new arthritis therapy with oxidative burst inducers. *PLoS Med.* 2006. **3**: 1625–1636.

58 **Gelderman, K. A., Hultqvist, M., Holmberg, J., Olofsson, P. and Holmdahl, R.**, T cell surface redox levels determine T cell reactivity and arthritis susceptibility. *Proc. Natl. Acad. Sci. USA* 2006. **103**: 12831–12836.

59 **Essex, D. W.**, Redox control of platelet function. *Antioxid. Redox Signal.* 2009. **11**: 1191–1225.

60 **Holbrook, L.-M., Watkins, N. A., Simmonds, A. D., Jones, C. I., Ouwehand, W. H. and Gibbins, J. M.**, Platelets release novel thiol isomerase enzymes which are recruited to the cell surface following activation. *Br. J. Haematol.* 2010. **148**: 627–637.

61 **Holbrook, L. M., Sasikumar, P., Stanley, R. G., Simmonds, A. D., Bicknell, A. B. and Gibbins, J. M.**, The platelet-surface thiol isomerase enzyme ERp57 modulates platelet function. *J. Thromb. Haemost.* 2012. **10**: 278–288.

62 **Calvete, J. J., Henschen, A. and González-Rodríguez, J.**, Assignment of disulphide bonds in human platelet GPIIIa. A disulphide pattern for the beta-subunits of the integrin family. *Biochem. J.* 1991. **274**: 63–71.

63 **Kamata, T., Ambo, H., Puzon-McLaughlin, W., Tieu, K. K., Handa, M., Ikeda, Y. and Takada, Y.**, Critical cysteine residues for regulation of integrin alphaIIbbeta3 are clustered in the epidermal growth factor domains of the beta3 subunit. *Biochem. J.* 2004. **378**: 1079–1082.

64 **Sun, Q. H., Liu, C. Y., Wang, R., Paddock, C. and Newman, P. J.**, Disruption of the long-range GPIIIa Cys(5)-Cys(435) disulfide bond results in the production of constitutively active GPIIb-IIIa (alpha(IIb)beta(3)) integrin complexes. *Blood* 2002. **100**: 2094–2101.

65 **Mor-Cohen, R., Rosenberg, N., Einav, Y., Zelzion, E., Landau, M., Mansour, W., Averbukh, Y. et al.**, Unique disulfide bonds in epidermal growth factor (EGF) domains of beta3 affect structure and function of alphaIIbbeta3 and alphavbeta3 integrins in different manner. *J. Biol. Chem.* 2012. **287**: 8879–8891.

66 **Butta, N., Arias-Salgado, E. G., Gonzalez-Manchon, C., Ferrer, M., Larrucea, S., Ayuso, M. S. and Parrilla, R.**, Disruption of the beta3 663–687 disulfide bridge confers constitutive activity to beta3 integrins. *Blood* 2003. **102**: 2491–2497.

67 **Chigaev, A., Zwartz, G. J., Buranda, T., Edwards, B. S., Prossnitz, E. R. and Sklar, L. A.**, Conformational regulation of alpha 4 beta 1-integrin affinity by reducing agents. "Inside-out" signaling is independent of and additive to reduction-regulated integrin activation. *J. Biol. Chem.* 2004. **279**: 32435–32443.

68 **Nolan, S. M., Mathew, E. C., Scarth, S. L., Al-Shamkhani, A. and Law, S. K.**, The effects of cysteine to alanine mutations of CD18 on the expression and adhesion of the CD11/CD18 integrins. *FEBS Lett.* 2000. **486**: 89–92.

69 **Smagghe, B. J., Huang, P. S., Ban, Y. E., Baker, D. and Springer, T. A.**, Modulation of integrin activation by an entropic spring in the {beta}-knee. *J. Biol. Chem.* 2010. **285**: 32954–32966.

70 **Jasuja, R., Passam, F. H., Kennedy, D. R., Kim, S. H., van Hessem, L., Lin, L., Bowley, S. R. et al.**, Protein disulfide isomerase inhibitors constitute a new class of antithrombotic agents. *J. Clin. Invest.* 2012. **122**: 2104–2113.

Abbreviations: **DTNB**: 5,5'-dithiobis (2-nitrobenzoic acid) · **HN**: haemagglutinin neuraminidase · **PDI**: protein disulfide isomerase

Full correspondence: Dr. A. Neil Barclay, Oxford Molecular Pathology Institute, Sir William Dunn School of Pathology, University of Oxford, South Parks Road, Oxford, United Kingdom, OX1 3RE
Fax: +44 (0)1865 275591
e-mail: neil.barclay@path.ox.ac.uk

Received: 20/7/2012
Revised: 22/10/2012
Accepted: 5/12/2012
Accepted article online: 11/12/2012

PLOS | ONE

RESEARCH ARTICLE

CD44 Binding to Hyaluronic Acid Is Redox Regulated by a Labile Disulfide Bond in the Hyaluronic Acid Binding Site

Helena Kellett-Clarke, Monika Stegmann, A. Neil Barclay, Clive Metcalfe*

The Sir William Dunn School of Pathology, University of Oxford, Oxford, United Kingdom

* clive.metcalfe@path.ox.ac.uk

OPEN ACCESS

Citation: Kellett-Clarke H, Stegmann M, Barclay AN, Metcalfe C (2015) CD44 Binding to Hyaluronic Acid Is Redox Regulated by a Labile Disulfide Bond in the Hyaluronic Acid Binding Site. PLoS ONE 10(9): e0138137. doi:10.1371/journal.pone.0138137

Editor: Junji Yodoi, Institute for Virus Research, Laboratory of Infection and Prevention, JAPAN

Received: June 8, 2015

Accepted: August 25, 2015

Published: September 17, 2015

Data Availability Statement: All relevant data are within the paper and its Supporting Information files.

Funding: This work was supported by Medical Research Council Grant No. G9826026. The funders had no role in study design, data collection and analysis, decision to publish, or preparation of the manuscript.

Competing Interests: The authors have declared that no competing interests exist.

Abstract

CD44 is the primary leukocyte cell surface receptor for hyaluronic acid (HA), a component of the extracellular matrix. Enzymatic post translational cleavage of labile disulfide bonds is a mechanism by which proteins are structurally regulated by imparting an allosteric change and altering activity. We have identified one such disulfide bond in CD44 formed by Cys77 and Cys97 that stabilises the HA binding groove. This bond is labile on the surface of leukocytes treated with chemical and enzymatic reducing agents. Analysis of CD44 crystal structures reveal the disulfide bond to be solvent accessible and in the–LH hook configuration characteristic of labile disulfide bonds. Kinetic trapping and binding experiments on CD44-Fc chimeric proteins show the bond is preferentially reduced over the other disulfide bonds in CD44 and reduction inhibits the CD44-HA interaction. Furthermore cells transfected with CD44 no longer adhere to HA coated surfaces after pre-treatment with reducing agents. The implications of CD44 redox regulation are discussed in the context of immune function, disease and therapeutic strategies.

Introduction

CD44 is an abundant, highly glycosylated transmembrane protein present on many leukocytes. The primary function of CD44 is to bind hyaluronic acid (HA) and mediate interactions between leukocytes and the extracellular matrix. One characteristic of CD44 is that it exists in many isoforms due to alternative splicing and different glycoforms and these control the HA binding function of CD44 [1]. CD44 is linked to many diseases, for example rheumatoid arthritis [2], cancer metastasis [3] and systemic lupus erythematosus [4]. Targeting CD44 with therapeutics has shown potential in rheumatoid arthritis [5,6] and various methods of modulating the CD44-HA interaction have been assessed in cancer therapy [7,8]. Regulation of CD44 activity is clearly an important and complex system with huge therapeutic potential. CD44 was revealed in recent screens for membrane proteins containing labile disulfide bonds [9] suggesting a role for the extracellular redox environment in regulation of CD44 activity.

Disulfide bonds formed between cysteine residues play an important role in the stabilisation and organisation of proteins but it is now apparent that a subset of these bonds are labile and

can function as redox switches [10]. Changes in the redox microenvironment through the secretion of thiol reductase and protein disulfide isomerase (PDI) enzymes can impart post translational allosteric structural changes in proteins [11] resulting in modulation of protein and cellular function. Post translation control of disulfide bonds is essential for maintaining haemostasis with many blood proteins under redox control [12]. For example, in the early stages of thrombus formation activated platelets secrete PDI which reduces two disulfide bonds in the integrin αIIbβ3 on the platelet surface. This results in allosteric switching of fibrinogen cross linking and inhibition of PDI inhibits thrombus formation (redox control of platelet function is reviewed in [13]).

There is evidence that post translational control of disulfide bond topology also plays a role in regulation of the immune system. Activation of T cells results in up regulation of thioredoxin-1 (Trx1), a ubiquitous thiol reductase enzyme [14], and results in increased thiols at the T cell surface [15,16], which can be inhibited with thiol reductase inhibitors [15]. Activated dendritic cells also secrete Trx1 [17] which can reduce disulfide bonds at the surface of both the dendritic cells and co cultured T cells [18]. This surface reduction is inhibited by introducing regulatory T cells [18]. Immunisation of mice leads to an increase in free thiols at the surface of the leukocytes [14] as does LPS induced endotoxemia [9]. A key question towards understanding the role of redox reduction of surface proteins in immune responses is which proteins contain the reduced disulfide bonds?

This was addressed for the first time when we recently developed a mass spectrometry based screen to identify proteins on the cell surface of leukocytes that contain a labile disulfide bond [9]. More than 50 different proteins were identified on the cell surface of a mouse 2B4 T-cell hybridoma that potentially contain such bonds. To demonstrate the efficacy of the screen we followed up CD132, the common γ signalling chain of the interleukin-2 (IL-2) family of cytokine receptors with functional assays and showed that function of the IL-2 receptor could be controlled through reduction of a labile disulfide bond at the CD132/IL-2 binding interface [19].

CD44 was consistently found in these screens for membrane proteins with labile disulfide bonds and herein we explore the HA binding function of CD44 in response to protein redox state. We show a novel mechanism by which CD44 can be regulated by enzymes known to be secreted into the extracellular environment during inflammation. The implications for the function of CD44 and other HA binding proteins of the link module family are discussed together with possibilities for new avenues of manipulating these interactions for therapeutic purposes.

Materials and Methods

Human and mouse CD44 Fc proteins were purchased from R&D systems. Biotinylated rat anti-mouse/human CD44, (clone IM-7) and biotinylated goat anti rat IgG were purchased from Abcam. HRP-conjugated anti human and mouse Fc and FITC and DyLight 800 conjugated avidin were purchased from AbD Serotec. Peptide-N-Glycosidase F (PNGase F) was purchased from New England Biolabs. Deuterated N-ethylmaleimide (ethyl-D5) was from Cambridge Isotopes. Everything else was purchased from Sigma-Aldrich.

TCEP-HCl reduction and differential thiol labelling of the GFETCR peptide of CD44 on the surface of 2B4 cells

Murine T cell hybridoma cells, 2B4 Saito [20] (~1 x 10^8 cells) were reduced with TCEP-HCl (2.5 mM in PBS containing 1% BSA), reacted with maleimide-PEO2-Biotin (MPB), the biotinylated cell surface glycoproteins purified, digested with PNGase F and trypsin and analysed

by MS [9]. Non reduced MPB labelled cells were used as a control to determine background levels of free cysteines on the cell.

Kinetic trapping of disulfide bond reduction in hCD44-Fc chimeras

hCD44 Fc-chimera (5 μg in PBS) was added to 10kDa 500 μl centrifugal concentrators (Vivacon 500, Sartorious). Two samples were reduced with TCEP-HCl (100 μl of 2.5 mM in PBS for 15 minutes at 4°C) and Trx1 (100 μl of 1 μM Trx1 supplemented with 100 nM TR1 and 200 μM NADPH for 90 minutes at 37°C). A non-reduced control sample was treated with 100 μl of PBS at 37°C for 90 minutes. After washing, reduced disulfides were kinetically trapped by alkylating with NEM (100 μl 1 mM in PBS for 30 minutes at 4°C). After washing the chimeras were denatured (10 mM TCEP-HCl in 8M urea for 1 hour at room temperature), washed and any remaining cysteines alkylated with D5-NEM (100 μl of 1 mM in PBS for 30 minutes at 4°C). The samples were deglycosylated and trypsin digested [9].

Mass spectrometry

After desalting on a C18 micro column, the samples were resuspended in 0.1% formic acid containing 2% acetonitrile and analysed on a Ultimate 3000 UHPLC (Dionex) coupled to a QExactive mass spectrometer (Thermo Fisher Scientific). Samples were injected directly on an in-house packed 25 cm C18 (Bishoff 3 micron bead diameter) column. Separation of peptides was achieved with the following gradient 5–30% buffer B over 90 min, 30–55% buffer B over 20 minutes and 98% buffer B for 5 minutes (buffer A: 0.1% formic acid, buffer B: 0.1% formic acid in acetonitrile) at a flow rate of 300nl/minute. Data were acquired in a data-dependent mode, automatically switching from MS to collision induced dissociation MS/MS on the top 20 most abundant ions with a precursor ion scan range of 350–1650 m/z. Full scan MS spectra were acquired at a resolution of 70,000 and MS/MS scans at 17,500 at a target value 3×10^6 and 1×10^5 ions respectively. Dynamic exclusion was enabled with exclusion duration of 40 seconds.

Semi-quantitative label free analysis of GFETCR from 2B4 cells

Label free analysis was performed (Progenesis QI for Proteomics software, Nonlinear Dynamics) and aligned precursor features were searched with Mascot. MS/MS spectra were searched against the UniProt mouse database. Precursor mass tolerance was 10 ppm and a fragment ion tolerance was 0.02 Da with a minimum ion score of 20. The precursor ion charge state was 2+, 3+ and 4+. Variable modifications were defined as deamidation on asparagine and glutamine, oxidation on methionine and alkylation with MPB or IAA on cysteine. The enzyme specificity was set to trypsin with a maximum of two missed cleavages. All searches were performed against a concatenated target/decoy database, providing an empirical false discovery rate (FDR) and results are reported at a 1% target/decoy FDR for both peptides and proteins. Aligned chromatography features identified as MPB and MPB+H_2O alkylated GFETCR in both control and TCEP-HCl reduced samples were visually compared.

Quantitative data analysis of disulfide bond reduction of kinetically trapped hCD44-Fc

The data files from all of the mass spectrometry runs were combined and searched against the human Swiss-Prot database using Peaks 7 proteomics studio (Bioinformatics Solutions Inc. On, Canada). Precursor mass tolerance was 10 ppm and a fragment ion tolerance was 0.01m/z with up to three missed trypsin cleavage sites per peptide allowed. Variable modifications were defined as deamidation on asparagine and glutamine, oxidation on methionine and alkylation

with NEM or D5-NEM (and hydrolysed variants) on cysteines. *de-novo*, peaks-db, SPIDER and peaks PTM algorithms were sequentially used to search against a concatenated target/decoy database, providing an empirical FDR and results are reported at a 1%t target/decoy FDR for both peptides and proteins. 2+ ions and retention time windows were extracted for peptides containing cysteine residues from the hCD44 hyaluronic binding domain (HABD) and the Fc region of the chimera. Precursor ion areas for NEM and D5-NEM alkylated (and hydrolysed variants) peptides were extracted using MS1 filtering in Skyline. The reduction of each cysteine is calculated from the following ratio (total NEM area/total D5-NEM area) where total NEM area and total D5-NEM area are the sum of normal and hydrolysed forms of NEM and D5-NEM (plus any other variants such as oxidised methionine and deamidation) and normalised against the control ratio for each peptide.

Generation of a CD44 transfected CHO cell line

The coding sequence was amplified from a full length cDNA using the high fidelity polymerase pfu Ultra AD (Agilent) with the following primers:

hCD44−14 MluI F 5′ GCGTAACGCGTCCCGGACACCATGGACAAG

hCD44 1146* NotI R 5′ CGGCGGCCGCTTA CACCCCAATCTTCATGTCCAC

Segments of the primers that generate restriction sites are underlined and the stop codon is denoted by italics in the reverse primer.

The amplified product was cloned into the vector pHR Sin, based on the HIV retrovirus. 293T cells were transiently transfected with pHR Sin plasmids together with pMD.G and p8.91 [21] in 6-well plates using Genejuice (Merck, Darmstadt, Germany) according to the manufacturer's instructions. Growth media had been changed immediately prior to transfection with DMEM supplemented with 10% FCS. Supernatant was harvested at 48–72 hours post-transfection passed through a 0.45 micron filter to remove cell debris. Transduction was achieved by adding virus-like particles in 2 ml of supernatant to $2x10^5$ CHO K1. Cells were incubated overnight before the supernatants were replaced with fresh growth medium. After 3 days cells bearing an enhanced level of cell surface CD44 with concomitant elevated levels of HA binding (as determined by staining with fluorescein labelled HA) were isolated by FACS and maintained as a line.

CD44-Fc HA plate binding assays

ELISA plate wells were coated with 5mg/ml HA in carbonate-bicarbonate coating buffer, pH 9.6 for 18 hours at 4°C, washed with PBS containing 0.05% tween-20 and blocked with 1% BSA for 3 hours at room temperature. Human (h) and mouse (m) CD44-Fc protein were diluted to 5mg/ml in PBS and reduced with either TCEP-HCl (2.5 mM for 20 minutes at 4°C) or Trx1 (100 μl of 1 μM Trx1 supplemented with 100 nM TR1 and 200 μM NADPH for 90 minutes at 37°C) after which reduced chimeras were alkylated by 5 mM NEM for 30 minutes at 4°C. A non reduced control samples were treated with 5 mM NEM only. The stock solutions were serially diluted to concentrations of 5000, 2500, 1250, 625, 313, 156, 78, 39, 20, 10, 5 and 2.5ng/ml (plus 5mg/ml to determine maximal binding), added to HA coated ELISA plates in triplicate and left to equilibrate at room temperature for 1 hour. Bound CD44-Fc was probed with HRP-conjugated anti-human Fc or HRP conjugated anti-mouse Fc with colorimetric quantitation using 3,3',5,5'–tetramethylbenzidine substrate, quenched with 5% H_2SO_4 and optical densities recorded at 450 nm. Binding isotherms were constructed and normalised by plotting mean absorbances for each CD44-Fc concentration as a fraction of the maximal binding and equilibrium dissociation constants (K_D) determined by fitting a one site binding model to the data in

Graphpad Prism 6.0 software. Quoted K_Ds and the final figures are the average of three independent experiments.

Staining of reduced cysteines on hCD44 transfected CHO cells and western blot for CD44

CHO hCD44+ cells (~1x10^7 each sample) were washed twice with ice cold PBS and reduced with either TCEP-HCl (1ml of 2.5 mM in PBS/1%BSA for 15 minutes at 4°C) or Trx1 (1ml of 100 μl of 1 μM Trx1 supplemented with 100 nM TR1 and 200 μM NADPH for 90 minutes at 37°) after which they were washed x2 with ice cold PBS and resuspended in 100uM Dylight-800-maleimide in PBS for 30 mins at 4°C to label reduced cell surface disulfide bonds. Non reduced cells were labelled as a control. After washing x5 with ice cold PBS the cells were lysed in 1ml of 1% digitonin for 30 minutes on ice. The lysates were cleared of cell debris by centrifugation at 11,000g for 20 minutes, and a sample mixed 1:1 with non-reducing SDS-PAGE sample loading buffer, heated to 95°C for 5 minutes and loaded onto Novex 4–12% bis-tris SDS PAGE gels, resolved in SDS-MES buffer at 180V and visualised on a LICOR™ Odyssey imaging system at 700 nm for the protein molecular weight markers and 800 nm for the labelled samples. The gel was transferred on nitrocellulose membrane and probed with biotinylated IM-7 CD44 specific monoclonal antibody that was detected with streptavidin-Dylight-680 and visualised on a Licor Odyssey imaging system. Scans of the gel and the blot were aligned via the protein molecular weight standards using Licor image studio software.

Immunoprecipitation of reduced CD44 from hCD44 transfected CHO cells

Dynabead-M280 streptavidin coated magnetic beads (1 μg per immunoprecipitation) saturated with biotinylated IM7 CD44 antibody (10 μg per immunoprecipitation) were added to lysates and rotated at 4°C for 4 hours. The beads were isolated, washed x4 with ice cold 0.1% digitonin in PBS and heated at 95°C for 10 minutes in 50 μl of 100 mM glycine-HCl, pH 2.8. 10 μl of the eluent was mixed 1:1 with non-reducing SDS-Page sample loading buffer, centrifuged at 11,000g for 10 minutes, loaded onto Novex 4–12% bis-tris SDS PAGE gels and resolved in SDS-MES buffer at 180V and visualised on a LICOR™ Odyssey imaging system at 700 nm for the protein molecular weight markers and 800 nm for the labelled samples.

hCD44 transfected CHO cell adhesion assay

ELISA plate wells were coated with 5mg/ml HA in carbonate-bicarbonate coating buffer, pH 9.6 for 18 hours at 4°C, control HA free wells were treated with coating buffer alone. Plates were washed with PBS containing 0.05% Tween 20 and blocked with 1% BSA for 3 hours at room temperature. hCD44 transfected CHO cells were fluorescently labelled using a Vybrant® Cell Adhesion Assay Kit (Life technologies). Cells (5x10^7) were reduced with TCEP-HCl (1ml of 2.5 mM in PBS/1%BSA for 15 minutes at 4°C) or Trx1 (1ml of 100 μl of 1 μM Trx1 supplemented with 100 nM TR1 and 200 μM NADPH for 90 minutes at 37°) after which they were washed twice in ice cold PBS and alkylated with 5 mM NEM in PBS for 30 mins at 4°C. Non reduced cells were also alkylated as a control. After resuspension in DMEM supplemented with 5% FCS, 1x10^6 cells were added to HA coated and control wells respectively, each condition in quintuplicate. Cells were left to adhere for 45 minutes at 37°C after which wells were carefully washed with PBS to remove non adherent cells. Total fluorescence was recorded at 517 nm and data from each individual well was normalised to the mean total fluorescence of the five non reduced hCD44+CHO cells binding HA coated wells, the mean of which was defined as 100%

binding. In order to represent the variability of the binding assay the results are graphed as composites of 15 wells per experimental condition (five wells per condition form three independent experiments) and significance of reduction was determined by applying non paired T tests to each condition relative to the control.

Results

CD44 contains disulfide bonds that are potentially labile

Potentially labile disulfide bonds can be characterised and identified by their configuration (labile bonds are normally–RH Staple,–LH Hook or–/+RH Hook), the strain energy of the covalent bond between the sulphur atoms and accessibility to reductases (defined as the solvent accessibility of the cysteines making up the bond) [11]. The crystal structure of the N-terminal globular HABD of murine CD44 in complex with a HA octosaccharide [22] is shown in Fig 1A. The HABD consists of the link module, typical of many hyaladherins which contains a shallow HA binding groove. The link module contains two conserved disulfide bonds and Cys57-Cys123 (Cys53-Cys118 in human) which stabilises the core and (Cys81-Cys101 (Cys77-Cys97 in human)) which is located at the bottom of the HA binding groove and stabilises it and is in contact with bound HA. There is a third disulfide bond Cys32-Cys134 (Cys28-Cys129 in human) which stabilises an area of the HABD formed by C and N terminal extensions to the link module.

Structural analysis of the disulfide bonds using the bioinformatics methods of [23] in the HABD of CD44 (Fig 1B) reveals two potentially labile disulfide bonds. Both the HA binding groove disulfide and (Cys32-Cys134 (Cys28-Cys129 in human) in the link module extension have solvent accessibility in excess of 50 $Å^2$. Furthermore they have high bond strain energy and potentially labile configurations of–LH Hook and–RH Staple respectively. The third disulfide bond, Cys57-Cys123 (Cys53-Cys118 in human)), is buried in the globular core of the HABD and has low strain energy and a non-labile spiral configuration.

A disulfide bond in CD44 is labile on the human and mouse leukocyte surface

Previously as part of a large scale mass spectrometry screen we identified CD44 on the surface of a mouse T cell hybridoma 2B4 to contain a reduced, and therefore potentially labile disulfide bond [9]. Further analysis of the data reveals the peptide GFETCR, containing Cys81 from the disulfide bond that stabilises the HA binding to be alkylated with MPB when CD44 is purified from TCEP-HCl or human thioredoxin-1 (Trx1) reduced cells. This indicates that this cysteine originated from a labile disulfide bond that was reduced when the cells were treated. On untreated control cells the Cys81 was not labelled with MPB therefore MPB alkylation and hence disulfide bond reduction appears to be dependent upon exogenous reducing agents. These screens are non-quantitative and provide no information on the extent of reduction of the labile bond at the cell surface therefore a more quantitative mass spectrometry workflow was designed. As the amount of cysteine biotinylation by MPB is proportional to the amount of reduction of the disulfide bond then if the disulfide bond is labile and therefore MPB labelled, then more protein from reduced cells will be captured on avidin beads than from control cells. Progenesis QI software suite was used to align the total ion current chromatograms (TICs) from control and TCEP-HCl reduced 2B4 hybridoma cells. Fig 2 shows the region of the TICs where MPB labelled GFETCR elutes in both the control (Fig 2A) and the TCEP-HCl reduced (Fig 2B) cells. The peak area of GFETCR is much greater in the TCEP-HCl reduced sample than in the control where the peak for GFETCR does not rise above background levels.

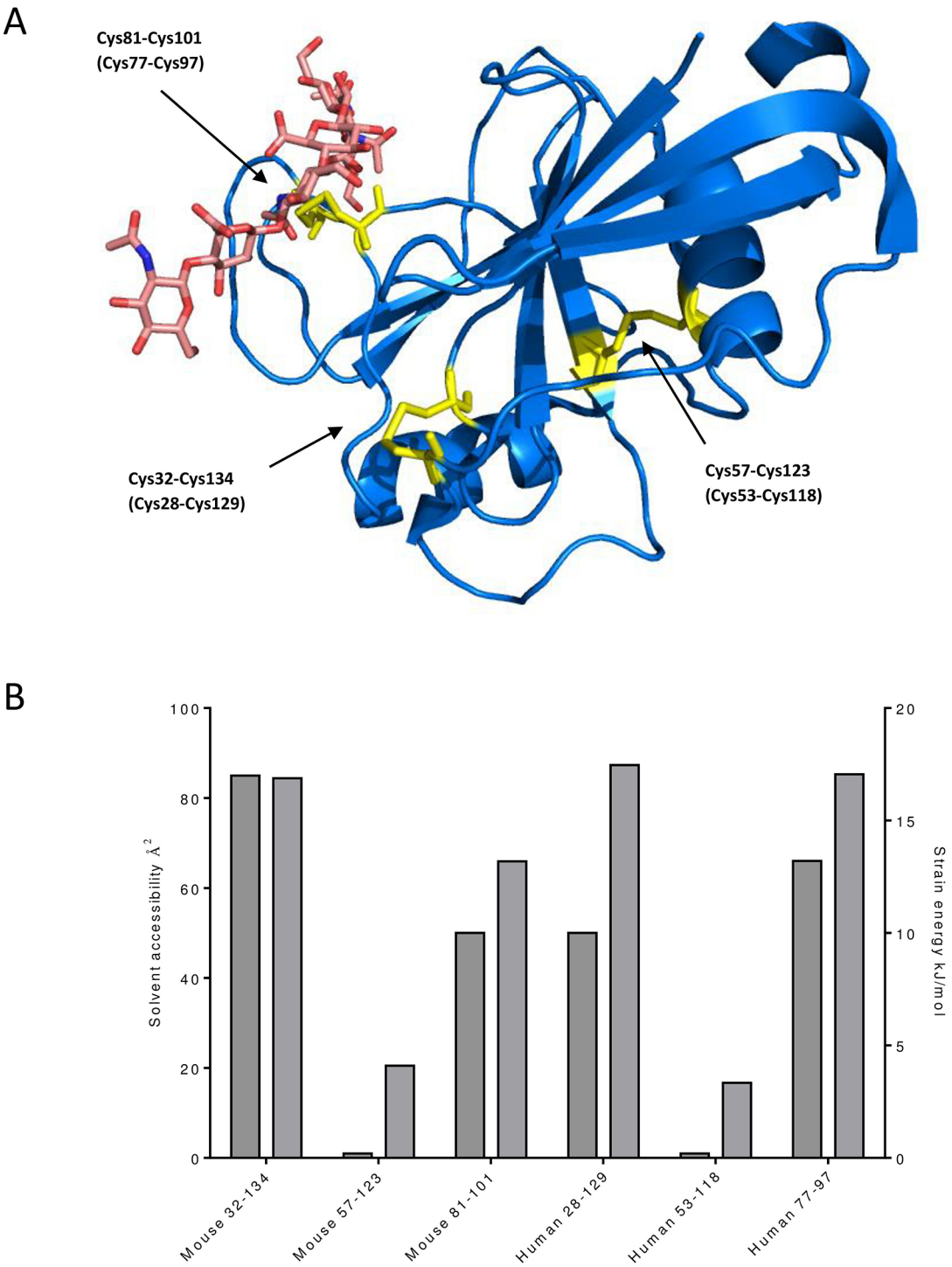

Fig 1. (A) Crystal structure of the HABD of murine CD44 in complex with an HA 8-mer (adapted from PDB ID:2JCQ). The protein backbone is represented as a blue cartoon. The HA 8-mer is shown as pink sticks. Disulfide bonds are shown as yellow sticks and the cysteine residues from which they are formed are numbered according to their position in the mouse CD44 sequence (human numbering is shown in parenthesis). (B) For each disulfide bond dark grey bars show solvent accessibility and light grey bars show bond strain energy calculated from the PDB coordinates (PDB ID:2JCQ for mouse and 1UUH for human, the coordinates for HA were removed from 2JCQ prior to analysis) **using** (http://powcs.med.unsw.edu.au/research/adult-cancer-program/services-resources/disulfide-bond-analysis-tool/disulfide-bond).

doi:10.1371/journal.pone.0138137.g001

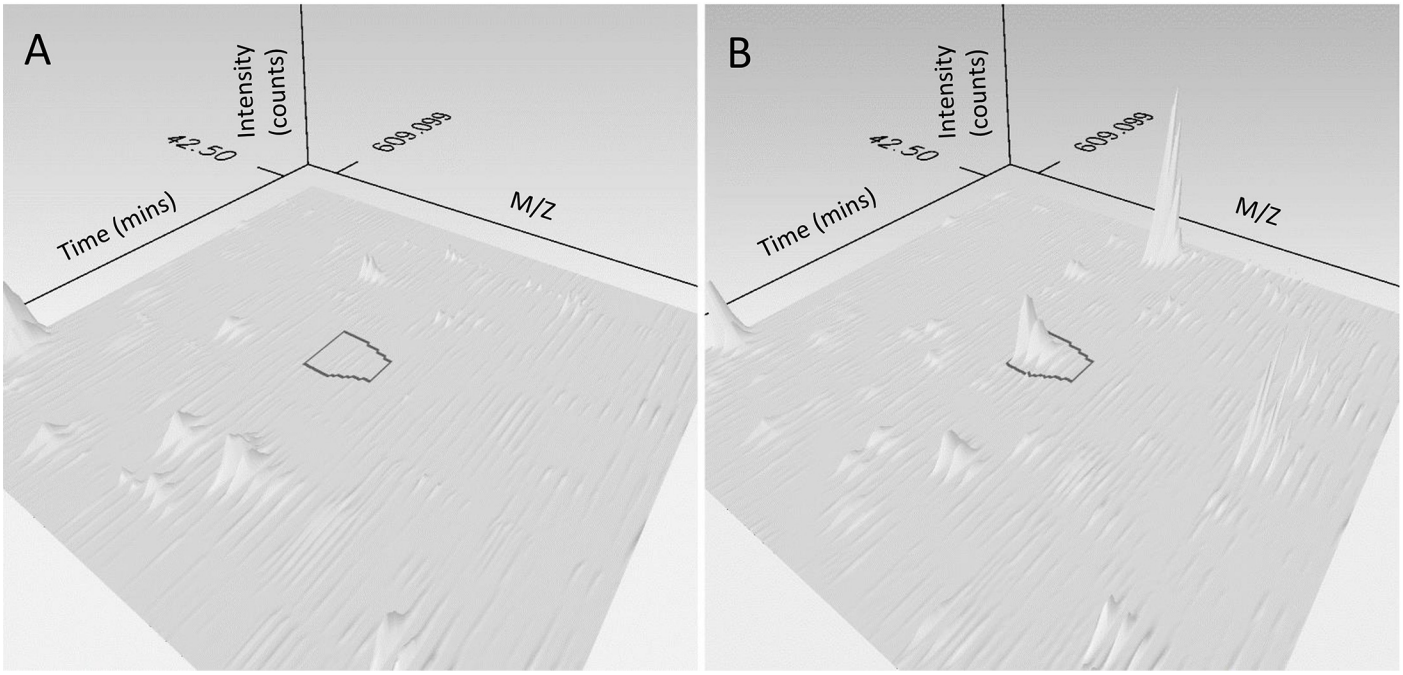

Fig 2. Aligned 3D total ion current chromatograms using Progenesis QI in the area of chromatographic space where MPB labelled GFETCR elutes for (A) control 2B4 cells and (B) TCEP-HCl reduced 2B4 cells. The peak corresponding to MPB labelled GFETCR is outlined in black and is visibly larger in the TCEP-HCl reduced cells. Other peptides are seen in both the control and TCEP-HCl reduced samples, ones with increased area after TCEP-HCl treatment suggests they are from proteins containing labile disulfide bonds.

doi:10.1371/journal.pone.0138137.g002

Other local spectral features unrelated to CD44 are seen in both the control and TCEP-HCl reduced samples, and some of the intensities are greater in the TCEP-HCl reduced sample, suggesting the peptides are from other proteins enriched through MPB labelling of redox labile disulfide bonds. A second cysteine containing peptide TEAADLCQAFNSTLPTMDQMK which contains Cys57 from the disulfide bond buried deep in the link module is consistently identified in the mass spectrometry screens but is never labelled with MPB, suggesting that it forms a disulfide bond in CD44 that is stable towards reduction, as was predicted by the structural analysis. Combining these observations show that the disulfide bond in the HA binding groove in CD44 is labile on the surface of the 2B4 T cell hybridoma, being readily reduced by TCEP-HCl. Subsequently this disulfide was observed to be labile under many differing conditions in screens from several other mouse and human leukocytes as summarised in Table 1. All subsequent experiments were performed on human CD44 and therefore human numbering will be used from this point onwards.

The disulfide bond in the HA binding groove of recombinant soluble CD44 is preferentially reduced

A key factor in determining whether the reduction of the labile disulfide bond in CD44 has a functional effect is the extent to which it occurs. This was tested using samples of human Fc chimera fusion protein, hCD44-Fc which were reduced with either TCEP-HCl or Trx1 for 20 and 90 minutes respectively. The resultant redox state of hCD44-Fc was kinetically trapped by alkylating free cysteines liberated from disulfide bond reduction with NEM. A control sample of hCD44-Fc was alkylated with NEM without prior reduction to obtain background levels of free cysteines. The labelled fusion proteins were then denatured with urea and further reduced

Table 1. Cell types and treatments for which the allosteric disulfide has been observed.

Species	Cell Type	Treatment	HA peptide	Labile?	Globular peptide	Labile?[c]
Mouse	2B4	Control	GFETCR	No	TEAADLCQAFNSTLPTMDQMK	No
		TCEP-HCl		Yes		No
		Trx1		Yes		No
		GILT[a]		Yes		No
Human	Platelets	Control	ALSIGFETCR	No	TEAADLCK	-
		TCEP-HCl		Yes		-
		DTT		Yes		-
Human	MEG-01	Control	ALSIGFETCR	No	TEAADLCK	-
		TCEP-HCl		Yes		No
Human	Namalwa	Control	ALSIGFETCR	No	TEAADLCK	-
		TCEP-HCl		Yes		-
Human	PBMC	Control	ALSIGFETCR	Yes	TEAADLCK	No
		TCEP-HCl		Yes		No
		SEA+IL-2[b]		Yes		No

[a] gamma-interferon-inducible lysosomal thiol reductase.

[b] MLR supplemented with staphylococcal enterotoxin A super antigen.

[c]–is not detected in the mass spectrometry run.

doi:10.1371/journal.pone.0138137.t001

with TCEP-HCl and the remaining disulfide bonds in hCD44-Fc were alkylated with deuterium labelled NEM, D5-NEM. After deglycosylation with PNGase F, digestion with porcine trypsin, and LC-MS-MS analysis, Peaks-7 was used to search the data against the UniProt human protein database [24] and four high ranking cysteine containing peptides were chosen to quantify the reduction of the disulfide bonds. TEAADLCK (Cys53) and ALSIGFETCR (Cys77) from the hCD44 HABD plus PEVTCVVVDVSHEDPEVK (Cys144) and NQVS LTCLVK (Cys250) from each of the immunoglobulin domains of the Fc region of the fusion protein. Precursor ion areas were extracted for the 2+ ion of each modified peptide along with two topisomers, examples of extracted ion chromatograms for ALSIGFETCR before and after reduction with TCEP are shown in Fig 3A. The total area for each peptide for each condition was determined by adding the normal and hydrolysed forms of the NEM together. The amount of reduction is determined by ratio of NEM peptide areas to D5-NEM peptide areas and is summarised in S1 Table. For each of the two replicates the increase in the NEM/ D5-NEM precursor ion area ratios for a given peptide after reduction are normalised to the control (Table 2) and plotted in Fig 3B. After reaction with TCEP-HCl and Trx1 the NEM:D5-NEM ratio of ALSIGFETCR (Cys77-Cys97) increases >20 fold over the control whereas TEA ADLCK (Cys53-Cys118) only increases to approximately 12 fold after Trx1 reduction and <10 fold after TCEP-HCl reduction. The Cys77-Cys97 disulfide bond from the HA binding groove is more reactive, thus more labile than the Cys53-Cys118 disulfide bond in the core of the link domain, corroborating the evidence seen in the cell surface screens. As expected, the peptides from buried disulfide bonds in the tightly folded immunoglobulin domains of the Fc region showed no significant reduction, and serve as an internal control. Both of the cysteines from the Cys28-Cys129 disulfide bonds do not reside in tryptic peptides that are compatible with mass spectrometry so their reduction state could not be determined.

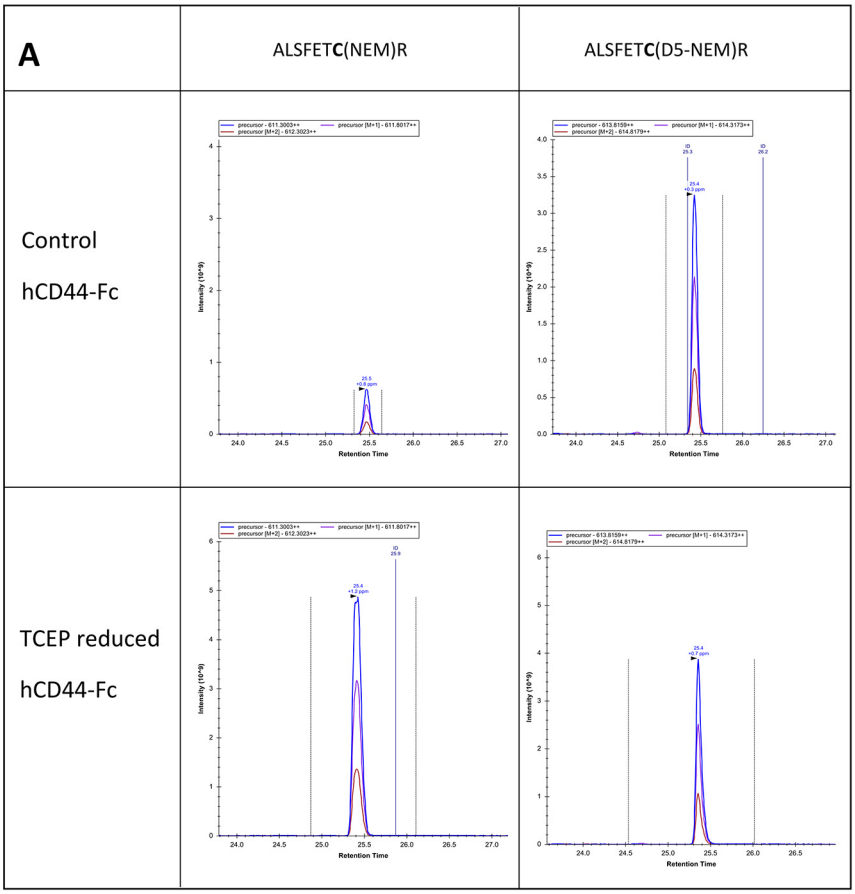
A
ALSFETC(NEM)R
ALSFETC(D5-NEM)R
Control
hCD44-Fc
TCEP reduced
hCD44-Fc
Retention Time
Intensity (10^9)

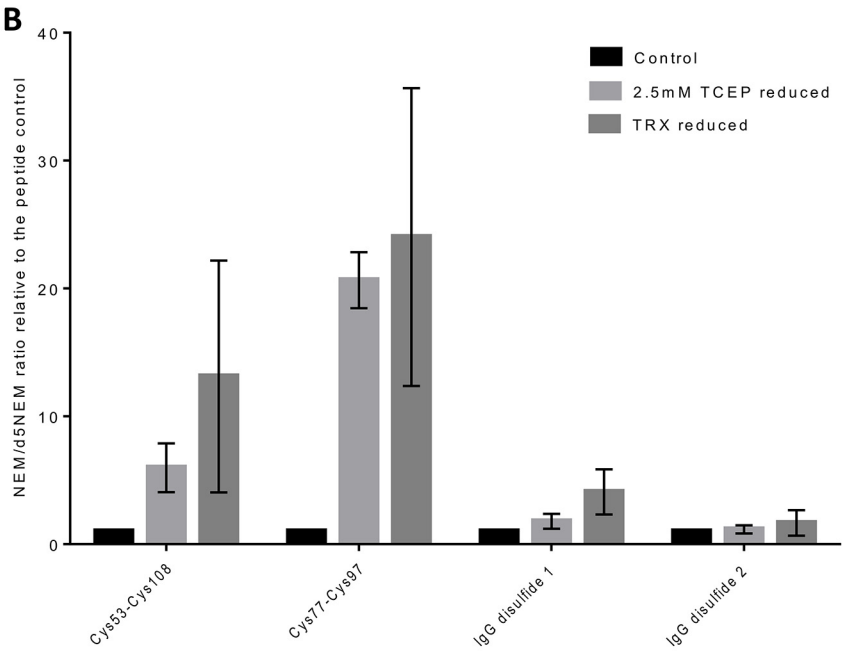
B
NEM/d5NEM ratio relative to the peptide control
Control
2.5mM TCEP reduced
TRX reduced
Cys53-Cys108
Cys77-Cys97
IgG disulfide 1
IgG disulfide 2

Fig 3. The Cys77-Cys97 disulfide bond is the most reactive in hCD44-Fc chimera after treatment with TCEP-HCl and Trx1 followed by kinetic trapping with NEM. (A) Extracted ion chromatograms for NEM and D5-NEM labelled ALSIGFETCR in non reduced control and TCEP reduced hCD44-Fc. In the control the NEM labelled peptide has a much smaller area than the D5-labelled peptide showing that the Cys77-Cys97 disulfide bond is predominantly oxidised. After reduction with TCEP the area of NEM labelled peptide is increased relative to D5-NEM labelled peptide indicating that the disulfide bond has been significantly reduced. Peak integration boundaries are shown as dotted lines and the times of any MS/MS switching events are indicated. (B) Summary of the ratio of the extracted ion chromatograms for NEM labelled to D5-NEM labelled peptides. Peptide ALSIGFETCR contains Cys77 is from the disulfide bond in the HA binding groove. TEAADLCK contains Cys53 and is from the disulfide buried in the core of the link domain. PEVTCVVVDVSHEDPEVK and NQVSLTCLVK are from the Fc region of the chimera. Columns represent the fold change of the NEM/D5-NEM ratio of each peptide for TCEP-HCl reduced chimera (medium grey), Trx1 reduced chimera (light grey) relative to non-reduced control chimera (dark grey). Mean and SEM of ratios from two reductions are shown.

doi:10.1371/journal.pone.0138137.g003

Disulfide bond reduction of recombinant soluble CD44 inhibits HA binding

To test the effect that reduction of the disulfide bond in the CD44 HA binding groove has on HA binding function we conducted binding experiments with plate bound HA. Both hCD44-Fc and mCD44-Fc were reduced as above with either TCEP-HCl or Trx1 and alkylated with NEM. Non reduced controls were alkylated without prior reduction. The binding of both hCD44-Fc (Fig 4A) and mCD44-Fc (Fig 4B) to plate bound HA was significantly inhibited by treatment with TCEP-HCl. For Trx1 reduction, which is more biologically relevant, a full titration was performed for hCD44-Fc (Fig 4C) and mCD44-Fc (Fig 4D). Combined data from three experiments gave equilibrium dissociation constants (K_D) of 4.5 ± 0.41 nM for hCD44-Fc and 180 ± 2.7 nM for mCD44-Fc respectively. After reduction, binding to HA was almost completely inhibited. The HA binding groove disulfide bond is therefore not only labile but is also functional, acting as a redox sensitive switch controlling HA binding.

CD44 can be reduced on the surface of transfected CHO cells

Mass spectrometry is an excellent tool to screen the cell surface proteome as a whole to determine which proteins contain labile disulfide bonds. However it is expensive and requires complex and lengthy sample preparation so is not practical to routinely check for reduction of a specific cell surface protein prior to cellular assays. To address this we developed a gel based assay to quantify CD44 reduction on the surface of CHO cells transfected with a full length hCD44 construct, which express high levels of CD44 on their surface (Fig 5A and 5B). CHO-hCD44 cells were reduced with TCEP-HCl and Trx1 under conditions previously shown by mass spectrometry to reduce the HA binding groove disulfide bond in CD44 on the surface of cells (Table 1) and in CD44-Fc chimeras which subsequently inhibits HA binding. Cysteines

Table 2. Summary of NEM/D5-NEM peptide ratios and fold changes relative to controls determined from the summed extracted ion chromatogram areas of the indicated peptides calculated in S1 Table.

Peptide	NEM/D5-NEM ratio						NEM/D5 NEM ratio change relative to control					
	Replicate 1			Replicate 2			Replicate 1			Replicate 2		
	Control	TCEP	Trx1	Control	TCEP	Trx1	Control	TCEP	Trx1	Control	TCEP	Trx1
ALSIGFETCR	0.05	1.21	1.89	0.15	2.81	1.88	1.00	22.83	35.66	1.00	18.45	12.37
TEAADLCK	0.06	0.47	1.31	0.24	0.99	0.98	1.00	7.88	22.19	1.00	4.07	4.05
NQVSLTCLVK	0.08	0.19	0.48	0.44	0.53	1.02	1.00	2.37	5.85	1.00	1.21	2.32
TPEVTCVVVDVSHEDPEVK	0.16	0.13	0.41	0.19	0.28	0.12	1.00	0.85	2.66	1.00	1.48	0.66

doi:10.1371/journal.pone.0138137.t002

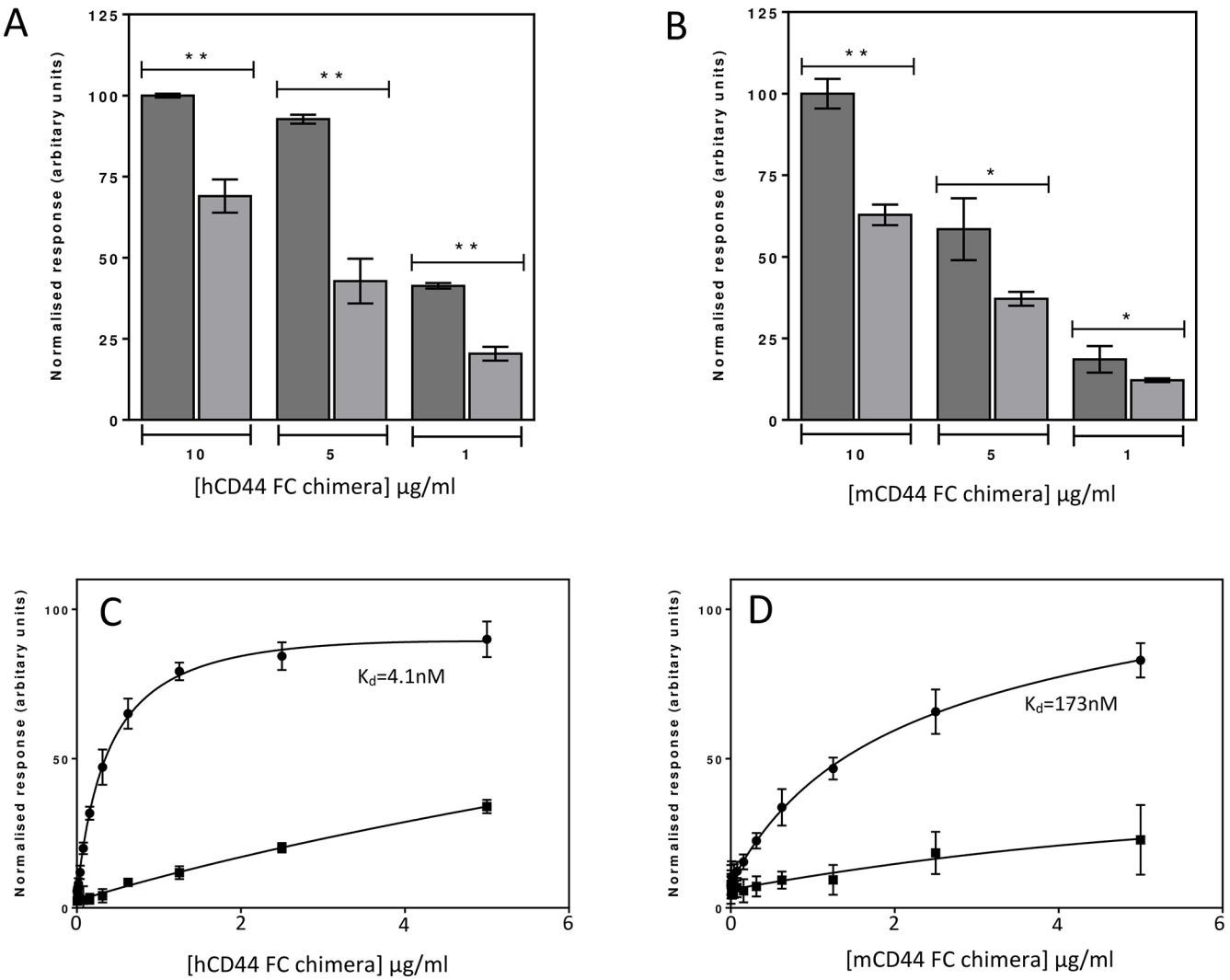

Fig 4. TCEP-HCl reduction of CD44 inhibits binding to HA. (A) hCD44-Fc and (B) mCD44-Fc binding to plates coated with 50 µg/ml HA. Columns represent non reduced control CD44-Fc (dark grey) and TCEP-HCl reduced CD44-Fc (light grey). Mean and SEM of peptide chromatographic areas from three experiments are shown, the differences between non reduced and TCEP-HCl reduced chimera: *, $P < 0.05$; **, $P < 0.01$. Titrations of Trx1 reduced (C) human CD44-Fc and (D) mouse CD44-Fc binding to plates coated with 50 µg/ml HA. For both mouse and human CD44-Fc titrations the binding curves represent non reduced control CD44-Fc (black circles) and Trx1 reduced CD44-Fc (black squares). Binding curves are constructed from data of three independent experiments and equilibrium dissociation constants were determined by fitting to a single binding site model.

doi:10.1371/journal.pone.0138137.g004

on the surface of CHO-CD44 cells resulting from disulfide bond reduction were alkylated with Dylight-800™ conjugated maleimide allowing reduced proteins to be visualised on a LICOR™ imaging system at 800 nm where proteins containing reduced cysteines show up as green bands (Fig 5C). Control cells were alkylated without prior reduction. The overall level of reduced cysteines is increased after reduction with both TCEP-HCl and Trx1 (Trx1> TCEP-HCl>>control). After scanning, the gel was transferred to nitrocellulose membrane and western blotted for CD44. Upon overlaying the western blot with the gel the red CD44 band overlays with the green bands at around 85kDa, which is the expected mass of the CD44 construct. Other bands containing reduced protein are seen in this assay and increase in intensity upon reduction relative to the non-reduced control and represent other membrane proteins with labile disulfide bonds. To determine if other proteins of similar weight are also being

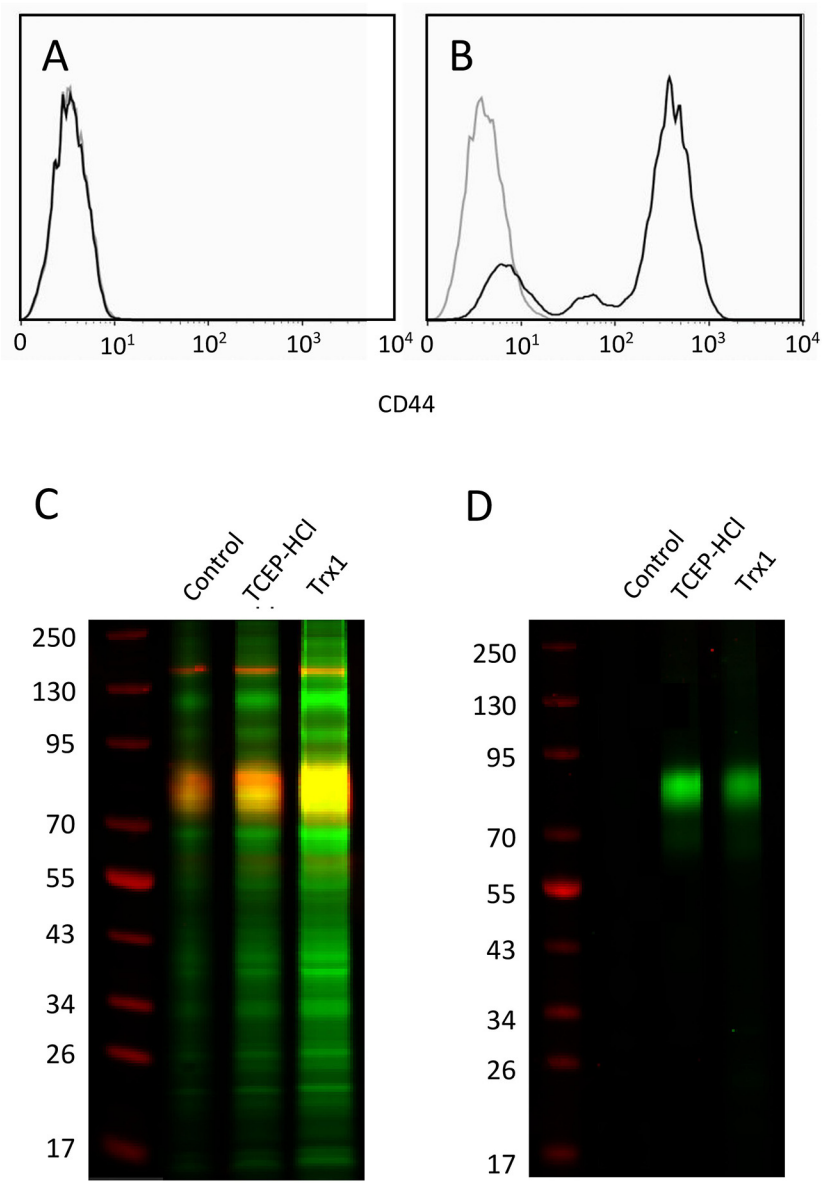

Fig 5. Levels of CD44 determined by flow cytometry analysis of (A) untransfected CHO K1 cells and (B) hCD44 transfected CHO cells. Light grey trace is isotype control, black trace is anti-CD44. (C) Non reduced SDS-PAGE gel showing reduced proteins on the surface of hCD44 transfected CHO cells after reduction (green bands) overlaid with a western blot of CD44 (red). (D) non reduced SDS-PAGE gel of eluted proteins which contain reduced disulfide bonds (green bands) from a CD44 immunoprecipitation of hCD44 transfected CHO cells that had been reduced with either TCEP-HCl or Trx1.

doi:10.1371/journal.pone.0138137.g005

reduced and contributing to the signal in the CD44 region, the lysate was immunoprecipitated with anti-CD44 coated magnetic beads and visualised in the LICOR™ scanner (Fig 5D). Intense green bands at around 85kDa can be seen in both TCEP-HCl and Trx1 reduced CHO-CD44 cells but not in the control cells confirming CD44 is reduced on the surface of CHO-CD44 cells after treatment with both TCEP-HCl and Trx1.

Reduction of CD44 transfected CHO cells inhibits HA binding

The effect of reducing CD44 on the surface of transfected CHO cells was investigated using a CD44 dependent cell adhesion assay to plate bound HA and is shown in Fig 6. CHO-K1 or CHO-hCD44 cells were stained with calcein and subjected to reduction with either TCEP-HCl or Trx1 and alkylation with NEM. Control CHO-hCD44 cells were alkylated with NEM without prior reduction. hCD44 transfected CHO-K1 cells show a significant increase in binding to HA relative to untransfected CHO-K1 cells. Similarly CHO-hCD44 cells do not bind to wells in the absence of HA, verifying that the binding of CHO-hCD44 cells to HA is dependent upon CD44 cell surface expression. Reduction of CD44 on CHO-hCD44 as described previously inhibits the CD44-HA binding and abolishes adhesion of CHO-hCD44 cells to HA coated plates providing further evidence that reduction can lead to loss of HA binding by CD44 with effects on cell adhesion.

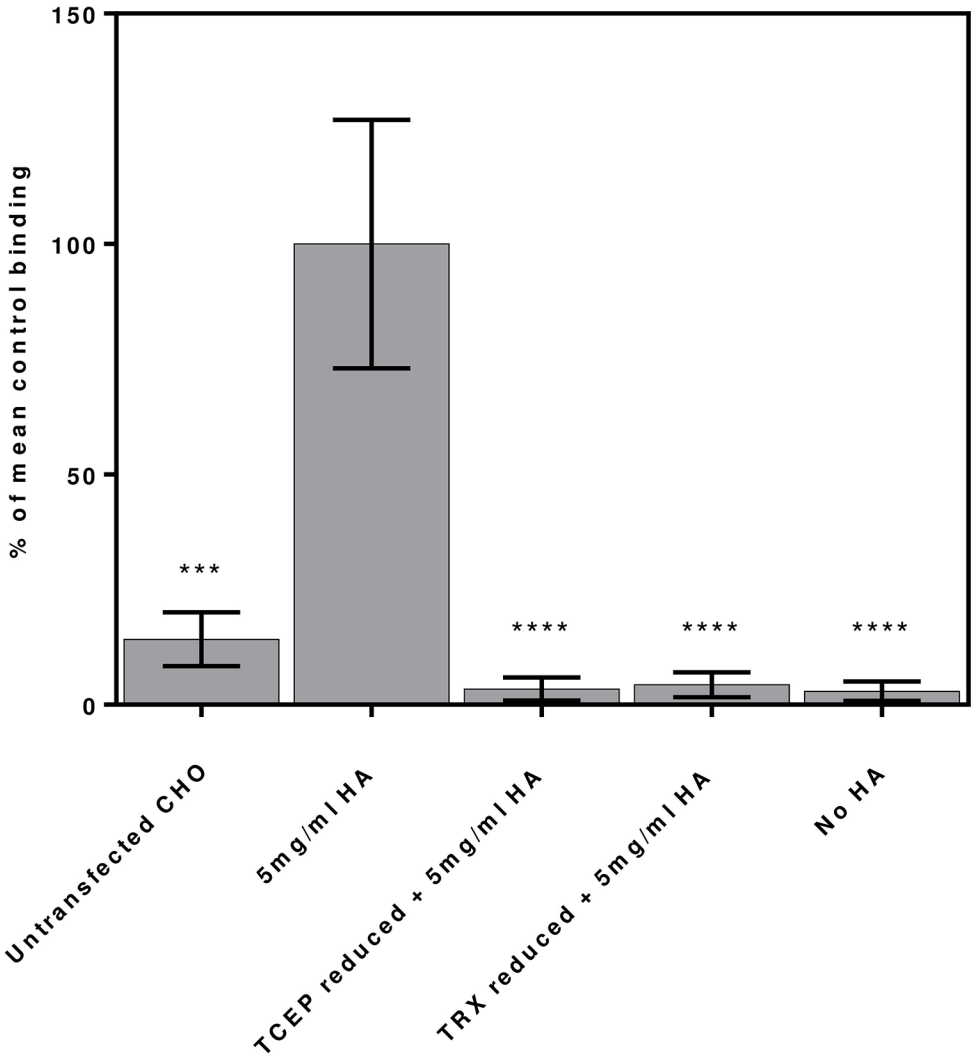

Fig 6. Cell adhesion assay showing the effect of TCEP-HCl and Trx1 reduction of untransfected and hCD44 transfected CHO cells binding to HA coated plates. Binding data are compositions of three independent experiments all normalised assuming non reduced CHO-hCD44 binding to HA coated wells as 100% response. Mean and SEM of total fluorescence are shown. The differences from control: *, P < 0.05; **, P < 0.01; ***, P < 0.001; ***, P < 0.0001

doi:10.1371/journal.pone.0138137.g006

Discussion

CD44 belongs to a family of HA binding proteins called hyaladherins that contain the link module protein fold. Two disulfide bonds are conserved across the link domain superfamily, one at the core of the link module which stabilises the fold and one which resides in the shallow groove which forms the binding site for HA. Type B link module proteins such as CD44 have N and C terminal extensions to the link module which are stabilised via a third disulfide bond. We have shown that the disulfide bond in the HA binding groove of CD44 (Cys77-Cys97) and not the disulfide bond in the core of the link module (Cys53-Cys108) can be reduced under redox conditions that mimic those found in inflammation.

Mass spectrometry screens identify reduced Cys77-Cys97 on a variety of human and mouse cell lines which had been subjected to reduction by the chemical reductant TCEP, and a spectrum of thiol reductase enzymes such as Trx1. Cys77-Cys97 was also reduced in CD44 purified from human PBMC's that had been activated by superantigen. Previously, CD44 purified from splenocytes of mice subjected to LPS induced endotoxaemia was deemed to contain a reduced disulfide bond but the identity of the bond was never determined [9]. Detailed kinetic analysis of the rate of reactions of the link domain disulfide bonds in recombinant soluble CD44 confirm that the Cys77-Cys97 disulfide bond is more reactive than Cys53-Cys108 due to its exposed orientation on the surface of CD44 and its reactive–LH hook configuration. The redox state of the third disulfide bond in the link module extension (Cys28-Cys129) could not be determined due to incompatibility of the tryptic peptides which contain the cysteines with the mass spectrometry experiments.

Reduction of the Cys77-Cys97 disulfide bond negatively regulates binding function. Reduced soluble CD44 can no longer bind HA and cells expressing CD44 no longer adhere to HA coated surfaces after treatment with TCEP and Trx1. As the Cys77-Cys97 disulfide bond not only stabilises the HA binding groove but is also in direct contact with bound HA, so reduction of this disulfide bond appears to destabilise both the structure of binding groove and the interaction with HA and thus acts as a redox switch.

There is precedence for such regulation *in vivo*. CD44 is upregulated on the surface of T cells after activation [25], however HA binding function needs to be 'switched on'. Receptor clustering [26] and relieving steric inhibition of the HA binding site by enzymatic removal of sialic acid moieties capping N-linked glycosylation sites [27,28] have been suggested as mechanisms for induction of HA binding. Once initiated HA binding activity is transient only lasting a few days after activation [29] allowing T cells migrate through the blood circulatory system to sites of inflammation [30]. The loss of HA binding is not due to CD44 down regulation as levels remain high long after the immune challenge has been cleared [31] suggesting that the protein structure and ligand binding is modulated in some way independent upon CD44 expression levels at the cell surface. Inhibition of HA binding by enzymatic reduction of the labile disulfide bond described here by reductases secreted at sites of inflammation could account for the observations.

Redox regulation of proteins through the enzymatic reduction of labile allosteric disulfide bonds is a widespread phenomenon. About 30 proteins have been shown to modulate their function through allosteric switching (reviewed in [12,32]) with many more predicted to contain allosteric disulfide bonds through data mining [23] molecular modelling [33] and experimental screens [9]. A variety of different functions have been shown to be affected by allosteric disulfide bonds in membrane or extracellular proteins. These include integrins where the interaction of platelet integrin αIIbβ3 with fibrinogen is regulated by PDI [34]. Cytokine receptors where CD132, the common gamma chain of the IL-2 family of cytokine receptors contains an allosteric disulfide bond at the interface with bound IL-2 and its redox state controls IL-2

binding and signalling [19]. The T cell surface antigen CD4 has been shown to homo dimerise through an allosteric disulfide bond in domain 2, which alters its function from a co stimulatory molecule [35] to a receptor involved in HIV viral fusion and infection [36]. These studies extend the range of different functions to include an important adhesion protein CD44.

Redox modulation of HA binding in the hyaladherins may be important in regulation of the movement of leukocytes through the lymphatic system during immune responses and inflammation. Conversely as CD44 is a marker for chronic autoimmune disease [37] and plays an important role in cancer metastasis [3] inhibiting the CD44/HA interaction though redox changes offers a mechanism of regulating such processes. Targeting allosteric disulfide bonds has recently been highlighted as a strategy of controlling protein function in disease [38] either by targeting the enzymes involved in the process or the modified protein. CD44 is a particularly attractive target for this approach given its involvement in inflammation and cancer. The ability to regulate the CD44/HA interaction through therapeutic manipulation of the redox state of the Cys77-Cys97 disulfide bond could provide a handle towards limiting leukocyte migration to sites of inflammation in autoimmune disease and the migration of metastatic cancer cells thought the lymphatic system.

Supporting Information

S1 Table. Extracted ion chromatogram peak areas for all of the peptides used in the kinetic trapping experiment.
(PDF)

Acknowledgments

We would like to thank Suneale Banerji for supplying the hCD44+ CHO cell line and Svenja Hester and Philip Charles in the University of Oxford central proteomics facility for help with mass spectrometry and data analysis. We are grateful to Marion H. Brown, Suneale Banerji and David Jackson for providing helpful comments and discussion in preparation of this manuscript. This work was supported by the Medical Research Council Grant No G9826026.

Author Contributions

Conceived and designed the experiments: CM ANB. Performed the experiments: CM HKC MS. Analyzed the data: CM MS. Wrote the paper: CM MS ANB.

References

1. Isacke CM, Yarwood H. The hyaluronan receptor, CD44. Int J Biochem & cell Biol. 2002; 34: 718–721.
2. Haynes BF, Hale LP, Patton KL, Martin ME, McCallum RM. Measurement of an adhesion molecule as an indicator of inflammatory disease activity: Up-regulation of the receptor for hyaluronate (CD44) in rheumatoid arthritis. Arthritis & Rheum. 1991; 34: 1434–1443.
3. Jothy S. CD44 and its partners in metastasis. Clin & Exp Metastas-. 2003; 20: 195–201.
4. Yung S, Chan TM. The role of hyaluronan and CD44 in the pathogenesis of lupus nephritis. Autoimmune Dis. 2012;2012.
5. Mikecz K, Dennis K, Shi M, Kim JH. Modulation of hyaluronan receptor (CD44) function in vivo in a murine model of rheumatoid arthritis. Arthritis Rheum. 1999; 42: 659–668. PMID: 10211879
6. Mikecz K, Brennan FR, Kim JH, Glant TT. Anti-CD44 treatment abrogates tissue aedema and leukocyte infiltration in murine arthrtis. Nat Med. 1995; 1: 558–563. PMID: 7585123
7. Misra S, Heldin P, Hascall VC, Karamanos NK, Skandalis SS, Markwald RR, et al. Hyaluronan-CD44 interactions as potential targets for cancer therapy. FEBS J. 2011; 278: 1429–1443. doi: 10.1111/j.1742-4658.2011.08071.x PMID: 21362138

8. Zhang S, Wu CC, Fecteau J-F, Cui B, Chen L, Zhang L, et al. Targeting chronic lymphocytic leukemia cells with a humanized monoclonal antibody specific for CD44. Proc Natl Acad Sci. National Acad Sciences; 2013; 110: 6127–6132. doi: 10.1073/pnas.1221841110 PMID: 23530247
9. Metcalfe C, Cresswell P, Ciaccia L, Thomas B, Barclay AN. Labile disulfide bonds are common at the leucocyte cell surface. Open Biol. 2011; 1. doi: 10.1098/rsob.110010
10. Hogg PJ. Disulfide bonds as switches for protein function. Trends Biochem Sci. 2003; 28: 210–214. PMID: 12713905
11. Schmidt B, Ho L, Hogg PJ. Allosteric disulfide bonds. Biochemistry. 2006; 45: 7429–7433. doi: 10.1021/bi0603064 PMID: 16768438
12. Butera D, Cook KM, Chiu J, Wong JWH, Hogg PJ. Control of blood proteins by functional disulfide bonds. Blood. 2014; 123: 2000–2007. doi: 10.1182/blood-2014-01-549816 PMID: 24523239
13. Essex DW. Redox control of platelet function. Antioxidants & redox Signal. 2009; 11: 1191–1225. doi: 10.1089/ARS.2008.2322
14. Castellani P, Angelini G, Delfino L, Matucci A, Rubartelli A. The thiol redox state of lymphoid organs is modified by immunization: role of different immune cell populations. Eur J Immunol. 2008; 38: 2419–2425. doi: 10.1002/eji.200838439 PMID: 18792398
15. Lawrence DA, Song R, Weber P. Surface thiols of human lymphocytes and their changes after in vitro and in vivo activation. J Leukoc Biol. 1996; 60: 611–618. PMID: 8929552
16. Pellom ST, Michalek RD, Crump KE, Langston PK, Juneau DG, Grayson JM. Increased cell surface free thiols identify effector CD8+ T cells undergoing T cell receptor stimulation. PloS one. 2013; 8. doi: 10.1371/journal.pone.0081134
17. Angelini G, Gardella S, Ardy M, Ciriolo MR, Filomeni G, Di Trapani G, et al. Antigen-presenting dendritic cells provide the reducing extracellular microenvironment required for T lymphocyte activation. Proc Natl Acad Sci United States Am. 2002; 99: 1491–1496. doi: 10.1073/pnas.022630299
18. Yan Z, Garg SK, Kipnis J, Banerjee R. Extracellular redox modulation by regulatory T cells. Nat Chem Biol. 2009; 5: 721–723. doi: 10.1038/nchembio.212 PMID: 19718041
19. Metcalfe C, Cresswell P, Barclay AN. Interleukin-2 signalling is modulated by a labile disulfide bond in the CD132 chain of its receptor. Open Biol. 2012; 2. doi: 10.1098/rsob.110036
20. Wild MK, Cambiaggi A, Brown MH, Davies EA, Ohno H, Saito T, et al. Dependence of T cell antigen recognition on the dimensions of an accessory receptor–ligand complex. J Exp Med. 1999; 190: 31–42. PMID: 10429668
21. Naldini L, Blömer U, Gallay P, Ory D, Mulligan R, Gage FH, et al. In vivo gene delivery and stable transduction of nondividing cells by a lentiviral vector. Science. American Association for the Advancement of Science; 1996; 272: 263–267. Available: http://www.sciencemag.org/content/272/5259/263.short
22. Banerji S, Wright AJ, Noble M, Mahoney DJ, Campbell ID, Day AJ, et al. Structures of the Cd44-hyaluronan complex provide insight into a fundamental carbohydrate-protein interaction. Nat Struct & Mol Biol. 2007; 14: 234–239. doi: 10.1038/nsmb1201
23. Wong JWH, Hogg PJ. Analysis of disulfide bonds in protein structures. J Thromb Haemost. 2010; 2345–2345. doi: 10.1111/j.1538-7836.2010.03894.x
24. Consortium U. UniProt: a hub for protein information. Nucleic Acids Res. 2014;
25. DeGrendele HC, Kosfiszer M, Estess P, Siegelman MH. CD44 activation and associated primary adhesion is inducible via T cell receptor stimulation. J Immunol. 1997; 159: 2549–2553. PMID: 9300670
26. Lesley J, Kincade PW, Hyman R. Antibody-induced activation of the hyaluronan receptor function of CD44 requires multivalent binding by antibody. Eur. J. Immunol. 1993; 23: 1902–1909. PMID: 7688309
27. Lesley JF, Hyman R, English NM. Site-specific De-N-glycosylation of CD44 Can Activate Hyaluronan Binding, and CD44 Activation States Show Distinct Threshold Densities for Hyaluronan Binding. Cancer Research. 1998; 58: 3736–3742 PMID: 9721887
28. Faller CE, Guvench O. Terminal sialic acids on CD44 N-glycans can block hyaluronan binding by forming competing intramolecular contacts with arginine sidechains. Proteins. 2014; 82: 3079–3089. doi: 10.1002/prot.24668 PMID: 25116630
29. Lesley J, Howes N, Perschl A, Hyman R. Hyaluronan binding function of CD44 is transiently activated on T cells during an in vivo immune response. J Exp Med. 1994; 180: 383–387. PMID: 7516415
30. DeGrendele HC, Estess P, Siegelman MH. Requirement for CD44 in activated T cell extravasation into an inflammatory site. Science. 1997; 278: 672–675. PMID: 9381175
31. Baaten BJG, Li C-R, Deiro MF, Lin MM, Linton PJ, Bradley LM. CD44 regulates survival and memory development in Th1 cells. Immunity. 2010; 32: 104–115. doi: 10.1016/j.immuni.2009.10.011 PMID: 20079666

32. Cook KM, Hogg PJ. Post-Translational Control of Protein Function by Disulfide Bond Cleavage. Antioxidants & redox Signal. 2013; doi: 10.1089/ars.2012.4807

33. Zhou B, Baldus IB, Li W, Edwards SA, Gräter F. Identification of allosteric disulfides from prestress analysis. Biophys J. 2014; 107: 672–681. doi: 10.1016/j.bpj.2014.06.025 PMID: 25099806

34. Essex DW, Li M. Redox control of platelet aggregation. Biochemistry. 2003; 42: 129–136. doi: 10.1021/bi0205045 PMID: 12515547

35. Maekawa A, Schmidt B, Fazekas de St Groth B, Sanejouand Y-H, Hogg PJ. Evidence for a domain-swapped CD4 dimer as the coreceptor for binding to class II MHC. J Immunol. 2006; 176: 6873–6878. PMID: 16709847

36. Matthias LJ, Azimi I, Tabrett CA, Hogg PJ. Reduced monomeric CD4 is the preferred receptor for HIV. J Biol Chem. 2010; 285: 40793–40799. doi: 10.1074/jbc.M110.190579 PMID: 20974843

37. Estess P, DeGrendele HC, Pascual V, Siegelman MH. Functional activation of lymphocyte CD44 in peripheral blood is a marker of autoimmune disease activity. J Clin Investig. 1998; 102: 1173–1182. PMID: 9739051

38. Hogg PJ. Targeting allosteric disulphide bonds in cancer. Nat Rev Cancer. 2013; 13: 425–431. doi: 10.1038/nrc3519 PMID: 23660784